PRACTICAL APPLICATIONS OF MICROBIAL FUEL CELL TECHNOLOGY IN WINERY WASTEWATER TREATMENT

by

Tianlong Liu

M.A.Sc., South China University of Technology, 2012
B. Eng., Qilu University of Technology, 2007

A THESIS SUBMITTED IN PARTIAL FULFILLMENT OF

THE REQUIREMENTS FOR THE DEGREE OF

DOCTOR OF PHILOSOPHY

in

THE COLLEGE OF GRADUATE STUDIES

(Civil Engineering)

THE UNIVERSITY OF BRITISH COLUMBIA

(Okanagan)

January 2020

The following individuals certify that they have read, and recommend to the College of Graduate Studies for acceptance, the dissertation entitled:

PRACTICAL APPLICATIONS OF MICROBIAL FUEL CELL TECHNOLOGY IN WINERY WASTEWATER TREATMENT

submitted by Tianlong Liu in partial fulfillment of the requirements for

the degree of DOCTOR OF PHILOSOPHY

Examining Committee:

Dr. Deborah Roberts, Faculty of Applied Science
Supervisor

Dr. Sumi Siddiqua, Faculty of Applied Science
Co-supervisor

Dr. Thomas Johnson, Faculty of Applied Science
Supervisory Committee Member

Dr. Louise Nelson, Irving K. Barber School of Arts and Sciences
Supervisory Committee Member

Dr. Karen Perry, Irving K. Barber School of Arts and Sciences
University Examiner

Dr. Christopher Simmons, University of California, Davis
External Examiner

Abstract

Microbial fuel cell (MFC) technology shows promise as an alternative to conventional wastewater treatment systems due to renewable energy production and the potential to treat wastewater. The goal of this study was to solve challenges when applying MFC to winery wastewater treatment. A 100 mL air cathode MFC using carbonaceous material as the electrodes was designed and fabricated, inoculated with winery sludge and fed with synthetic winery wastewater.

The pH was found to be essential for the enrichment and maintenance of the MFC. An optimum pH of 6.5 maintained by phosphate buffer (PB) provided stable MFC performance for both power production and chemical oxygen demand (COD) removal. When the reactor was maintained at 1000 mg/L COD, the highest COD removal rate was reached within 4 hours (h) and overall removal reached ~80% within 60 h, the maximum output voltage was obtained within 0.5 h and lasted for 60±3 h. A COD:PB ratio (COD(mg/L):PB(mM)=100:1) was suggested to counter pH fluctuations during MFC operation. With sufficient buffer, the COD removal rate and energy recovery efficiency were linearly related to SWW strength until the system limit was reached. Dog food was an effective alternative feed to maintain an active microbial population during the off season. An external resistance set close to the internal resistance maximized the treatment efficiency, whereas a higher external resistance increased energy recovery. Allowing time for a mature biofilm to form reduced the internal resistance of the reactor and provided better output power density.

A numerical model developed in this work predicted the output voltage from experiment but did not predict the COD removal rate well. The explanation was the existence of a complex mixed culture in the reactor consuming more COD and an increasing role of planktonic organisms at higher concentration. The model also revealed that the anode contributed ~2.5x higher to COD removal than the cathode, and that increasing the anode biofilm thickness resulted in a higher output power.

Lay Summary

Microbial fuel cell (MFC) technology can be used to treat wastewater and generate electricity. This study investigated using an MFC to treat winery wastewater containing rich organic compounds. An MFC reactor was designed and fabricated using synthetic winery wastewater as fuel. A pH of 6.5 maintained with phosphate buffer was found optimum for the MFC performance. When maintained at optimum pH the reactor performed better when fed a higher concentration of wastewater. Adding dog food could effectively keep the wastewater reactor active during the off season. The MFC was able to generate electricity when using either wastewater or dog food as fuel. The MFC performed better as it aged. A numerical model was able to provide promising simulation results, which can be used to predict reactor performance and provide optimization solutions. It also revealed that at a higher feed concentration the organisms in the liquid phase should not be ignored.

Preface

A version of Chapter 3 has been presented in part in the poster *Electricity generation from winery wastewater using air cathode microbial fuel cell: addressing the practical issues* at the *68th Annual Conference of the Canadian Society of Microbiologists,* and as oral presentation *Investigating the effects of pH and buffer on MFC treating winery wastewater* in the 2019 Annual Conference of the Canadian Society for Bioengineering (CSBE).

A version of Chapter 3 chapter has been submitted to *Journal of Water Process Engineering* as Tianglong Liu, Anupama Vijaya Nadaraja, Justin Friesen, Kiranpreet Gill, Man In Lam, and Deborah J Roberts, Practical control of the hydrogen ion concentration in a microbial fuel cell treating winery wastewater. I did the experiments and drafted the manuscript, Nadaraja did the microbiological analysis and revised the manuscript, Friesen, Gill and Lam helped on the routine sample analysis, Roberts finalized the manuscript.

A version of Chapter 4 has been presented in part in the poster *Effect of seasonal variations in feed on power production and the microbial population in a microbial fuel cell* in the 2019 Annual Conference of the Canadian Society for Bioengineering (CSBE), and submitted to *Water Research* as Tianglong Liu, Anupama Vijaya Nadaraja, Jiaming Shi and Deborah J Roberts, *Stable performance of MFC treating winery wastewater irrespective of seasonal variations*. I did the experiment and drafted the manuscript, Nadaraja did the microbiological analysis and revised the manuscript, Shi helped on the routine sample analysis, Roberts finalized the manuscript.

A version of Chapter 6 is being prepared for publication.

Table of Contents

List of Tables

List of Figures

List of Symbols

Symbol	Description	Unit
a_C	e- transfer coefficient of cathode	-
$b_{res,,A}$	endogenous decay coefficient for active biomass,	/h
c_i	species concentration	mol/L
D_i	diffusion coefficient of the species	dm^2/s
$D_{O2,PTFE}$	diffusivity of oxygen in PTFE	$\mu m^2/s$
E^0_A	standard reduction potential for the anodic e- acceptor	V
E^0_C	standard reduction potential for the cathode	V
E_A	potential of the anodic e- acceptor	V
E_C	cathode potential	V
F	Faraday's constant	C/mol
F_{adv}	advection flux term	$mol/(dm^2.s)$
F_{dif}	diffusion flux term	$mol/(dm^2.s)$
F_{mig}	migration flux term	$mol/(dm^2.s)$
f^0_e	the fraction of e- directed by HAB from the cathode to O_2	unitless
f^0_s	the fraction of e- that go from the cathode to biomass	unitless
$[H^+]$	proton concentration	mol/L
$[H^+]_{cat/liq}$	proton concentration at the cathode|liquid interface	mol/L
$[H^+]_{ini}$	initial proton concentration in anode	mol/L
I	current	A
I_d	current density	mA/m^2
$i_{0,A}$	anodic limiting current density	A/m^2
i_A	current density in anode biofilm	A/m^2
i_C	current density in cathode	A/m^2
J	diffusion rate per area	$mmol/(dm^2.s)$
K_{O2}	half velocity constant for oxygen	mmol/L
K_{sub}	half velocity constant for substrate	mmol/L
K_{Sub}	half velocity constant for substrate	mmol/L
k_{bio}	biofilm conductivity	S/m
k_{O2}	oxygen reduction rate per area	$mmol/(dm^2.s)$
L_{cat}	thickness of catalyst	m

n	the influence factor	unitless
$n_{e\text{-}/b}$	e- equivalence of active biomass	mmole-/ mg VS($C_5H_7O_2N$)
$n_{e\text{-}/eth}$	e- equivalence of ethanol	mmol e- / mmol ethanol
$n_{e\text{-}/glu}$	e- equivalence of glucose	mmol e- / mmol glucose
$n_{e\text{-}/sub}$	e- equivalence of substrate	mmol e- / mmol substrate
n_{O2}	e- equivalence of oxygen	mmol e- / mmol oxygen
n_{sub}	number of moles of substrate added	mol
$[O_2]_{air}$	oxygen concentration in air	mmol/L
$[O_2]_{cat/liq}$	oxygen concentration at the cathode/liquid interface	mmol/L
$[O_2]_{PTFE}$	oxygen concentration in PTFE layer	mmol/L
$[O_2]_{PTFE\|cc}$	oxygen concentration at the PTFE|carbon cloth interface	mmol/L
P_d	power density	mW/m^2
P_{max}	maximum power	W
q	flowrate of the reactor as a continuous system	m^3/h
R	ideal gas constant	J/mol/K
R_a	anodic resistance	Ω
R_c	cathodic resistance	Ω
R_{Ext}	external resistance	Ω
R_{Int}	internal resistance	Ω
R_Ω	ohmic resistance	Ω
$r_{COD/eth}$	COD equivalence of ethanol	mg COD / mmol ethanol
$r_{COD/glu}$	COD equivalence of glucose	mg COD / mmol glucose
$r_{COD/sub}$	COD equivalence of substrate	mg COD / mmol substrate
r_i	species reaction rate	mol/(L.S)
$r_{O2,C}$	oxygen reduction rate	mmol/(L.s)
$r_{res,A}$	endogenous respiration rate in anodic biofilm	mg VS / (L.s)
$r_{sub,A}$	substrate reaction rate in anodic biofilm	mmol / (L.s)
S_A	surface area of anode	m^2
S_C	projected surface area of cathode	m^2
$[Sub]^0_A$	stand anodic e- acceptor concentration	mol/L
$[Sub]_A$	anodic e- acceptor concentration	mol/L
$[Sub]_{bio}$	substrate concentration in biofilm	mmol/L
T	temperature	K
V	output voltage of MFC	V

v_A	effective volume of anode chamber.	m^3
x	location in biofilm	m
X_b	volume fraction of active biomass	unitless
y	location in PTFE layer	μm
Y_b	active biomass growth yield	mg VS / mg COD
$Y_{bio,HAB}$	HAB biomass yield	mol HAB / mol substrate
$Y_{O2,HAB}$	oxygen yield	mol O_2 / mol substrate
ΔCOD	change of COD before and after treatment	mg/L
ΔH	combustion heat	kJ/mol
η	local potential in biofilm	V
$\eta_{act,A}$	anode activation overpotential	V
$\lvert\eta_{act,A}\rvert$	anodic activation loss	V
$\eta_{act,KA}$	half maximum rate for anodic activation overpotential	V
$\lvert\eta_{con,A}\rvert$	anodic concentration loss	V
η_{MFC}	energy recovery ratio	unitless
η_{ohmic}	ohmic loss	V
μ_b	specific growth rate of active biomass	/h
ρ_b	density of active biomass	mg VS / L
σ	the energy transfer coefficient	unitless

List of Abbreviations

avg.	average
AAB	autotrophic aerobic bacteria
AEM	anion-exchange membrane
AFMBR	anaerobic fluidized membrane bioreactors
BB	bicarbonate buffer
BDL	below detection limit
BOD	biological oxygen demand
BPM	bipolar membrane
BSL	Biological Solution Laboratory
CEM	cation exchange membrane
CNTs	carbon nanotubes
COD	chemical oxygen demand
COD_{24}	COD after 24 hours
CSBE	Canadian Society for Bioengineering
DC	direct current
emf	electromotive force
EAB	electrochemically active bacteria
EIS	electrochemical impedance spectra
EPS	extracellular polymer substances
ER	external resistance
FDF	filtered dog food
FISH	Fluorescent In Situ Hybridization
g	gram
h	hour
HAB	heterotrophic aerobic bacteria
HRT	hydraulic retention time
IC	Ion Chromatography
ID	internal diameter
L	liter
min	minute
MFC	microbial fuel cell

MPPT	maximum power point tracking
Nafion	perfluorosulfonic acid
OCV	open circuit voltage
OD	outer diameter
ORL	organic loading rate
P/O	perturbation/observation
PB	phosphate buffer
PC	polarization curve
PDMS	poly(dimethylsiloxane)
PEM	proton exchange membrane
PPy	polypyrrole
PTFE	polytetrafluoroethylene
PVDF	poly(vinylidene fluoride)
RDF	raw dog food
RT	retention time
std.	standard deviation
SA	surface area
SCOD	soluble chemical oxygen demand
SEM	Scanning Electron Microscopy
SRT	solid retention time
SWW	synthetic winery wastewater
TCOD	total chemical oxygen demand
TSS	total suspended solids
UCM	ultracentrifugation membrane
VFA	volatile fatty acids
VSS	volatile suspended solids
WWTP	wastewater treatment plant

Acknowledgements

I offer my enduring gratitude to the faculty, staff and my fellow students at the UBC, who have inspired me to continue my work in this field. I owe particular thanks to my supervisor Dr. Deborah J. Roberts, for her motivation, guidance, encouragement, patience, and financial support. She granted me a great flexibility and freedom in my research. Her immense knowledge, enthusiasm and positive attitude towards science set a pattern for me. I am deeply honored and fortunate to have her as the supervisor for my Ph.D study and the mentor for my life. I extremely appreciate and would like to thank my co-supervisor Dr. Sumi Siddiqua for her constant guidance, advice, and kind encouragement. I have been deeply influenced by her work enthusiasm and precious support. I would also like to thank my committee members Dr. Louise Nelson and Dr. Thomas Johnson for their support, encouragement and insightful comments on my research.

I wish to express my sincere thanks to Dr. Anupama Vijaya Nadaraja for her selfless support and knowledge sharing in research, and her friendship in daily life. I sincerely thank Dr. Ian Foulds for his tutoring and guidance on experiments. I would like to thank mechanist Durwin Bossy, laboratory manager Alec Smith, technician Michelle Tofteland for their assistance in machine shop and laboratory. I am grateful to undergraduate students Justin Friesen, Jiaming Shi and Man In Lam for their help on experiments. I wish to thank my colleagues and friends in UBC and Kelowna for their support and friendship.

I would also like to thank my Canadian family (the Taiji family), Bruce and Jane Taiji, Sian, grandma and grandpa for their love, support and encouragement during my PhD study. They regard us as family members, for me they defined the word ‘Canada’.

Finally, but foremost, I am deeply grateful to my dad, mom and sister for their unconditional love, support and understanding over all these years. I own my special thanks to my wife Fang Fang for her love, encouragement and accompanying on my PhD adventure. All my achievements would not have been possible without their constant encouragement and support.

Chapter 1. Literature Review

1.1 Introduction

Wastewater treatment is the most basic sanitation need to protect the environment and potential drinking water reserves from polluted water. Inadequate treatment of organic wastewater and subsequent discharge into receiving water bodies is a major reason for water quality deterioration in many countries. Currently activated sludge processes are the most accepted sewage and industrial wastewater treatment systems in many countries. While the activated sludge process produces excellent results within reasonable processing times, the process is microbiologically-, chemical-, and energy-intensive requiring high capital and operation/maintenance costs (Sustarsic, 2009). The aeration process required in activated sludge process accounts for 75% of wastewater treatment plant (WWTP) energy costs (Kokabian and Gude, 2015). In United States 3-4% of the electricity produced is consumed by water infrastructure whose operational cost is mostly electricity (Logan, 2008; EPA, 2014). These costs make treating industrial wastewater to meet discharge standards a challenge. There is a growing demand for more environmentally friendly and less energy demanding bioprocesses to manage various organic wastewaters.

Harnessing energy from wastewater is considered as a ground-breaking technology that can decrease our reliance on fossil fuels. It is estimated that wastewater contains as much as 9.3 times the energy consumed using current technologies (Shizas and Bagley, 2004). Capturing this energy could result in a sustainable wastewater treatment solution. Two types of energy are locked in wastewater, thermal energy (74%) and chemical energy (26%); both can be recovered. Thermal energy capture requires a heat pump and is subject to the temperature of wastewater (Scott et al., 2016). Chemical energy is present in two forms, nutritional elements such as nitrogen and phosphorus (0.7 kWh/m^3) and organic matter (1.79 kWh/m^3) (McCarty et al., 2011). Efficient extraction of the energy locked in organic matter reduces pollution and decreases the

operational cost of the treatment process. The present research investigates an alternative way to treat wastewater rich in organic matter while recovering the chemical energy inherent to the wastewater.

1.2 Winery wastewater

Wastewater from the wine industry contains a significantly high amount of biodegradable organic matter. The wine market has expanded rapidly in the global scenario and is expected to reach a global consumption of more than 30 billion liters during the period 2016-2020 (PR Newswire Association, 2016). Wine production globally is increasing substantially to meet the growing worldwide demand. In 2018 global wine production was about 282 million hectoliters, an increase of about 12.4% compared to 2017 (OIV, 2018). One of the major challenges faced by the wine industry is treating the large amount of winery wastes which include solid organic waste, wastewater, recalcitrant materials (e.g. polyphenols, tannins, lignin), greenhouse gases, packaging wastes, detergents, and food waste if they have restaurants (Ioannou et al., 2015; Litaor et al., 2015).

1.2.1 Winery wastewater constituents

Winery wastewater originates from various washing operations during the crushing and pressing of grapes, cleaning of surfaces and equipment, rinsing of bottles, barrels and fermentation tanks (Malandra et al., 2003). Understanding the characteristics of winery wastewater is crucial for the optimization of winery wastewater treatment. The characteristics of winery wastewater from the literature are summarized in Table 1-1. As shown in the table, winery wastewater was reported to have high chemical oxygen demand (COD) concentrations (up to 76,900 mg/L), biological oxygen demand (BOD) (up to 22,400 mg/L), and variable amounts of total solids (TS) that range from 150 to 18,000 mg/L (Conradie et al., 2014; Fillaudeau et al., 2008; Mosse et al., 2011). The high COD in wastewaters poses serious environmental issues if not treated properly and if it reached streams or irrigation systems (Conradie et al., 2014; Serrano et al., 2011).

Table 1-1 Summary of characteristics of winery wastewater

Parameter	Value (range)	Reference
COD (mg/L)	320-49105	Iaonnou et al., 2015
	675-76900	Welz et al., 2016
	15000-44900	Fillaudeau et al., 2008
	340-49105	Conradie et al., 2014
BOD (mg/L)	310-410	Rajagopal et al., 2013
	181-22418	Conradie et al., 2014
pH	4-8	Bolzonella et al., 2019
	3.6-10.5	Welz et al., 2016
Total Solids (mg/L)	150-200	Rajagopal et al., 2013
	190-18000	Conradie et al., 2014
Suspended solids (mg/L)	1000-5137	Conradie et al., 2014
Total P (mg/L)	40-60	Rajagopal et al., 2013
	10-270	Welz et al., 2016
Total N (mg/L)	310-410	Rajagopal et al., 2013
	10-176	Welz et al., 2016
Sugar (mg/L)		Welz et al., 2016
Glucose	0-1596	
Fructose	0-506	
Maltose	0-889	
Ethanol (mg/L)	4900	Fillaudeau et al., 2008
Organic acids (mg/L)		Fillaudeau et al., 2008
Tartaric acid	0-1794	
Malic acid	0-583	
Lactic acid	0-770	
Succinic acid	0-1121	

1.2.2 Current treatment technology

Currently employed treatment systems for winery wastewater include physicochemical technologies such as electrodialysis, reverse osmosis, photo-fenton, ozonation processes, and biological systems such as activated sludge, sequencing batch reactors, rotating biological reactors, fixed bed biofilm reactors, membrane bioreactor, biofilm reactors, and constructed wetlands (Litaor et al., 2015). A recent review by Ioannou et al. (2015) critically evaluated the currently applied treatment systems including physicochemical, advanced oxidation processes, membrane filtration and separation, biological, and a combination of biological and advanced oxidation processes for winery wastewater. They concluded that depending on the wine processing systems used in specific wineries, the nature and properties for winery wastewater vary, hence, developing a generalized treatment strategy is a difficult task. They also suggested more advanced treatment processes with higher waste removal efficiency and cost effectiveness, that are environmentally sensitive and technically reliable for large scale applications are needed.

1.3 Microbial fuel cell

The microbial fuel cell (MFC) is a recently developed technology that shows promise over conventional wastewater treatment systems due to bioelectricity generation, renewable energy production and the potential to treat wastewater (Huggins et al., 2013; Logan, 2008). Even though the first observation of electricity generation by bacteria was made in 1911 (Potter, 1911), the majority of the research has been performed in the last 20 years.

In conventional anaerobic digestion, methane produced is cleaned and used as combustion fuel or in chemical fuel cells for generating electricity. Usually one third of the biogas produced is used to generate electricity and the rest is used for combustion to heat the digester (Pham et al., 2006). In comparison MFCs convert the chemical energy locked in wastewater components directly to electricity. Moreover, bioelectrical systems like MFCs do not have to cater to methanogens and so will not experience the inherent problems of anaerobic digestion such as poor performance at low temperature and low substrate concentrations (Rabaey and Verstraete, 2005). Additionally, compared to aerobic systems, the lower sludge production in these systems will minimize the challenges and operating costs associated with sludge treatment and disposal.

Just like a typical fuel cell, an MFC system includes an anode, a cathode and electrolyte. The redox reaction occurring in MFCs results in electron release and transfer through biochemical or electrochemical reactions at the electrodes therefore forms current. One serves as the electron donor and the other acts as the acceptor. For example, if glucose acts as the electron donor and O_2 acts as the electron acceptor, the half reactions will be:

$$C_6H_{12}O_6 + 12H_2O \rightarrow 6HCO_3^- + 30H^+ + 24e^- (Anode) \quad \text{eq. 1-1}$$

$$O_2 + 4H^+ + 4e^- \rightarrow 2H_2O\ (Cathode) \quad \text{eq. 1-2}$$

In an MFC, the theoretical cell voltage or electromotive force (emf) of the overall reaction (anode and cathode potential difference) determines if the electron flow (current) is formed, as shown in Equation 1-3. ΔE_{cell} needs to be a positive value in MFC system.

$$\Delta E_{cell} = \Delta E_{cathode} - \Delta E_{anode} \quad \text{eq. 1-3}$$

A classic MFC system consists of an anode chamber and cathode chamber physically separated by a separator which is usually a proton exchange membrane (PEM) (Logan, 2008). Electrochemically active bacteria (EAB) inoculated in the anode chamber oxidize the substrate (e.g. glucose) and transfer electrons to the anode, electrons then move to the cathode through an external load. Meanwhile protons (H^+) pass through the PEM to the cathode (or the cathode chamber filled with electrolyte if it is a dual chamber MFC), where protons react with oxygen and electrons to form water with or without the presence of catalyst.

1.3.1 MFC design

Various designs for MFCs have been reported in laboratory studies including single chamber, dual chamber, cylindrical, H-shape dual chamber, tubular, etc. (Liu et al., 2004; Mathuriya, 2014; Miran et al., 2015; Samsudeen et al., 2015). The dual chamber MFC is a classic design, which consists of an anode and cathode installed in two chambers separated by a PEM. It is commonly used in lab mechanistic studies; however, the complexity and space requirement of this design limit its application when scaling up (Logan, 2010). The single-chamber MFC has been proposed as an alternative. A classic single chamber MFC has only one anode chamber, with the cathode exposed to air directly, therefore, it is also called an air cathode MFC. The schematic of an air cathode MFC fed wastewater is illustrated in Figure 1-1.

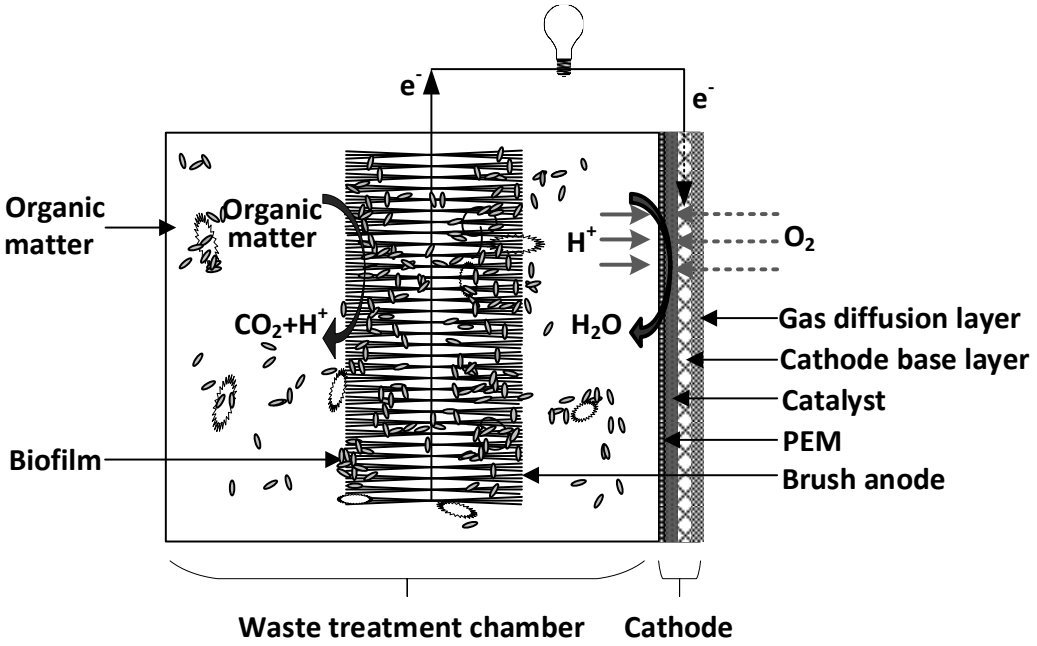

Figure 1-1 The schematic of a single chamber MFC fed wastewater

The design presented in Figure 1-1 depicts an anode as a brush shape which significantly increases the specific surface and allows more contact with biofilm. The cathode can be assembled with or without the PEM. Diffusion layers used on the air side of the cathode improve the system performance significantly by limiting oxygen diffusing to the anode and decreasing the loss of water instantaneously. In practical applications the anode and cathode are usually processed with a water-proof treatment to obtain better durability (Cao et al., 2009). This chapter focuses on the design, operation and application of the air cathode MFC.

1.3.2 MFC performance influence factors

Current studies have demonstrated that MFC performance is greatly influenced by a number of factors, including the MFC configuration, electrode materials, presence/absence of PEM, and operational parameters such as pH, temperature, and retention time (RT) (Gil-Carrera et al., 2013; Liu and Logan, 2004; Walter et al., 2016). MFC configuration is subject to factors such as the size of the MFCs, the number of units (e.g. the length of the cascade, how they are connected), hydraulic retention time, fuel quality, anode

surface area, etc. (Walter et al., 2016; Wang et al., 2016). In addition to the structural material of an MFC, a size limitation has appeared that compared to large-volume units, small scale units tend to produce higher energy densities due to higher surface area-to-volume ratio (SA:V) of the electrode macro-surface area to chamber volume, as well as the distance between electrodes (Walter et al., 2016). MFC cascade is one approach to boost power generation up to practically usable level through stacking/connecting small units together. It has been reported that the cascade stacking strategies (both in parallel and series) enhanced both the power production and treatment efficiency without catalysts when compared to single large units with the same volume. Another advantage of this strategy is that substrate starvation and imbalances did not result in cell-voltage reversal (Ledezma et al., 2013).

1.3.2.1 Anode

A variety of materials have been attempted to use as the anode to improve performance and economic viability, e.g. metal and metal oxides, composite materials, especially carbonaceous materials (Deval et al., 2016; Hernández-Fernández et al., 2015; Logan, 2008; Siegert et al., 2014; Sonawane et al., 2014). Carbonaceous materials are most widely used as anodes as they are relatively inexpensive, meanwhile providing good conductivity, chemical stability as well as biocompatibility (Logan et al., 2006; Zhou et al., 2013).

The anode arrangement and the anode surface area have significant effects on MFC performance. Three types (brush shape, plane shape and packed granules) of anode arrangement are widely researched. Reports showed that carbon brush anodes achieved higher efficiency than plane carbon cloth or packed carbon granules on both power production and COD removal (Logan, 2008; Molognoni, 2014; Shehab et al., 2014). Physical/chemical treatment (e.g. ammonia, acid, or thermal treatment) of the electrode surface has shown promising improvements over untreated in power production. Ammonia treatment increased the surface charges of carbon cloth, therefore, facilitating adhesion of bacteria during reactor start-up and improving the efficiency of electron transfer from the bacteria to the surface (Cheng and Logan, 2007). Acid or thermal

treatment of carbonaceous material improved the surface of the anode by the increase in protonated N to total N and the decrease of oxygen-to-carbon (O/C). Wang et al. (2009) reported that a heat treated (450 °C for 30 min) carbon mesh anode resulted in a maximum power density of 922 mW/m^2 (46 W/m^3), a 3% improvement over a mesh anode cleaned with acetone (893 mW/m^2; 45 W/m^3). When the carbon mesh was treated by a high temperature ammonia gas process (700 °C for 60 min in 5% ammonia gas), the power increased to 1015 mW/m^2 (51W/m^3). Liu et al. (2014) showed that the performance of an air-cathode single-chamber microbial fuel cell increased 38.1% when carbon cloth anodes were modified with formic acid.

Another possible anode modification option is the electrodeposition of metallic oxide onto the surface of carbonaceous anodes. Zhang et al. (2014) reported that depositing manganese dioxide (MnO_2) onto carbon felt resulted in up to 24.5% increase in power density compared to bare carbon felt anodes. This was explained as the synergistic effect of the material properties (biocompatibility, high specific surface area and pseudocapacitive behavior), which facilitated electron transfer.

The application of metals as MFC electrodes has been studied widely as they are more conductive than carbon-based materials. Since the corrosiveness of many metals is a major drawback of their application as electrodes (Bataineh et al., 2006; Siegert et al., 2014; Zhu and Logan, 2013), non-corrosive metals such as stainless steel, titanium and gold have been used as base materials for anodes (Sonawane et al., 2014). However, many studies failed to achieve higher power generation efficiency compared to carbon materials, the main disadvantage is that their smooth surface hinders the adhesion of the bacteria. (Crittenden et al., 2006; Liang et al., 2017; F. Zhang et al., 2011a; Zhang et al., 2010).

Overall, among the various materials studied, carbonaceous materials are still widely used for MFC anodes for their acceptable economic feasibility and performance. Further improvement such as surface modification and elemental dosing is a promising direction for efficiency improvement.

1.3.2.2 Cathode

Air and aqueous phase cathodes are two common cathode configurations used in MFCs. The main difference is that air cathodes expose the reaction area to air directly, whereas in aqueous phase cathodes a cathodic electrolyte is used in a separate chamber. Air cathodes are widely used due to their simple design; they do not require aeration and offer high power densities. The air cathode typically consists of three layers: a hydrophobic diffusion layer exposed to the air, a conductive supporting material which sometimes also works as a diffusion layer, and a blend of catalyst and binder in contact with the water (Min et al., 2005). As described previously, oxygen is required in the cathode for the redox reaction, but it should be limited from diffusing deep into the anode chamber to avoid efficiency loss. The diffusion layer placed on the air side of the cathode controls the diffusion efficiency of oxygen. A schematic design of the air cathode is shown in Figure 1-2 as an example. The carbon cloth is coated with one base layer (carbon black mixed with polytetrafluoroethylene (PTFE) and four diffusion layers (PTFE) on the air side, and a support layer blended with Pt as catalyst on the solution side. Cheng et al. (2006) found an increase of 42% on the maximum power density was obtained using this design compared to a cathode without diffusion layers.

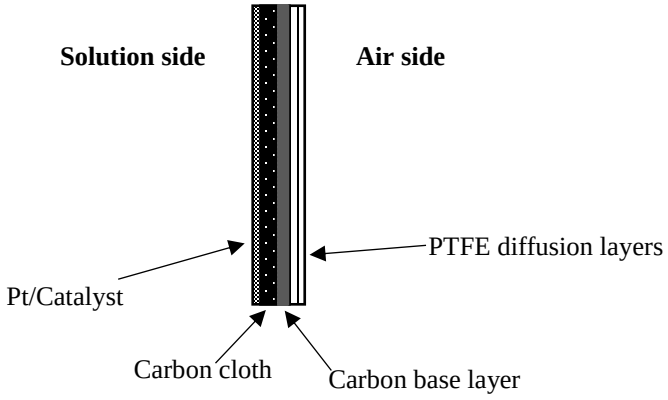

Figure 1-2 The schematic diagram of an air cathode

Similar to the anode, carbonaceous materials such as carbon cloth or carbon paper are commonly used as supporting material in cathodes (Logan et al., 2006; Mink et al., 2014). Copper, stainless steel and nickel mesh have also been used as the conductive supporting layer; however, corrosion and high cost limited their further application (Siegert et al., 2014; F. Zhang et al., 2011a; Zhang et al., 2012, 2010).

The binder used to fix the catalyst onto the electrode includes perfluorosulfonic acid (Nafion) (Wang et al., 2010), PTFE (Logan, 2008; Wang et al., 2010; Zhang et al., 2009), poly(vinylidene fluoride) (PVDF) (Yang et al., 2014), or poly(dimethylsiloxane) (PDMS) (Luo et al., 2011; F. Zhang et al., 2011a; Zhang et al., 2010). The performance varies widely based on the material, fabrication process, and running conditions. Cheng and Wu (2013) reported using Nafion as catalyst (Pt) binder improved the maximum power density by 14% compared with PTFE as binder. However, the >500 times higher price of Nafion is the drawback compared to other binders.

A catalyst bonded to the cathode can be chosen from many catalytic materials; Pt or Gold (Au) are the most commonly used and provided the best performance. To overcome the drawback of using Pt due to its high price, many researchers have chosen to either reduce the amount of Pt used or consider an alternative replacement. Cheng et al. (2006) reported that when Pt loading was decreased from 0.5 to 0.1 mg/cm^2 there was no substantial loss of maximum power densities. Other studies have reported important advances as well in developing new catalysts such as graphene, nanomaterials, macrocyclic compounds, etc. (Zuo et al., 2016); however, their performances have not exceeded carbon materials with Pt (Liang et al., 2017; Yang et al., 2014; Zhu and Logan, 2013).

Another essential factor impacting the property of cathodes is that the resistance contributed by both material and fabrication technology, will eventually reflect on the internal resistance of the MFC. To minimize this resistance the cathode and the membrane have been manufactured separately before assembly to ensure a good contact. A promising new configuration has been developed known as membrane cathode assembly, for example, pressing the PEM (or cation exchange membrane) on the air cathode (Hoskins et al., 2014; Mohanakrishna et al. , 2012; Zhang et al., 2015).

1.3.2.3 Membrane as separator

Membrane separators offer several advantages such as physical separation between anode and cathode preventing short-circuit, limiting oxygen diffusion from the cathodic to the anodic side, and thereby boosting the columbic efficiency of MFC. A number of factors (internal resistance, oxygen diffusion ability, biofouling) are essential for MFC performance. A widely used proton exchange membrane (PEM) is Perfluorinated ionomer such as DuPont™ Nafion® due to their high ionic conductivity and high mechanical and chemical resistance (Logan, 2008; Samsudeen et al., 2015). However, these are very expensive, making their large-scale application unfeasible. Other cation-exchange membranes (CEM), anion-exchange membranes (AEM), bipolar membranes (BPM) and ultracentrifugation membranes (UCM) were also tested. Anion exchange membranes were found to improve cell efficiency in MFC, however, lack of flexibility to change operational conditions with these membranes limit their MFC applications (Liu et al., 2011; Philamore et al., 2015; Scott et al., 2016; You et al., 2017). Membranes based on cloth and glass fibers as the separators have shown the potential to effectively maintain a high level output power and low oxygen diffusion efficiency; however, these materials might degrade with time and might not be feasible for long term operations (Siegert et al., 2014). A few studies used clay-based membranes which showed long term stability (Behera et al., 2013; Ghadge and Ghangrekar, 2014). Another interesting inexpensive alternative membrane tested was natural rubber which showed long term power production compared to conventional materials, but it required further validation and modifications to make it feasible for commercial MFC applications (Winfield et al., 2014).

Many groups have studied different configurations such as membraneless MFC, which assembles the PEM directly on flexible carbon cloth, or uses rigid carbon paper without PEM coating (Cusick et al., 2011; Huang et al. 2011; Jiang et al., 2016). The common design of membraneless MFC is to place anode and cathode into two ends of a chamber without PEM or CEM as the separator. Results showed some advantages includes lower internal resistances and less operational costs (Jang et al., 2004; Zhou et al., 2013).

1.3.3 MFC operational parameters

The major limiting factor of practical MFC application is low power output; various strategies have been developed for better improvement. Operational parameters including pH, temperature, external and internal resistance, ionic strength, solids and hydraulic retention time, and the addition of mediators play crucial roles in power generation; hence, optimizing these parameters receives significant attention (Gil et al., 2003; Goswami and Mishra, 2018; Liu et al., 2005b).

1.3.3.1 pH

Electrolyte pH at both the anode and cathode chambers of MFC is the most critical factor affecting the overall MFC efficiency. A neutral pH is usually maintained in the anode chamber due to the preference for neutral pH by anodic microbial community bacteria for their growth and metabolic activities (J. T. Li et al., 2013; Zhuang et al., 2010). Several studies substantiated this finding. A decline in current generation was observed in the absence of buffer after 5 hours (h) of operation with a starting pH of 7; the increase and decrease of pH resulted in less microbial activity, anodic electron transfer and slower cathodic reaction and finally reduced MFC efficiency in unbuffered conditions (Gil et al., 2003). A similar observation was reported by Ren et al. (2007), that a significant decrease in power production occurred when pH dropped to 5.2 from 7 due to acidic products of fermentation in a dual chamber MFC. However, a few studies reported MFC operation under acidic and alkaline conditions. An air cathode MFC could tolerate an electrolyte pH as high as 10 with optimal pH 8 and 10, and it was observed that the anodic bacterial activity and cathode oxygen reduction altered electrolyte pH by supplying or consuming protons (He et al., 2008). Another study showed that an MFC operated under acidic conditions in the anode chamber for chemical wastewater treatment showed effective performance with respect to power output compared to the corresponding neutral and alkaline conditions; however, substrate degradation was higher at neutral pH (Raghavulu et al., 2009). A more detailed literature review regarding MFC pH is presented in Chapter 3. In

this study the impact of pH on MFC fed winery wastewater was investigated, the optimum pH and buffer strength were determined.

1.3.3.2 Temperature

Temperature is another factor which influences MFC performance in terms of substrate removal and power generation by altering system kinetics, microbial metabolism, membrane permeability and internal resistance (Goswami and Mishra, 2018; Martin et al., 2010). An increased power output was usually observed in mesophilic temperatures compared to low temperatures; this could be attributed to the enhanced anodic biofilm formation and activity and membrane conductivity, increase in conductivity of wastewater which lowers the overall internal resistance of the system (Gonzalez del Campo et al., 2013; Larrosa-guerrero et al., 2010; Liu et al., 2005a). Interestingly, a sustainable power output was observed in MFCs operated at 15 °C; however, the start-up time to reach reproducible voltage output was significantly increased and it was also observed that MFC performance was improved by using a warm start-up temperature (30 °C) before changing the temperature to 4 C or 10 °C (Cheng and Logan, 2011). Another study showed that an MFC operated at low temperature (10 °C and 5 °C) using a mixed anodic community showed a sustainable performance compared to pure-culture (*Shewanella*) at 10 °C. However, the electrogenic activity of anodic bacteria was substantially reduced at 5 °C (Tkach et al., 2017).

1.3.3.3 External resistance (R_{Ext})

The external resistance affects many parameters that determine MFC performance, such as biofilm morphology, microbial diversity, microbial metabolism, anode potential, power output and stability (del Campo et al., 2016; Jung and Regan, 2011; Liu et al., 2016; Lyon et al., 2010; Rismani-Yazdi et al., 2011). Therefore, control of external resistance is significant to improve MFC efficiency and it may change as operational parameters change such as temperature, pH, influent strength, influent composition etc. (Pinto et al., 2011). Maximum output power occurs only when the external resistance equals the internal resistance. Aelterman et al. (2008) observed that low methane production and stable power output were only obtained

when external resistance was set close to the MFC internal resistance in an MFC with a mixed consortium. Higher external resistance usually resulted in lower power production but higher COD removal (del Campo et al., 2016). Katuri et al., (2011) observed distinct differences in anodic bacterial communities in MFCs operated under different external resistances and found that electrogenic bacteria enriched under higher current densities led to sustainable power and higher substrate removal. Electrochemical impedance spectra (EIS) analysis showed a positive correlation between internal resistance and external resistance with an increase in anodic biofilm mass and extracellular polymer substances (EPS) at higher external resistance (Liu et al., 2016). Chapter 5 reports a study of the impact of external resistance on MFC fed wastewater.

1.3.3.4 Internal resistance (R_{Int})

The internal resistance is identified as another key performance driver for MFC operation as high internal resistances limits power output (Fan et al., 2008; Manohar and Mansfeld, 2009; Zhang and Liu, 2010). The major detection methods include the polarization curve method, current interruption method, Electrochemical impedance spectra (EIS) analysis, and phase locked amplifier (Aelterman et al., 2006; Fan and Li, 2016; He et al., 2008). An introduction of the polarization curve method that was used in this thesis is given in Section 2.3. An expanded literature review on internal resistance is given in Chapter 5.

1.3.3.5 Ionic strength

Ionic strength determines the resistance to ion migration within the electrolyte, which is a source to the internal resistance. It also impacts the anodic biofilm activity as high salt can inhibit the microbial community. NaCl is commonly used as an electrolyte to improve the mass transfer of charged particles (Gil et al., 2003). Jang et al. (2004) showed an increase in current generation from 3.5 to 7.7 mA by increasing salt concentration in the cathode compartment from 0.1 to 1 M. Other research showed that increasing the ionic strength of solution from 100 to 400 mM by adding NaCl increased power output from 720 to 1330 mW/m^2 in a single chamber MFC (Liu et al., 2005a). Mohan and Das (2009) observed increasing NaCl concentration up to 10 mM improved power output with a maximum of 12.8 mW/m^2 in a

dual chamber MFC, however, further increase to 15 mM decreased power output; they suggested that the optimum salt concentration was limited by the salt tolerance of the anodic microbial community. Aaron et al. (2010) observed that increasing the ionic strength of anodic fluid from 0.037 M to 0.37 M resulted in a decrease of total internal resistance from 22.5Ω to 13.0 Ω and an increase of the maximum power density from 378 to 793 mW/m^2. Miyahara et al. (2015) reported that increasing the NaCl concentration from 0 to 1.8 M in a single chamber MFC inoculated with rice paddy-field soil and continuously supplied with acetate showed an increase in power output, after that power production decreased markedly and they suggested that the optimum salt concentration in MFC was determined by solution conductivity and salt tolerance of EABs. Similar studies about highly salt tolerant bacteria and archaea in MFC have also been reported. A salt tolerant strain of *Shewanella marisflavi* capable of reducing Fe (III) generated 3.6 mW/m^2 power at a high ionic strength of up to 291 mM (Huang et al., 2010). Halo tolerant archaea (*Haloferax volcanii* and *Natrialba magadii*) produced maximum power of 500.98 and 50.39 mW/m^2 at ionic strengths 2.9 and 3.6 M, respectively (Abrevaya et al., 2011). The concentration and output power varied but all showed the trend that the salt tolerant strains were capable of power generation at higher ionic strength.

1.3.3.6 Retention time

Similar to conventional treatment methods such as activated sludge, solid and hydraulic retention time (SRT and HRT) are critical parameters for stable MFC performance especially when operated with a complex inoculum under continuous flow conditions (Kim et al., 2015; You et al., 2006). The SRT of the reactor affected the anodic microbial population; it's influence on direct and indirect electron transfer mechanisms was reported to account for more than 95% of the total electricity production (D'Angelo et al., 2017; Mateo et al., 2018). HRT or SRT could be as short as several hours in many studies. You et al. (2006) reported a maximum power density of 103±2 mW/m^2 with an average COD removal up to 71% at a HRT of 2 h was obtained in an air cathode MFC using domestic wastewater as substrate; however, an increased HRT (10-30 h) was found to benefit COD removal but voltage was unstable. Cetinkaya et al., (2017) designed a dual chamber MFC producing the maximum power when HRT was set at 12 h and organic loading rate of 10,000

mgCOD/L/day, however, the MFC performance decreased when the HRT was reduced to 6 h. They suggested the possible reason for lower MFC performance could be washing out of the microbial population due to the short HRT. Other studies reported much longer HRT/SRT lasting several days. Calignano et al. (2015) demonstrated that a stable and reproducible power output was obtained from an additive manufacturing wastewater MFC operated for more than 5 months (R_{Ext} = 10-820 Ω) with a continuous feed of anodic organic substrates and an HRT of ~6 days. Santos et al. (2017) reported an optimum HRT of 7.5 days for effectively obtaining maximum power output, voltage and removing COD, ammonium and phosphate in a cyclically fed glycerol-based microbial fuel cell. The study of Mateo et al. (2018) evaluated different SRT for an air cathode MFC with activated sludge and observed a higher power density (0.2 A/m^2) at SRT of 10 days.

1.3.3.7 Mediators

Initially researchers enhanced power production by the addition of artificial exogenous mediators such as neutral red, methylene blue, meldola's blue, azure A, thionine, anthraquinone 2,6-disulfonic acid, cobalt sepulchrate, and Fe (III)EDTA (Bond and Lovley, 2003; Du et al., 2007; Park and Zeikus, 2000). These mediators facilitated the transfer of electrons between planktonic microbial cells and the anode for electrochemically inactive microbes (Fultz and Durst, 1983; Gil et al., 2003; Roller et al., 1984). A good mediator should be able to cross the cell membrane easily, able to accept electrons from the electron carriers of the electron transport chains, possess a high electrode reaction rate, have a good solubility and stability in the anolyte, not be absorbed by the microorganisms and not toxic to them, and be inexpensive (Ieropoulos et al., 2005; Miroliaei et al., 2014). Some bacteria produce endogenous metabolites such as humic acids, anthraquinones, oxyanions, etc. which can act as mediators (Bond and Lovley, 2003).

Compared to other MFC applications there are few reports documenting the use of mediators in MFC fed winery wastewater. Recently, Penteado et al. (2017) investigated the long-term influence of ferricyanide as mediator in the cathode chamber of a dual chamber MFC and observed enhancement of MFC efficiency.

However, a significant concentration of mediator was detected in the anode chamber resulting in declining MFC performance due to toxicity imparted by the mediator to anodic microbes.

The discovery of direct electron transfer between the microbial community and the anode through nanowires in biofilms led researchers towards mediator-less MFC and the importance of biofilm formation. Kim et al. (1999) reported electrochemical activity in anaerobically-grown cells of the iron-reducing bacterium, *S. putrefaciens* IR-1 without the addition of any electrochemical mediator. There are several reports on highly efficient mediator-less MFCs and attempts were made to improve power efficiency by altering electrode materials and operational parameters in mediator-less MFC. Stable and long-term power by a mediator-less MFC was first reported by Chaudhuri and Lovely (2003) using a novel microorganism, *Rhodoferax ferrireducens*, that could oxidize glucose to CO_2 and quantitatively transfer electrons to graphite electrodes. Later, a mediator-less MFC was designed and optimised using artificial wastewater as substrate (Moon et al., 2006). They obtained a power density of 0.56 W/M^2 with 300 mg/L of COD fed at the rate of 0.53 mL/min at 35 °C. Venkata Mohan et al. (2008) evaluated the effect of biofilm formation on the anodic surface in a single chamber mediator-less MFC for treating wastewater. A significant improvement (power, substrate consumption rate, coulomb efficiency) was observed as a function of anodic biofilm coverage. Zou et al. (2008) constructed the anode of a mediator-less MFC using polypyrrole (PPy) coated carbon nanotubes (CNTs) and *Escherichia coli* as the biocatalyst, and achieved 228 mW/m^2 in the absence of exogenous electron mediators. Roh and Kim (2012) reported a power density of 252 mW/M^2 in a mediator-less MFC with carbon nanotubes (CNTs)/graphite felt composite electrodes. A mediator-less MFC inoculated with *Cupriavidus basilensis* could produce a power of 902 and 310 mA/m^2 with acetate and phenol as substrates, respectively under a constant external resistor of 1 kΩ. Park et al. (2016) obtained a voltage of 800-900 mV using a mediator-less MFC inoculated with *S. oneidensis*. A previous study reported an interesting development on mediator-less MFC where electroactive property was triggered in a non-electrogenic strain of *E. coli* by applying an electric pulse of specific magnitude (Nandy et al., 2016).

1.3.4 MFC Microbiology

Microbial communities define the performance of an MFC, and anodic biofilms play a key role in determining the power generation by effectively decomposing the complex substrates and transfer of electrons to the anode (Feng et al., 2008; Greenman et al., 2009; Wrighton et al., 2008). Different microbial communities including bacteria (Logan et al., 2006; Lovely, 2008), archaea (Abrevaya et al., 2011) and yeast (Ganguli and Dunn, 2009) have been reported as potential candidates for inclusion in MFCs. Bacterial mediated MFCs are the predominant form. Electrochemically active microorganisms are frequently isolated from MFC's operated with diverse inoculum such as marine and fresh water sediments (Holmes et al., 2004; Rowe et al., 2015), or wastewater sludge (Feng et al., 2016; Zuo et al., 2008). Exoelectrogenic bacteria reported to date belong to *Proteobacteria*, *Firmicutes*, *Acidobacteria*, and *Bacteroidetes* (Bond and Lovley, 2003; Logan and Regan, 2006; Sun et al., 2010; Wrighton et al., 2008). A list of bacteria reported to show exoelectrogenic activity is given in Table 1-2.

Table 1-2 Electrochemically active bacteria

Bacteria	Phylogenetic classification	Power/current output	Reference
Erwinia dissolvens	Proteobacteria (γ)	0.22 mW	Vega and Fernández, 1987
Desulfovibrio desulfuricans	Proteobacteria (δ)	-	Cooney et al., 1996
Shewanella putrefaciens	Proteobacteria (γ)	≅ 0.04 mA	Kim et al., 2002
Clostridium butyricum	Firmicutes	0.22 mA	Lee et al., 2001
Geobacter metallireducens	Proteobacteria (δ)	-	Champine et al., 2000
Geobacter sulfurreducens	Proteobacteria (δ)	65 mA/m^2	Bond and Lovley, 2003
Aeromonas hydrophila	Proteobacteria (γ)	0.3 mA	Pham et al., 2003
Escherichia coli	Proteobacteria (γ)	0.47 mA/m^2	Park and Zeikus, 2003
Rhodoferax ferrireducens	Proteobacteria (α)	31 mA/m^2	Chaudhuri and Lovley, 2003
Enterococcus faecium	Firmicutes	4.31 mA/m^2	Rabaey and Verstraete, 2005
Desulfobulbus propionicus	Proteobacteria (δ)	28.35±4.72 mA/m^2	Holmes et al., 2004
Geothrix fermentans	Acidobacteria	0.31 mA	Bond and Lovley, 2003
Pseudomonas aeruginosa	Proteobacteria (γ)	0.1 mA	Rabaey and Verstraete, 2005
Gluconobacter oxydans	Proteobacteria (α)	7.23 mW	Reshetilov et al., 2006
Rhodobacter sphaeroides	Proteobacteria (α)	790 mW/m^2	Cho et al., 2008
Klebsiella pneumoniae	Proteobacteria (γ)	409.71 mW/m^2	Zhang et al., 2008
Rhodopseudomonas palustris	Proteobacteria (α)	2720±60 mW/m^2	Xing et al., 2008
Acidiphilium cryptum	Proteobacteria (α)	12.7 mW/m^2	Borole et al., 2008
Bacillus subtilis	Firmicutes	1.05 mW/cm^2	Nimje et al., 2009
Geopsychrobacter electrodiphilus	Proteobacteria (δ)	~8.89 mA/cm^2	Holmes et al., 2009
Lactococcus lactis	Firmicutes	~3 A/m^3	Freguia et al., 2009
Arcobacter butzleri	Proteobacteria (Ɛ)	296 mW/L	Fedorovich et al., 2009
Comamonas denitrificans	Proteobacteria (β)	35 mW/m^2	Xing et al., 2010
Thermincola potens	Firmicutes	~15 mA	Wrighton et al., 2011
Arcobacter butzleri	Proteobacteria (Ɛ)		Toh et al., 2011
Dysgonomonas oryzarvi	Bacteroidetes	50 μA/cm^2	Kodama et al., 2012
Lysinibacillus sphaericus	Firmicutes	≈270 mA/m^2	Nandy et al., 2013
Cupriavidus basilensis	Proteobacteria (β)	902 mA/m^2	Friman et al., 2013
Enterobacter ludwigii	Proteobacteria (γ)	440 mA/m^2	Feng et al., 2014
Ochrobactrum anthropi	Proteobacteria (α)	89.1±1.2 mW/m^2	Wang et al., 2016

The possible mechanisms of electron transfer resulting in power generation via cell respiration include direct electron transfer, direct election transfer through pili (nanowires), mediated electron transfer and oxidization of secondary metabolites, as summarized in the reviews by Schaetzle et al. (2008) and Logan (2009). The different modes of electron transfer are through multiheme cytochromes (Myers and Myers, 1992), natural or artificial electron mediators or shuttles (Lovley et al., 1996; Marsili et al., 2008; Newman and Kolter, 2000; Von Canstein et al., 2008) or by nanowires (pili) produced by bacteria (Gorby et al., 2006; Reguera et al., 2005). Initially only a few bacteria such as *Geobacter* or *Shewenlla* were shown to be capable of direct electron transfer via nanowires. The number of reports on bacterial species having nanowires is increasing. For example, Eaktasang et al. (2016) reported *Desulfovibrio desulfuricans*, a predominant sulfate-reducing bacterium found in soils and sediments produced nanoscale bacterial

appendages which helped it to colonize the surface of insoluble or solid electron acceptors and facilitated direct electron transfer.

Many studies show that a mixed biofilm community was found to be advantageous over single species. A mixed biofilm community comprised of exoelectrogenic proteobacteria *Shewanella oneidensis*, *Geobacter sulfurreducens* and *Geobacter metallireducens* was capable of accelerated electron transfer through positive interactions between the isolates within the community (Prokhorova et al., 2017). Another study showed that mixed species biofilms could transfer electrical currents over a distance up to 1 mm suggesting the possibility of interspecies interactions (Li et al., 2016). Contradictory to this, a recent study showed that using artificial biofilms of pure cultures fed lactate provided constant power generation and a stable performance in an MFC (Kaiser et al., 2017). A better understanding of electrochemically active microbial communities, their metabolic pathways and interactions will help to expand MFC to wider applications.

1.4 MFC used in wastewater treatment

Wastewater is a rich source of diverse organics, therefore, an ideal substrate for MFC to release the chemical energy locked within and convert it to electrical energy, meanwhile reducing the pollutant content. Initial studies on MFC for wastewater studies focused on increasing power generation. Synthetic wastewaters were largely used in fundamental studies to elucidate the working principle and the mechanisms to improve energy recovery and organic removal efficiencies (Malandra et al. 2003). Recent studies have used actual wastewaters from various waste sources (agricultural, domestic, industrial, etc.) to demonstrate the potential application of MFCs (Janicek et al., 2014; Logan, 2008). These are required because actual wastewater composition is quite different from the synthetic wastewaters.

1.4.1 MFC treating industrial wastewater

Industrial wastewaters from wine and brewery, starch, molasses, chocolate, dairy, paper etc. have been successfully used as substrate for MFCs; a considerable COD removal efficiency accompanied with

electricity generation was achieved in previous attempts (Huang et al., 2011; Mathuriya, 2014; Penteado et al., 2016b). However, when compared to synthetic wastewaters the power production was comparatively low (Jadhav and Ghangrekar, 2009; Malandra et al., 2003; Venkata Mohan et al., 2010).

Wen et al. (2010) reported a steady COD removal efficiency of 92-96% (3.87-4.24 kg COD/(m^3·d)) using an external resistance of 100 Ω in a sequential anode-cathode MFC using raw brewery wastewater. Zhuang et al. (Zhuang et al., 2012) tested a tubular air-cathode MFC stack at two organic loading rates (ORLs) (1.2 and 4.9kg COD/m^3d), five non-Pt MFCs connected in series and parallel circuit modes treating swine wastewater. They observed the parallel stack achieved 83.8% of COD removal and 90.8% of NH_4^+-N removal at 1.2 kg COD/m^3d, and 77.1% COD removal and 80.7% NH_4^+-N removal at 4.9 kg COD/m^3d with continuous electricity production. A stacked MFC with 90 L capacity was reported to produce a power density of 1.1 W/m^3 treating brewery wastewater (Dong et al., 2015). A novel pilot scale stacked MFC with granular activated carbon packed bed electrodes achieved a power density of 51±2 W/m^3 and a COD removal efficiency of 97% within 48 h operated in fed batch mode (Wu et al., 2016). A maximum of 400±8 mW/m^2 (12 W/m^3) was produced using raw domestic wastewater in a stackable MFC reactor with 29 m^2/m^3 of cathode area (He et al., 2016). Ge and He (2016) developed a 200 L modularized MFC system consisting of 96 MFC modules which could remove more than 75% of the total COD and 90% of the suspended solids in 300 days operation using municipal wastewater. One study reported that COD removal in MFC was slightly slower (12 days) than an aerated system (10 days) but much faster than an unaerated lagoon (25 days) (Huggins et al., 2013). Significant biomass reduction in an MFC as compared to activated sludge treatment has also been reported (Asai et al., 2017; Gude, 2016; Huggins et al., 2013).

Due to the lower performance of MFC in terms of COD removal, a post treatment process or integrating MFC with conventional treatment technologies, such as anaerobic digestion, struvite precipitation, algae treatment, membrane filtration, etc. to promote the practical application of MFCs and improve the sustainability of wastewater treatment process was proposed (Li et al., 2014). Shin et al. (2016) reported developing an anaerobic fluidized membrane bioreactors (AFMBRs) which could achieve 89±3% removal

of the COD, with an effluent of 36±6 mg COD/L over 112 days operation using MFC treated domestic wastewater.

A few modelling studies proposed large scale MFC for wastewater treatment. Dannys et al. (2016) proposed a two chamber MFC process to treat 84 L/h of wastewater with an inlet COD of 3000 mg/L with an overall COD conversion of 91.9% and electricity generation is 26.4 kWh, 107% of the operational requirement.

Table 1-3 summaries some studies reported for the practical implementation of MFC in industry wastewater treatment. Single chamber MFCs are more widely attempted with a better performance compared to dual chamber MFCs. These studies revealed the potential of MFC as an alternative treatment method for industrial wastewaters meanwhile recovering energy.

Table 1-3 MFC tested for different industrial wastewater

Wastewater substrates	Design	Power/current density	Reference
Food industrial wastewater (rice/starch/meat/etc.)	SCMFC*	0.9-1.15 A/m^2	Heilmann and Logan, 2006; Lu et al., 2009
		0.1-2 W/m^2	Hamamoto et al., 2016; Yamashita et al., 2016
	DCMFC**	0.08 A/m^2	Liu et al., 2009
Food waste	SCMFC	100-200 W/m3	Goud et al., 2011; Gude, 2016
	DCMFC	0.015-0.5 A/m^2	X. Li et al., 2013; Nimje et al., 2012; Oh and Logan, 2005
Paper industry	SCMFC	0.125-2.5 A/m^2	Chen et al., 2019; Huang and Logan, 2008; Huggins et al., 2013; Velasquez-Orta et al., 2011
Petroleum Industry (oil sands/oil refinery/etc.)	SCMFC	0.08-3.87 W/m^2	Choi and Liu, 2014; Yang et al., 2016
	DCMFC	0.045-334 W/m^3	Addi et al., 2018; Guo et al., 2016; Srikanth et al., 2016
Brewery/distillery wastewater	SCMFC	0.25-100 A/m^2	Feng et al., 2008; Mohanakrishna et al., 2012; Velasquez-Orta et al., 2011; Wen et al., 2009
Agricultural/diary wastewater (cheese/diary/farm)	SCMFC	0.015-7 A/m^2	Ichihashi and Hirooka, 2012; Min et al., 2005; Nimje et al., 2012; Scott and Murano, 2007; Velasquez-Orta et al., 2011
		5.7 W/m^3	Ayyaru and Dharmalingam, 2011
	DCMFC	42 mA/m^2	Stamatelatou et al., 2010
		27 W/m^3	Cecconet et al., 2018
Municipal/domestic/urban wastewater	SCMFC	1.7-51 W/m^3	Liu et al., 2004; Liu and Logan, 2004; Wang et al., 2009
		0.05-0.1 W/m^2	Liu et al., 2011
	DCMFC	0.018 mA/cm^2	Rodrigo et al., 2010
Landfill leachate	SCMFC	0.34-20.9 W/m^3	Puig et al., 2011; Vázquez-Larios et al., 2014
	DCMFC	0.0004 mA/cm^2	Greenman et al., 2009
Medical wastewater	SCMFC	177.36 W/m^3	Velvizhi and Venkata Mohan, 2011
	DCMFC	3-15 W/m^3	Aelterman et al., 2006; Rabaey and Verstraete, 2005

*SCMFC – single chamber MFC ** DCMFC– dual chamber MFC

1.4.2 MFC treating winery wastewater

Due to the rich composition in sugars, vitamins, minerals, and redox-active mediators winery wastewater can be a promising feedstock for MFC technology (Vidyalakshmi et al., 2009). However, only a few reports are available on the application of MFC to the winery industry. Research shows several challenges for MFC application in winery wastewater such as unbalanced nutrient composition, the presence of recalcitrant organics, the presence of alternate electron acceptors like sulphate, acidic pH, etc. for MFC application in winery wastewater treatment (Jo et al., 2015; Li et al., 2014; Pepe Sciarria et al., 2015). A summary of the studies of MFC treating winery wastewater is shown in Table 1-4.

Table 1-4 Literature review of MFC treating winery wastewater

WW Source	Design/ Flow Regime*	Anode Chamber (mL)	Inlet COD (mg/L)	HRT (h)	pH	COD depletion (mg/L/D)	COD removal (%)	Max. power density (mW/m2)	Study Duration	Source
WWW	AC	28	2200	144	7.2	238.3	65	278	18 days	Cusick et al. 2010
WWW (MEC)	AC/C	910x10^3	1000-2000	24	6.4	-	62±20	-	40 days	Cusick et al. 2011
Bad wine	DC	125	7800	144	6.4–7.0	1534 1300 1066	59 50 41	- 3820	6 days	Rengasamy and Berchmans, 2012
WWW	DC/B	70	6850	84	6.5	1000	17	465	41 days	Penteado et al., 2016b
White wine lees	AC/B	28	6400	NG**	7.0±0.2	-	90	263	31-33 days	Sciarria et al, 2015
Red wine lees	AC/B	28	10100	NG**	7.0±0.2	-	27	111	31-33 days	Sciarria et al, 2015
WWW	DC/B	70	6850	28.8	6.5	600	10	3250	92 days	Penteado et al., 2016a
WWW	DC/SB	4	6850	52.8	6.5	650	11	890	>5 weeks	Penteado et al., 2017
WWW	DC/SB	4	6850	52.8	6.5	480	7	-	>5 weeks	Penteado et al., 2017
WWW	DC/SB	4	6850	52.8	6.5	270	4	-	>5 weeks	Penteado et al., 2017
WWW	DC/SB	4	6850	1.92	6.5	597	8.5	90	5 weeks	Penteado et al., 2018
WWW	DC/SB	20	6850	9.6	6.5	1076	15.6	730	5 weeks	Penteado et al., 2018

*WWW-Winery wastewater, DC-dual chamber, AC-air cathode, B-batch, C-continuous, SC-semicontinuous

** the information in the article was not sufficient to provide an HRT.

As shown above, it was also observed that a neutral pH (6.4-7.2) was chosen for all the studies. The HRT varied from as low as 1.9 h to 144 h (6 days) in the studies. None of the studies was directed specifically at examining an optimal HRT with regard to COD removal and so interpreting the data is difficult. The pilot scale test by Cusick et al. (2011) achieved a very high COD removal (90%) in a low retention time (24 h). Most studies were lab scale reactors (4-125 mL) except for the Cusick et al. (2011) study which was an MEC not MFC. The inlet COD varied from 1000 to 10100 mg/L and the studies averaged 33% COD

removal efficiency, which is much lower compared to existing treatment technology such as activated sludge. The highest COD removal efficiency for lab scale studies was reported as 90% for winery wastewater starting with 6400 mg/L COD and achieving 90% removal, this leaves 640 mg/L COD which could still require some polishing treatment before discharge, depending on the method for discharge (Pepe Sciarria et al., 2015). The studies from Penteado's group (Penteado et al., 2016a, 2016b, 2017, 2018) were not designed to maximize COD removal and so a low bias is introduced by this body of work.

Studies addressed some inherent important issues with winery wastewater treatment with MFC. Penteado et al. (2016) reported that nutrient imbalance i.e. low nitrogen and phosphorus ratio compared to high COD was a limiting factor in power generation and COD removal in their study with winery wastewater feed. They found that increasing the concentration of phosphorus and nitrogen in the feed solution increased Coulombic efficiency from 2% to almost 15% with a maximum power density from 105 to 465 mW/m^2. Attempts were made to improve MFC performance. Penteado et al. (2016) reported that decreasing sludge retention time (SRT) increased electricity generation with an increase in coulombic efficiency from 3.4% to almost 42.2% and maximum power density from 58 to 890 mW/m^2. However, no significant improvement in COD removal was observed in this study by altering SRT. Comparison of three commonly used electrode materials: carbon felt, carbon cloth and carbon paper (both anode and cathode) in MFC for winery waste water treatment showed a difference in performance (Penteado et al., 2017). It was observed that MFC equipped with carbon felt produced the highest voltage and power (72 mV and 420 mW/m^2, respectively), with lowest values with carbon paper (0.2 mV and $8.37x10^{-6}$ mW/m^2, respectively). A similar observation was also made in terms of COD removal highest average organic matter consumption rate (650 mgCOD/L/d) and 270 mgCOD/L/d using carbon felt and carbon paper, respectively.

1.5 Research needed to advance MFC use to treat winery wastewater

MFC technology can be considered promising for wastewater treatment and energy recovery; however, there are still some obstacles that must be overcome. The above studies revealed the potential of MFC for

winery wastewater treatment applications; however, the targets of these studies were power production, not COD removal, leaving significant work required to allow scaling an MFC to an actual treatment process. Overcoming the practical issues of deploying MFC to treat winery wastewater demands more attention, especially on the impact and further understanding of operational parameters including pH, seasonality, treatment efficiency, and optimization strategy. A mathematical model specifically developed to predict/simulate the application of MFC to wastewater treatment will be useful for others as it will allow them to predict power and efficiency based on feed components, which has not been reported.

1.6 Thesis objectives

The present research was developed to investigate the use of MFC to treat winery wastewater to optimize the treatment and energy recovery efficiency. The specific objectives of this study were as follows:

- Design and fabricate an MFC reactor for the treatment of winery wastewater.
- Investigate the pH and buffer impact on MFC fed winery wastewater
- Investigate the impact of seasonal changes of the winery wastewater as feed stock on the efficiency of MFC reactors
- Investigate the impact of external and internal resistance on MFC treating winery wastewater
- Develop a numerical model to simulate the operational parameters of MFC treating winery wastewater

After this introduction and literature review, Chapter 2 provides the methodology of design and fabrication, operation of MFC reactors, and analytical methods used. Chapters 3 to 6 present the detailed methods and results addressing the research objectives. Chapter 7 presents the final conclusions.

Chapter 2. Methodology

This chapter presents the design, fabrication and operation of an air cathode MFC reactor. It also describes the analytical methods used to characterize influent winery wastewater and treated effluent water as well as the collection of electrochemical data from the MFC treatment systems. The calculations and statistics used to analyze collected data and compare different test conditions are also included.

2.1 MFC design and fabrication

A tubular shape single chamber air cathode MFC similar to the one proposed by Liu and Logan (2004) but with 100 mL working volume, was designed and constructed for the tests reported in this thesis. The larger volume provided more sample for analysis, but also required a longer HRT. The MFC design is shown in Figure 2-1, each component is explained below.

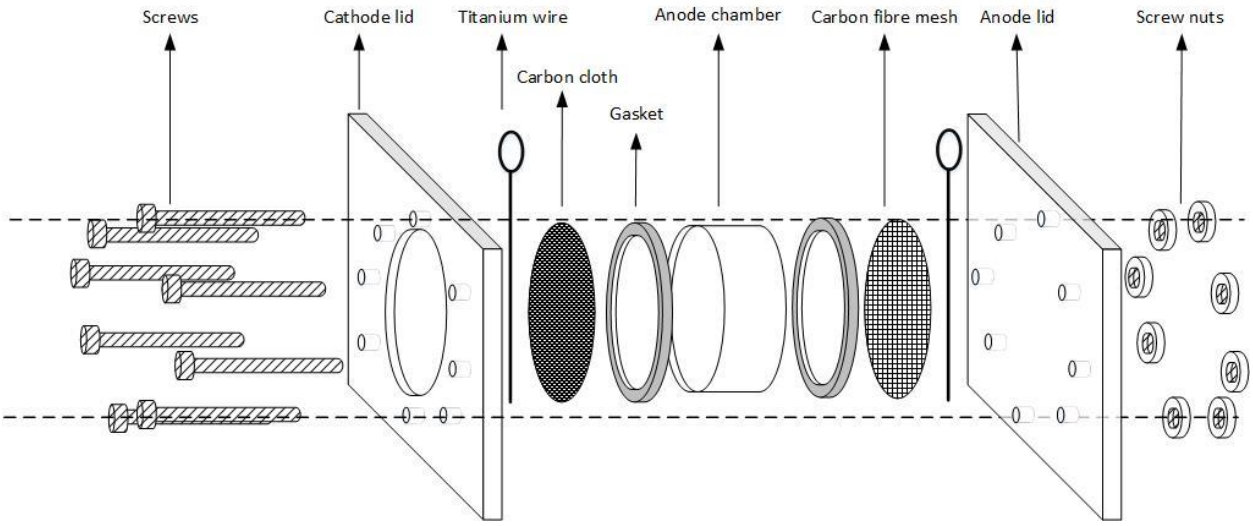

Figure 2-1 The design of an air cathode MFC with 100mL working volume

2.1.1 Electrode lids and chamber

The chamber and endcaps of the lab-scale MFC reactor need to be strong enough to hold the liquid and prevent leakage, and transparent enough to allow observation of bacterial growth. The anode and cathode endcaps were cut from a 5 mm-thick polycarbonate sheet. Both endcaps were 108.0 mm × 108.0 mm with eight ports (Ø 6.1 mm) four corners and four sides for assembly. A Ø 76.2 mm circular port was drilled in the centre of the cathode cap to allow air to reach the cathode. The anode chamber was an 18 mm-long acrylic tube with 76.2 mm internal diameter (ID) and 82.6 mm outer diameter (OD) cut off by an electric table saw, both ends were polished using sand paper to get a smooth finish. Two 3.0 mm sampling ports were drilled in the top of the anode chamber for sampling and gas collection. Both polycarbonate sheets and acrylic tubes were purchased from Industrial Plastics & Paints (Kelowna, BC, Canada). Silicon gaskets (ID 76.2 mm, OD 82.6 mm, thickness 2 mm) were used at each end of the anode chamber to allow a leakage-proof seal. All the pieces were finished in the machine shop of the School of Engineering, UBC Okanagan (Kelowna, BC, Canada).

2.1.2 Electrodes

A challenge for the selection of materials for MFC construction is to identify low cost, highly efficient materials. Various types of electrode materials have been discussed in Chapter 1. Internal resistance is an essential factor that must be considered during selection as high internal resistance would cause potential loss and decrease the energy recovery efficiency. The internal resistance is usually contributed by electrode materials, PEM, coating material, and assembly technology.

2.1.2.1 Anode

Anode materials must be highly conductive and non-corrosive, have a high specific surface area with a high porosity, and be cost effective (Logan et al., 2006). Carbonaceous electrodes (carbon cloth, carbon mesh, graphite brush, graphite granules) and metal electrodes (stainless steel mesh, titanium mesh/brush,

aluminum-alloy mesh, etc.) are commonly used. Carbonaceous electrodes show good biocompatibility, chemical stability and conductivity, and are less expensive for potential industrial application (Wei et al., 2011). In this study a 3k carbon fiber mesh with high specific surface area (Industrial Plastics & Paints, Kelowna, BC, Canada) was used as the anode material. The carbon fiber mesh was trimmed to a round piece (Ø 79 mm) using a sharp utility knife to fit the anode chamber. Fine fiber pieces were removed with special attention to prevent leakage while fabricating. The projected surface area of anode was measured as 45.60 cm^2.

2.1.2.2 Air Cathode with PEM and catalyst

The cathode is the most challenging component to fabricate in an air cathode MFC as it is the place where the triple-phase reaction (water, solid catalyst, air) occurs (Logan et al., 2006; Zhang et al., 2011b). The selection of cathode material is similar to anode as they follow similar principles (highly conductive, non-corrosive, low cost), the difference is that a catalyst (usually Pt) is usually applied onto the cathode to increase reaction efficiency. A PEM isolates the catalyst from the cathode, improves coulombic efficiency by preventing fuel crossover and oxygen diffusion from cathode to anode (Liu and Logan, 2004). Nafion, as the PEM as well as the binder, has shown promising results as described in Section 1.3.2.2.

In this research the air cathode design is given in Figure 1-2. The base material is a piece of carbon cloth pre-coated with Nafion and 20% Pt on Vulcan carbon, and additional 410-µm-thick PTFE layer (Fuel cell Store, Collage station, TX, USA). The cathode was fabricated similarly to that of Cheng et al. (2006) and Middaugh (2006) but with additional modifications. Briefly, the non-catalyst side of carbon cloth was coated with carbon suspension (by mixing 12 µL of 40% PTFE (in water) and 1.56 mg of carbon black per cm^2 of cathode) using small painting brush, then air dried for 2 h and heated at 370 °C for 20 min. The diffusion layer was applied by adding a layer of 60% PTFE in a uniform fashion onto the same side, heated at 370 °C for 15 min. After cooling down to room temperature, the PTFE coating step was repeated three more times to obtain 4 layers. At last the carbon cloth was trimmed to a round piece (Ø 79 mm), a 20 mm

(L) × 5 mm (W) tail on the edge was left for better circuit connection. The projected surface area of cathode was measured as 45.60 cm^2, same as the anode.

2.1.3 MFC assembly and monitoring

Each component was carefully organized as shown in Figure 2-1, rubber gaskets (ID 74.0 mm, OD 82.6 mm) were placed at both ends of the anode chamber tube to ensure better sealing. A piece of 5 cm-long titanium wire (Titanium ≥99.98% metals basis, Ø 0.5 mm, from VWR Canada) was paired to each electrode with a tail left outside to ensure proper connection to the external circuit. All pieces were assembled together using 2-inch screws (Home Depot, Kelowna, BC, Canada) to finalize the MFC setup. All reactors were filled with water and left for 72 h to make sure there was no sign of leakage.

The anode was connected to the cathode externally through a resistor to complete the circuit. The real-time voltage on the external load was monitored using NI USB 6210 Multifunction I/O device and recorded by NI SignalExpress 2015 every 2 min. Assembly stages and the monitoring station are shown in Figure 2-2.

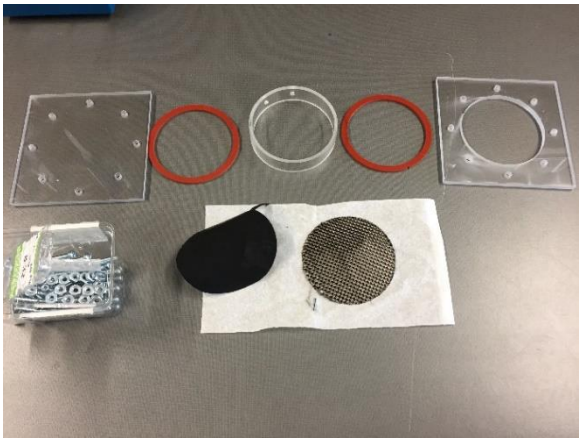

a)

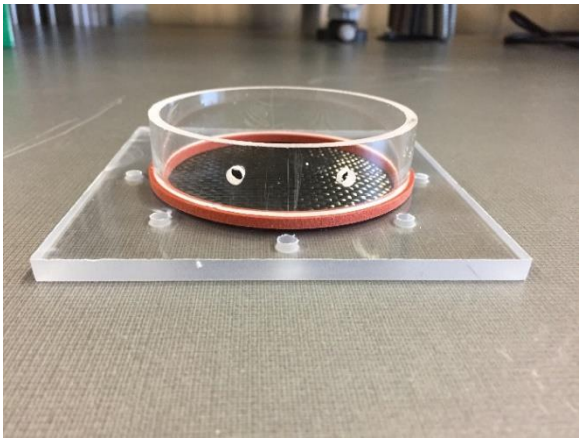

b)

c1)

c2)

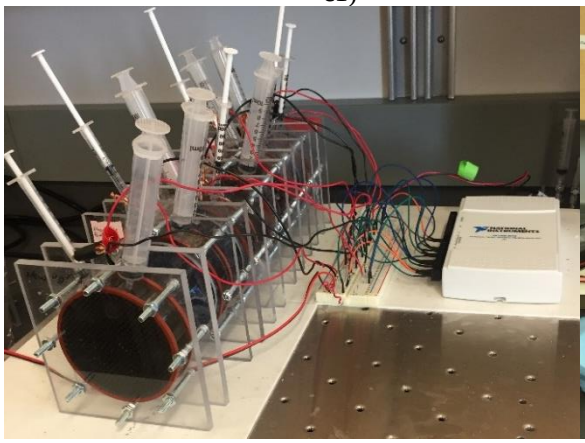

d1)

d2)

Figure 2-2 Air cathode MFCs assembly and their monitoring station
a) Components needed for the fabrication of an MFC reactor; b) MFC assembly process (top to bottom: anode chamber, gasket, carbon fibre mesh, anode endcap); c1) and c2) Final assembly of MFC reactors; d1) and d2) The MFC monitoring station showing the reactors, NI-USB6210 I/O multifunction device and computer

2.2 MFC Operation

In this study the air cathode MFC reactors were operated in batch mode and fed with synthetic winery wastewater (SWW) medium. Medium was changed by replacing 80% of the volume with fresh feed based on either voltage drop or COD consumption. Samples were taken for measurements from the MFCs daily and immediately before/after each feed. Voltage on external load was continuously monitored as described in Section 2.1.3.

2.2.1 Feed preparation

2.2.1.1 Winery wastewater collection and characterization

The winery wastewater was collected from our industrial partner Tantalus Vineyards (Kelowna, BC, Canada) March 2017, June 2017 and September 2017. The wastewater was characterized immediately after collection; the rest was kept in 4-liter jugs and stored at 4 °C for future use. Characterization included pH, conductivity, total chemical oxygen demand (TCOD), soluble chemical oxygen demand (SCOD), total suspended solids (TSS), volatile suspended solids (VSS), polyphenols, volatile fatty acids (VFA), protein, total nitrogen (N) and phosphorus (P) (methods described in analytical method Section 2.3); the results are presented in Table 2-1.

Table 2-1 Characterization results of winery wastewater collected from Tantalus Vineyards

Parameters	March 2017	June 2017	September 2017
pH	4.1-4.3	5.1-5.4	3.9-4.3
Conductivity (µS/cm)	840±30	690±90	1070±120
TCOD (mg/L)	7150±370	3140±430	11000±2580
SCOD (mg/L)	2230±180	1010±230	6720±490
TSS (mg/L)	3710±410	2760±540	6300±2500
VSS (mg/L)	3700±410	1350±370	5800±2100
Polyphenols (mg/L)	22.4±3.7	14.7±2.9	79.6±17.0
VFA (mg/L)	420±84	35±7	1170±360
Protein (mg/L)	BDL	BDL	BDL
Total N (mg/L)	BDL	BDL	BDL
Total P (mg/L)	BDL	BDL	BDL

2.2.1.2 Synthetic winery wastewater medium preparation

Wine production is seasonal, starting in September and finishing in March; therefore, the availability of winery wastewater is highly restricted. To overcome this a simulated wastewater was developed based on a literature survey and our characterization data. A ten times concentrated synthetic winery wastewater (10x SWW) medium with the addition of a group of trace metals (Cang et al., 2004) was prepared using white wine containing 9% (v/v) ethanol and 67 g/L sugar (Moscato, Barefoot Wine and Bubbly, Modesto, CA, USA). The 10x SWW medium contained 41.91 mL of wine (COD: 238000 mg/L as measured) per liter, 755.2 mg/L of NH_4Cl, 173.6 mg/L of KH_2PO_4. (CNP ratio 250:5:1), 10 mL/L mineral solution (contained 50 g/L $(NH_4)_6Mo_7O_{24}{\cdot}4H_2O$, 0.05 g/L $ZnCl_2$, 0.3 g/L H_3BO_3, 1.5 g/L $FeCl_2{\cdot}4H_2O$, 10 g/L $CoCl_2{\cdot}6H_2O$, 0.03 g/L $MnCl_2{\cdot}6H_2O$, and 0.03 g/L $NiCl_2{\cdot}6H_2O$).

Two types of buffer were prepared for this study, phosphate buffer (PB) and bicarbonate buffer (BB). One liter (L) of 0.1 M PB was prepared by adding 20.209 grams (g) of sodium phosphate dibasic (Na_2HPO_4) and 3.394 g of sodium phosphate monobasic (NaH_2PO_4) to 900 mL of RO water, adjusting pH to 7.4 (using HCl or NaOH) and diluting to 1 L. One liter of 0.1 M bicarbonate buffer was prepared by adding 8.401 g sodium bicarbonate ($NaHCO_3$) to 900 mL of RO water, adjusting pH to 6.5 (using HCl) and diluting to 1 L. Sodium chloride (NaCl) solution (1 M) was prepared by dissolving 58.440 g into 1 L of RO.

The feed medium was prepared by mixing the solutions described above in different ratios depending on the experiment. For example, 100 mL of medium (COD 1000 mg/L, PB 10 mM, NaCl 100 mM, pH 6.5) was prepared by mixing the solutions listed in Table 2-2, then titrating pH to 6.5 using HCl or NaOH, and adjusting the volume to 100 mL. After preparation the medium was sparged with nitrogen gas for 10 min before feeding to reactors to minimize dissolved oxygen.

Table 2-2 Recipe of 100 mL of SWW medium (COD 1000 mg/L, PB 10 mM, NaCl 100 mM, pH 6.5)

Solution needed	Volume
10x concentrated SWW	10 mL
0.1 M PB solution	10 mL
1 M NaCl solution	10 mL
RO water	60 mL

2.2.2 MFC inoculation and start-up

The 100 mL MFCs were inoculated with 5 mL of anaerobic sludge (VSS = 3700 mg/L) collected from the anaerobic chamber of the wastewater treatment plant in Tantalus Vineyards. The start-up medium was prepared by mixing 10 mL of 10x SWW and 10 mL of 1 M NaCl solution and diluting to 100 mL with RO water to reach a final COD of 1000 mg/L. The pH was adjusted to the desired pH with HCl or NaOH. Phosphate or bicarbonate buffer was or was not added depending on the experimental objectives. The medium was deaerated by sparging with nitrogen gas for 10 min prior to feed.

2.2.3 External resistance

Many studies with pure cultures and simple substrates such as acetate or glucose found higher COD removal with low external resistances, for example Liu et al. (2016) and many researchers use external resistance in the range 0.5 to 1 KΩ (Jung and Regan, 2011; Lyon et al., 2010; Tursun et al., 2016). Other studies (Katuri et al., 2011) found no significant difference in peak power when the external resistance was between 0.1 to 50 KΩ in a mixed culture MFC fed municipal wastewater and del Campo et al., (2016) reported that an increase in external resistance resulted in better COD removal especially with a mixed microbial population. Based on these studies a 10 KΩ was chosen as the external resistance for this study unless otherwise specified.

2.3 Analytical methods

The performance of the MFCs was evaluated with regard to wastewater treatment efficiency and power production efficiency. Wastewater treatment efficiency was assessed by analyzing water samples from the anode chamber regularly and power production efficiency was evaluated by periodic electrochemical analysis. The analytical methods are detailed as follows:

2.3.1 Chemical parameters

2.3.1.1 pH and Conductivity

The pH and conductivity of MFCs were measured using Thermo Scientific Orion 1119000 5-Star Benchtop multiparameter meter. Probes used were Cole-Parmer Accumet pH Probe and Orion 013605MD Conductivity Probe (Thermo Fisher Scientific, Collage Station, TX, USA). The pH probe was calibrated using standardized buffer solutions weekly to ensure accuracy.

2.3.1.2 COD

COD was measured using Standard Methods (Eaton et al. 2005) to determine the quantity of oxygen consumed by impurities in water based on dichromate solution reduction under specified conditions. The procedure is described below:

- Preparation of reagents:

The silver sulfate catalyst solution was prepared by dissolving 22 g of silver sulfate (Ag_2SO_4) into 2.5 L concentrated sulfuric acid (H_2SO_4) (sp gr 1.84). Potassium dichromate digestion solution was prepared by adding 10.216 g of oven dried potassium dichromate ($K_2Cr_2O_7$), 167 mL of concentrated sulfuric acid (H_2SO_4) and 33.3 g of mercuric sulfate ($HgSO_4$) to ~750 mL of water, mixed, let cool, and adjusted to 1 L.

- Preparation and measurement of COD

Digestion solution (1.5 mL) and silver sulfate catalyst solution (3.5 mL) were placed into a clean COD tube with bottle top dispenser (Fisherbrand™), followed by the addition of wastewater sample/standards/blank (2.5 mL) down the side of the tube so that a layer is formed on top of the reagents. The tube was sealed and mixed thoroughly by shaking vigorously or using a Vortex mixer (Fisherbrand™, NH, US), then incubated at 150±2 °C for 2 h using a Block heater (AccuBlock™ Digital Dry Baths, by Labnet Internationa Inc.). After cooling to room temperature, the absorbance of the COD solution was measured at 600 nm using

SPECTRONIC 20D+ Digital Spectrophotometer (Thermo Fisher Scientific, TX, USA). The measurement range of this method is 25 mg/L to 800 mg/L.

- Calibration:

Standard potassium acid phthalate solution (1 mL = 1 mg COD, 1000 ppm COD) (Ricca Chemical™) was purchased from Fisher Scientific. COD standards (50, 100, 200, 400, 600, and 800 mg/L) were prepared by diluting the commercial standard solution in water. A COD standard calibration curve was plotted using absorbance vs COD (mg/L), as shown in Figure 2-3. The trendline equation was used to calculate the COD of unknown samples. COD standard calibration curve was run for each new batch of COD tubes prepared to ensure the accuracy.

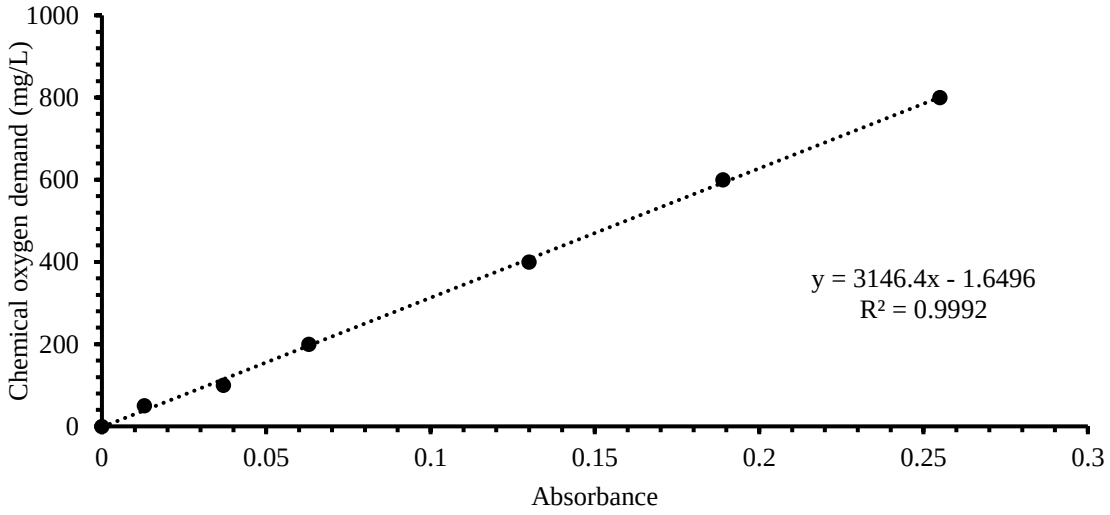

Figure 2-3 Typical COD calibration curve for spectrophotometric COD method

2.3.1.3 Total N and total P

Total N and total P were simultaneously determined using Dionex™ ICS-3000 Ion Chromatography System (Thermo Scientific, Sunnyvale, CA, USA) after alkaline persulfate digestion (De Borba et al., 2014). The alkaline persulfate reagent (0.15 M $K_2S_2O_8$ in 0.15 M NaOH) was prepared by adding 10 mL of 1.5 M NaOH to approximately 80 g of RO water, followed by dissolving 4 g of potassium persulfate in

a 100 mL volumetric flask. The solution was sonicated for 10 min to completely dissolve the solid material and then diluted to 100 mL with RO water. The alkaline persulfate solution was prepared daily and stored at 4 °C when not in use.

The alkaline persulfate digest was performed by adding 2 mL of alkaline persulfate digestion to 4 mL of sample in a glass digestion tube. The digestion tube was capped and then placed in a heating block set at 120 °C for 60 min. After the digestion was complete, the tube was allowed to cool to room temperature. The cooled solution was diluted by a minimum of 1:10 (total dilution 1:15), filtered, then injected into the Ion Chromatography (IC) for NO_3^- and PO_4^{3-}. The detection limit for NO_3^- and PO_4^{3-} was 1 mg/L in the IC sample. The IC procedure is discussed in the following section.

2.3.1.4 Volatile fatty acids (VFA), NO_3^- and PO_4^{3-} measurement by Ion Chromatography

The presence of VFA was measured using the Dionex ICS-3000 system. The Dionex ICS-3000 system integrates an ion chromatograph with an electrolytic eluent generator, dual pump with vacuum degas, a six-port injection valve fitted with a 10 µL injection loop, a heated conductivity cell, and a column heater set at 35 °C. A Thermo Scientific Dionex™ AS-AP Autosampler was used for sample processing. A Thermo Scientific Dionex™ IonPac™ AG11HC Guard Column (50 × 4 mm) and Dionex™ IonPac™ AS11HC Analytical Column (250 × 4 mm) were used for all analytical separations. The flow rate of the dual pump was set as 1 mL/min. The KOH eluent was electrolytically generated with the Thermo Scientific Dionex™ EGC III RFIT™ KOH Eluent Generator Cartridge to produce the following conditions: 1-15 mM KOH from 0 to 13 min, 15-60 mM from 13 to 20 min, 60 mM from 20 to 22 min, 60-1 mM from 22 to 23 min, and 1 mM from 23 to 25 min. VFA, Total N (as NO_3^-) and total P (as PO_4^{3-}) samples were detected by suppressed conductivity with a Thermo Scientific Dionex™ AERS™ 500 Anion Electrolytically Regenerated Suppressor (4 mm) operating at 223 mA current in the recycle mode. Thermo Scientific Dionex™ Chromeleon™ Chromatography Data System (software version 7.1.1) was used for system

control and data processing. The IC response (signal peak area) for each analyte was converted to concentration using a standard curve for each analyte.

The samples for IC measurement were filtered through clean 0.45 µm syringe filters immediately after collection to remove solids and prevent change of ionic concentrations over time caused by microorganisms. Samples were refrigerated at 4 °C if not analyzed immediately.

2.3.1.5 Total suspended solids (TSS) and Volatile suspended solids (VSS)

TSS and VSS was measured using Standard Methods (Eaton et al., 2005). Briefly, 50 mL of a well mixed wastewater sample was filtered through a pre-weighed glass fibre filter (diameter 47 mm, pore size 0.45 µm). The filter was dried at 105 °C to a constant weight (24 h). The new mass of the filter and sample was measured, TSS was determined by subtraction of the initial weight. The dried filter after TSS was measured was ignited at 550 °C for 1 h, the weight loss of the filter was recorded as VSS.

2.3.2 Electrochemical parameters

2.3.2.1 Polarization curve

A polarization curve analysis is a common technique used to characterize the current density as a function of voltage by changing the external resistance. Usually polarization is plotted by using current density I_d (mA/m^2) as X and MFC output voltage (V) as Y.

I_d is calculated by normalizing current by electrode surface area (usually the anode).

$$I_d = \frac{I}{S_A} \qquad \text{eq. 2-1}$$

where I_d is current density, I is the current and S_A is the surface area of anode.

In this study the polarization curve was determined by varying the external resistance and measuring voltage after the system reached a steady state or 30 min after changing the external resistance, whichever came first.

2.3.2.2 Power density curve

A power density (P_d) curve is plotted using current density as X and power density (normalizing P by electrode surface area or effective chamber volume) as Y. Power density curve was used to estimate maximum power output. Power (P) can be calculated by either.

$$P = VI \qquad \text{eq. 2-2}$$

or

$$P = \frac{V^2}{R_{Ext}} \qquad \text{eq. 2-3}$$

where V is output voltage, R_{Ext} is the external resistance.

Power density (P_d) and current density (I_d) were calculated by dividing the power and current by the surface area (m^2) of the anode.

P_d is calculated by

$$P_d = \frac{P}{S} \qquad \text{eq. 2-4}$$

$$I_d = \frac{I}{S} \qquad \text{eq. 2-5}$$

where S is the surface are of anode or cathode.

Figure 2-4 shows an example of a polarization curve and a power density curve of a reactor 200 days after inoculation. As shown in the graph, the maximum output power density value (52.1 mW/m^2) and current density (0.295 mA/m^2) were measured. A more detailed discussion regarding the analysis is given in Chapter 5.

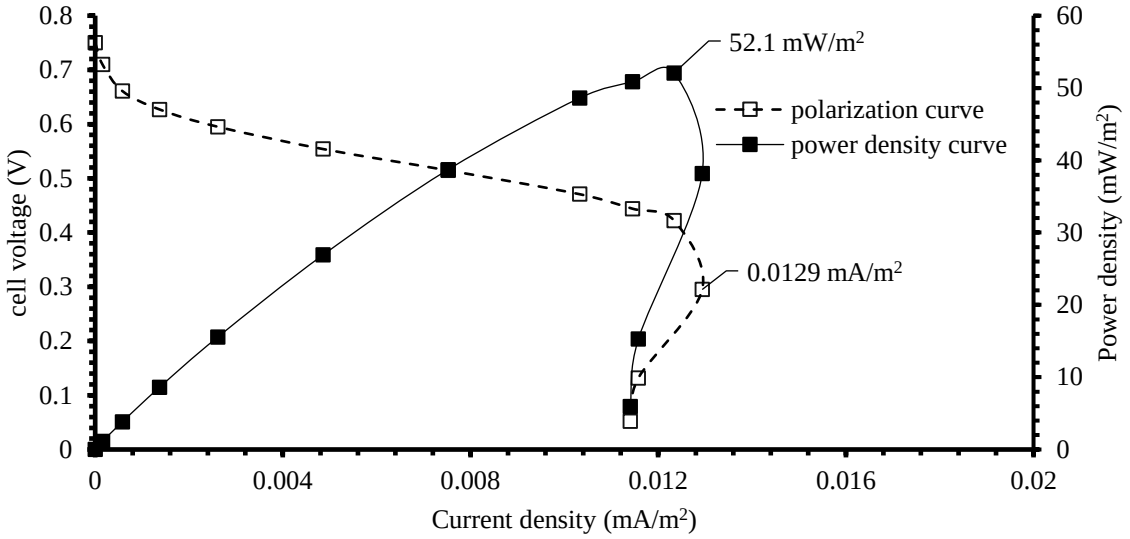

Figure 2-4 Polarization and power density curve of a reactor 200 days after inoculation

2.3.2.3 Internal resistance (R_{Int}).

Internal resistance was evaluated using polarization slope method. A plot of circuit current (I) vs output voltage (V) is developed and the slope of interested range of the polarization curve is the internal resistance. An example of the estimation is given in Figure 2-5, the polarization curve presents the correlation between cell current and the output voltage of an MFC reactor after 200 days of operation. There are three types of losses occurring in the system, activation loss, ohmic loss and mass transport loss. The internal resistance is the slope of the dashed line, which reveals the linear trend of ohmic loss of the reactor. In this case the R_{Int} is estimated as 377Ω.

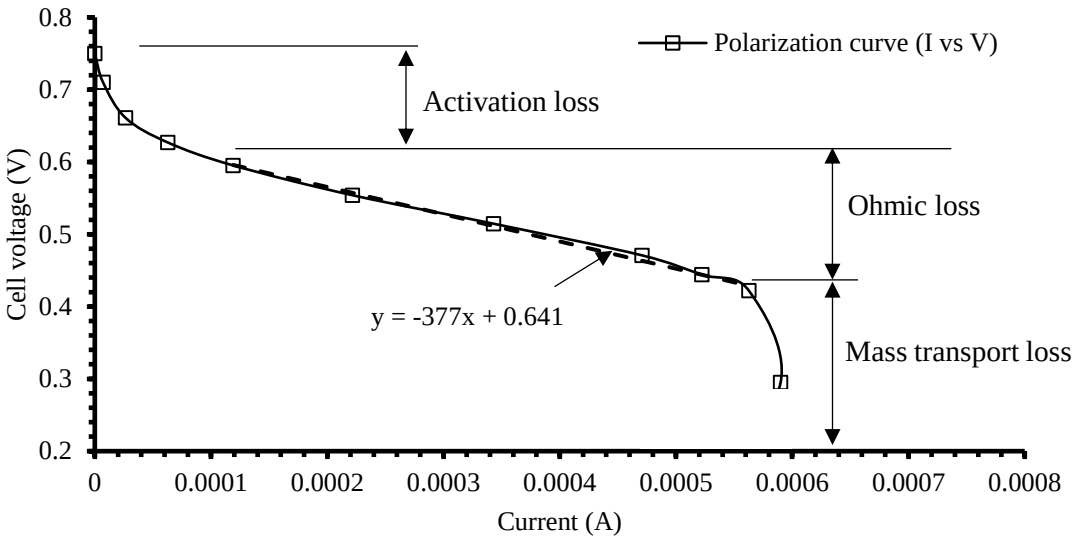

Figure 2-5 Polarization curve and the internal resistance of a reactor 200 days after inoculation

As discussed in Section 1.3.3.3, the potential maximum power output of an MFC (or any power source) is obtained when R_{Ext} equals to R_{Int} of the power source. This is also known as the maximum power transfer theorem (Jacobi's law), it could be mathematically demonstrated as follows:

Consider the MFC is in a DC circuit, based on Ohm's law,

$$I = \frac{V}{R_{Int} + R_{Ext}} \qquad \text{eq. 2-6}$$

Power (P) is:

$$P = I^2 R_{Ext} = \frac{V^2}{(R_{Int} + R_{Ext})^2} \cdot R_{ext} = \frac{V^2}{\frac{R_{Int}^2}{R_{Ext}} + 2R_{Int} + R_{Ext}} \qquad \text{eq. 2-7}$$

As shown in eq. 2.7, the denominator should be minimum to obtain maximum power, the 1st derivative of denominator with respect to R_{Ext} therefore should be 0. Differentiation of the denominator with respect to R_{Ext},

$$\frac{d\left(\frac{R_{Int}^2}{R_{Ext}} + 2R_{Int} + R_{Ext}\right)}{dR_{Ext}} = -\frac{R_{Int}^2}{R_{Ext}^2} + 1 = 0 \qquad \text{eq. 2-8}$$

Therefore, the maximum power will be obtained when R_{Ext} =R_{Int}.

This theory is used to calculate the maximum power transfer across the circuit but not the maximum efficiency. Higher output efficiency can be reached when R_{Ext} is higher than the R_{Int} of the source, as a higher percentage of the source power is utilized by the external load instead of lost inside the source, but the magnitude of the load power is lower since the total circuit resistance (R_{Ext}+R_{Int}) increased.

2.3.2.4 Columbic and energy efficiency

Columbic efficiency (C_E) is defined to express the total electron recovery from the organic matter in wastewater (Logan, 2008). The columbic efficiency is calculated based on the ratio of electrons used as the current flow to the total amount of electrons in substrate,

$$C_E = \frac{Coulombs\ recovered}{Total\ coulombs\ in\ substrate} \qquad \text{eq. 2-9}$$

When considering COD removal in wastewater, for a continuous system C_E can be expressed as

$$C_E = \frac{8I}{Fq\Delta COD} \qquad \text{eq. 2-10}$$

where 8 is a constant based on the molecular weight of O_2 (32) and the number of electrons exchanged per mole of O_2 (4), F is Faraday's constant, q is the flowrate of the reactor as a continuous system, and ΔCOD is the change of COD before and after treatment.

For a batch system, C_E is calculated as

$$C_E = \frac{8\int_0^{t_b} Idt}{Fv_A\Delta COD} \qquad \text{eq. 2-11}$$

where v_A is the effective volume of anode chamber.

The energy efficiency of MFC, η_{MFC}, is the energy recovered in the system compared to the total energy in the substrate.

$$\eta_{MFC} = \frac{\int_0^t V\, Idt}{\Delta H n_{sub}} \qquad \text{eq. 2-12}$$

where V is the output voltage of MFC, ΔH is the combustion heat, n_{sub} is the number of moles of substrate added.

2.3.3 Microbial analysis

Samples from MFCs were subjected to routine microscopy analysis under bright field (40x and 100x objectives) using Zeiss Fluorescent microscope. Biofilm samples taken of the biosolids on the surface of electrodes in an active reactor were analyzed by Tescan Mira 3 XMU Scanning Electron Microscope (SEM) (Brno, Czech Republic). Sample (1 mL) was fixed with 1.25% glutaraldehyde made in phosphate buffer (pH 7.4) for 2 h, then dehydrated in ethanol series (30, 50, 100%) for 20 min each. Bacterial samples were deposited on the SEM tray and platinum coated to improve conduction. The SEM acceleration voltage was adjusted to 20 kV for most of the cases, and the working distance was 14 mm.

2.4 Measures to assure confidence in results

A variety of measures was carried out to assure the confidence of the results.

2.4.1 Replication of reactors

A total of 7 identical single chamber air cathode MFC reactors (100 mL) as described in Chapter 2.1 were carefully fabricated. The internal resistance of each blank reactor (filled with SWW medium prior to inoculation) was measured as 1.2±0.2 KΩ using a multimeter, suggesting consistent fabrication technique. A pre-study was conducted in the reactors before changing the test parameters. For this, the reactors were inoculated and operated under identical conditions (same inoculation sludge, external resistance, feed,

buffer and salt concentration), the output voltage for all reactors (reactors #1-7 operated at SWW COD 1000 mg/L, NaCl 100 mM, PB 100 mM, pH 6.5) showed the same pattern, achieved 0.60±0.01 V with a maximum output period of 35±2 h. The COD removal was also similar at 80±5 % per cycle. An example of the voltage production for each reactor after 60 days of operation is shown in Figure 2-6. These reactors were then selected for later studies.

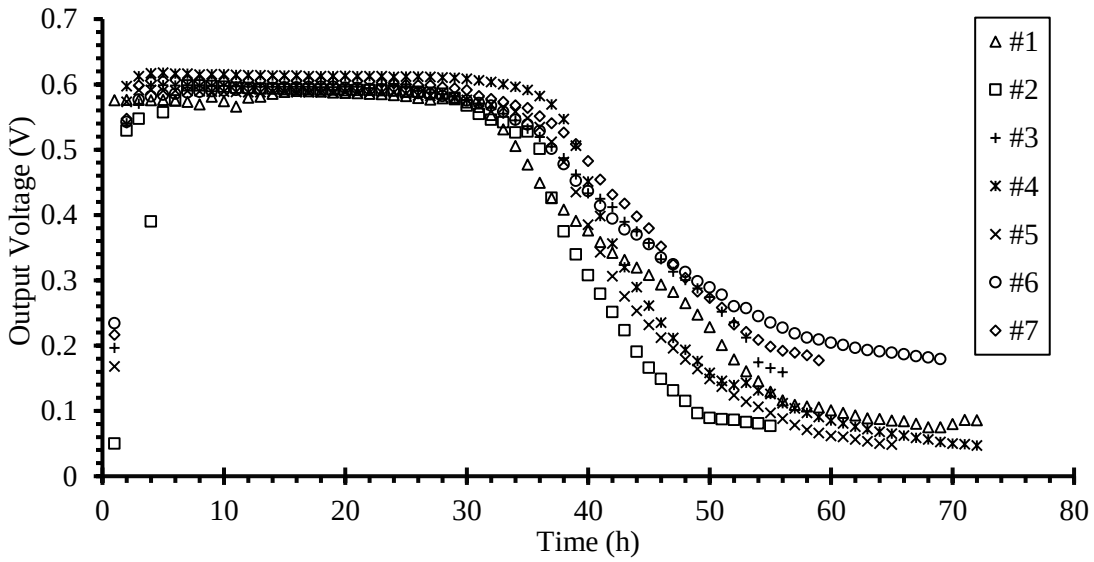

Figure 2-6 An example of the performance of 7 reactors in the pre-study. Numbers in the legend identify 7 individual reactors created in this research.

2.4.2 Replication of analytical methods

In all the studies presented in this thesis, the COD, TSS, VSS, IC analysis were assured by taking triplicate analysis of each sample. The pH measurements were performed by taking triplicate reading for each sample.

2.4.3 Replication of steady state

Each set of experiments was carried out until steady state was reached. An analysis of steady state performance was conducted over multiple cycles for each test condition. The steady state performance of the reactors was evaluated from a total of 1000+ cycles over the period from April 2017 to September 2018 for the overall study, and 247 cycles were eventually chosen and reported in this thesis. Data presented in

this research was evaluated with average (avg.) and standard deviation (std.) at the form of avg. ± std. (n= numbers of cycle).

Chapter 3. Investigation of pH and Buffer Impact on MFC Treating Winery Wastewater

This chapter presents the study designed to determine the optimum pH for the treatment of winery wastewater using the MFC reactors designed in Chapter 2.1 and fed synthetic winery wastewater. The use of buffered or unbuffered conditions was also tested. A comparison of the effect of using phosphate buffer or bicarbonate buffer on the power generation and COD degradation efficiency of MFC reactors was then studied. Finally, the optimum phosphate buffer concentration was determined. The contents of this chapter were presented in part in the poster *Electricity generation from winery wastewater using air cathode microbial fuel cell: addressing the practical issues* at the *68th Annual Conference of the Canadian Society of Microbiologists*, and as oral presentation at the 2019 Annual Conference of the Canadian Society for Bioengineering (CSBE) for presentation. A version of this chapter is under review by the *Journal of Water Process Engineering*.

One of the drawbacks for biological winery wastewater treatment is the pH, which varies (3.6-10.5) but is mostly acidic with little natural buffering capacity (Rosso and Bolzonella, 2009; Welz et al., 2016). The pH plays a significant role in biological treatment processes by affecting the growth and metabolism of microbial communities (Metcalf & Eddy, 2014). It is also critical in MFCs treating wastewater, not only the bacterial growth, but also the energy recovery efficiency. Many groups had observed a neutral to alkaline pH was favourable for MFC performance when fed with municipal or synthetic wastewater (He et al., 2008; Jadhav and Ghangrekar, 2009; Li et al., 2013; Puig et al., 2011). The neutral pH is more favourable for microbial growth, anodic attachment and electrogenic activity (Franks et al., 2009; L. Zhang et al., 2011). Ren et al. (2007) found that due to the production of acidic products from fermentation, the output power of a dual-chamber MFC decreased dramatically when the pH went down to 5.2; the power recovered rapidly when the pH was adjusted to 7.0. Jadhav and Ghangrekar (2009) found out in dual chamber MFCs fed synthetic wastewater, the more different the pH between the anode chamber, the higher

the current obtained. They further concluded that the difference of pH acted as a driving force for proton transport. The pH of a single chamber impacts on both anodic and cathodic reactions. A higher pH (8-10) inhibits the bacterial activities but might benefit the cathodic reaction thus improving the overall performance of MFC (He et al., 2008). Fan et al. (2007) demonstrated 38.6% improvement on performance of MFCs using a pH 9 bicarbonate buffer compared to a pH 7 phosphate buffer (PB).

In laboratory studies, proper pH maintenance is accomplished by the addition of buffers. However, highly acidic wastewaters such as winery effluents require the addition of tremendous amounts of caustic soda or buffer which can increase operational cost drastically. Additionally, when applying MFC systems to winery wastewater treatment, a buffer can act as a sink for protons thereby limiting voltage production. The literature reports documenting the treatment of winery wastewater all maintained a pH of 6.4-7.2 in buffered solutions, for instance, 6.4-7.0 (Rengasamy and Berchmans, 2012), 6.5 (Penteado et al., 2015, 2016, 2071, 2018), 7.2 (Cusick et al., 2010) and 7.0±0.2 (Pepe Sciarria et al., 2015). Penteado et al. (2016) reported a 17% COD removal and 0.12 V output voltage (R_{Ext} = 120 Ω, P_d = 465 mW/m^2) when fed a dual chamber MFC with winery wastewater (6850 mg/L) with pH adjusted to 6.5 using $NaHCO_3$. Pepe Sciarria et al. (2015) obtained COD removal of 27% (initial COD 6400 mg/L) and 83% (initial COD 10100±300 mg/L), maximum output voltage of 0.42±0.03 V (R_{Ext} = 1 kΩ) and 0.34 V (R_{Ext} = 1 kΩ), using two single chamber air cathode MFCs fed with white and red wine lees respectively (initial pH adjusted to 7.0±0.2 using 100 mM phosphate buffered saline solution). To cover the range of all pH reported from the literature with consideration to minimize the usage of buffer, 4.5, 5.5, 6.5 and 7.5 were chosen for this study.

3.1 Experimental design and analytical methods

The air cathode MFCs used for this study were fabricated and operated as described in Section 2.1 and 2.2. MFCs were inoculated using anaerobic winery wastewater sludge, operated in batch mode fed with synthetic winery wastewater (SWW) as described in Section 2.2. Each reactor was loaded with an external resistance of 10 KΩ (unless otherwise stated). The output voltage was monitored using NI USB 6210

Multifunction I/O device and recorded by NI SignalExpress 2015 every 2 min. Analytical methods are described in Section 2.3.

Initially, reactors were maintained by feeding SWW regularly to achieve a repeatable performance. A volume of 80 mL of reactor supernatant was replaced with the same volume of fresh feed when the output voltage dropped to 50% of the maximum output voltage. Occasionally, longer term monitoring was performed and, in those cases feed replacements were done when the voltage dropped to 90% of maximum.

3.1.1 Determination of the optimum pH

The pH of the feed solution was adjusted from 4.0±0.1 to 6.5 by adding 100 mM PB (pH 7.4). After attaining a steady state performance, the pH of the reactor and feed solution was adjusted from 6.5 to 7.5 using NaOH. Once a new steady state was verified the pH was returned to 6.5 followed by lowering to 5.5, then increasing to 6.5 and finally to 4.5. Each pH was maintained for a period of at least two weeks or the time required to achieve a steady state.

3.1.2 Comparison of reactor performance under buffered and unbuffered conditions

Since the addition of buffering materials is expensive, and biofilms can maintain environmental conditions separate from the bulk conditions, two MFC reactors were setup to compare the MFC performance under buffered and unbuffered conditions. One reactor was fed with SWW with PB (100 mM, pH 6.5). The other reactor was fed with SWW without any buffer but NaOH to adjust pH to 6.5.

3.1.2.1 Phosphate buffer and bicarbonate buffer Comparison

To investigate how different buffers maintained pH in the MFC fed with winery wastewater, two buffers - phosphate buffer and bicarbonate buffer each at 100 mM were prepared as described in Section 2.2.1.2. To test the effect of these two buffers on MFC performance, two reactors were inoculated with the same sludge

and run under the same conditions (SWW medium, COD 1000 mg/L, pH 6.5, NaCl 100 mM), HCl or NaOH were used to adjust the pH to 6.5.

3.1.2.2 Optimum buffer concentration

After PB was determined as the more effective buffer, the optimum buffer concentration was studied. The reactor was fed with SWW (COD 1000 mg/L, NaCl 100 mM, pH 6.5) with 100 mM PB, then PB concentration in the feed was decreased to 50, 25, 10, 5 and 2.5 mM, respectively, after at least one-week of steady state was reached for each concentration. At last 2x SWW medium with 10 mM PB (COD 2000 mg/L, PB 10 mM, NaCl 100 mM, pH 6.5) was fed for comparison.

3.1.3 Chemical electrochemical and microbial analysis

The winery wastewater for characterization and sludge for reactor inoculation were taken from the anaerobic tank from Tantalus Vineyards at March 2017. Samples were taken per requirement and the physical chemical parameters: pH, conductivity, COD, total N and P, VFA was measured by following the procedures described in Section 2.3.1. Electrochemical parameters were monitored and calculated as described in Section 2.3.2.

3.2 Results and discussion

Figure 3-1 presents an example of the results generated during this study (the output voltage and COD of a reactor maintained at optimum condition). Batch experiments all showed the same general pattern. The voltage increased sharply (T=0 h) and reached a plateau initially and then declined as the COD in the batch was removed. This is because the microorganisms in the anode chamber degrade the organic matter for growth and transfer electrons extracellularly to the anode, the electron flow through external load (known as the current) as shown in Figure 1-1. The potential difference between anode and cathode (output voltage in this case) as the driving force of the electron flow was continuously recorded by the monitoring system.

After the organic matter (measured as COD) declined to around 100 mg/L, the output voltage started to drop. At the end of the cycle the COD and output voltage both declined to an insufficient level, that defines a complete batch and the reactor was re-fed (T=96 h in Figure 3-1). In many studies the reactor was refed when the voltage dropped to ½ maximum rather than allowing the decline to continue, at this point COD removal was 83% complete. An obvious time shift was observed between the rapid COD removal phase and output voltage decline phase. The proposed reason is that the electrons and protons produced during COD removal accumulated due to limitation of the circuit (e.g. the external resistance) and the capacity of reactor. In Figure 3-1 it took ~20 h for the accumulation to clear.

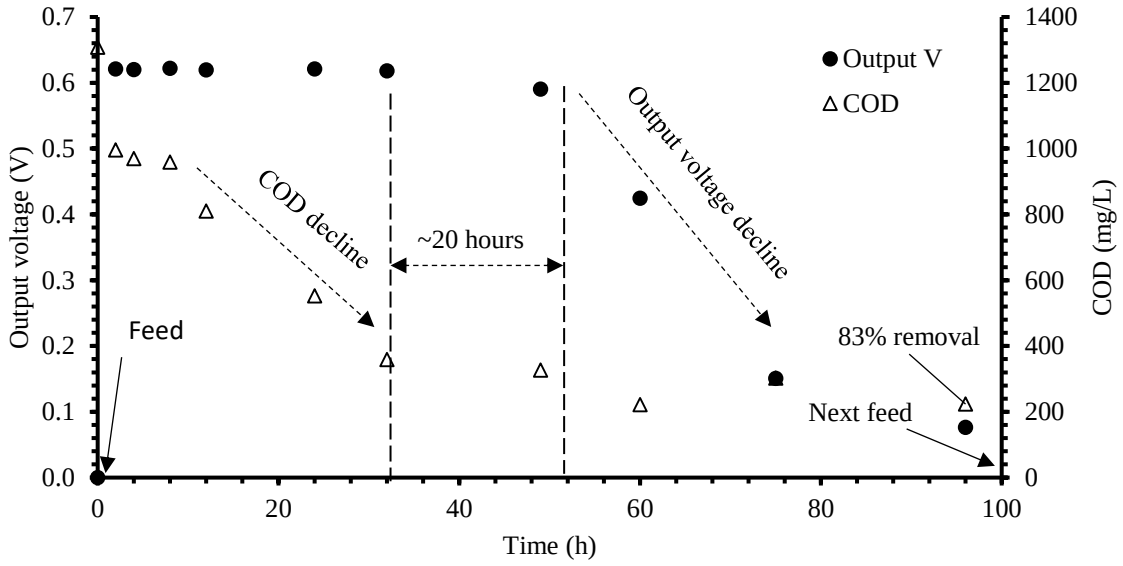

Figure 3-1 An example of the performance of a reactor fed SWW maintained at optimum condition

3.2.1 Determination of the optimum pH for MFC fed SWW

The pH 6.5 reactor reached steady state performance after 30 days of operation. Figure 3-2 presents the first 20 days of enrichment. As can be seen the maximum voltage and the period of maximum voltage production increased over the first five feeds and then were relatively constant for feeds 6 and all subsequent feeds. Table 3-1 presents a summary of the average and standard deviation of the maximum power production and duration period for maximum power production for 10+ steady state feed cycles. The duration was determined as the time to the rapid drop in production interpreted as the time to reach 90% of the maximum

voltage in each batch. Multiple cycles at pH 6.5 showed the same pattern and the voltage remained stable at 0.63±0.01 V for 60 h from feeding prior to drop. Interestingly, increasing pH to 7.5 resulted in 20 times decline (0-0.03 V) in maximum output voltage. There was a drastic decline in voltage observed at pH 5.5 and 4.5, respectively. Figure 3-3 presents example output voltages of the reactor once it reached steady state at each pH.

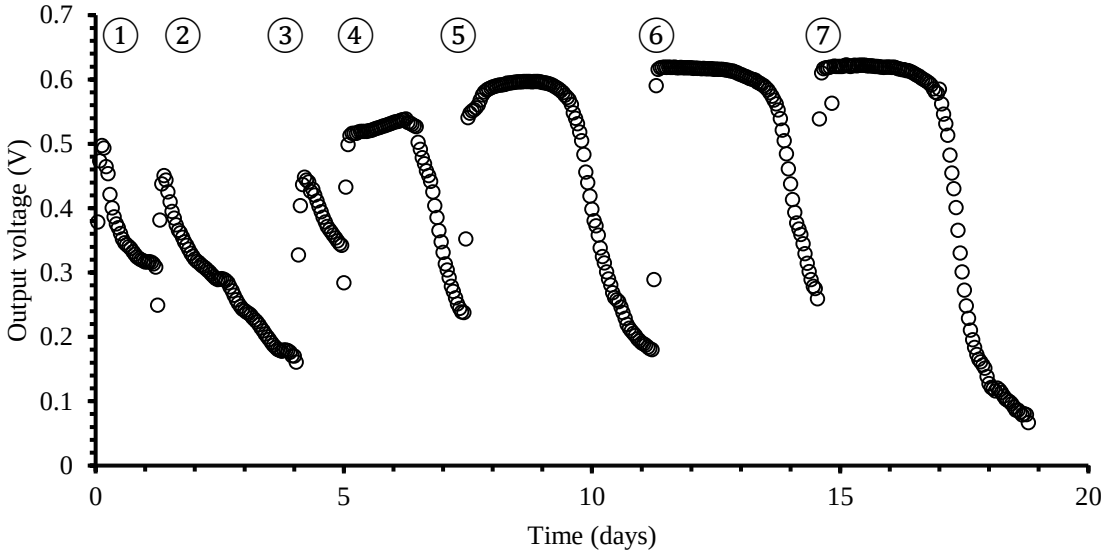

Figure 3-2 Output voltage of MFC operated at pH 6.5 showing the enrichment process (COD 1000mg/L, ER=10 KΩ). The numbers indicate successive feed cycles

Table 3-1 Comparison of reactor performance when fed SWW medium under different pHs

pH of reactor	Final pH	Maximum output (V)	Maximum output period (h)	COD removal (%)	Maximum C_E (%)
7.5	7.4±0.1	0.03±0.02	2±2	68±15	0.02
6.5	6.5±0.1	0.63±0.01	60±3	77±7	1.8
5.5	5.5±0.2	0.07±0.03	2±1	61±28	0.07
4.5	3.6±0.3	0.06±0.04	5±2	85±11	0.20

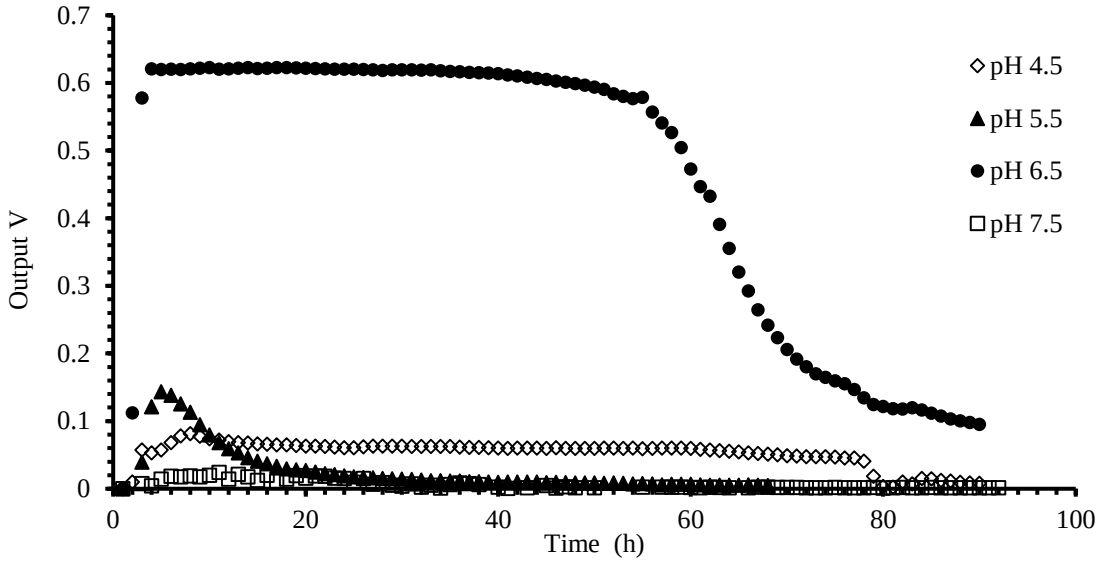

Figure 3-3 Output voltage in a representative MFC batch
Reactor was fed with SWW medium (COD 1000 mg/L) with 100 mM PB but adjusted to different initial pHs (ER=10 KΩ)

The highest average COD removal of 85±11% was observed at pH 4.5, followed by 77±7% at pH 6.5, 68±15% at pH 7.5 and 61±28% at pH 5.5. The highest coulombic efficiency (C_E) was 1.80% obtained from pH 6.5 reactor, which is much higher compared to 0.02% in pH 7.5, 0.07% in pH 5.5 and 0.20% in pH 4.5 reactor. This suggested that the optimum pH improved the output power efficiency and meanwhile increased the columbic efficiency. The reactor at pH 7.5 reached the lowest output voltage (0.03±0.02 V) and columbic efficiency; possibly this can be due to proton scavenging resulting in limiting the cathodic reaction (Min et al., 2005), and poor proton transfer at the reduced proton concentration gradient across the PEM. Also pH 7.5 is favourable for methanogenesis which could contribute to the COD consumption (Jadhav and Ghangrekar, 2009). The increased COD removal at pH 4.5 is most likely due to proliferation of yeast. Yeast present in winery wastewater were from the wine making process. Yeast favoured lower pH therefore overcame the bacterial population in the reactor, which led to high COD degradation efficiency but low output voltage since they do not export electrons.

A microscopic analysis of reactor biomass revealed yeast cells flourishing in samples from pH 4.5 (Figure 3-4) that were not observed in samples from the reactor operated at other pHs. The high COD removal and

low voltage at pH 4.5 MFC is attributed to the consumption of the organics by yeast and loss of the active electrogenic population. There are a number of studies on potential application of yeast in MFCs but all are restricted to mediator based MFCs (Gunawardena et al., 2008; Sayed et al., 2015). In other research *Saccharomyces cerevisiae* cells was reported as unsatisfactory as a fuel cell catalyst due to their lethargic responses to external substrates (Schaetzle et al., 2008). The most preferred yeast in the wine making process is *S. cerevisiae* (Goold et al., 2017) and hence a yeast mediated MFC would not be suitable to treat winery wastewater and the pH should be kept higher than 4.5 to prevent yeast proliferation.

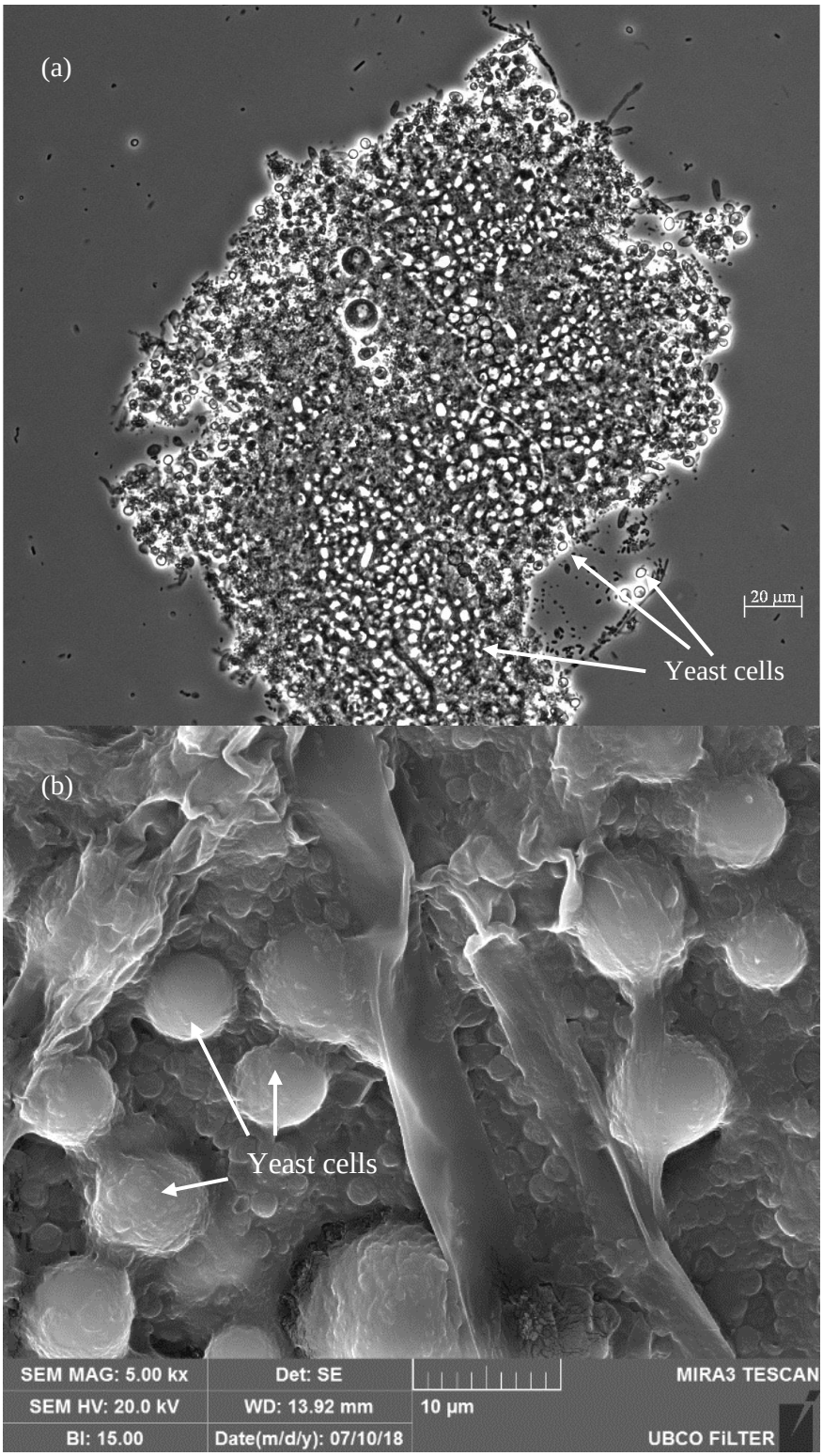

Figure 3-4 Images showing the flourishing of yeast cells in pH 4.5 reactor
(a) Microscope image showing the yeast cells in anode chamber; (b) SEM image showing the yeast cell accumulating on the cathode

3.2.2 Impact of buffer on MFC performance fed SWW

As mentioned earlier, winery wastewater is highly acidic and requires a tremendous amount of buffer which is costly for wineries. This section examined if buffer could be omitted, altered to a less expensive one, or at least reduced to a minimum while maintaining pH efficiently.

3.2.2.1 Determination of the need for buffering

Figure 3-5 presents examples of the output voltage of MFC fed SWW under buffered and unbuffered conditions with pH adjusted to 6.5 for three consecutive cycles two weeks after inoculation. The first two cycles were 24 h each and the third one was left for 96 h to allow the COD and output voltage to completely decline to the minimum. Table 3-2 presents a summary of pertinent data. A maximum voltage of 37±3 mV was obtained in buffered SWW 6 h after feeding. However, the MFC fed with unbuffered SWW showed only a maximum voltage of 20±5 mV which is a 47% decline in power production when compared to the buffered MFC. The duration of the maximum voltage output period was extended to 10-15 h (Table 3-2). The pH was maintained constant (6.5±0.1) in buffered MFC whereas the pH was dropped to 3.3-4.1 in the unbuffered reactor. The buffered MFC also reached higher COD removal rate (81.6%) compared to unbuffered one (60.6%) in 24 h, whereas in 48 h both achieved ~85% COD removal (84.3% in buffered MFC and 85.6% in unbuffered MFC).

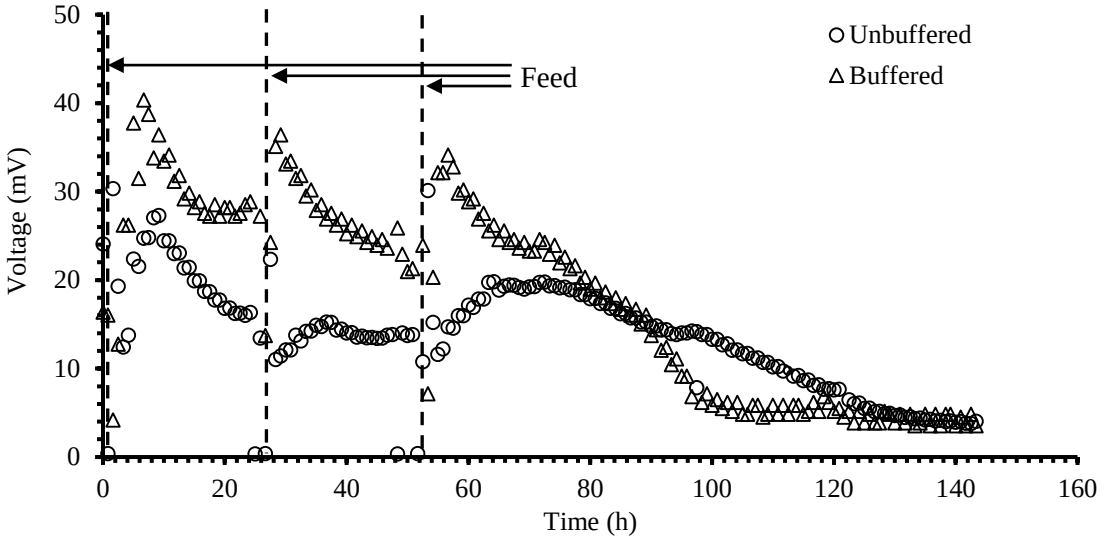

Figure 3-5 Output voltage of MFC fed SWW at pH 6.5 under buffered and unbuffered conditions after 14 days of acclimation

Table 3-2 MFC performance under buffered and unbuffered conditions after 14 days of acclimation

	Buffered (100 mM PB)	Unbuffered (with NaOH)
Feed frequency (h)	24	24
Initial pH	6.5±0.1	6.5±0.1
Final pH	6.5±0.1	3.7±0.4
Maximum output voltage (mV)	37±3	20±5
Maximum output period (h)*	10-15	4±1
COD removal (%)	83±1	73±13

*Maximum output period represents the lasting time of peak voltage measured during each cycle.

3.2.2.2 Determination of appropriate buffer

After determining an optimum pH for MFC fed winery wastewater and the fact that pH buffer improved performance, the next step was to determine an appropriate and cost-effective buffer. PB has been commonly used in MFC studies for pH maintenance at the lab scale; it is considerably more expensive and rarely used in field reactors. Fan et al. (2007) reported when using a pH 9 bicarbonate buffer the MFC fed performed better (power density increased 38.6%) compared to using pH 7 PB. They also declared that when using bicarbonate buffer, increasing the pH from 7 to 8 resulted in a 42.2% power density improvement. However, they used a simple medium (acetate) instead of complicated wastewater. Since the pH of winery wastewater is initially low, it would take a considerable amount of carbonate to reach 9.

Two reactors were setup to compare PB and bicarbonate buffered SWW on reactor performance. Both MFCs were established identically except one used 100 mM PB and the other 100 mM bicarbonate buffer. The output voltage from the reactor fed bicarbonate buffered SWW is presented in Figure 3-6; the first two weeks (1-13 days) showed the period when the initial pH was 6.5, after that the initial pH was adjusted to 9 until the end of this experiment. Two or three cycles under each pH were left longer to allow both COD and output voltage to decline. Results indicated adjusting pH from 6.5 to 9 resulted in a ~40% improvement of output voltage (70±10 mV vs 100±10 mV) but no apparent difference in COD removal (79±7% vs 74±8%). The output voltage of bicarbonate buffered reactor under both pHs was far less compared to PB buffered reactor. One typical complete cycle chosen from each reactor after steady state is presented in Figure 3-7 for clearer understanding; the maximum output voltage under PB buffered condition was 6 to 10 times higher than bicarbonate buffered condition. The reactor performance among different buffer conditions is listed in Table 3-3 for better comparison. Interestingly, our results showed that the energy recovery efficiency (in terms of power generation) of bicarbonate buffered reactor was much less compared to PB buffered reactor, this is opposite to what Fan et al. (2007) observed. In addition, the bicarbonate buffered reactor showed wider fluctuations in pH. When fed with pH 6.5 medium adjusted with bicarbonate buffer, the pH ended up at 7.1±0.2 after 24 and 72 h; similarly, when fed with pH 9 bicarbonate buffered SWW medium, the pH changed to 8.5±0.4 after 24 and 72 h. In contrast, PB was able to maintain pH to 6.5±0.1 even after 120 h of operation.

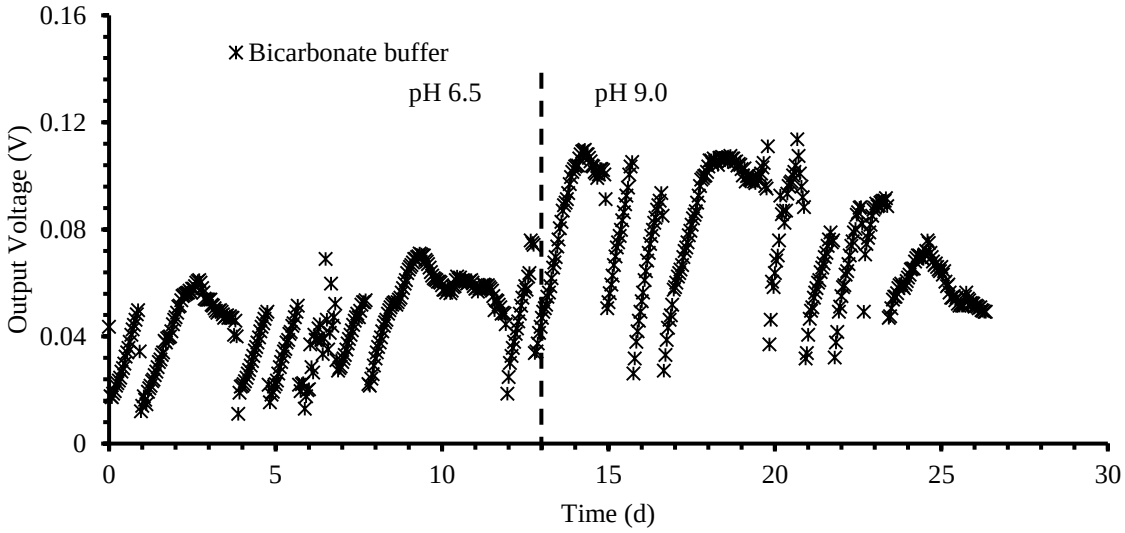

Figure 3-6 Output voltage of MFC fed SWW and buffered with bicarbonate

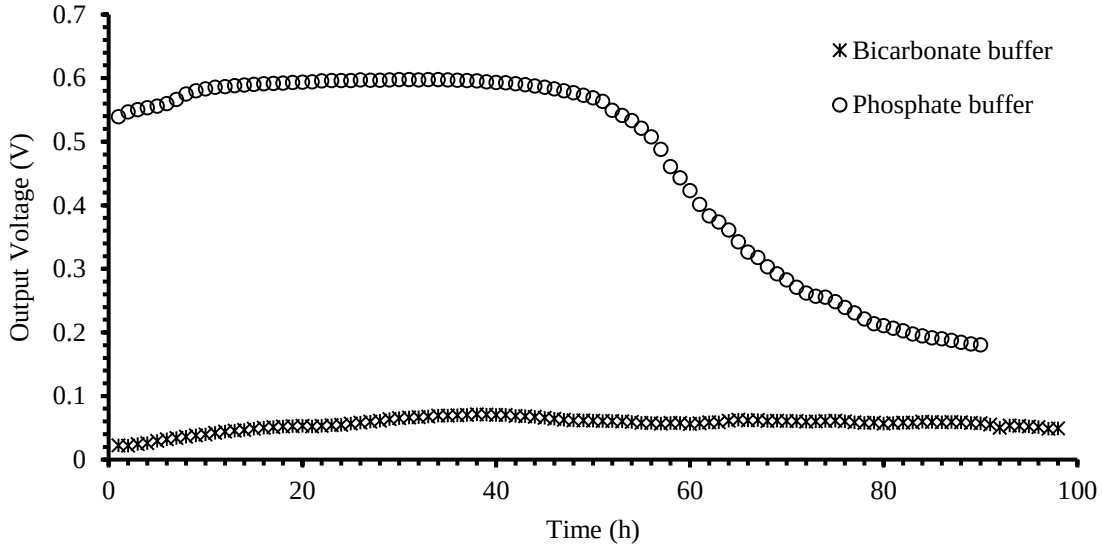

Figure 3-7 Output voltage of MFC fed SWW with pH 6.5 adjusted by BB and PB, respectively

Table 3-3 Comparison of reactor performance under different buffer conditions

	Unbuffered (with NaOH)	PB Buffered (100 mM)	Bicarbonate Buffered (100 mM, Initial pH 6.5)	Bicarbonate Buffered (100 mM, Initial pH 9)
Feed frequency (h)	24	72-96	24-72	24-72
Initial pH	6.5±0.1	6.5±0.1	6.5±0.1	9±0.1
Final pH	3.7±0.4	6.5±0.1	7.1±0.2	8.5±0.4
Maximum output (mV)	20±5	630±10	70±10	100±10
Maximum output period (h)	4±1	60±3	26±7	30±5
COD removal (%)	73±13	77±7	79±7	74±8

The COD removal in the bicarbonate buffered reactor (both at pH 6.5 and pH 9) was not different than the COD removal in the PB buffered reactor (pH 6.5). The proposed reason is that non EAB bacteria were still able to remove organic matter, however, the unstable/basic pH did not favor EAB; this led to less exo-electron transfer efficiency that eventually was reflected in the output power. In addition, the basic environment acts as a proton sink which limited the proton concentration, thereby also decreasing the proton transportation rate to the cathode. Reactors using either buffer performed better than in unbuffered conditions (Table 3-3), as EAB favored neutral conditions; a buffered system would balance the protons that were continuously generated when microorganisms break down large molecules into small acids. In contrast, the protons kept accumulating in the unbuffered reactor, resulting in a rapid pH drop which was harmful to EAB. This leads to the conclusion that PB worked better in terms of electrical energy recovery when using MFC treat winery wastewater. In addition, this once again proved that buffer (no matter bicarbonate or phosphate) is necessary for stable MFC treatment of wastewater in terms of both power production and COD removal.

3.2.2.3 Optimum buffer concentration

Since the bicarbonate buffer did not work as effectively as PB in terms of power production, decreasing the buffer concentration as an alternative way to bring down the buffer cost was investigated. The steady state, pH, maximum output voltage, and COD removal efficiency were recorded or calculated for each PB concentration and are shown in Table 3-4. The Buffer concentration up to 5 mM could maintain a constant pH (6.5±0.2) but further reducing the buffer concentration to 2.5 mM resulted in a pH decline to 5.3 within 24 h. Figure 3-8 presents an example of voltage production during one steady state feed cycle in reactors with 10, 5, and 2.5 mM PB concentration. When the buffer exceeded 10 mM the voltage curves were not significantly different from 10 mM PB SWW, so are not presented in the figure.

Table 3-4 Summary of effects of PB concentration (n=5)

PB conc. (mM)	100	50	25	10	5	2.5
Final pH	6.5±0.1	6.5±0.1	6.5±0.1	6.5±0.2	6.5±0.2	5.3±0.2
Max output V (V)	0.55	0.54	0.6	0.61	0.57	0.55
COD removal (%)	83.4±3.9	84.5±4.0	79.8±4.1	87.0±4.1	76.2±7.7	64.3±19.3
CE (%)	1.8±0.1	1.8±0.1	1.8±0.1	1.8±0.1	1.8±0.1	1.7±0.2

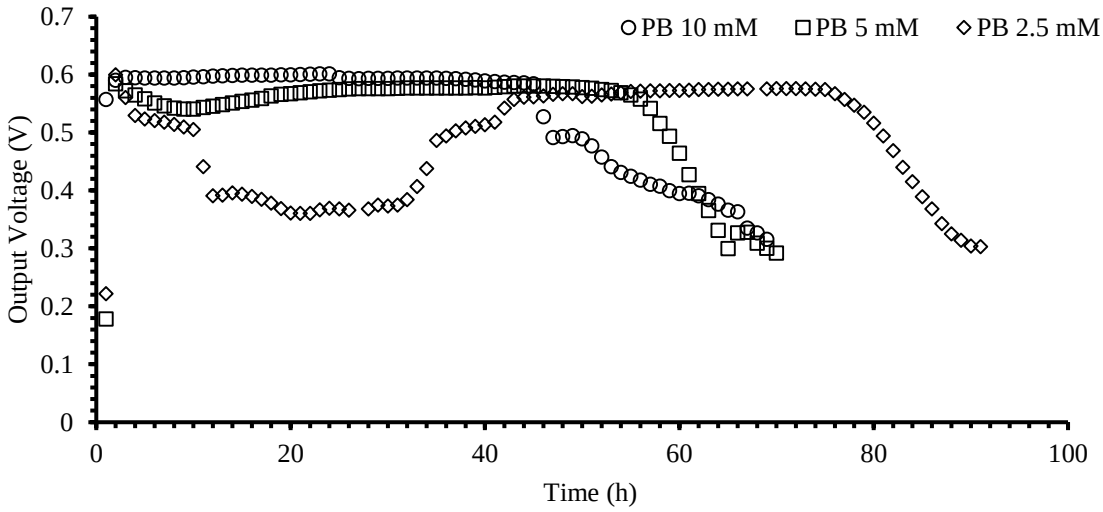

Figure 3-8 Output voltage of MFC reactor under different PB concentration

Although the output voltage increased when the PB concentration was reduced from 100 to 25 and decreased when the PB was decreased from 10 to 5 mM, and again when the PB concentration was reduced from 5 mM to 2.5 mM, it is interesting finding that the coulombic efficiency was similar but with a slightly higher fluctuation when 2.5 mM PB was used (1.8±0.1 at 5-100 mM vs. 1.7±0.2 at 2.5 mM) Table 3-4. This indicated that insufficient buffer capacity may lead to temporary pH changes but this did not decrease the columbic efficiency as the culture adjusted the pH back to 6.5 (Figure 3-9b).

The pH disturbance due to insufficient PB strength also caused a dramatic difference of COD removal efficiency. The reactor fed with 10 mM PB achieved 58% COD removal in 24 h and 77% in 72 h, whereas 2.5 mM PB reactor reached only 27% in 24 h and 46% in 72 h, as shown in Figure 3-9. The fluctuations of pH due to insufficient buffer are closely correlated to the output voltage, and the change in the pattern of the COD removal rate. When using 10 mM buffer the pH was maintained at 6.5 constantly, the reactor reached a maximum rate of 12% COD removal per hour (~120 mg/LCOD/h) within 4 h right after feed.

However, using 2.5 mM PB the maximum COD removal rate was postponed to 30-35 h, at 6.4% COD removal per hour (~46 mg/LCOD/h). This was also when the pH raised back to 6.

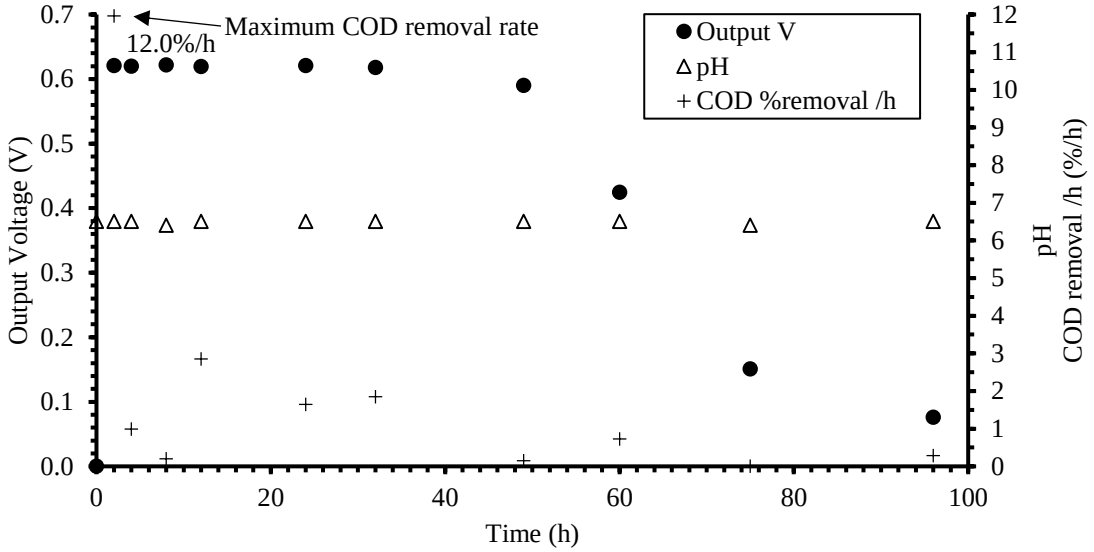

a) MFC reactor fed SWW with 10 mM PB

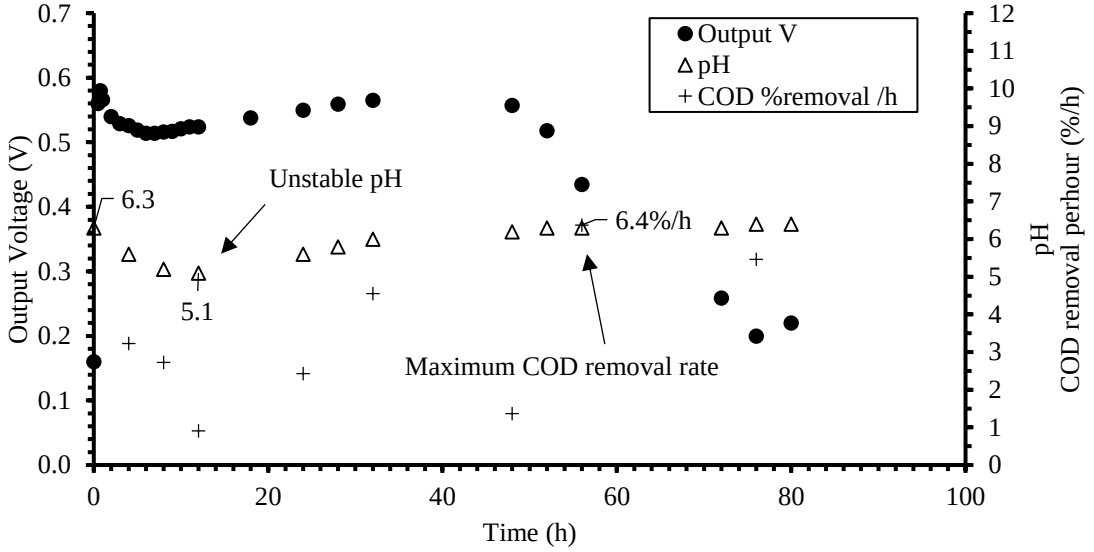

b) MFC reactor fed SWW with 2.5 mM PB

Figure 3-9 MFC performance comparison under different PB strength

To further investigate the correlation of COD and buffer strength, the feed was changed from 2000 mg/L COD with 20 mM PB to 2000 mg/L COD with 10 mM PB (Figure 3-10). The output voltage dropped sharply from 0.6 V to 0.25 V after 70 h and slowly increased to 0.57 V at 150 h and lasted until the end of

the feed cycle. The pH was initially 6.5 right after feed, and then slowly dropped down to 6.0±0.2 after 48 h, further down to 5.2±0.2 by 70 h to 120 h and then increased to 6.0±0.2 by 150 h. The trend of pH correlates with the performance of output voltage, which indicated that when increasing the COD strength from 1000 mg/L to 2000 mg/L, 10 mM PB was not able to maintain the pH stable at 6.5, and this affected the output voltage. To support this finding the reactor was fed 2000 mg/L SWW medium with 20 mM PB buffer. The output voltage was stable at 0.63±0.02 V for 120 h and dropped down slowly and smoothly after that. The pH was well maintained at 6.5±0.1 during the cycle. This suggests that when changing the COD of feed, the PB concentration needs to be adjusted proportionally. A COD:PB ratio (COD(mg/L):PB(mM)=100:1) is proposed for future experiments. This finding is further discussed in Section 4.3.2.

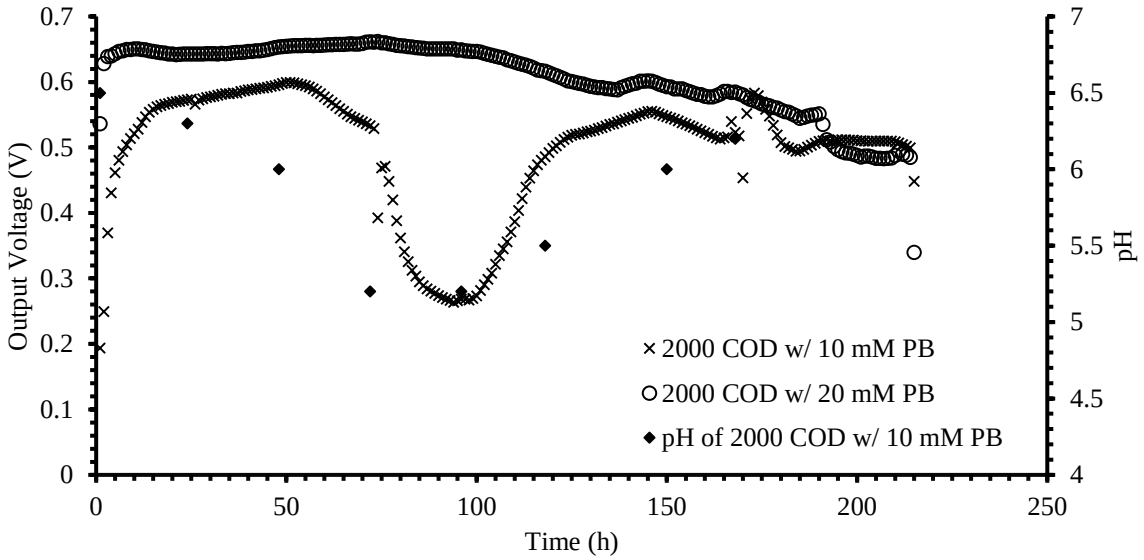

Figure 3-10 Output voltage of MFC at steady state when fed 10 and 20 mM PB buffered 2x strength SWW (2000 mg/L COD, 10 and 20 mM PB, 100 mM NaCl, pH 6.5)

The temporary pH changes within this range most probably inhibited the activity of EAB. Previous studies suggest a working pH range of 6-9 for MFC fed pure substrate (acetate or glucose) or wastewater; many studies report an optimum pH of 6-6.5 (Fan et al., 2007; Jadhav and Ghangrekar, 2009; Raghavulu et al., 2009; Zhang et al., 2011). An acidified anode can inhibit bacterial activity and affect the performance and stability of the biofilm (Oliveira et al., 2013). One report was found using a single chamber MFC to treat

low-pH (pH 4.4) distillery wastewater directly without buffering and obtained stable voltage generation, but whether the power generation efficiency would improve under neutral pH was not examined (Kim et al., 2014). In this study we found adjusting acidic medium to 6.5 using sufficient buffer improved the power generation efficiency dramatically. Even with insufficient buffer strength, the total COD removal and energy recovery were not impacted, but the process took longer to achieve the same level of conversion.

3.2.3 MFC performance under optimum pH and concentration

3.2.3.1 COD removal under optimum pH

The pH 6.5 MFC reactor was observed to show the best performance when steady state was compared to other initial pH, using a PB concentration of 10mM, 10K ER, and 100mM salt concentration. The time versus output voltage and COD removal are plotted in Figure 3-11. The highest COD removal rate was reached within 4 h after each feed, the maximum Output voltage was measured 0.5 hour after fed and lasted for 50 h. The COD removal reached 80% within 60 h. The highest COD removal rate was obtained at 0-4 h, after that the removal rate dropped down to 22-37 mg/L/h until 32 h, then 0-10 mg/L/h after 32 h (Figure 3-11).

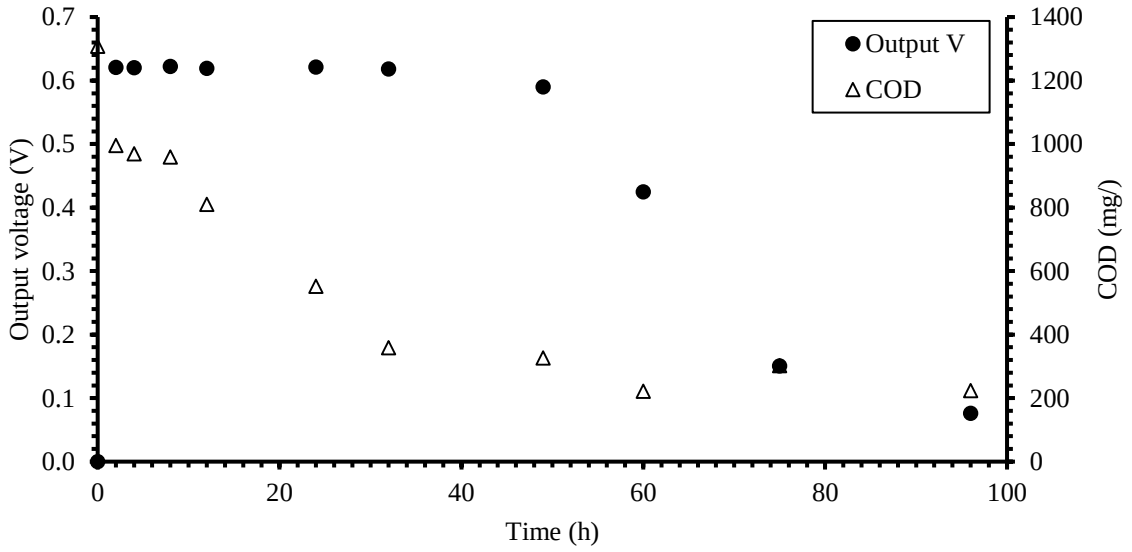

Figure 3-11 Output voltage performance of an MFC reactor maintained at pH 6.5

3.2.3.2 Polarization analysis

The polarization and power density curve of a reactor maintained with SWW medium of pH 6.5 with 10 mM PB for 120 days are shown in Figure 3-12. The power density curve revealed the maximum power density reached was 44 mW/m^2 when using a 1 KΩ resistance. Internal resistance calculated from the slope of straight portion was 491 Ω. This suggested that output power can be optimized through adjusting the external resistance; a further study related to this and the change of internal resistance with increased incubation time is presented in Chapter 5.

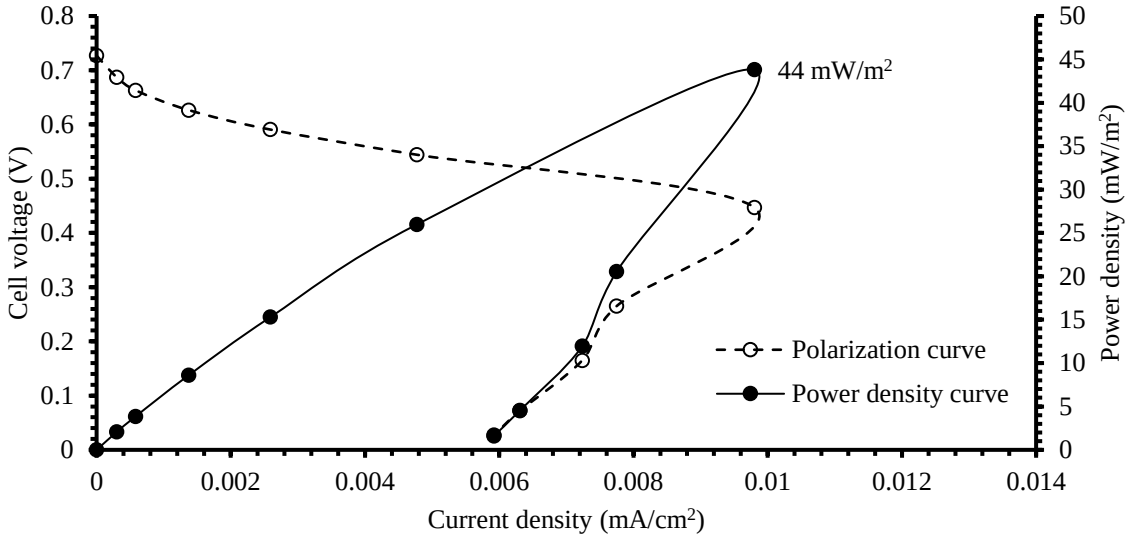

Figure 3-12 Polarization and power density curve of a reactor maintained at pH 6.5 fed SWW for 120d

3.2.4 Microbiology

Biofilm growth was observed on both the anode and cathode of an active reactor maintained with SWW medium with 10 mM PB (Figure 3-13). The Biofilm on the cathode was much thicker (~1 mm) compared to anode (0.2-0.5 mm); SEM images (Figure 3-14) showed a thick porous layer on the cathode, and growth of bacteria on the surface of the anode carbon fiber. The thick biofilm on the cathode may be because oxygen diffusion occurring in the cathode favored the growth of aerobic bacteria from the sludge used for inoculation. This benefits the system by limiting oxygen diffused into the anode area; however, if the

cathodic biofilm was allowed to develop too thick it would decrease the proton transportation efficiency. Additionally, the external resistance used may have affected the activity of the cathodic biofilm. A more detailed study regarding the impact external resistance therefore was carried on and is presented in Chapter 5.

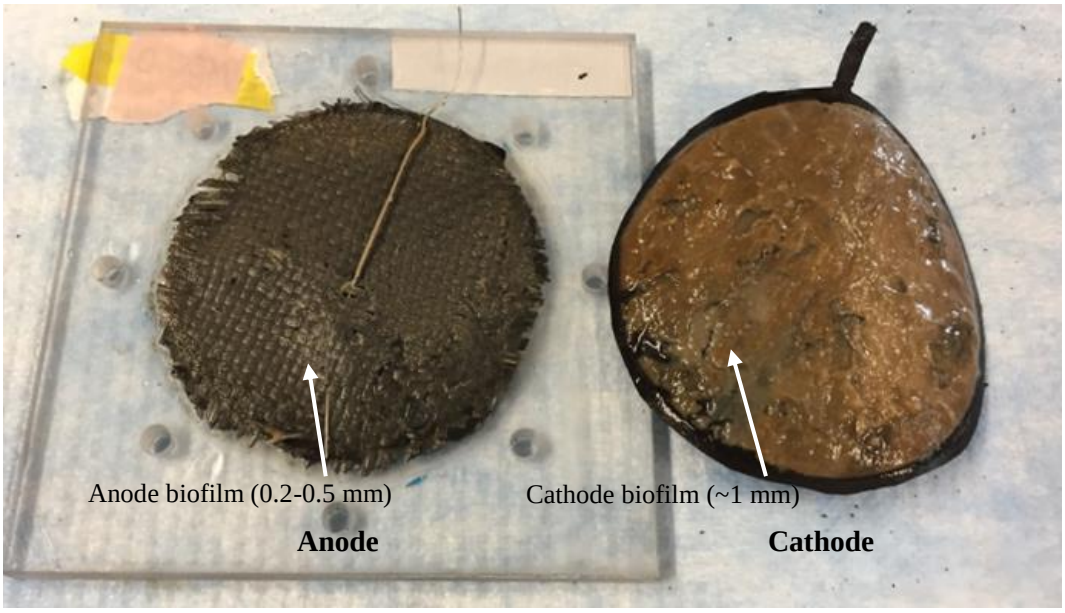

Figure 3-13 Digital photo showing biofilm on anode (left) and cathode (right) from an active MFC reactor 250 days after inoculation

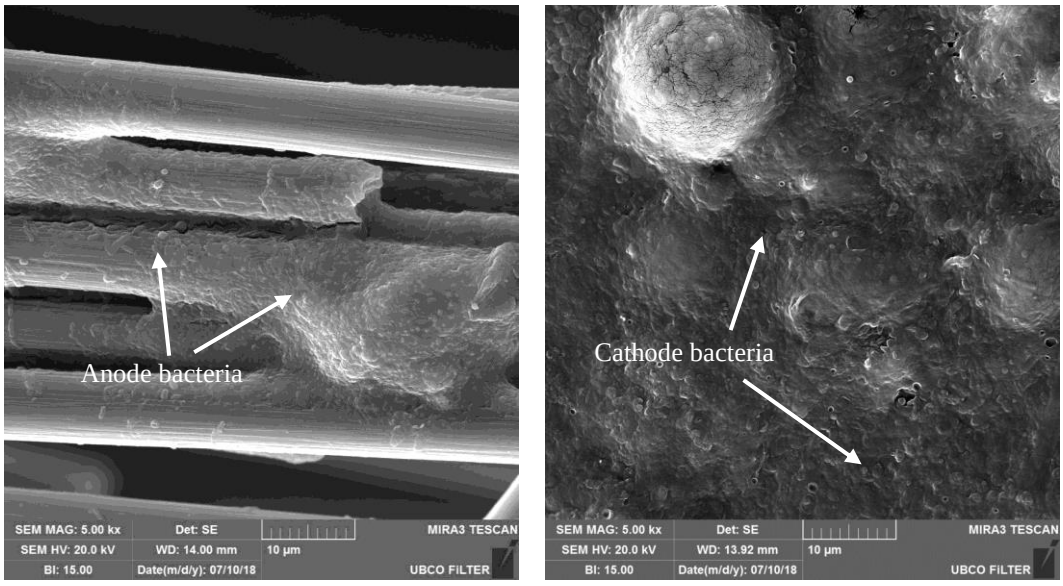

Figure 3-14 SEM images showing the growth of bacteria on anode (left) and cathode (right) of MFC maintained with 10 mM PB

3.3 Summary

This chapter investigated the impact of pH on the performance of MFC fed winery wastewater. The optimum pH (6.5) was found for MFC when fed with 1000 mg/L SWW obtaining the maximum voltage (0.63 V, R_{Ext} = 10 KΩ) and a stable COD removal (77±7%). Low pH (4.5) resulted in the growth of yeast and a decrease in the power production. A proper buffer is required to maintain the reactor at pH 6.5 for optimum and stable performance on both output power and COD removal. Phosphate buffer was found to be more effective than bicarbonate buffer of the same concentrations. A minimum buffer concentration of 10 mM is required to maintain the reactor pH at pH 6.5 when fed SWW (COD 1000 mg/L); insufficient buffer strength caused a drop in efficiency of COD removal and power generation. When the reactor was maintained at pH 6.5 and 10 mM PB, the highest COD removal rate was reached within 4 h after feed. The maximum output voltage was obtained 0.5 hour after feed and lasted for 60±3 h, COD removal reached 80% within 60 h. COD strength was correlated to the buffer strength; a COD:PB ratio (COD(mg/L):PB(mM)=100:1) was proposed for future experiments.

Chapter 4. Investigation of The Effect of Seasonality on MFC Treating Winery Wastewater

This chapter presents the study of the impact of seasonal changes in winery wastewater as feed stock on the efficiency of MFC reactors, including the consequences of feed change in both type of feed supplied and COD concentration of feed. A version of this chapter has been submitted to *Water Research.*

Winery wastewater characteristics vary from winery to winery and are significantly influenced by the types of wine produced and the local climate (Welz et al., 2016). Winery wastewater loads also vary seasonally, with the highest organic loads produced during vintage, and low organic loads during the idle phase (Sirrine et al., 1977; SWBC, 2018). The challenge of seasonality must be considered when developing a system to treat winery wastewater.

4.1 Tantalus Vineyards winery effluent treatment system

Tantalus vineyards produces 20,000 cases of wine per year. Based on the estimation of 0.2 to 4 L of wastewater produced per liter of wine (Vlyssides et al., 2005; Welz et al., 2016), the winery effluent could be up to 720 m^3, considering household and some agricultural wastewater would also need treatment. Tantalus Vineyards chose to build its own treatment system instead of discharging the effluent to the municipal sewage system. This was not only a benefit to the city in regards of reducing pressure on the municipal system, but also decreased the operating cost itself as they would not have to pay COD charges. Mr. David Patterson, the general manager and winemaker of Tantalus Vineyards shared that the cost for wastewater disposal was reduced by 50% after the system was established, and the investment on this project should be recovered within 10 years. The flowchart of the treatment system is shown in Figure 4-1.

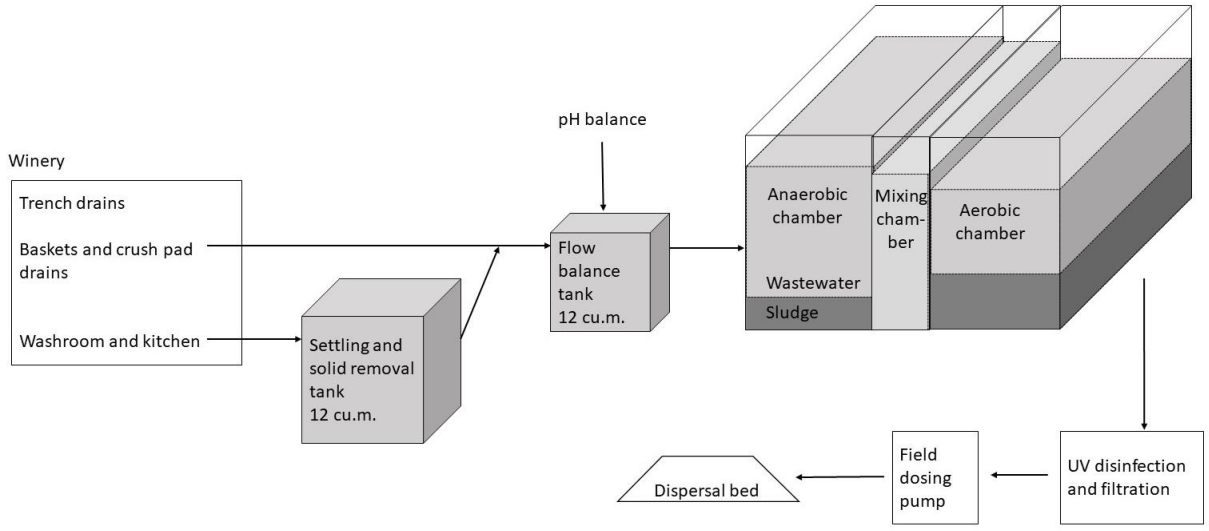

Figure 4-1 The wastewater treatment system in Tantalus Vineyards (Kelowna, BC, Canada)

The main stages of the system include a flow balance tank that pumps approximately 6 cubic meter treatment batches, a pH sensor and metering pump located in the flow balance tank to neutralize the pH for each batch, followed by a 12 cubic meter anaerobic tank for suspended solids collection, settling and fermentation, an aerobic bioreactor with a timed air blower and diffusers for aeration. Between cycles sludge settles and clear effluent is decanted and disinfected with UV light and is pumped to dispersal field after filtration through bag filters. This system has several advantages, it produces a high-quality effluent that is suitable for direct irrigation and, the odor of wine waste is eliminated. In addition, the system meets the domestic sewage regulations and the effluent has no measurable impact on the groundwater.

However, there are challenges, just like every system. In addition to the high initial investment, the system requires experience to be effectively maintained and operated. The challenge that will be discussed in this chapter, is the maintenance of an active population throughout the year especially in idle seasons. In other words, an alternative carbon source during the low flow season is required to keep the microorganisms in the reactor alive, so that they can maintain activity and will immediately respond when the vintage season kicks in.

4.1.1 Seasonality of wine production

Wineries face two busy seasons each year. The busiest season starts from early September to late October in the northern hemisphere (or February to March in the southern hemisphere), when the grapes are harvested from the vineyard. In this season the grapes are picked and destemmed before being crushed for primary fermentation. Cultured yeast is added during the fermentation process to break down the sugars and produce alcohol, meanwhile carbon dioxide gas is generated as a by-product. Sometimes the pre-fermentation process is followed by an additional pressing process to separate the juice from pomace depending on the type of wine; white wine requires this pressing process whereas red wine does not. This season lasts for two to six weeks and produces half of the year's wastewater. This wastewater (generated during fermentation and settling, pressing, equipment cleaning, or sometimes accidental spillages) also has the highest contaminant burden, with COD up to 45,000 mg/L as introduced in Chapter 1. The highest COD of wastewater samples in this season collected from Tantalus Vineyards was 13,086 mg/L (Chapter 2).

The second busy season occurs during February and March, where the secondary fermentation starts. This process usually happens in large stainless-steel vessels at a low pH (< 3.5), where lactic acid bacteria degrade the malic acid to lactic acid to remove the bitter and harsh taste caused by the malic acid (Jussier et al., 2006). This process also produces a fair amount of wastewater from the filtration, bottling, and cleaning procedures. The pH of wastewater from this season varies widely, as the fermentation process produces acidic effluent, whereas the cleaning process generates alkaline wastewater (caustic soda is used to remove the potassium bitartrate crystals adherent to the walls of the tanks). This suggests that the pH of the inlet wastewater for the treatment system will change within a short period; therefore, a system neutralization strategy is strongly required.

In addition to the two seasons mentioned above, bottle cleaning and the daily equipment cleaning process also produce wastewater. This wastewater contains the lowest COD compared to others.

In summary, the flowrate and strength of winery wastewater depends highly on the seasons, the types of wine and winemaking techniques. To overcome this challenge and maintain microbial activities in the reactor during the long off season which can last for six to seven months, Tantalus Vineyards invented a novel idea, to feed the reactor with dog food. The reactor was fed with a bag of dog food (10 kg) purchased from a local store (Costco Warehouse in Kelowna, BC) monthly to supply additional nutrition. The fact that the system is consistently able to recover swiftly when the vintage season starts shows this method is effective.

The research in this chapter was conducted to investigate the impact of feed source (winery wastewater and dog food) and feed strength (high and low COD) on MFC performance.

4.2 Experimental design and analytical methods

Air cathode MFCs as shown in Figure 2-1 were fabricated as described in Section 2.1 and 2.2 for this study. MFCs were inoculated using anaerobic winery wastewater sludge as described in Section 2.2 except that 10 mL of 100 mM phosphate buffer (PB) were added to maintain the pH at 6.5. Each reactor was loaded with an external resistance of 10 KΩ and the output voltage on the resistance was monitored using NI USB 6210 Multifunction I/O device. The output voltage data were recorded by NI SignalExpress 2015 every 2 min. Experiments regarding the effect of feed type and the effect of SWW COD strength were carried out, respectively, to investigate how the reactor responded to seasonal changes. The analytical methods described in Section 2.3 were used to follow MFC reactor performance.

4.2.1 Media preparation

SWW medium was prepared as described in Section 2.2.1.2. The amount of dog food was estimated based on the information given by Tantalus Vineyards. The treatment plant in Tantalus Vineyards was maintained by dumping one bag of dog food (10 kg) into the anaerobic tank monthly during the off season (late March to August, and November to January). The effective working volume of the treatment plant is 6 cubic

meters; treated water was discharged weekly during the off season. Assuming 50% of the working volume was discharged every week,

then,

Hydraulic Retention Time (HRT) = 7 days / 50% = 14 days, eq. 4-1

Volume of treated effluent / month (30 days) = 6 m^3 × (30 days / 14 days) = 12.86 m^3, eq. 4-2

$$\text{Concentration of dog food (mg/L)} = \frac{10\ \text{kg} \times (1\times10^6\ \text{mg / kg})}{12.86\ \text{m}^3 \times (1\times10^3\ \text{L / m}^3)} = 778\ \text{mg/L}. \quad \text{eq. 4-3}$$

The COD of dog food was measured to be 1330 mg COD per 1 g of dog food, therefore, the COD of raw dog food (RDF) medium is

1330 mg COD / 1g dog food × 778 mg/L dog food = 1035 mgCOD/L. eq. 4-4

Two types of media, RDF and filtered dog food medium (FDF) were prepared to understand the impact of using dog food on MFC performance. Dog food pellets (average diameter 6 to 8 mm) were first ground to a fine powder using a mortar and pestle before medium preparation. RDF was prepared by adding 0.778 g of dog food powder to 1 L of RO water, FDF was prepared by filtering the RDF medium with glass fiber filters (pore size 1.5 µm, diameter 47 mm). Concentrated FDF (10x FDF) was prepared by making a 10x concentrated RDF medium (7.78 g of dog food powder into 1 L of water) and then filtering this.

4.2.2 Experimental design for effect of seasonality on MFC treating winery wastewater

Initially, two reactors were established and fed with SWW (COD 1000 mg/L, PB 10 mM, NaCl 10 mM, pH 6.5) for at least two months to inoculate the anode and achieve a stable performance; the medium was changed when the voltage dropped to at least 50% of the maximum output as described in Section 2.2.1.2 for each reactor unless otherwise specified.

The first reactor was used to investigate the effect of feed type in 6 phases. No additional pH buffer was added when fed with RDF, FDF or 10x FDF as the pH was stable at 6.8±0.2 during the process.

Phase 1 – Inoculation phase – SWW feed (>two months),

Phase 2 – RDF feed (two months),

Phase 3 –FDF feed (two weeks),

Phase 4 – 10x FDF feed (two weeks),

Phase 5 – 2nd RDF feed (1 month),

Phase 6 – Return to SWW (1 month).

The second reactor was set up to investigate the impact of SWW strength on MFC performance and operated as follows,

Phase 1 – Inoculation phase – SWW feed (>two months),

Phase 2 – 2x SWW (2000 mg/L COD, 20 mM PB, 100 mM NaCl, pH 6.5) (1 month),

Phase 3 – 3x SWW (3000 mg/L COD, 30 mM PB, 100 mM NaCl, pH 6.5) (1 month),

Phase 4 – 4x SWW (4000 mg/L COD, 40 mM PB, 100 mM NaCl, pH 6.5) (1 month),

Phase 5 – 10x SWW (10,000 mg/L COD, 100 mM PB, 100 mM NaCl, pH 6.5) for 1 cycle (as a stress test to study the response of the system under COD stress conditions).

4.3 Results and discussion

Results suggest that the changing of both type and strength of feed resulted in changes in the performance of the reactors. This indicated that the seasonality is indeed an important factor when applying MFC technology to winery wastewater treatment.

4.3.1 Effect of changing MFC feed composition

The manufacturer's analysis of dog food composition is listed in Table 4-1 and shows that the raw dog food is rich in crude protein, carbohydrate, and crude fat. This will result in slow degradation rate by microorganisms compared to SWW, which is composed of sugar, ethanol, and volatile fatty acids (VFAs). The manufacturer does not include COD or other oxygen demand measures as part of their analyses. Medium prepared from dog food thereby was characterized in the lab to determine COD, pH and conductivity important to MFC operation. The results indicate that the FDF (10x) medium had higher soluble COD and conductivity compared to RDF medium as expected (Table 4-2).

Table 4-1 Dog food composition

Composition	Percentage
Crude protein	27%
Carbohydrate	20%
Crude Fat	16%
Crude Fibre	4%
Moisture	10%
Zinc	200 mg/kg
Selenium	0.35 mg/kg
Vitamin E	150 IU/kg
Taurine	0.1%
L-Carnitine	30 mg/kg
Omega-6 Fatty acids	2.5%
Omega-3 Fatty acids	0.4%
Total Microorganisms	2200000 CFU/kg

-Retrieved from the bag of dog food (Small Formula Chicken & Vegetable) produced by Kirkland Signature

Table 4-2 Dog food and dog food medium composition measured in lab

	Dog food pellets (1 g)	RDF (0.778 g/L)	FDF (10x)
TCOD (±SD)	1330 mg / 1 g dog	1200±100 mg/L	1000±80 mg/L
SCOD (±SD)	-	130±20 mg/L	940±60 mg/L
pH (±SD)	-	6.8±0.2	6.7±0.2
Conductivity (±SD)	-	340±70 µS/cm	900±110 µS/cm

4.3.1.1 Phase 1 – reactor start-up

After one month of start-up with SWW the initial reactor consistently showed a typical maximum output voltage of 0.64 V immediately after feeding which lasted for 1.8 days (43 h) before declining. The COD

removal for each cycle during this period was 84±10%. An example of this performance can be seen in the first 7 days of Figure 4-2.

4.3.1.2 Phase 2 – first feed change, SWW to RDF

Immediately after the feed changed to RDF the reactor performed differently, the maximum voltage output period lasted 150 h, it took 8.12 days (195 h) to remove 94% of the COD during the first feed cycle. The degradation process sped up with a shorter best performance period (0.52±0.02 V, 55-60 h) with a slightly lower COD removal rate per cycle (89±2%). The culture adjusted to the new feed within 3 feed cycles (Figure 4-2).

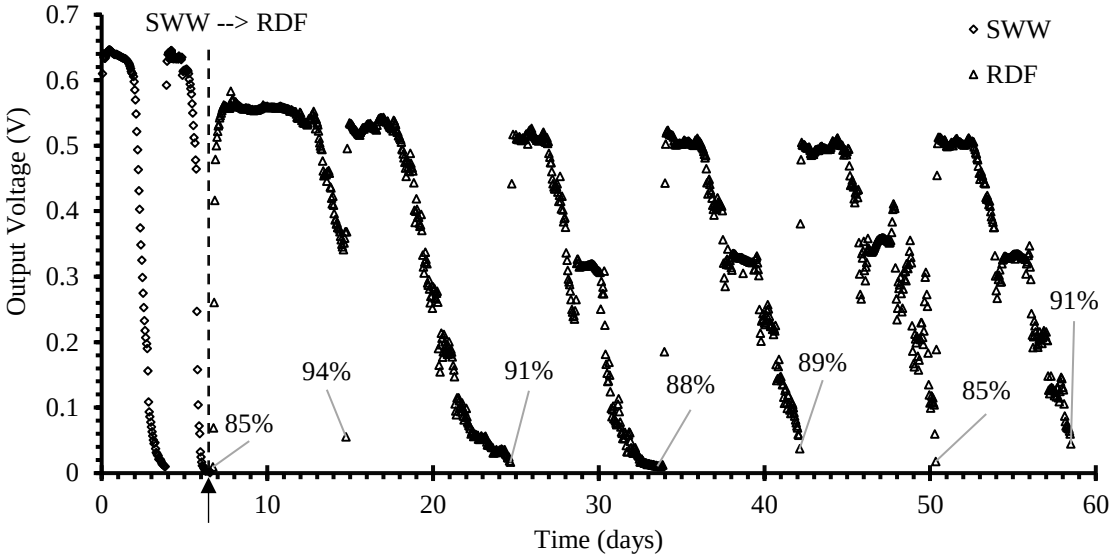

Figure 4-2 MFC output voltage and COD removal efficiency when changed from SWW to RDF
The symbols represent the output voltage, the numbers showed in the graph represent the COD removal between a measurement directly after the feed to just before the next feed.

A typical cycle of the output voltage and COD of the reactor when fed with SWW and RDF after reaching steady state are given in Figure 4-3. The COD after 24 h (COD_{24}) was down from 1308 mg/L to 551.7 mg/L when fed SWW, compared to 663 mg/L to 76 mg/L when fed RDF. It is necessary to point out that the COD measured when fed RDF was soluble COD as the medium was prepared by dissolving dog food

powder into RO water, and the dog food particles were observed to quickly settle down to the bottom of the reactor several minutes after each feed.

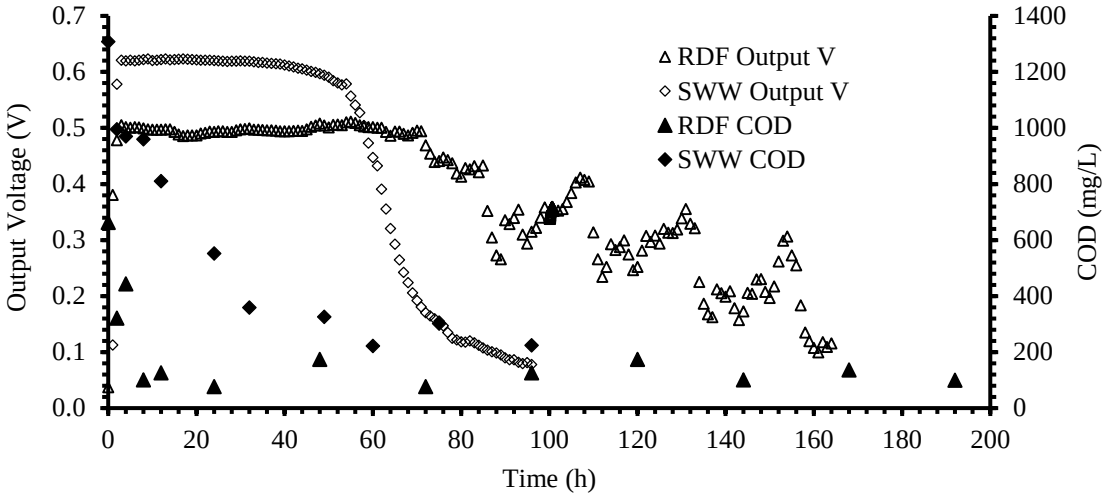

Figure 4-3 Output voltage performance comparison when MFC's were fed SWW or RDF

An interesting common phenomenon was noticed, when the voltage of the reactor declined to about 50%-60% of the of the maximum value (from 0.54 V to ~0.3 V); it fluctuated between 0.28-0.35 V for around 3 days (70-80 h) before further descending, as shown in the last four cycles in Figure 4-2 and in Figure 4-3. Several tests were carried out to better understand the possible reason for this phenomenon.

The impact of sunlight was first investigated. In this lab the MFC station was near a window, which was exposed to direct sunlight from about 11 am to 2 pm in the summer. This was close to the time when the short voltage recovery stage occurred. A test was carried out by covering the MFC reactor with a box made from opaque wood to block the sunlight completely; a gap on the back side of the box was left open to allow air exchange. During this test the phenomenon still appeared, which indicated that it was not directly caused by sunlight. The direct sunlight as an energy source may have also caused an increase of the environmental temperature, which may result in a temporary improvement of the output voltage.

The impact of the room temperature was further considered, which was set to 20 °C but in practice showed a considerable range (±3 °C) every day. The highest temperature (~22 °C) was reached from 12 pm to 3

pm, and the lowest at midnight. The output voltage declined when the temperature decreased and recovered a bit when the temperature went up the next day. Other studies have shown that an increase in temperature led to the increase of both power output and COD removal. The higher temperature enhanced membrane permeability and microbial metabolism, meanwhile reducing the internal resistance due to higher internal liquid conductivity (Gonzalez del Campo et al., 2013; Jadhav and Ghangrekar, 2009; Martin et al., 2010; Michie et al., 2011; Qiang et al., 2011; Tang et al., 2012). In this study, the change of temperature could have acted on the microbial activity in the reactor which was reflected in the output voltage. This also explained why this phenomenon appeared at the voltage declining stage. Initially the reactor had enough nutrition so that the rate limiting step of electricity generation in this stage was cathode surface area (as described previously). However, after the maximum output period (0.54±0.02 V, 150 h), the COD load caused the biological system to become the limiting factor. In addition to the COD strength, the environmental temperature probably contributed to the fluctuation of voltage.

Another proposed reason for this assumption is the occasional dissolution of dog food particles providing additional carbon. This was tested by examining the COD measurements during this period, they ranged unstably from 117 mg/L to 254 mg/L as shown in Figure 4-3. This indicated that carbon periodically leached out from the settled dog food chunks and was then used as fuel for the reactor. This observation was reinforced with each feed of the reactor with RDF medium (Figure 4-2). Correspondingly, it was eased when the feed was changed to FDF (Figure 4-4) or SWW (Figure 4-5), both of which contain only soluble organic matter. The results show that the degradation of RDF takes more time when compared to SWW when fed at the same COD strength only reaching ~85% removal in 9 days vs 3 days for SWW. This is advantageous since dog food would have to be added less frequently to maintain reactor health.

4.3.1.3 Phase 3&4 – RDF to FDF and 10x FDF

To further investigate if the regularities in reactor performance observed during RDF feeding were due to the impact of particle dissolution, the feed was filtered (FDF). The output voltage and COD removal are

shown in Figure 4-4. After changing from RDF to FDF, the maximum output voltage dropped slightly from 0.54 V to 0.5 V and the reactor showed a much shorter stable performance period (8 h during the first two cycles and 4 h for the following cycles), the COD removal reached 79% (from 346 mg/L to 70 mg/L) during the first cycle, then performed stably at 51-53% removal for several cycles. Sediment (mostly dog food particles from previous feeds) were observed to reduce to an insignificant amount after 3 cycles, which indicated the decomposition of dog food particles that settled down to the bottom was complete and the voltage measured was due only to the energy from the current feed.

The COD of the FDF was 10x lower than the COD of RDF so 10x FDF was prepared. The 10x FDF more accurately simulates the RDF in terms of COD. A much longer stable performance was observed when the reactor was fed 10x FDF (40-45 h). The COD removal efficiency increased immediately from 51-53% to 88% per cycle. This suggested the reactor was more active when fed with higher strength medium, resulting in longer lasting output voltage and higher COD removal efficiency.

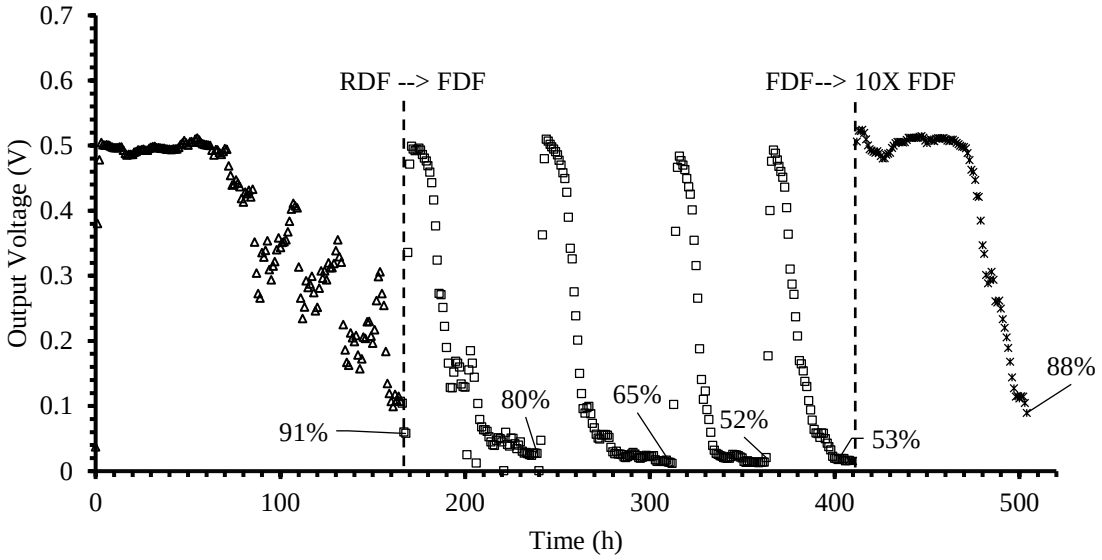

Figure 4-4 MFC output voltage and COD removal efficiency when changing from RDF to FDF
The numbers showed in the graph represent the COD removal between a measurement directly after the feed to just before the next feed.

4.3.1.4 Phase 5&6 RDF to SWW

To simulate the transition back to active production season, the reactor was changed back to RDF for one month (phase 5) and finally changed back to SWW for another month (phase 6), the maximum output voltage when changed from RDF to SWW (Figure 4-5) increased immediately from 0.52 V to 0.64 V without any lag phase, with similar COD removal efficiency (85±4% for RDF vs 85±3% for SWW).

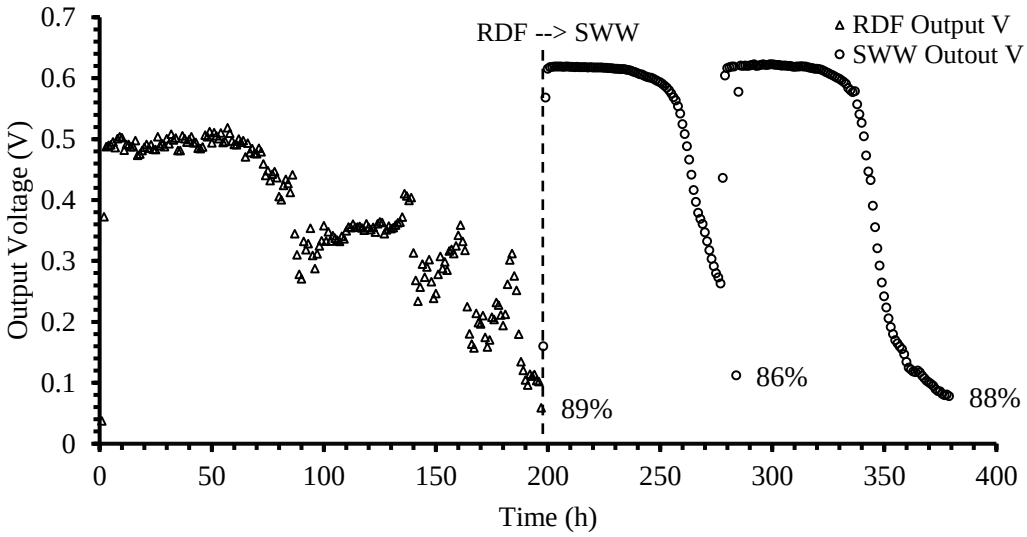

Figure 4-5 MFC output voltage and COD removal efficiency when changing from RDF to SWW
The numbers showed in the graph represent the COD removal between a measurement directly after the feed to just before the next feed.

4.3.1.5 Discussion of the impact of seasonal changes in reactor feed

A summary of the reactor performance during the experiments to examine the effect of feed type is shown in Table 4-3. The pH, COD removal efficiency, power generation and energy recovery efficiency are presented for comparison.

Table 4-3 Comparison of reactor performance when fed different feed stocks

Phase	1 (n=18)	2 (n=8)	3 (n=4)	4 (n=4)	5 (n=4)	6 (n=18)
Media fed	SWW	RDF	FDF	10x FDF	RDF	SWW
Media COD (mg/L) (±SD)	1000±20	1200±100	100±8	1000±80	1200±100	1000±20
Phosphate buffer (mM)	10	-	-	-	-	10
Initial COD (mg/L) (±SD)	930±20	1100±70	190±50	870±40	1040±30	920±40
pH (±SD)	6.5±0.2	6.8±0.2	6.7±0.1	6.7±0.1	6.8±0.2	6.5±0.2
COD removal in 24h (%) (±SD)	82±5	37±3	62±8	81±1	39±3	82±5
COD removal / cycle (%) (±SD)	84±10	90±3	65±14	83±4	89±4	85±3
Feed frequency (days)	3	8-9	3	4	8-9	3
Max. output V (V) (ER=10KΩ)	0.64	0.54	0.50	0.52	0.54	0.64
Max. output P (mW/m^3) (R_{Ext}=10KΩ)	410	290	250	270	290	410
Max. output period (h) (90% of Max V)	55-58	55-63	4	60-65	55-63	55-58
Total Electrical Energy (J/cycle)	10.1±0.6	9.5±0.8	1.5±0.1	6.5±0.6	9.5±0.8	10.1±0.6
Energy/ΔCOD ($x10^{-3}$ kWh/kgCOD) (±SD)	32±2	28±3	4.6±0.4	20±2	28±3	32±2

- *pH and COD removal efficiency*

The pH after the reactor was fed with SWW was stable at 6.5±0.2; 10 mM PB buffer was able to maintain the pH as shown in Chapter 3. Feeding with RDF, FDF and 10x FDF resulted in a stable pH (6.8±0.2 or 6.7±0.1), revealed that the culture was able to maintain a stable neutral pH without the addition of any buffer when dog food was used as feed.

The COD of all media was around 1000 mg/L except FDF which was close to 100 mg/L. The best COD removal rate in the first 24 h was achieved (~82%) when fed SWW, followed by 10x FDF (81%) and FDF (62%). The COD removal when fed RDF was much lower compared to any other medium, 37% removed. As discussed in Chapter 3 and Section 4.1, SWW contains only soluble components and is rich in sugars and small molecules such as VFAs and ethanol, which are easier to degrade. FDF is ~94% soluble, whereas RDF contains only ~11% of rapidly soluble components (SCOD:TCOD = 130 mg/L : 1200 mg/L), which means that most components need more time for solubilisation and decomposition. This also explains why the COD of FDF medium is only 8-10% of the COD of RDF (103 mg/L vs 1170 mg/L). In addition, RDF is rich in crude protein, crude fat and crude fibre as shown in Table 4-1, all of which degrade more slowly than the sugars, VFAs and ethanol in the SWW.

It worth pointing out that when fed FDF the COD removal rate for the first 24 h was relatively low (62±8%) compared to other feeds, initially the COD was 190±50 mg/L and dropped down to 80-100 mg/L within 24 h and kept stable until the end of the cycle. This is similar to what was observed from all reactors, that the lowest COD obtained when using MFC treating winery wastewater was 100-400 mg/L depending on the feed strength. After reaching this stage the reactor will contribute neither output power nor COD removal. This has also been observed by other researchers (Gude, 2016; Penteado et al., 2016b; Walter et al., 2016).

More importantly, the results for the final feed change (from RDF to SWW) indicated that the system reacted swiftly when changed back to SWW medium, both on output voltage and COD removal. This affirmed that dog food is a good choice as an alternative feed during the off season, which can maintain the system in an active stage and allow a quick response to the upcoming busy season.

- *Power generation efficiency*

The maximum output voltage and power (0.64V, 410 mW/m^3, ER=10 KΩ) was obtained when fed SWW. Three types of DF feed resulted in similar performance although RDF was slightly better than FDF and 10x FDF. When looking into the maximum output period, SWW, RDF and 10x FDF all resulted in 55-65 h of maximum output whereas FDF only sustained power production for 4 h. The results were expected considering the 10 times difference on the inlet COD between FDF and any other feed.

- *Electrical energy recovery efficiency*

The highest electrical energy recovery was achieved when the reactor was fed SWW providing 10.1±0.6 Joules per cycle and 32(±2) $x10^{-3}$ kWh/kg COD. The reactor fed RDF was close, achieving at about 9.5±0.8 Joules per cycle and 28(±3) $x10^{-3}$ kWh/kg. When comparing the feed frequency (3 days for SWW and 8-9 days for RDF) it indicated that although RDF lasted much longer as nutrient source, the total electrical energy amount recovered per cycle and per kg of COD was similar when compared to SWW.

4.3.2 Effect of SWW strength on MFC performance

As described in Section 4.1.1, winery production can result in wastewater of varying COD concentration depending on the activity. To observe the impact of SWW medium strength on MFC performance, SWW medium with increasing COD strength was prepared and fed to the reactor as described in Section 2.2.1. The PB concentration was kept at the ratio of COD (mg/L) : PB (mM) = 100:1 when increasing COD strength as determined in Chapter 3. This adjustment led to an improvement on not only the stability of the output voltage, but also the COD removal efficiency, power generation and energy recovery efficiency. Examples of output voltages for each stage during stable performance are shown in Figure 4-6. It shows that increasing the COD strength of the SWW resulted in small increases in output voltages. The most marked difference was sustainability of the reactor's maximum output period. The shape of the output voltage curves also changed with the strength of the feed. When fed with lower COD levels power production dropped quickly and smoothly. As the feed COD increased the output voltage curve reflected a more gradual but fluctuating decline. This was more obvious when the reactor was fed 4x strength feed. One of the proposed reasons was the temperature, as described in the previous section. The fluctuating of the output voltage appeared on a daily basis which corresponded to the temperature change. Another reason proposed is the growth and decomposition of biofilm. The increase of feed strength caused an increased growth of biofilm, which can result in the change of internal resistance and conductivity, which is reflected on the output power. This is further discussed in Chapter 5. The reactor performance when fed different feed strengths is summarized in Table 4-4.

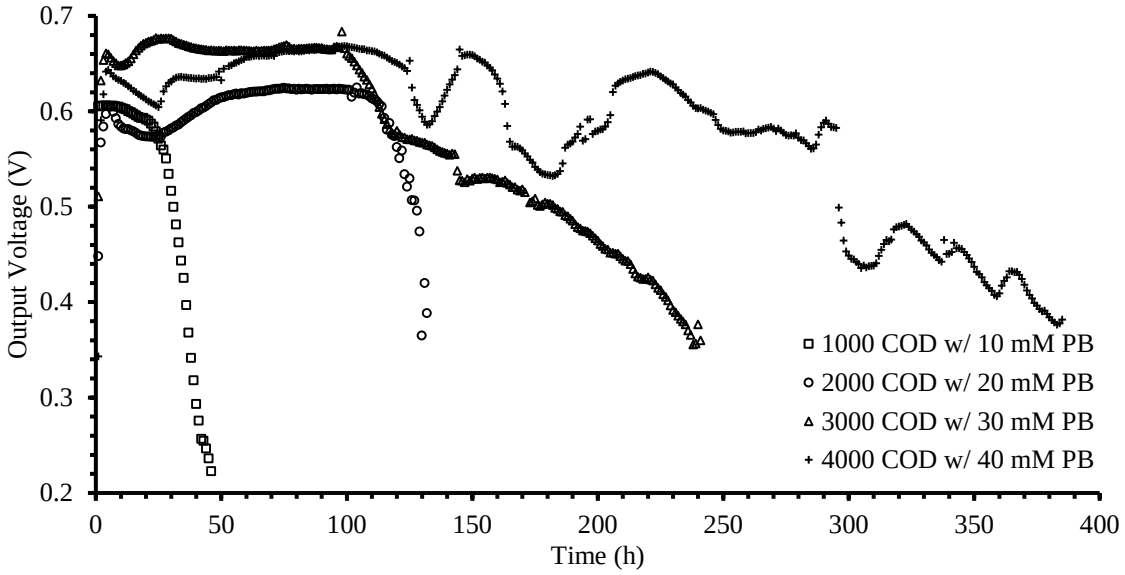

Figure 4-6 Output voltage of steady state when fed with different strength of SWW

Table 4-4 Comparison of reactor performance under different feed strength

Phase	1 (n=9)	2 (n=6)	3 (n=4)	4 (n=2)	5 (n=1)
Media COD (mg/L)	1000	2000	3000	4000	10000
Phosphate buffer (mM)	10	20	30	40	100
Initial COD (mg/L)	933±79	1616±32	2436±171	3619±310	8945
pH	6.5±0.2	6.5±0.2	6.5±0.2	6.5±0.2	6.5±0.2
COD removal 24h (%)	79±3	73±4	67±1	59±1	27
COD removal / cycle (%)	82±7	86±5	90±3	91±4	96
Feed frequency (days)	3	5-6	10-12	14-16	28
Max. output V (V)	0.60	0.62	0.68	0.67	0.67
Max. output P (mW) (ER=10KΩ)	0.036	0.038	0.046	0.045	0.045
Max. output period (h) (90% of Max V)	45	120	112	196	366
Total Electrical Energy (J/cycle)	9.77	16.8	29.0	46.8	88.4
Energy/ΔCOD (kWh/kgCOD)	0.033	0.033	0.036	0.042	0.041

4.3.2.1 pH and COD removal efficiency

It was observed that the pH was well maintained at 6.5±0.2 if the COD to buffer ratio (COD(mg/L):PB(mM)) was 100:1. The COD removal efficiency within 24 h (both by percent and by concentration) and per feed cycle when fed with different medium strength is presented in Figure 4-7. The results revealed that within the first 24 h after each feed the COD removal (%) decreased linearly

corresponding to the increase of the feed strength. The concentration removed also increased linearly. This suggested that the reactor's absolute COD removal amount within first 24 h right after feed would increase if the inlet COD concentration increased. However, the total COD removal (%) per cycle was logarithmically related to the strength of feed medium. This indicates that there is a maximum efficiency in the reactor. The maximum efficiency can be estimated based on the correlations obtained in Figure 4-7.

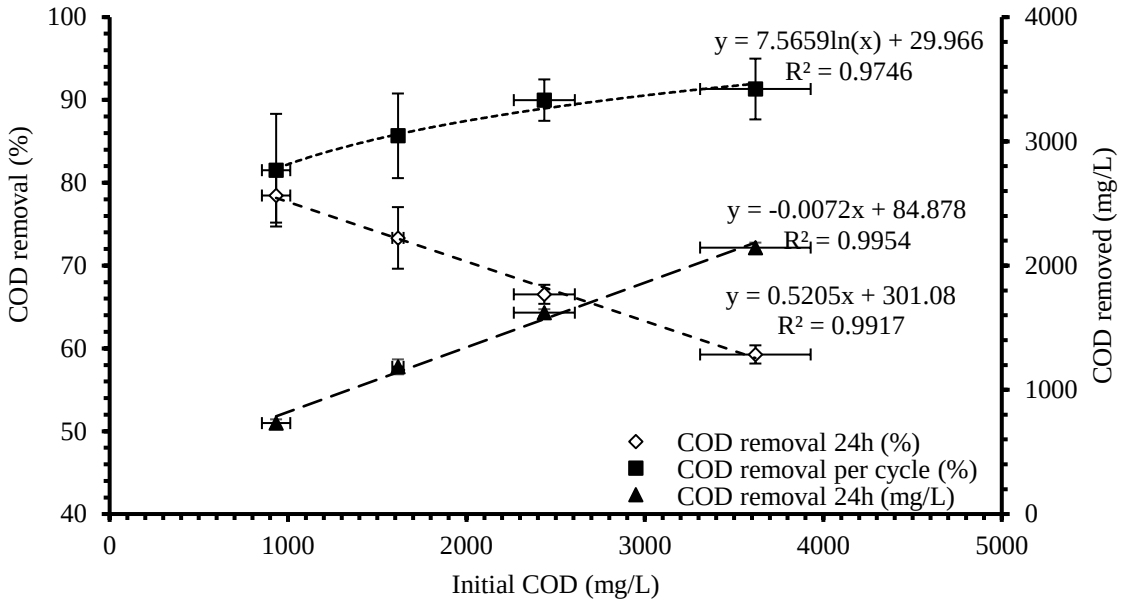

Figure 4-7 COD removal efficiency when fed with different strength of SWW

Firstly, the minimum COD that can be reached after treatment in MFC fed SWW is assumed to be 100 mg/L as discussed in Section 4.3.1.5. Assume the maximum treatment capacity for MFC is X mg/L. Therefore,

treatment efficiency Y (%)

$$Y = 7.5659 \ln(X) + 29.966, \quad \text{eq. 4-5}$$

since the maximum treatment efficiency Y approaches to 100%, and

$$Y = (X-100) / X = 100\%. \quad \text{eq. 4-6}$$

Therefore,

$$100 = 7.5659 \ln(X) + 29.966, \quad \text{eq. 4-7}$$

$$X = 10470 \text{ (mg/L)}, \quad \text{eq. 4-8}$$

and,

$$Y = (10470\text{-}100) / 10470 = 99.04 \text{ (\%)}. \quad \text{eq. 4-9}$$

Correspondingly, the COD removal efficiency after 24 h (COD_{24}) can be calculated when the COD of medium fed being 10470 mg/L as

$$COD_{24} \text{ (mg/L)} = 0.5205 \times (10470) + 301.08 = 5750.6 \text{ (mg/L)}, \quad \text{eq. 4-10}$$

$$COD_{24} \text{ (\%)} = 0.0072 \times (10470) + 84.87 = 30.43 \text{ (\%)}. \quad \text{eq. 4-11}$$

As discussed in Section 2.2.1, the maximum COD of winery wastewater measured from Tantalus Vineyards is 11000 mg/L. To verify if the reactor can handle the full strength SWW, 10x strength SWW medium was made (10000 mg/L COD, 100 mM PB, 100 mM NaCl, pH 6.5) and fed to the same reactor right after 4x strength SWW medium was tested. The results show that the pH was stable at 6.5±0.2 and, the COD removal (%) within 24 h and per cycle reached 27% and 96%, respectively, which are a bit lower than expected (30.4% and 99.0%). However, when considering the maximum capacity of the reactor can be due to the surface area of electrodes, the treatment efficiency under maximum COD strength could be limited by the cathode surface area, as the maximum output power was stable at 0.045-0.046 mW without any improvement when the inlet COD of SWW was above 3000 mg/L as shown in Table 4-4.

4.3.2.2 Power generation and energy recovery efficiency

The maximum output voltage and power improved slightly when the inlet COD increased and finally reached the highest reading (0.67-0.68 V, 0.045-0.046 mV/m^3, ER = 10 KΩ) when inlet COD was above 3000 mg/L as shown in in Table 4-4. After this the increase of feed strength only led to a longer maximum

output period, e.g., when the feed COD changed from 3000 mg/L to 4000 mg/L, the maximum output period increased from 112 h to 196 h, and then to 366 h when the inlet COD reached 10,000 mg/L.

The total electrical energy recovery efficiency (J/cycle) and energy recovered per kg COD (kWh/ΔCOD) were found to be linearly related to the inlet COD in the range of 1000 mg/L to 4000 mg/L, and the total electrical energy recovery showed an excellent correlation to the initial COD ($R^2 = 0.9955$) as shown in Figure 4-8.

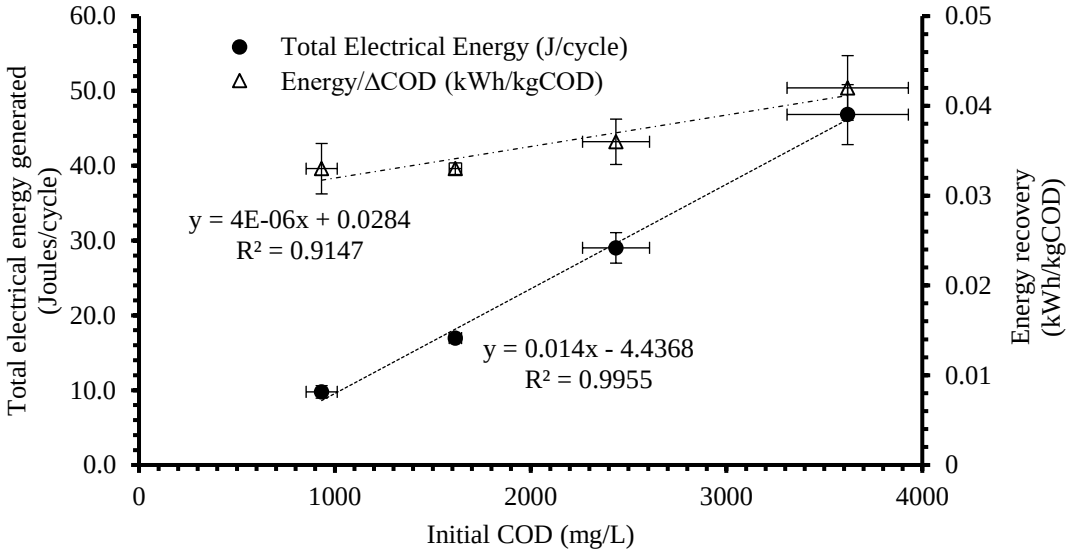

Figure 4-8 Recovered energy under different COD loads

However, when testing with 10,000 mg/L inlet COD, the actual values were lower than the expected trends (88.40 J/cycle vs 129.63 J/cycle, and 0.041 kWh/kgCOD vs 0.064 kWh/kgCOD). This can also be explained by the maximum capacity of the reactor being limited by the cathode area. Similar to the power generation efficiency, the electrical energy recovery efficiency would not be improved when the inlet COD was above a certain level (between 4000 mg/L to 10,000 mg/L). To overcome this obstacle an MFC reactor with more electrode surface area would need to be compared.

4.4 Summary

This chapter investigated the impact of seasonality on the performance of MFC fed winery wastewater. The results suggest that dog food is an efficient alternative feed for the winery wastewater system during the off season. When used as the MFC feed, it can effectively maintain the activity of the microbial system and boost the maximum output period without pH buffer addition. This feed was less efficient in terms of power generation and electrical energy recovery efficiency when compared to the same strength of synthetic winery wastewater. However, the purpose of adding dog food was not to produce power.

The performance of MFC fed synthetic winery wastewater highly depends on the COD strength of the feed. With sufficient buffer supply to maintain pH stable at 6.5, the COD removal (mg/L/24h) and energy recovery efficiency are linearly related to the strength of synthetic winery wastewater until the system limit of MFC reactor was reached, after that the increase of feed strength solely resulted in longer time without any efficiency improvement (both on COD removal and electrical energy recovery). In sum, changes on both feed type and strength led to changes in performance of the MFC reactors. This indicates that the seasonality of wine production is an important factor and can be addressed with specific operational design considerations.

Chapter 5. Investigation of The Effect of Operational Factors on MFC Treating Winery Wastewater

To enhance the performance of MFC, the limiting factors that can cause inefficiency or energy loss must be investigated. This chapter presents the study of the effect of external resistance, salt and the operational age on the performance of MFC reactors fed SWW medium. The external resistance was investigated as a control strategy to regulate the performance of an MFC reactor. Increasing the salt concentration (340 mM) was evaluated as a strategy to reduce the internal resistance. Additionally, the operational time of the system was investigated as a factor to determine if it affected the internal resistance (R_{Int}) and determined the overall performance of an MFC.

- *External resistance as a control on MFC performance*

The external resistance (R_{Ext}) applied to the circuit and the internal resistance (R_{Int}) of the MFC are two parameters that dramatically impact the system performance. The external resistance impacts the treatment efficiency, electricity production and stability, as well as the microbiological activity including microbial diversity, microbial population evolution, biofilm morphology, microbial metabolism and anode potential of MFC (del Campo et al., 2016; Jung and Regan, 2011; Liu et al., 2016; Lyon et al., 2010; Rismani-Yazdi et al., 2011). The external resistance equals to the ratio between the cell voltage (the potential difference of the cathode and anode) and the current (the number of electrons transferred through the circuit within a certain period) (del Campo et al., 2016). It controls the output voltage by limiting the flow of electrons (Jung et al., 2011). A low external resistance or high anode potential encourage the microorganisms in a mixed culture to use the anode for electrode respiration; therefore, a thicker and high diversity anodic biofilm community will be achieved (Liu et al., 2016), whereas higher external resistance or lower anode potential will discourage electron transfer to the electrode, thereby altering the metabolic activities and diversity of the anodic microbial community. Similar to other power sources, the power generation of an

MFC reactor can be maximized from enhanced loading rates when operated under an external load close to its internal resistance (Aelterman et al., 2008). Regulating external resistance while considering the impact of other operational parameters such as temperature, pH, feed strength and composition can optimize MFC performance (Pinto et al., 2011).

Automatic control strategies have been adopted to MFC study to obtain optimal conditions for power production; these strategies keep an optimal external resistance on the system to minimize the ohmic loss occurring during operation (Clauwaert et al., 2008). The commonly used strategy for external load optimization is usually referred to as Maximum Power Point Tracking (MPPT). The MPPT algorithm is used to maximize the MFC power extraction under all conditions by matching the external resistance to the internal resistance as it changes due to the operational conditions. Pinto et al. (2011) used a simple perturbation/observation (P/O) algorithm to maximize MFC power output by adjusting external resistance to the internal resistance of MFCs fed with either acetate or synthetic wastewater. The P/O algorithm achieved a highly improved coulombic efficiency when the MFC was operated under complex conditions such as various influent compositions, organic loads, and temperatures. A similar study was also reported by Premier et al. (2011), which showed that the power production and coulombic efficiency were improved by 530% and 540%, respectively, when using a logic based controlled external load instead of a static resistive load. These studies show that higher power can be achieved by controlling resistance impedance.

Previous studies have mainly focused on optimizing the power production of MFC. When considering MFC as a wastewater treatment technology, the effect of the external resistance control strategy specifically on COD removal efficiency demands more attention. Due to the complexity of the microbial diversity, feed composition and running conditions, many researchers reported various results. In general, lower external resistance leads to higher COD degradation efficiency, with the increase of external resistance the COD removal will decrease (Kim et al., 2014; Li and Chen, 2018; Liu et al., 2016). Aelterman et al. (2008) reported that low methane production and stable power output were only obtained when external resistance was set close to the internal resistance in an MFC with a mixed consortium. Katuri et al., (2011) observed

distinct differences in anodic bacterial communities under a different external load and found that electrogenic bacteria enriched under higher current densities led to more sustainable power and higher substrate removal. Electrochemical impedance spectra (EIS) analysis showed a positive correlation between internal resistance and external resistance, with an increase in anodic biofilm mass and extracellular polymer substances (EPS) at higher external resistance (Liu et al., 2016). Other research reported conflicting results. del Campo et al. (2016) reported the increase in external resistance resulted in lower power production but better COD removal, suggesting treatment efficiency was enhanced when the external resistance was higher; this is in contrast to other studies. The proposed reason was that the majority of organic matter in the anode chamber was consumed by non EAB bacteria, which resulted in better waste treatment but little power generation.

Previous studies also focused on feeding with pure feed (such as acetate or glucose) or synthetic feed and pure cultures. In this study, the impact of external resistance on a lab scale MFC inoculated with a complex mixed culture was investigated, to explore the external resistance as a control strategy on the reactor in terms of wastewater purification and power generation efficiency.

- *Factors affecting internal resistance (R_{Int})*

Internal resistance is a critical parameter of MFC performance (Fan et al., 2008; Manohar and Mansfeld, 2009; Zhang and Liu, 2010). The R_{Int} is partitioned into three components: anodic resistance (R_a), cathodic resistance (R_c), and ohmic resistance (R_Ω) (Liang et al., 2007). Single chamber MFCs typically perform better than dual chamber MFCs due to lower cathode and membrane resistances (Fan et al., 2008). In the review on internal resistance of MFCs by Fan and Li (2016), they emphasised the importance of monitoring the internal resistance for enhancing power output as well as ensuring stable reactor performance.

In addition to selecting suitable electrode material, an alternative way to decrease internal resistance is to increase anode fluid ionic strength, which reduces the solution resistance (Aaron et al., 2010). Ionic strength determines the resistance of ion migration within the electrolyte. NaCl is commonly used as an electrolyte

to increase the ionic strength and improve the mass transfer of charged particles (Gil et al., 2003). Jang et al. (2004) observed a rise in current generation from 3.5 up to 7.7 mA by increasing cathodic salt concentration from 0.1 to 1 M in dual chamber MFC. Another research showed that increasing the ionic strength of the anodic solution from 100 to 400 mM by adding NaCl improved power output from 720 to 1330 mW/m^2 in a single chamber MFC (Liu et al., 2005a). Mohan and Das (2009) observed that increasing the salt concentration up to 10 mM NaCl improved power output with a maximum of 12.8 mW/m^2 in a dual chamber MFC; however, further increase to 15 mM decreased the power output. They suggested that the salt concentration is limited by the salt tolerance capacity of the anodic microbial community. Aaron et al. (2010) observed that increasing the ionic strength of the anodic fluid from 0.037 M to 0.37 M resulted in a decrease of total internal resistance from 22.5 Ω to 13.0 Ω and an increase of the maximum power density from 378 to 793 mW/m^2.

To overcome the inhibition of anodic communities by salt, some studies have reported the inoculation of salt tolerant bacteria and archaea in their MFC. A salt tolerant strain of *Shewanella marisflavi* capable of reducing Fe (III) and generating power (3.6 mW/m^2) at a high ionic strength of up to 291 mM was previously reported (Huang et al., 2010). High salt tolerant archaea (*Haloferax volcanii* and *Natrialba magadii*) produced maximum power of 50.98 and 5.39 $\mu W/cm^2$ at ionic strengths 2.9 and 3.6 M, respectively (Abrevaya et al., 2011). Miyahara et al. (2015) reported that increasing the NaCl concentration from 0 to 1.8 M in a single chamber MFC inoculated with rice paddy-field soil and continuously supplied with acetate showed an increase in power output up to 504±41 mW/m^2 (NaCl = 0.1 M); after that power production decreased markedly (1.6±0.3 mW/m^2 when NaCl = 1.8 M) and they suggested that the optimum salt concentration in MFC is determined by solution conductivity and salt tolerance of EAB.

In addition, the performance of an MFC can change within the overall time it has been operated. This can be due to the change in the internal resistance, as it reflects the growth of the electrode biofilm, and the accumulated changes contributed by various parameters (such as aqueous conductivity changes, possible electrode corrosion, electrode aging, and biofilm fouling on cathode membrane) will result in changes to

the MFC performance (Penteado et al., 2016a; Syron and Casey, 2015). Some studies reported the sludge age of each cycle (SRT) affected the reactor performance, for instance Penteado et al., (2016a) found that decreasing the SRT (7 day to 1 day) improved the coulombic efficiency (3.4% to 42.2%) and maximum power density (58 to 890 mW/m^2), but the change of SRT did not improve the COD removal rate which oscillated around 600 mg/L/d at all SRT studied. No report was found to investigate the impact of general reactor age on MFC performance.

In this study the impact of high salt condition (340 mM, 20 g/L) and the incubation age on MFC internal resistance, with their reflection on the performance of MFC reactors (in terms of output power and COD removal) were tested.

5.1 Experimental design and analytical methods

MFC reactors were fabricated as described in Section 2.1 The medium preparation and inoculation process are detailed in 2.2 with further adjustment. After inoculation reactors were operated in batch mode fed SWW medium until steady state was reached. Each reactor was loaded with an external resistance, the output voltage was monitored using NI USB 6210 Multifunction I/O device and recorded by NI SignalExpress 2015 every 2 min.

5.1.1 External resistance

One reactor was chosen to study the impact of the external resistance. This reactor was inoculated with anaerobic winery sludge as described in Section 2.2 with 10 mM PB to maintain the pH at 6.5. The reactor was fed SWW medium as shown in Table 2-2 (COD 1000 mg/L, PB 10 mM, NaCl 10 mM, pH 6.5), the following experimental design was followed, analytical methods as described in Section 2.3 were regularly used to monitor the chemical and electrical parameters.

Phase 1 – Maintained until steady state was reached (R_{Ext} = 10 KΩ) (two months),

Phase 2 – Evaluated the internal resistance using polarization slope method (Section 2.3.2.3) to determine the minimum external resistance to be chosen,

Phase 3 – Changed to 2.5 KΩ and maintained until steady state was reached to obtain several cycles of stable performance (~1 month),

Phase 4 – Changed to 1 KΩ and maintained until steady state was reached to obtain several cycles of stable performance (~1 month),

Phase 5 – Changed to 0.5 KΩ and maintained until steady state was reached to obtain several cycles of stable performance (>1 month).

5.1.2 Internal resistance

An MFC reactor was used to investigate the impact of high salt conditions (340 mM). The reactor was inoculated as described in Section 2.2 except that 29.3 mL of 1 M NaCl solution and 10 mL of 100 mM phosphate buffer (PB) were added to make the final salt concentration of the medium at 340 mM (20.0 g/L) and pH of 6.5. After inoculation the reactor was maintained using high salt SWW medium (COD 1000 mg/L, PB 10 mM, NaCl 340 mM, pH 6.5).

Another reactor continuously fed with SWW medium (COD 1000 mg/L, PB 10 mM, NaCl 10 mM, pH 6.5) was monitored to investigate the impact of inoculation age on the internal resistance. The internal resistance of the reactor was initially measured using a MAS830L multimeter (Mastech Digital, Pittsburgh, PA, USA) after fabrication and prior to the inoculation. After inoculation it was evaluated using polarization slope method as described in Section 2.3.2.3. Samples from MFCs were subjected to routine microscopy analysis and SEM analysis as described in Section 2.3.3.

5.2 Results and discussion

5.2.1 Effect of external resistance on MFC performance

In this study, the reactor loaded with 10 KΩ external resistance reached steady state performance within the first 30 days of operation. After one month of stable performance, the internal resistance of the reactor was analyzed to determine the minimum external resistance required. Figure 5-1 presents an example of the output voltage during one steady state feed cycle under different external resistances. The duration was determined as the time to the rapid drop in power interpreted as the time to reach 90% of the maximum voltage. Reactors showed the same pattern with a stable output voltage at 0.63±0.01 V for 60-65 h from feeding prior to drop. The change from 10 KΩ to 2.5 KΩ resulted in a lower output voltage (0.52±0.01 V) and shorter maximum output period (52-55 h) but higher power density (23.7±0.9 mW/m^2 at 2.5 KΩ compared to 8.82±0.2 mW/m^2 at 10 KΩ) as shown in Table 5-1. Continuing to decrease the external resistance to 1 KΩ led to a slightly unstable initial output voltage within the first 24 h, similar to what was observed in Section 3.2.2.3 (Figure 3-8), when the buffer could not manage the pH. The pH during this period showed the same pattern decreasing to pH 5.7, and finally increasing back to 6.4±0.1 by 12 h. The power density reached a maximum of 27.4±0.9 mW/m^2 when the external resistance was 1 KΩ. When the external resistance was set to 0.5 KΩ, the output voltage was 51% lower than at 1 KΩ (from 0.35±0.01 V to 0.17±0.01 V) within 12 h after feeding, followed by a 30-hour stable output (0.15-0.17 V) and a smooth decline until the end of the cycle.

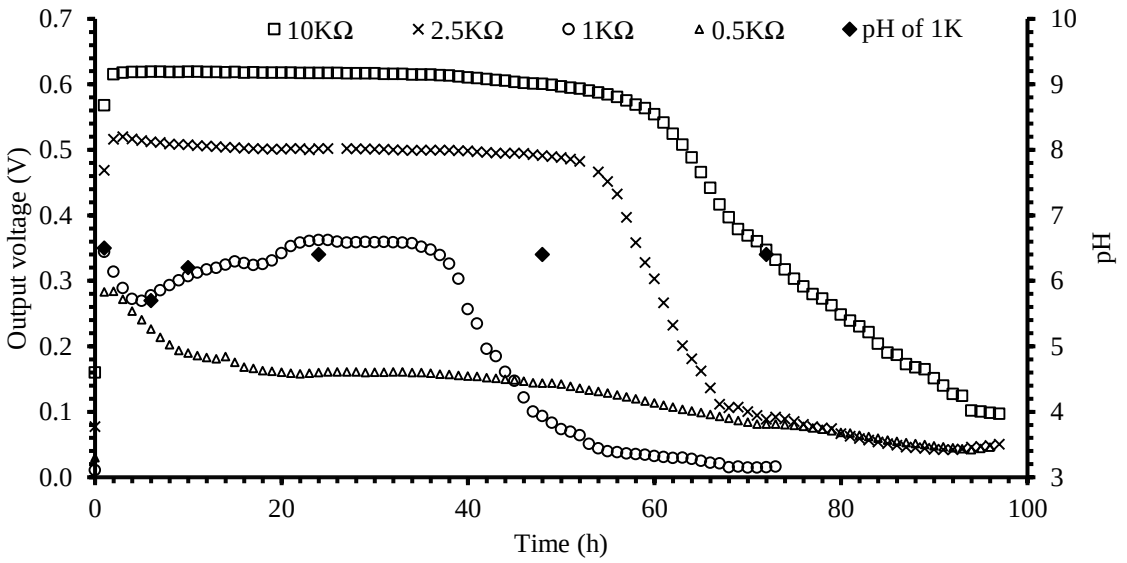

Figure 5-1 Output voltage of MFC at different external resistance at steady state in a single cycle with the pH of reactor when R_{Ext}=1 KΩ (COD 1000mg/L, PB 10 mM)

A comparison of the output voltage and COD degradation trend of the same reactor under different R_{Ext} (10 KΩ and 0.5 KΩ) is given in Figure 5-2. An MFC loaded with 0.5 KΩ took ~12 h to reach 85% COD removal, whereas with 10 KΩ it took ~60 h to reach a similar removal (87%). This indicated that decreasing external resistance led to an increase in the COD removal rate. A comparison of performance of MFC reactor loaded with different external resistance is given in Table 5-1.

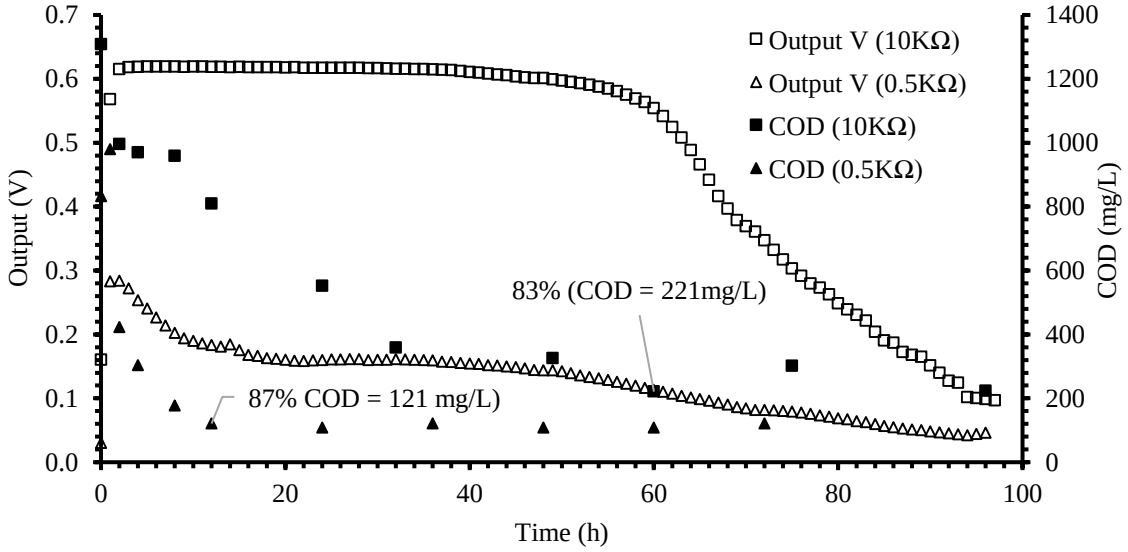

Figure 5-2 The output voltage and COD of reactors when using R_{Ext} 10 KΩ and 1 KΩ, respectively

Table 5-1 Comparison of reactor performance when loaded with different R_{Ext}

R_{Ext} (KΩ)	10	2.5	1	0.5
Phosphate buffer (mM)	10	10	10	10
Initial COD (mg/L) (±SD)	940±30	960±18	810±30	870±30
Final pH (±SD)	6.5±0.1	6.5±0.1	6.4±0.1	5.8±0.2
COD removal 24h (%) (±SD)	41±6	72±4.9	84±4	84±6
COD removal per cycle (%) (±SD)	84±5	83±7	86±2	83±6
Time consumed to reach 85% COD removal (h)	~60	32-36	~24	~12
Feed frequency (days)	4	4	4	4
Max. output V (V) (±SD)	0.63±0.01	0.52±01	0.35±0.01	0.17±0.01
Max. Power density (mW/m^3) (±SD)	400±10	1080±40	1250±40	560±80
Max. Power density (mW/m^2) (±SD)	8.8±0.3	23.7±0.9	27.4±0.9	12.2±1.7
Max. output period (h) (90% of Max V)	60-65	52-55	~40	-
Total Electrical Energy (J/cycle) (±SD)	10.4±0.4	25.0±1.0	19.8±0.6	12.0±1.7
Energy/ΔCOD (kWh/kgCOD) (±SD)	0.037±0.003	0.086±0.006	0.079±0.001	0.047±0.010
Coulombic Efficiency (%) (±SD)	1.70±0.10	5.0±0.4	6.7±0.2	8.3±1.1

- *pH and COD removal efficiency*

pH was measured each time a sample was collected and it was observed that the pH varied with the changes of external resistance. The pH was well maintained at 6.5±0.1 when R_{Ext} was 10 KΩ and 2.5 KΩ. However, the change of R_{Ext} to 1 KΩ led to a temporary pH drop 8 h after feed, followed by a gradual recovery within 24 h and stabilized to 6.4±0.1 as observed in Figure 5-1. Continuing to decrease the R_{Ext} to 0.5 KΩ led to a sharp pH drop to 5.8±0.2 within 8 h after feeding without recovery.

The COD removal rate accelerated dramatically with the decrease in R_{Ext}. The time needed to remove ~85% of COD (~800 mg/L) was plotted vs the R_{Ext} as shown in Figure 5-3. A linear relation was found between the log (R_{Ext}) and the time to reach 85% COD removal. This suggests that decreasing the external resistance can exponentially increase the COD removal rate before reaching the limitation of reactor (as shown in Section 4.3.2 the impact of SWW strength on MFC performance).

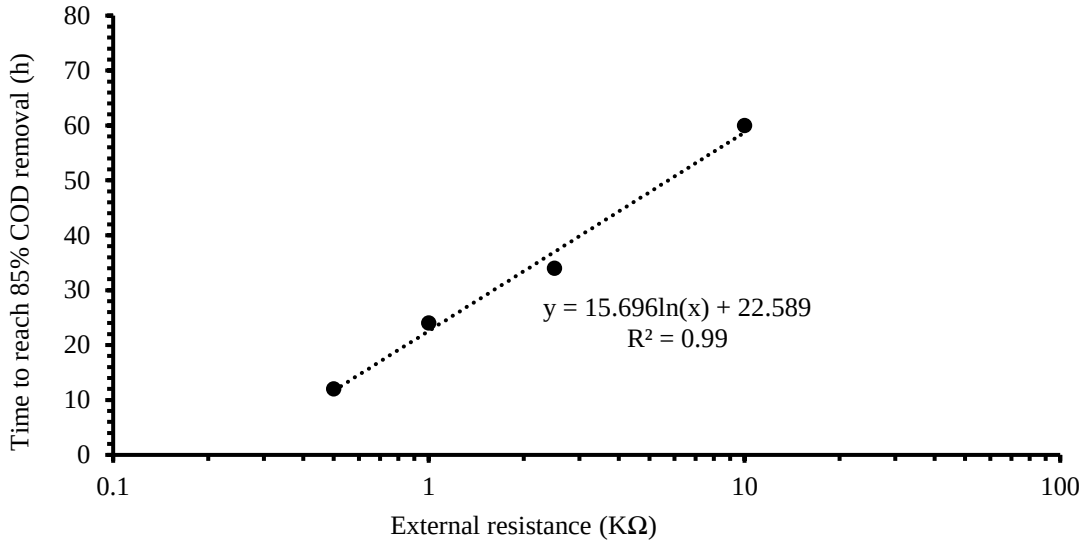

Figure 5-3 The time to reach 85% COD removal for an MFC reactor fed with SWW loaded with different external resistance (log R_{Ext})

These results suggested that decreasing external resistance resulted in the instability of pH by increasing the COD consumption rate. The faster COD degradation rate led to an accumulation of small acids and decrease in pH (proton concentration). The protons in the anode chamber diffused to the cathode, meanwhile electrons were transported to the anode by EAB and then to the cathode through an external circuit to complete the reduction reaction. Therefore, the power density improved with the increase of R_{Ext} and achieved the maximum (27.4±0.9 mW/m^2) at 1 KΩ. However, if R_{Ext} was decreased further to 0.5 KΩ, the protons accumulated and overcame the capacity of the pH buffer (PB 10 mM) and possibly the PEM (Nafion) diffusion capacity. Any of these resulted in proton accumulation in the anode chamber and caused the pH drop (Liu et al., 2016; Molognoni, 2014; Rismani-Yazdi et al., 2011).

- *Power generation and electrical energy recovery efficiency*

As observed in Table 5-1. The maximum power density improved with the decrease in R_{Ext} and reached the maximum at 27.4±0.9 mW/m^2 at 1 KΩ, compared to 8.8±0.3 mW/m^2 at 10 KΩ, then started to decline to 12.2±1.7 mW/m^2 when R_{Ext} continue to decrease to 0.5 KΩ. Meanwhile total Electrical Energy (25.0±1.0 J/cycle) and energy/ΔCOD (0.086±0.006 kWh/kg COD) were both obtained when R_{Ext} was 2.5 KΩ. The

decrease of R_{Ext} down to 0.5 KΩ also improved the COD removal efficiency (83±6%) and the columbic efficiency (8.3±1.1%), at which point the R_{Ext} was close to the R_{int}. This suggested that based on the purpose of the system, the R_{Ext} can be used as a control strategy by adjusting it to different levels. When the MFC is used for effective wastewater treatment, R_{Ext} should be kept close to R_{int} to obtain the highest removal rate. If the MFC system was designed to obtain the highest output power (in terms of power density), or highest energy recovery efficiency (Energy/ΔCOD), the R_{Ext} should be set higher than R_{int} to achieve the best performance.

5.2.2 Effect of inoculation age and high salt condition

The internal resistances of the blank reactors (filled with SWW medium prior to inoculation) used in this section were measured as 1.2±0.2 KΩ using a multimeter prior to study.

5.2.2.1 Effect of high salt condition

The internal resistance of the blank reactor (filled with high salt SWW medium prior to inoculation) used in this study was averaged as 1.2 KΩ. Within 5 months after inoculation the reactor had not reached a constant output voltage. The data in Figure 5-4 represents the last two month's output voltage data when loaded with a 10 KΩ resistor as R_{Ext}. An average of 0.22±0.15 V was obtained during this period.

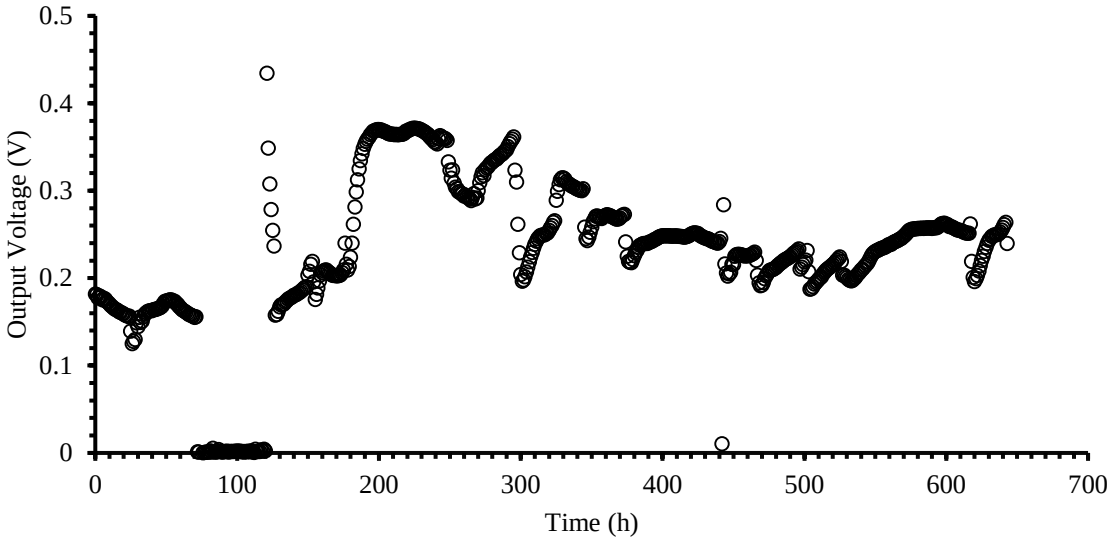

Figure 5-4 The output voltage of an MFC reactor fed with high salt SWW medium

The COD removal per cycle (24-72 h) obtained during the overall period was much lower (<40%) compared to the reactor maintained under 10 mM NaCl and, the average pH was 5.1±1.0 during the period. Yeast was observed during most of the microscopic analysis. It revealed that the inconsistent pH allowed yeast to grow even under high salt conditions. The internal resistance was constant at ~500 Ω after 60 days of inoculation. This was opposite to what Lefebvre et al. reported (2012), who showed that adding up to 340 mM NaCl reduced the internal resistance by 33% and increased the maximum power production by 30%. Our results indicated that 340 mM NaCl resulted in no improvement in internal resistance (~500 Ω in high salt conditions vs ~500 Ω in optimum conditions, both after 60 days incubation), but with 87% reduction in output power density (~1.20 mW/m^2 in high salt conditions vs 8.82±0.32 mW/m^2 in optimum conditions), and much less COD removal efficiency per cycle (<40% in high salt conditions vs 84±5% in optimum conditions).

The proposed reason is that although the increase of ionic strength helped reduce the internal resistance initially (1.2 KΩ vs 1.54 KΩ), the high salt condition prohibited the formation of EAB biofilms on the anode, meanwhile enhancing the formation of the thick EPS layer (>2 mm) on the cathode, which was two times thicker than the samples from typical cathodic biofilms in other studies (Figure 3-13). Meanwhile

oxygen diffusion also favors aerobic bacteria on the cathode. These would lead to the decrease of proton transport efficiency. EPS formed on the electrode especially the cathode would cause membrane fouling and decrease the efficiency of both energy recovery and COD removal (Syron and Casey, 2015). This could be observed in the SEM images and photo as shown in Figure 5-5. Anode SEM images (a1 and a2) showed fewer bacteria and thinner biofilms compared to the optimum conditions (Figure 3-14), meanwhile a tremendous EPS layer was clearly observed on both the anode and the cathode (a1, b1 and b2). The anode and cathode photo (c) showed the crystallization of NaCl on the cathode, meanwhile less biofilm was observed on the anode. Overall results indicated that no improvement on either power generation or COD removal was made by maintaining MFC in high salt conditions, compared to being fed with regular SWW medium.

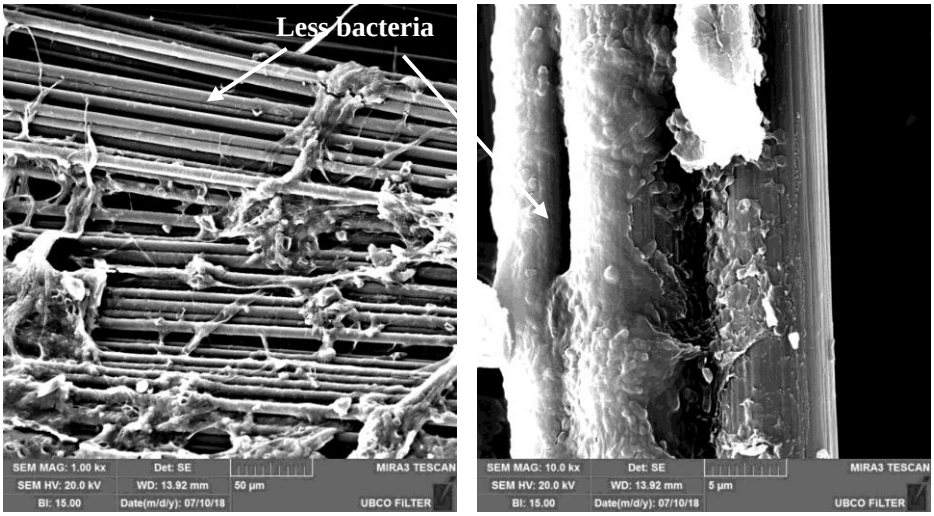

a1) a2)

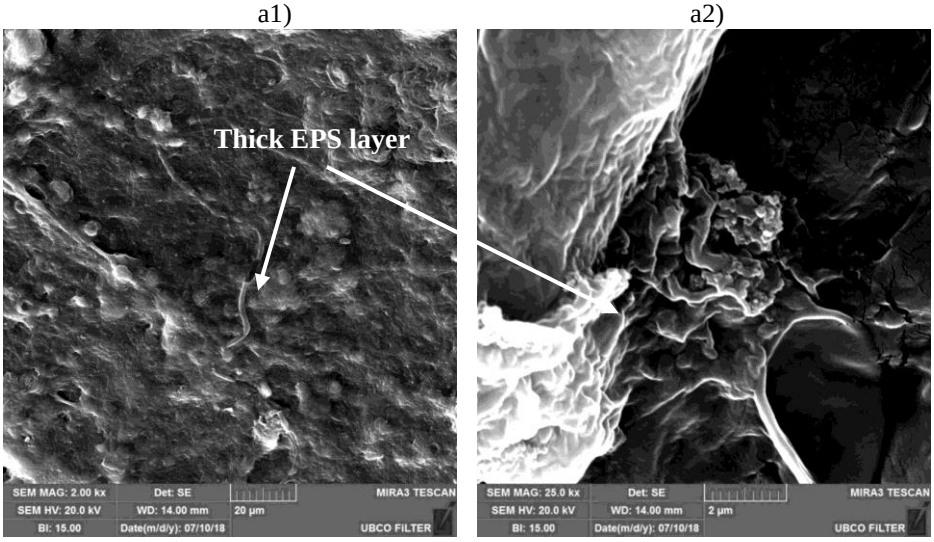

b1) b2)

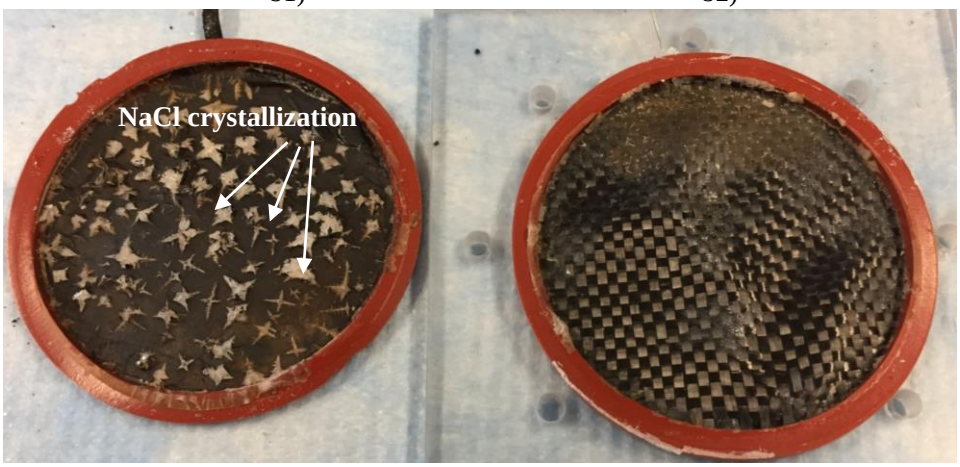

c)

Figure 5-5 SEM images and photo showing the anode and cathode under high salt condition
a1) and a2) showed the SEM images of the anode, b1) and b2) showed the SEM images of the cathode,
c) showed the salt crystallization and biofilm on electrodes

5.2.2.2 Reactor operational time

Polarization analysis conducted for the same reactor after different lengths of operation is shown in Figure 5-6. The maximum current density increased from 0.005 mA/cm^2 after 60 days to 0.020 mA/cm^2 after 250 days. The polarization curve showed three losses; activation, ohmic and mass transfer loss. The activation loss showed a similar pattern for all lengths of MFC operation; however, ohmic and mass transfer loss changed. The mass transfer loss decreased as the reactor aged. It was reported previously that mass transfer losses arise because of insufficient flux of reactant to the electrode or the flux produced from the electrode limits the reaction rate (Logan, 2008). In this study the proposed reason is that the optimum pH and sufficient maintenance favored the biofilm on the electrode, with longer time for biofilm formation, the reactor rate (higher maximum current density) increased and mass transfer losses decreased.

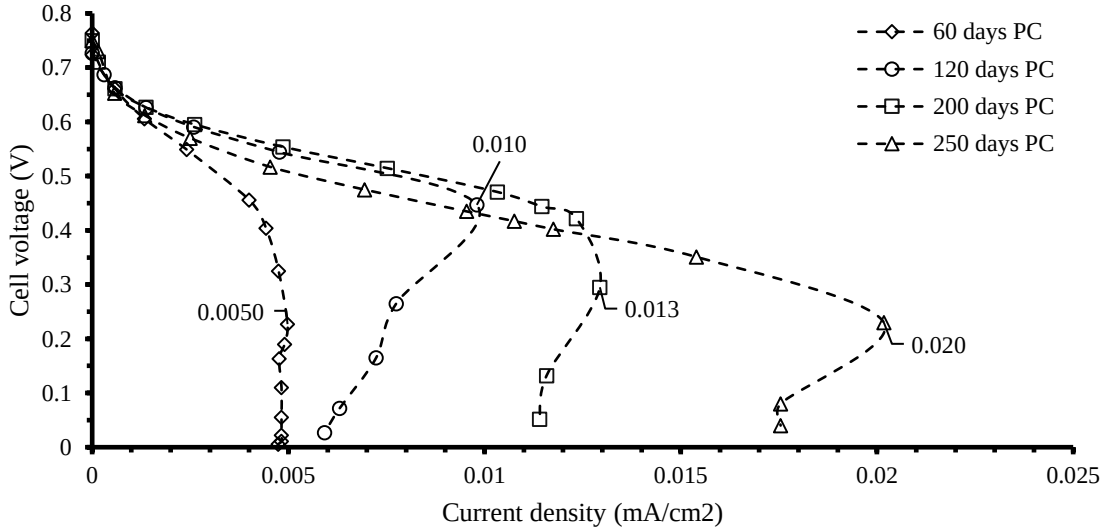

Figure 5-6 Polarization curve (PC) generated with MFC at pH 6.5 at different operational period
Values in legend stands for days after inoculation

The initial internal resistance of the blank reactor (containing SWW medium but without inoculation) was 1.54 KΩ. The internal resistance of the reactor at different times was evaluated using the polarization slope method as described in Section 2.3.2.3 and plotted in Figure 5-7. The internal resistance vs inoculation time was plotted as shown in Figure 5-8. As mentioned previously the slope of the region of interest can be

interpreted as the internal resistance. It was observed that after inoculation the internal resistance decreased between 0-120 days but became relatively steady after 120 days (0.4-0.5 KΩ), when the reactor was continuously maintained under optimum conditions.

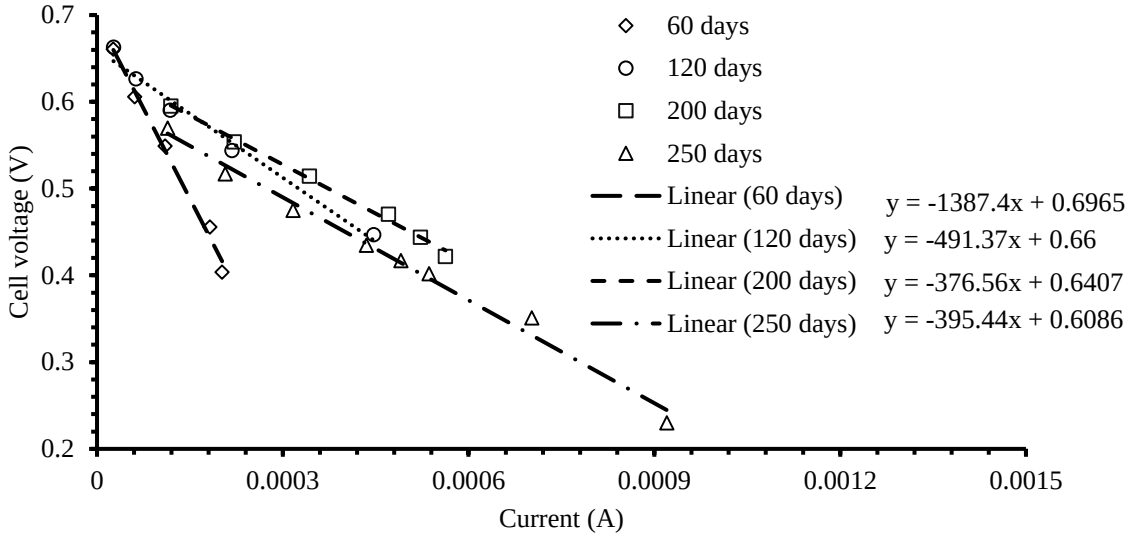

Figure 5-7 The internal resistance of reactors at different inoculation age
The days shown on the graph represent the days after inoculation

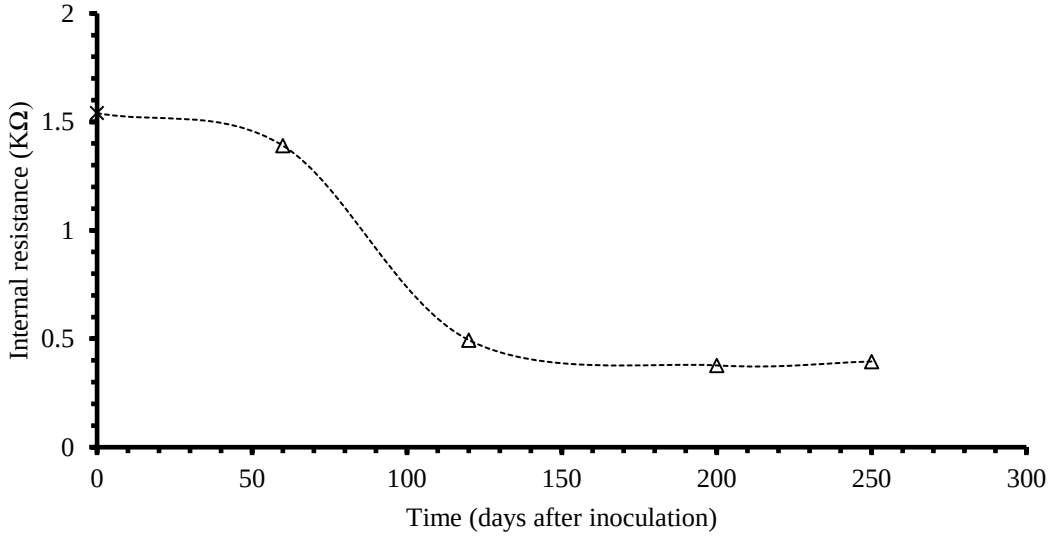

Figure 5-8 The internal resistance of the reactor at pH 6.5 at different operational periods

The power density curve (Figure 5-9) showed an increase in maximum power density with time, the maximum power density increasing to 50 mW/m^2 after 200 days and reaching 54.0 mW/m^2 at 250 days

(R_{Ext} = 500 Ω). This is a ~200% improvement compared to 18.2 mW/m^2 (1 KΩ) on the 120th day. It was also observed that a sharp decline in power density occurred after reaching maximum value at 120th day, whereas threshold power lasted longer at 250th day. As can be seen in both Figure 5-6 and Figure 5-9, increased current density eventually resulted in a large drop in voltage (or reflected as power density drop in Figure 5-9). This phenomenon, reported as 'Overshoot', was caused by the electron transfer limitation at the anode (Watson and Logan, 2011). During the polarization curve analysis process, the rapid increase of anode potential (due to rapidly lowering the external resistance within a short time interval) occurred; however, the current density was restricted due to electron transfer limitation at the anode (Ieropoulos et al., 2010). Watson and Logan (2011) therefore suggested that biofilms require much more time to adapt to the applied resistance, and so overshoot is observed.

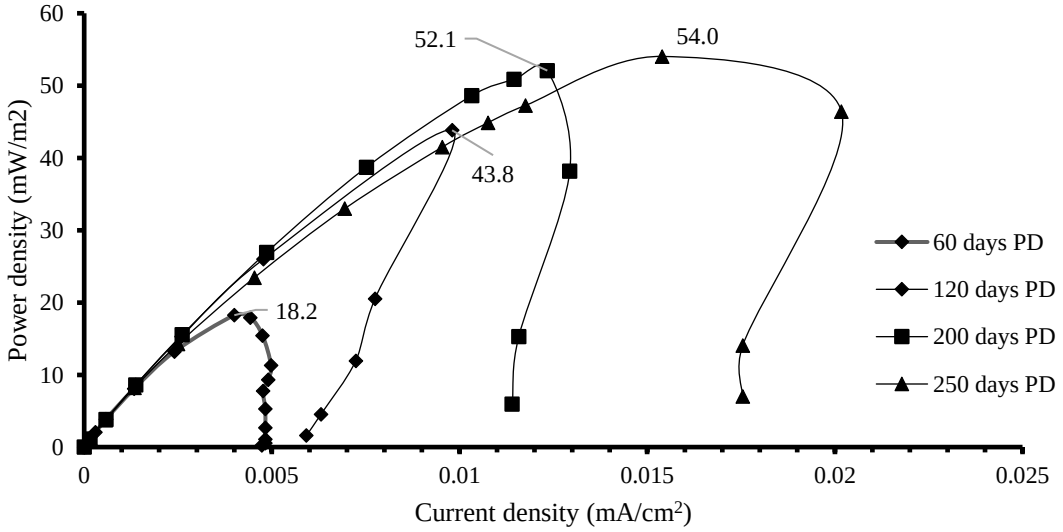

Figure 5-9 Power density curve (PD) generated with MFC at pH 6.5 at different operational periods
Values in legend stands for days after inoculation

SEM images of the bacteria and the biofilm on both anode and cathode from the reactor after 250 days are given in Figure 5-10, indicating the growth on the anode. A thick EPS layer and bacteria can also be observed on the cathode surface.

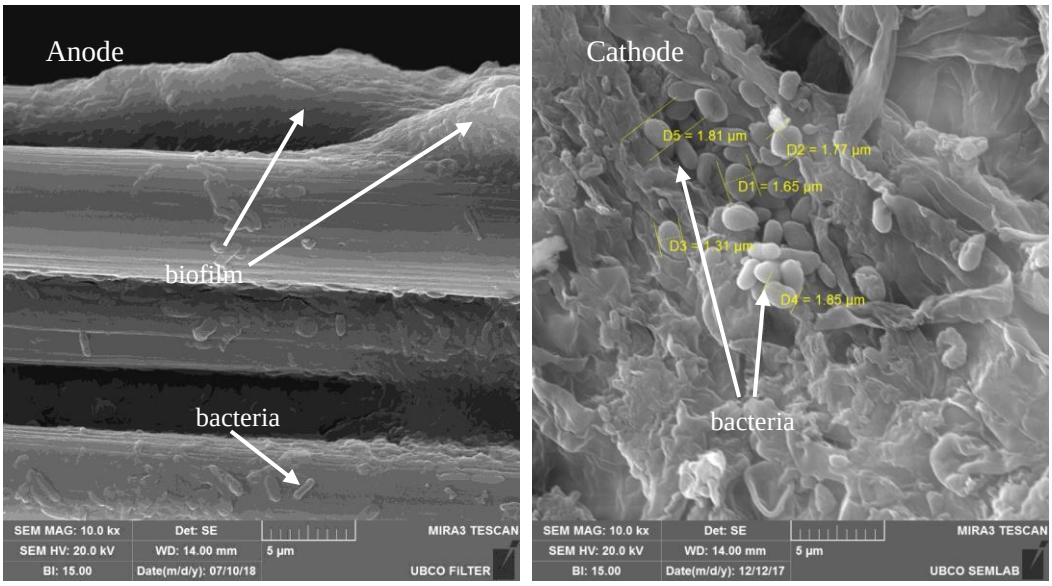

Figure 5-10 SEM images showing the biofilm on the anode (left) and cathode (right) of an MFC fed SWW medium after 250 days of inoculation

The results and images above indicate that the reactor maintained under optimum conditions (COD 1000 mg/L, PB 10 mM, NaCl 100 mM, pH 6.5) offered a suitable environment for the biofilm, led to stable COD removal and output power efficiency. More importantly, with a longer incubation time, the internal resistance was reduced due to formation of biofilm, leading to less energy loss and improved output power density.

5.3 Summary

This chapter shows that an external resistance control strategy can be used to optimize MFC system performance, however, the optimum external resistance would differ based on the main purpose of the system. When the MFC system is needed for a higher wastewater treatment efficiency, the external resistance should be kept close to internal resistance to obtain the highest removal rate. If the MFC system is designed to maximally extract energy from wastewater, the external resistance needs to be higher than internal resistance. Decreasing the external resistance close to internal resistance promoted the activation of EAB and resulted in faster COD degradation by exponentially improving the COD removal rate before

reaching the limitation of the reactor. The change of external resistance may change the pH due to the alteration of the COD consumption rate; therefore, proper pH buffer concentration adjustment is required. In addition, high salt conditions (340 mM) failed to improve the reactor performance; Increasing the time the reactor operated under optimum conditions, however, reduced the internal resistance and provided better output power density.

Chapter 6. Multi-substrate MFC model

This chapter presents the development of a comprehensive mathematical model of a single chamber MFC for winery wastewater treatment. Anode and cathode half-cell models were developed from the basic fundamental principles and linked together using the principles of mass and electron balance, and Ohm's law.

An MFC is a system including various electrical, electro-chemical, physical-chemical and biological processes. The existence of the biofilm on the anode (and cathode for a single chamber MFC) separates MFC from other fuel cells and, increases the difficulty in reactor maintenance and power prediction. Mathematical modelling is an effective tool to study and optimize MFC; however, the modelling and simulation of MFC system has received considerably less attention compared to tremendous experimental work conducted for MFC design and application accomplished in the last several decades. MFC models were initially adopted from classic fuel cell models, but with further modifications based on biological growth, substrate consumption and electron transport. The complexity of developing an MFC model, as well as its simulation and prediction capacity when compared to experimental data, are the main obstacles; this includes a simulation of microorganism behaviors, the impact of biofilm, the mass transfer and balance, the anode and cathode reaction kinetics, etc. (Logan et al., 2006; Marcus et al., 2007; Ortiz-Martínez et al., 2015).

MFC models are classified into specific models and comprehensive models (Ortiz-Martínez et al., 2015). Specific models are developed to study one or more key components, processes and parameters of the MFC, such as the simulation of polarization curve (Wen et al., 2009) and, the application of fuzzy control strategy in MFC (Yan and Fan, 2013). Comprehensive models are developed to study the overall behaviors and reactor performances, they are further categorized into two types, anode-limiting models and anode/cathode models. Anode-limiting models consider the anode as the limiting factor of the reactor performance, whereas anode/cathode models are developed without this assumption. When modelling an MFC system,

electrical processes are usually expressed by Ohm's law (for voltage, current, external and internal resistance); electro-chemical behaviors are simulated by the Nernst equation, the Nernst-Planck equation, and the Butler-Volmer equation (for anode and cathode reaction, charge balance, anode current density, etc.); physical-chemical processes are commonly accomplished by the application of Fick's diffusion laws (for the substrate/ion gradient concentrations); finally the biological processes are most usually simulated by the Monod equation (for the microorganism growth and substrate oxidization) (Ortiz-Martínez et al., 2015; Picioreanu et al., 2007; Pinto, 2011). In many studies combinations of various equations are required for a more accurate model, for example, microbiological metabolism in response to electron release can be determined by the combination of the Monod equation and Nernst equation and, electrochemical reactions can be more accurately simulated by combining the Monod and Butler-Volmer equation (Marcus et al., 2011, 2007; Merkey and Chopp, 2012).

The study reported by Marcus et al. (2007) provides an essential description of how the biofilm on MFC anode works. They developed a dynamic, one-dimensional, multi-species model for the anode simulating the biofilm-related (growth and mass transport) and electrochemical (electron conduction and charge-transfer) processes. This is the first reported conduction-based model of biofilm growth in MFC (Merkey and Chopp, 2012). They defined a term 'biofilm anode' to represent the anode with a layer of conductive biofilm matrix accepting electrons from biofilm bacteria and conducting electrons to the anode. Then they described the rate of substrate (electron donor) utilization and respiration using the Nernst-Monod equation, and developed the model by linking all the components using multiple balance equations. The electron donor mass balance defined the utilization of electron donor equal to the mass of electron donor that diffused into the biofilm. The electron balance assumed that the electrons derived from electron donor equaled to the electrons conducted through biofilm and the electrons used to support synthesis. The biomass mass balance assumed that the accumulation and advection of biomass equaled to the growth, respiration and decay. The model studied the dual-limitation in biofilm caused by the electron donor concentration and local potential, suggesting that the dual-limitation effect in biofilm could be alleviated by reducing biofilm

thickness and removing excess biomass. They also found out that the biofilm conductivity (k_{bio}) greatly affected the current density, substrate oxidization rate, and biomass distribution in biofilm. A larger k_{bio} resulted in a higher current density, substrate consumption rate, and local potential. Merkey and Chopp (2012) further extended this work to a two-dimension conduction based biofilm model to simulate the anodic biofilm growth, with additional consideration of the impact of liquid-biofilm and biofilm-anode interface. The term k_{bio} was also used in this model to express the conductivity of the biofilm. This model was more complete compared to other works. Simulation and validation results using previously reported data revealed that the current production of an MFC was limited by the nutrient delivery to the entire biofilm surface at the anode scale. Any reason limiting the nutrient delivery (e.g., bacteria colonies grew too large/thick on anodic biofilm) would decrease the current generation.

Sirinutsomboon (2014) reported a computational model simulating a single chamber air cathode MFC and studied the kinetic nature of the MFC processes. The air cathode was coated with PTFE diffusion layer and Pt/C catalyst layer. The feed medium was assumed to be molasses (mostly sucrose) and the electron acceptor was oxygen from the air. The substrate diffused through the anode bioflim and was oxidized by the bacteria in the bioflim. The consumption rate of molasses was estimated using the Nernst-Monod equation. The oxygen diffusion rate through the PTFE layer was expressed using Fick's second law of diffusion; the reduction rate was calculated by combining the Monod and Bulter-Volmer equations. The electrode potential and potential losses were estimated using the Nernst equation. The inputs of this model included the initial amount of molasses, biofilm thickness, pH, operation time, temperature, and chamber dimensions. This model was capable of predicting the concentration profiles of sucrose (as functions of time and location) and the open circuit voltage (as a function of time) for a given feed strength. It also suggested that increasing the anode bioflim thickness was more effective to obtain a higher output voltage when feeding higher COD medium (>5000 mg/L). The drawback of this model is that it considered the cathode as a pure chemical cathode, neglecting the existance of a cathodic biofilm that is usually present in an air cathode MFC. In addition more validations with experimental data are required for this model.

A more recent single chamber air cathode MFC model was developed by Ou et al., (2016) to understand the interrelation of biological, chemical, and electrochemical reactions at steady state. The difference between this model and the one by Sirinutsomboon (2014) is that both anode and cathode were assumed to be covered with biofilm formed by multi species bacteria in this model. The chemical species diffusion and electric migration were expressed in the anode model, meanwhile the diffusion and mass transfer were simulated in the cathode model. This model considered the impact of biological catalyst (autotrophic aerobic bacteria (AAB) in the cathode) and revealed that the biocatalyst had only minor impact in the oxygen reduction reaction in a cathode that includes a Pt/C catalyst (contributed only up to 8% of the total power). The impact of pH was also included in the model, suggesting that the transport of hydroxide was the cause of cathodic pH change. In addition, the power density and polarization curve generated from the cathode model fit well with experimental data.

The studies reported above showed the evolution of model development and the trend of increasing the complexity and diversity in modelling. Computational modelling and simulation is a powerful tool to further understand and improve MFC technology, especially when considering the cost and time saving compared to lab studies and field trials. In this chapter a mathematical model specifically for the application of air cathode MFC fed SWW medium was developed; the prediction results achieved from this model were compared to experimental data for verification and validation.

6.1 Model development and implementation

A mathematical model was developed to simulate steady state for a single chamber air cathode MFC reactor designed in Section 2.1. The MFC model contains a flat anode and a flat cathode and, the distance between the anode and cathode was constant. Figure 6-1 summarizes the system and input and output parameters. An anode half-cell model and cathode half-cell model were developed separately and combined using Ohm's law and substrate mass balance equations. The anode was considered as a biofilm anode with a complex mixed culture, the substrate (glucose/ethanol) consumption was described using the Nernst-

Monod equation, the respiration was also described using the Nernst-Monod equation to express the biomass self-degradation (cellular mass). The anodic potential was described using the Nernst equation. Ohm's law and an electron balance were used to link the above pieces together to a complete steady state anode half-cell. Meanwhile the cathode was assumed to be attached with a layer of biofilm containing only heterotrophic aerobic bacteria (HAB). Oxygen diffusion in the cathode was described using Fick's law of diffusion, and the oxygen reduction rate at the cathode was achieved through combining the Monod equation and the Butler Volmer equation. Similar to the anodic potential, the cathodic potential was also expressed through the Nernst equation and, the overall cathode half-cell model was linked using mass and electron balance in the cathode. Constants, assumptions and boundary conditions were obtained from published papers augmented by experimental data from lab studies.

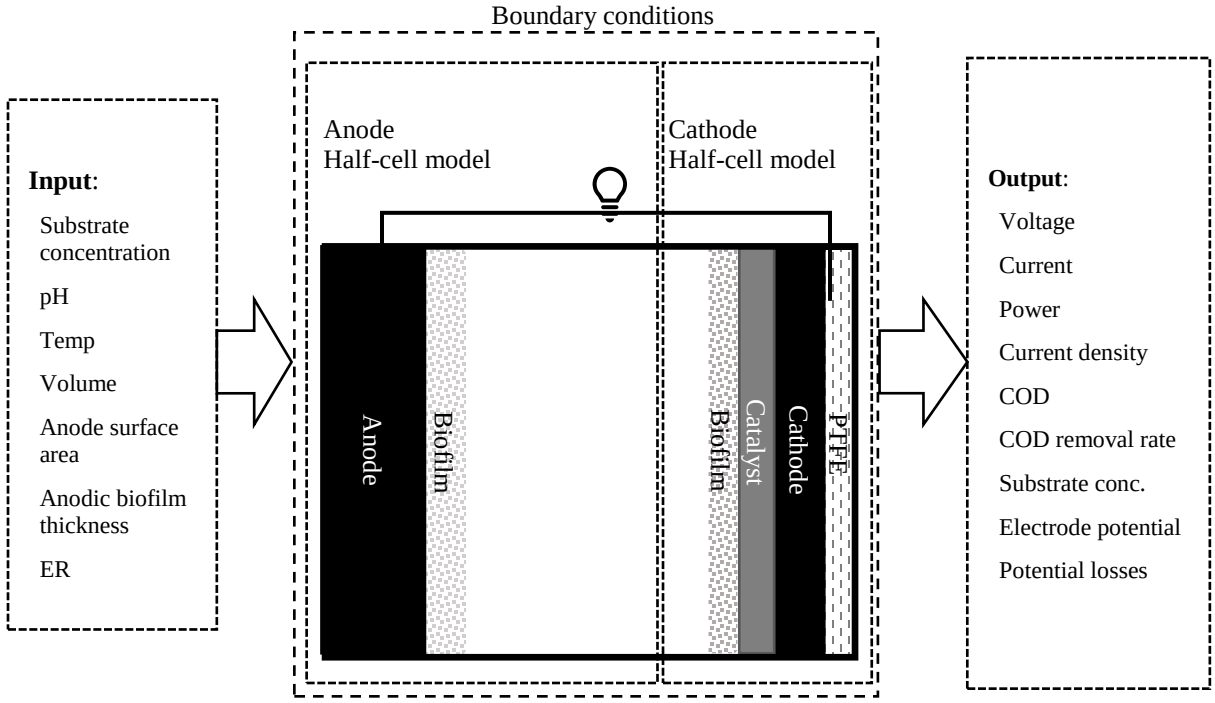

Figure 6-1 Model diagram of the air cathode MFC system

The completed air cathode MFC model was implemented using Microsoft Excel 365. The anode half-cell model and the cathode half-cell model were implemented in separate worksheets. Both anode and cathode model pages contain input area and output area as shown in Figure 6-2. The input area allows the user to

import constants and operational parameters as input; the output area presents the simulated results which include voltage, current, power, current density, COD and COD removal rate (overall and by anode/cathode, respectively), substrate concentration, anode/cathode potential and potential losses (activation, ohmic and concentration). The validation process comparing the simulated data to actual results (output voltage, COD degradation, feed composition and internal/external resistances) are accomplished in different worksheets as shown in Figure 6-3.

Table 6-1 shows the input variables and boundary conditions for each parameter in column 3. As the MFC model in this study was developed to simulate/predict experimental results, the values/ranges in column 4 were chosen to encompass the range expected for an MFC treating winery wastewater. Table 6-2 to Table 6-4 summarize the constants, assumed variables and calculated variables used in this study. These variables are further explained in Section 6.1.1 to 6.1.3.

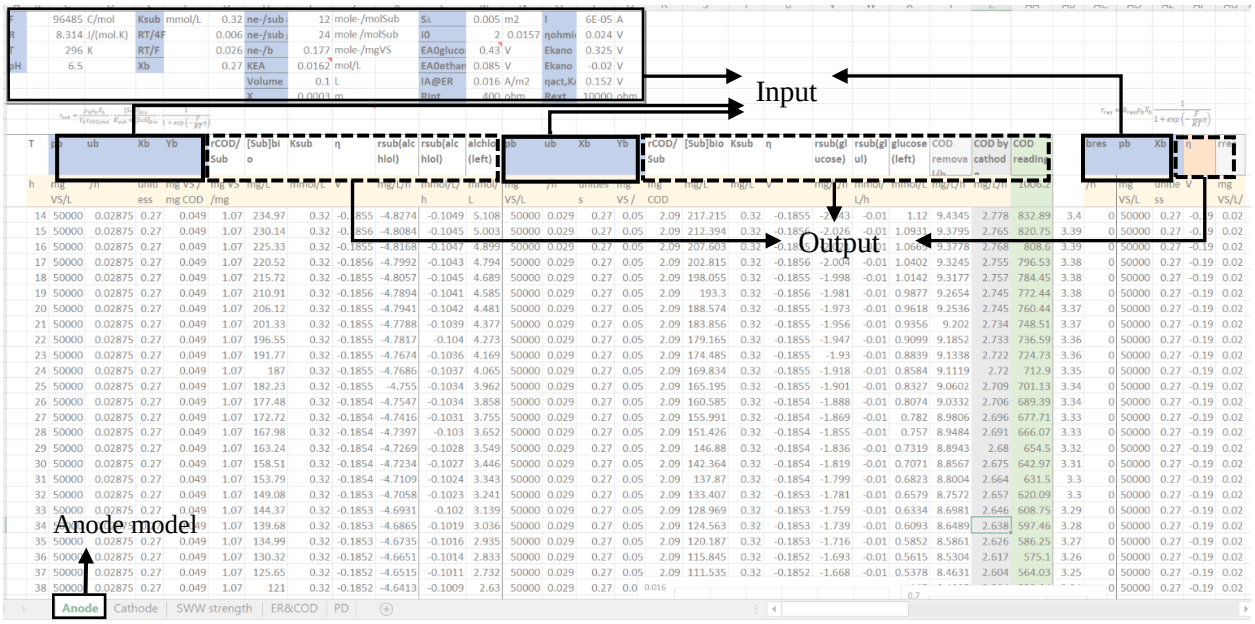

a) Screenshot of anode model showing the input and output

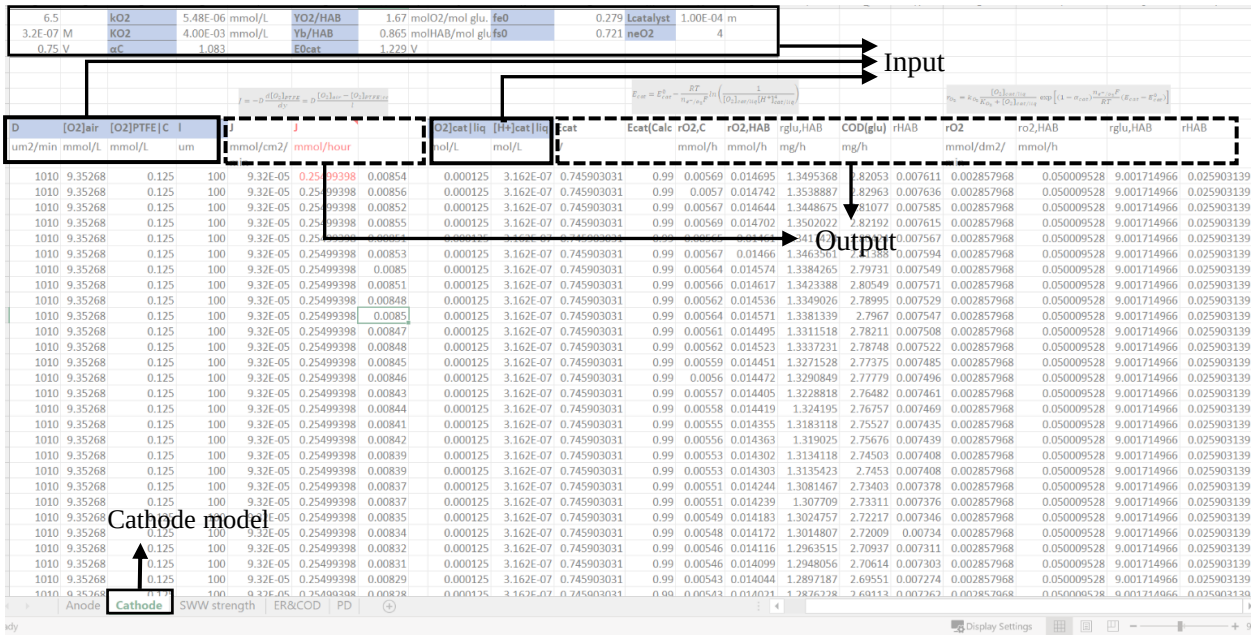

b) Screenshot of cathode model showing the input and output

Figure 6-2 Implementation of MFC model

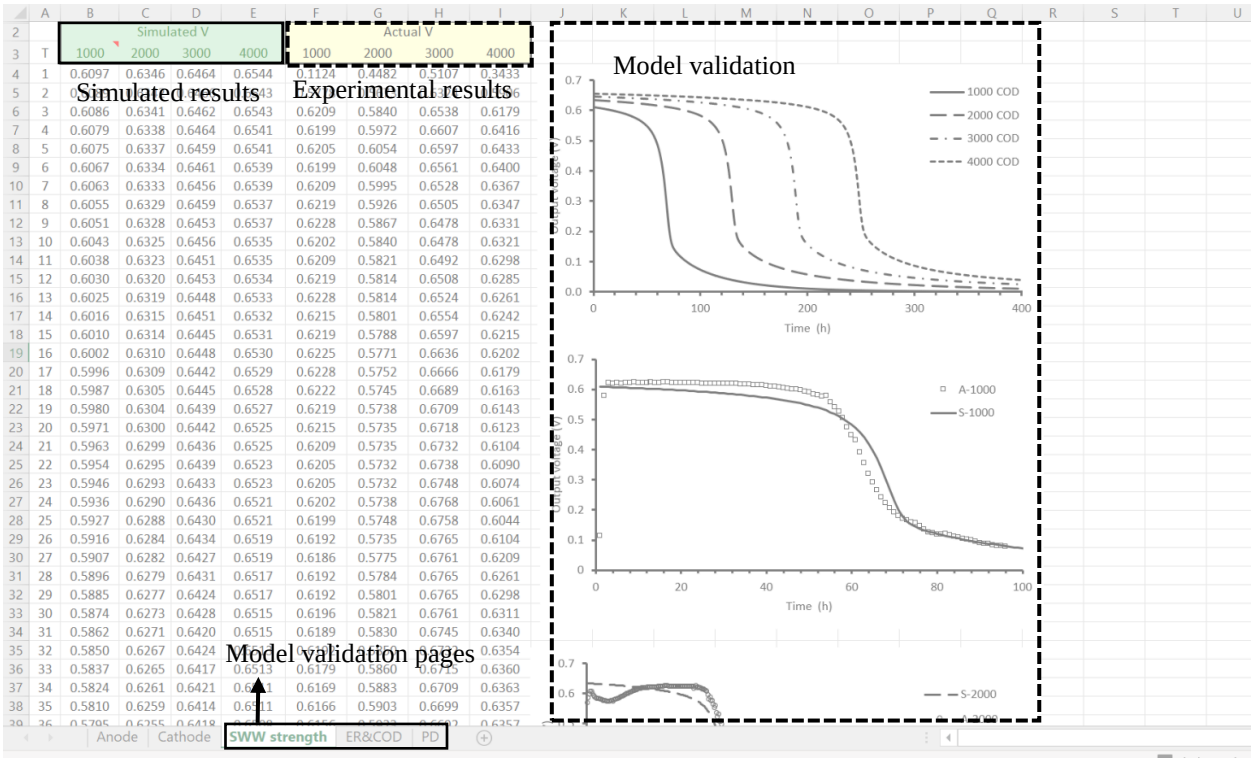

Figure 6-3 A screenshot of model validation pages

Table 6-1 Input variables and boundary conditions for MFC modelling

Symbol	Description	boundary conditions	Value used	Unit	Reference
$[Sub]_{bio}$	Substrate concentration in biofilm	0-2980 (Ethanol) 0-2810 (Glucose)	298-2980 (Ethanol) 281-2810 (Glucose)	mg/L	This study
R_{Ext}	External resistance	0- ∞	500-10000	Ω	This study
T	Temperature	296	296	K	This study
L_{cat}	Thickness of catalyst	0-0.001	0.0001	m	Assumed
S_A	Surface area of anode	0- ∞	0.00456	m^2	This study
S_C	Surface area of cathode	0- ∞	0.00456	m^2	This study
pH	pH in anode chamber	4.5-7	6.5	-	This study
x	Location in biofilm (biofilm thickness)	0-0.022	0.0003	m	Assumed
y	Location in PTFE layer (PTFE thickness)	0-22000	100	µm	Assumed (Ou et al., 2016)

Table 6-2 Constants for MFC modelling

Symbol	Description	Value	Unit	Reference
E^0_A	Standard reduction potential for the Anodic e- acceptor	0.43(glucose) 0.085(ethanol)	V	Constant
E^0_C	Standard reduction potential for the cathode	1.229	V	Constant
F	Faraday's constant	96,485	C/mol	Constant
n	Influence factor	+1 / -1		Constant
$n_{e-/eth}$	e- equivalence of ethanol	12	mmol e- / mmol ethanol	Eq. 6-2
$n_{e-/glu}$	e- equivalence of glucose	24	mmol e- / mmol glucose	Eq. 6-1
n_{O2}	e- equivalence of oxygen	4	mmol e- / mmol oxygen	Eq. 6-3
$[O_2]_{air}$	Oxygen concentration in air	9.35	mmol/L	Constant
R	Ideal gas constant	8.314	J/mol/K	Constant
$r_{COD/eth}$	COD equivalence of ethanol	1.07	mg COD / mmol ethanol	Eq. 6-2 & 6-3
$r_{COD/glu}$	COD equivalence of glucose	2.09	mg COD / mmol glucose	Eq. 6-1 & 6-3
$[Sub]^0_A$	Standard anodic e- acceptor concentration	1	mol/L	Constant

Table 6-3 Assumed parameters for MFC modelling

Symbol	Description	Value	Unit	Reference
a_C	e- transfer coefficient of cathode	1.083	-	Sirinutsomboon, 2014
$b_{res,,A}$	Endogenous decay coefficient for active biomass	0.0021	/h	Marcus et al., 2007
$D_{O2,PTFE}$	Diffusivity of oxygen in PTFE	$1.68x10^{-13}$	$\mu m^2/s$	Rharbi et al., 1999;
$i_{0,A}$	Anodic limiting current density	2	A/m^2	Assumed (this study)
K_{O2}	Half velocity constant for oxygen	0.004	mmol/L	Sirinutsomboon, 2014
K_{sub}	Half velocity constant for substrate	0.32	mmol/L	Marcus et al., 2007
k_{bio}	Biofilm conductivity	0.05	S/m	Merkey and Chopp, 2012
k_{O2}	Oxygen reduction rate per area	$9.13x10^{-8}$	$mmol/(dm^2.s)$	Sirinutsomboon, 2014
$n_{e-/b}$	e- equivalence of active biomass	0.177	mmol e- / mg VS ($C_5H_7O_2N$)	Marcus et al., 2007
R_{Int}	Internal resistance	400	Ω	Assumed (This study)
X_b	Volume fraction of active biomass	0.27	-	Assumed (This study)
Y_b	Active biomass growth yield	0.049	mgVS/mgCOD	Merkey and Chopp, 2012
$\eta_{act,KA}$	Half maximum rate for anodic activation overpotential	0.152	V	Assumed (This study)
μ_b	Specific growth rate of active biomass	0.0288	/h	Merkey and Chopp, 2012
ρ_b	Density of active biomass	50,000	mg VS/L	Merkey and Chopp, 2012
σ	Energy transfer coefficient	0.6	-	Grady et al., 2011,

Table 6-4 Calculated variables used in MFC modelling

Symbol	Description	Value	Unit	Equations
f^0_e	The fraction of electrons directed by HAB from the cathode to O_2,	0.279(glucose) 0.341(ethanol)	-	eq. 6-48 eq. 6-49
f^0_s	The fraction of electrons that go from the cathode to biomass	0.721(glucose) 0.659(ethanol)	-	eq. 6-48 eq. 6-49
$[H^+]_{cat/liq}$	Proton concentration at the cathode|liquid interface	$3.16x10^{-7}$	mol/L	eq. 6-42
J	Diffusion rate per area	$9.32x10^{-5}$	mmol/(dm^2.s)	eq. 6-41
$[O_2]_{PTFE\|cc}$	Oxygen concentration at the PTFE|carbon cloth interface	0.125	mmol/L	eq. 6-37 eq. 6-38
$[O_2]_{cat/liq}$	Oxygen concentration at the cathode/liquid interface	0.000125	mmol/L	eq. 6-42
$Y_{bio,HAB}$	HAB biomass yield	0.865 (glucose) 0.395 (ethanol)	mol HAB / mol substrate	eq. 6-52
$Y_{O2,HAB}$	Oxygen yield	1.67 (glucose) 1.02 (ethanol)	mol O_2 / mol substrate	eq. 6-53

6.1.1 Substrate modelling

The carbon substrates used for the anode chamber were designed to simulate SWW medium. The original wine sample used for SWW medium contains 9% (v/v) ethanol and 67 g/L sugar, with a volatile acidity (as acetic acid) of ~1.2 g/L. Volatile acidity expresses the concentration of volatile fatty acids in wine, which is generally perceived as the odour of vinegar. Acetic acid accounts for >93% of steam distillable acids in wine, other acids such as carbonic acid, sulfurous acid, lactic, formic, butyric and propionic acids also contribute to the volatile acidity but they are minor compared to acetic acid (Buick and Holdstock, 2003; Coulter, 2018). Sugar content in wine is mostly glucose, with a small amount of fructose and other sugars (Rengasamy and Berchmans, 2012; SWBC, 2018). Although various other components also exist in wine such as tannin, phenolics, vitamins, mineral elements (Oliveira et al., 2016), they are either negligible or do not contribute greatly to the COD when used as an MFC feed; therefore, are not discussed or used in the model.

In this model glucose and ethanol are considered as the main COD contributors and, the redox reactions occurring on the anode and cathode are listed as follows,

$$C_6H_{12}O_6 + 12H_2O \rightarrow 6HCO_3^- + 30H^+ + 24e^-(Anode) \quad \text{eq. 6-1}$$

or $$C_2H_6O + 5H_2O \rightarrow 2HCO_3^- + 14H^+ + 12e^- (Anode)$$ eq. 6-2

$$O_2 + 4H^+ + 4e^- \rightarrow 2H_2O\ (Cathode)$$ eq. 6-3

The COD of the substrate feed was calculated from the SWW medium components ethanol, sugar and acetic acid. In addition to the 10 mM PB and 10 mM NaCl, the SWW medium per liter (contains 4.191 mL of wine sample) results in the following concentrations:

$$M_{Ethanol}\ (g) = 4.191\ mL * (9\%\ v/v) * (0.789 g/mL) = 0.298\ g/L,$$ eq. 6-4

$$M_{Glucose}\ (g) = 4.191\ mL * 1/1000\ L/mL * 67\ g/L = 0.281\ g/L,$$ eq. 6-5

$$M_{Acetic\ acid}\ (g) = 4.191\ mL * 1/1000\ L/mL * 1.2\ g/L = 0.005\ g/L.$$ eq. 6-6

The COD of the three main components are calculated using eq. 6-1 to eq. 6-3:

$$COD_{Ethanol}\ (mg/L) = M_{Ethanol} \times 3MW_{O2} / MW_{Ethanol} \times 1000\ mg/g/L = 622\ mg/L$$ eq. 6-7

Similarly,

$$COD_{Glucose}\ (mg/L) = 300\ mg/L,$$ eq. 6-8

$$COD_{Acetic\ acid}\ (mg/L) = 5\ mg/L,$$ eq. 6-9

the overall COD

$$COD_{sum} = 620 + 300 + 5 = 927\ mg/L.$$ eq. 6-10

The pH of the wine (1.2 g/L (0.02 M) acetic acid) was verified as follows:

$$pH = pKa + \log([A^-]/[HA]) = 4.75 + \log((5.8 \times 10^{-4}\ M) / (0.02\ M)) = 3.21.$$ eq. 6-11

The estimated COD (COD_{sum}) is slightly less than the COD measured in previous studies (1000±20 mg/L). The proposed reason for this difference is the existence of small quantities of other organic acids (e.g. malic

and tartaric acids, citric acid, …), glycerol, and complex organic compounds such as tannins and phenolics (Oliveira et al., 2016). To simplify the validation process only the ethanol and sugar were considered as the COD contributors. The estimated pH is close to the pH measured in the lab (3.3±0.2); therefore, the estimation based on volatile acidity is acceptable.

In the model worksheet, the initial ethanol concentration (298 mg/L) and glucose concentration (281 mg/L) were given as input to the anode half-cell model (cell H11 and S11 respectively). With built-in equations as described in Section 6.1.2 and 6.1.3, the corresponding COD removal rate (by anode and cathode) and overall COD are calculated and presented in column Y, Z and AA respectively, the outputs after every hour were presented in row 12 and later, as shown in

Figure 6-4.

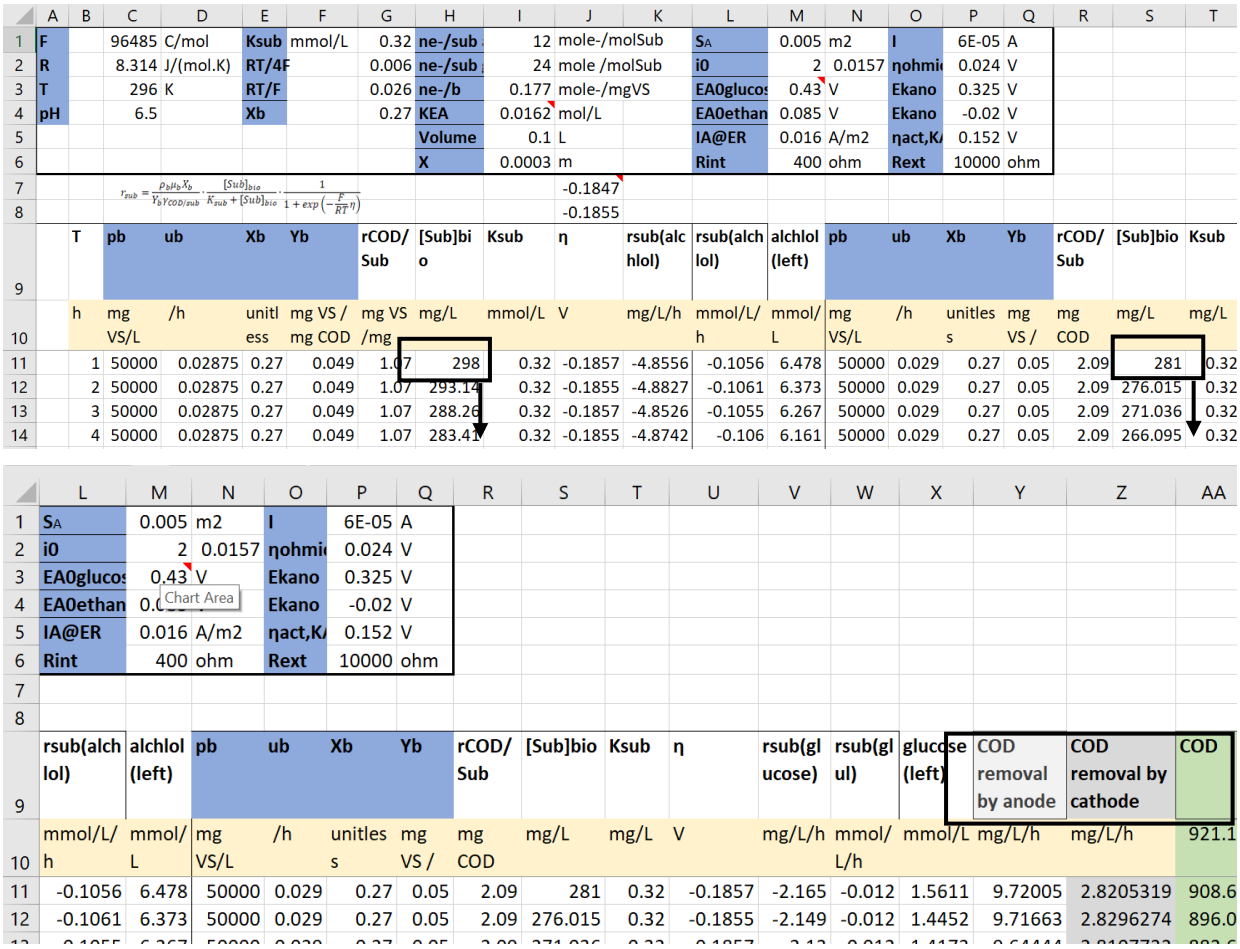

	A	B	C	D	E	F	G	H	I	J	K	L	M	N	O	P	Q	R	S	T
1	F		96485	C/mol	Ksub	mmol/L	0.32	ne-/sub	12	mole-/molSub		SA	0.005	m2	I	6E-05	A			
2	R		8.314	J/(mol.K)	RT/4F		0.006	ne-/sub	24	mole /molSub		i0	2	0.0157	ηohmi	0.024	V			
3	T		296	K	RT/F		0.026	ne-/b	0.177	mole-/mgVS		EA0glucos	0.43	V	Ekano	0.325	V			
4	pH		6.5		Xb		0.27	KEA	0.0162	mol/L		EA0ethan	0.085	V	Ekano	-0.02	V			
5								Volume	0.1	L		IA@ER	0.016	A/m2	ηact,KA	0.152	V			
6								X	0.0003	m		Rint	400	ohm	Rext	10000	ohm			
7				$r_{sub} = \frac{\rho_b \mu_b X_b}{Y_b Y_{COD/sub}} \cdot \frac{[Sub]_{bio}}{K_{sub} + [Sub]_{bio}} \cdot \frac{1}{1 + exp\left(-\frac{F}{RT}\eta\right)}$					-0.1847									
8											-0.1855									
9		T	pb	ub	Xb	Yb	rCOD/Sub	[Sub]bio	Ksub	η	rsub(alchlol)	rsub(alchlol)	alchlol (left)	pb	ub	Xb	Yb	rCOD/Sub	[Sub]bio	Ksub
10		h	mg VS/L	/h	unitless	mg VS / mg COD	mg VS /mg	mg/L	mmol/L	V	mg/L/h	mmol/L/h	mmol/L	mg VS/L	/h	unitless	mg VS /	mg COD	mg/L	mg/L
11		1	50000	0.02875	0.27	0.049	1.07	298	0.32	-0.1857	-4.8556	-0.1056	6.478	50000	0.029	0.27	0.05	2.09	281	0.32
12		2	50000	0.02875	0.27	0.049	1.07	293.14	0.32	-0.1855	-4.8827	-0.1061	6.373	50000	0.029	0.27	0.05	2.09	276.015	0.32
13		3	50000	0.02875	0.27	0.049	1.07	288.26	0.32	-0.1857	-4.8526	-0.1055	6.267	50000	0.029	0.27	0.05	2.09	271.036	0.32
14		4	50000	0.02875	0.27	0.049	1.07	283.41	0.32	-0.1855	-4.8742	-0.106	6.161	50000	0.029	0.27	0.05	2.09	266.095	0.32

	L	M	N	O	P	Q	R	S	T	U	V	W	X	Y	Z	AA
1	SA	0.005	m2	I	6E-05	A										
2	i0	2	0.0157	ηohmi	0.024	V										
3	EA0glucos	0.43	V	Ekano	0.325	V										
4	EA0ethan	0.0	Chart Area	Ekano	-0.02	V										
5	IA@ER	0.016	A/m2	ηact,KA	0.152	V										
6	Rint	400	ohm	Rext	10000	ohm										
7																
8																
9	rsub(alchlol)	alchlol (left)	pb	ub	Xb	Yb	rCOD/Sub	[Sub]bio	Ksub	η	rsub(glucose)	rsub(glul)	glucose (left)	COD removal by anode	COD removal by cathode	COD
10	mmol/L/h	mmol/L	mg VS/L	/h	unitless	mg VS /	mg COD	mg/L	mg/L	V	mg/L/h	mmol/L/h	mmol/L	mg/L/h	mg/L/h	921.1
11	-0.1056	6.478	50000	0.029	0.27	0.05	2.09	281	0.32	-0.1857	-2.165	-0.012	1.5611	9.72005	2.8205319	908.6
12	-0.1061	6.373	50000	0.029	0.27	0.05	2.09	276.015	0.32	-0.1855	-2.149	-0.012	1.4452	9.71663	2.8296274	896.0

Figure 6-4 Screenshots of model implementation (substrate consumption)

6.1.2 Anode steady state half-cell model

The anode structure contains two domains, a flat anode electrode (carbon fiber mesh) and the biofilm attached to it. The factors with significant impact on the anode are: the substrate used for electron donor (type and concentration), the microorganisms capable of substrate oxidization (accumulation of anodic biofilm), and the electrons for transfer to the anode (electrical potential) (Marcus et al., 2007). The following assumptions were made during the development of the half-cell model:

- The MFC was a tubular reactor with a volume 100 mL, the distance between anode and cathode was 2.2 cm.
- The anode biofilm was assumed to be mature. The biofilm was homogeneous, 0.3 mm thick and was well attached to the anode surface.
- The planktonic bacteria in the anode chamber were negligible.
- The reactor was batch fed with a pH buffered (PB 10 mM) medium containing 298 mg/L (6.46 mM) ethanol and 281 mg/L (1.56 mM) sugar which was assumed to be all glucose.
- The system was well buffered with a constant pH of 6.5.
- A constant anodic coulombic efficiency was assumed, which meant the ratio between the electrons conducted to the anode and electrons consumed by EAB for growth were constant.

6.1.2.1 Electron balance

In the anode, the electrons are derived from the substrate and are either 1) transferred to the anode (as current) or 2) utilized for microbial growth. The steady state of electron balance equation for the biofilm anode is presented in eq. 6-12 (Marcus et al., 2007; Merkey and Chopp, 2012):

$$Fn_{e^-/sub}\, r_{sub,A} + Fn_{e^-/b}\, r_{res,A} + k_{bio}\frac{\partial^2 \eta}{\partial^2 x} = 0 \qquad \text{eq. 6-12}$$

where

F = Faraday's constant, C/mol e^-,

$n_{e^-/sub}$ = electron equivalence of substrate (electron donor), mol e^- / mol substrate,

$n_{e^-/b}$ = electron equivalence of active biomass, mmol e^- / mg VS ($C_5H_7O_2N$),

$r_{sub,A}$ = substrate consumption rate in anodic biofilm, mmol / (L.s),

$r_{res,A}$ = endogenous respiration rate in anodic biofilm, mg VS / (L.s),

k_{bio} = biofilm conductivity, S/m,

η = local potential in biofilm, V,

x = location in biofilm, m.

The substrate consumption rate ($r_{sub,A}$) in the anodic biofilm is further described by the Nernst-Monod equation (Marcus et al., 2007; Merkey and Chopp, 2012; Sirinutsomboon, 2014) as:

$$r_{sub,A} = \frac{\rho_b \mu_b X_b}{Y_b \gamma_{COD/sub}} \cdot \frac{[Sub]_{bio}}{K_{sub} + [Sub]_{bio}} \cdot \frac{1}{1 + exp\left(-\frac{F}{RT}\eta\right)} \quad \text{eq. 6-13}$$

where

ρ_b = density of active biomass, mg VS / L,

μ_b = specific growth rate of active biomass, /h,

X_b = volume fraction of active biomass, unitless,

Y_b = biomass growth yield, mg VS / mg COD,

$\gamma_{COD/sub}$ = COD equivalence of substrate (electron donor), mg COD/ mmol substrate,

$[Sub]_{bio}$ = substrate concentration in biofilm, mmol/L,

K_{sub} = half velocity constant for substrate, mmol/L,

R = ideal gas constant, J/mol/K,

T = temperature, K.

As $\frac{\rho_b \mu_b X_b}{Y_b Y_{COD/sub}}$ is a constant for a specific reactor maintained at regular working condition, when the substrate concentration $[Sub]_{bio}$ increases, the local potential η and rate of substrate consumption r_{sub} also increase relatively until a plateau is reached. When the local potential η reaches the plateau at the steady state, the anodic electron acceptor (in this case the carbon cloth anode is limited by specific surface area and conductivity) and substrate oxidization will be the limit of substrate utilization rate (Marcus et al., 2007).

In addition to the exogenous respiration, the rate of endogenous respiration ($r_{res,A}$) of the biofilm for self maintenance is expressed using the Nernst-Monod equation as (Marcus et al., 2007; Merkey and Chopp, 2012):

$$r_{res,A} = b_{res,A} \rho_b X_b \frac{1}{1 + exp\left(-\frac{F}{RT}\eta\right)} \quad \text{eq. 6-14}$$

where

$b_{res,A}$ = endogenous decay coefficient for active biomass, /h.

As the current density in biofilm i_A can be expressed as

$$i_A = k_{bio} \frac{d\eta}{dx}. \quad \text{eq. 6-15}$$

The output current from anode I can be expressed as

$$I = \left(\int i_A \, dx\right) S_A \quad \text{eq. 6-16}$$

where

S_A = the surface area of anode.

The electron balance for biofilm anode can also be expressed by including i_A:

$$Fn_{e^-/sub}\, r_{sub} + Fn_{e^-/b}\, r_{res} + \frac{di_A}{dx} = 0. \quad \text{eq. 6-17}$$

6.1.2.2 Anode potential

The anode potential is related to the concentration of electron acceptor using the Nernst equation (Stumm and Morgan, 1996). Here the anode and biofilm anode are referred to as the 'anode electron acceptor', to be distinguished from the traditional soluble electron acceptor (Marcus et al., 2007):

$$E_A = E_A^0 - \frac{RT}{n_{e^-/sub}\, F} ln\left(\frac{[Sub]_A^0}{[Sub]_A}\right) \quad \text{eq. 6-18}$$

where

E_A = potential of the anodic electron acceptor, V,

E_A^0 = standard reduction potential for the anodic electron acceptor, V,

$[Sub]_A^0$ = standard anodic electron acceptor concentration (1 mol/L),

$[Sub]_A$ = anodic electron acceptor concentration, mol/L.

Meanwhile, the anode potential can be further expressed as:

$$E_A = E_A^0 - \eta_{ohmic} - \left|\eta_{con,A}\right| - \left|\eta_{act,A}\right| \quad \text{eq. 6-19}$$

where

η_{ohmic} = ohmic loss, V,

$\left|\eta_{con,A}\right|$ = anodic concentration loss, V,

$\left|\eta_{act,A}\right|$ = anodic activation loss, V.

In summary, the overall anodic potential loss is:

$$\eta_{ohmic} + |\eta_{con,A}| + |\eta_{act,A}| = \frac{RT}{n_{e^-/sub}\,F} ln\left(\frac{[Sub]_A^0}{[Sub]_A}\right). \quad \text{eq. 6-20}$$

The local potential (η) in biofilm:

$$\eta = \eta_{act,A} - \eta_{act,KA} \quad \text{eq. 6-21}$$

where

$\eta_{act,A}$ = anode activation overpotential, V,

$\eta_{act,KA}$ = half maximum rate for the anodic activation overpotential, V.

Each type of loss can be further derived as follows:

1) Anodic ohmic loss:

$$\eta_{ohmic} = IR_{Int}. \quad \text{eq. 6-22}$$

2) Concentration loss:

$$\eta_{\text{con,A}} = \frac{RT}{n_{e^-/sub}F} log\left(1 - \frac{i_A}{i_{0,A}}\right) + \frac{RT}{n_{e^-/sub}F} log\left(\frac{[H^+]}{[H^+]_{ini}}\right) \quad \text{eq. 6-23}$$

where

$i_{0,A}$ = anodic limiting current density, A/m^2,

$[H^+]$ = proton concentration, mol/L,

$[H^+]_{ini}$ = initial proton concentration in anode, mol/L,

3) Overall, activation loss is derived as

$$\eta_{act,A} = E_A - E_A^0 - \eta_{ohmic} - |\eta_{con,A}| = \frac{RT}{n_{e^-/sub}\,F} ln\left(\frac{[Sub]_A^0}{[Sub]_A}\right) - IR_{int} - |\eta_{con,A}|. \quad \text{eq. 6-24}$$

6.1.2.3 Substrate proton and HCO_3^- mass balance

The steady state mass balance of substrate and ions can be achieved by the transportation behaviors of chemical components in fluid, which include concentration-driven diffusion, electric field-included migration and advection (Bird et al., 2012; Ou et al., 2016). The mass balance equation therefore can be expressed using the Nernst-Planck equation as

$$\frac{\partial c_i}{\partial t} = \frac{\partial}{\partial x}\left(F_{dif} + F_{mig} + F_{adv}\right) - r_i \qquad \text{eq. 6-25}$$

where

c_i = species concentration, mol/L,

F_{dif} = diffusion flux term, mol/(dm^2.s),

F_{mig} = migration flux term, mol/(dm^2.s),

F_{adv} = advection flux term, mol/(dm^2.s),

r_i = species reaction rate, mol/(L.s).

This air cathode MFC is a batch system without stirring, therefore, the advection was not included (Ou et al., 2016). Migration would be most important for charged or partially charged substrates. The migration affects more when there is a high current density; we have not experimented with a high current density in the bulk phase, so the migration effect was neglected in this model (Merkey and Chopp, 2012; Zhang et al., 2015). The diffusion effect can be expressed as

$$F_{dif} = D_i \frac{\partial c_i}{\partial x} \qquad \text{eq. 6-26}$$

where D_i = diffusion coefficient of the species, dm^2/s.

Therefore, the mass balance equation can be expressed as

$$\frac{\partial c_i}{\partial t} = D_i \frac{\partial^2}{\partial x^2} c_i - r_i. \qquad \text{eq. 6-27}$$

The steady state mass balance of the substrate concentration in biofilm can be expressed as

$$\frac{\partial}{\partial t}[Sub]_{bio} = D_{sub,bio} \frac{\partial^2}{\partial x^2}[Sub]_{bio} - r_{sub}. \qquad \text{eq. 6-28}$$

The steady state mass balance of the proton concentration in biofilm can be expressed as

$$\frac{\partial}{\partial t}[H^+]_{bio} = D_{H^+} \frac{\partial^2}{\partial x^2}[H^+]_{bio} + n_{e^-/sub}\, r_{sub.} \qquad \text{eq. 6-29}$$

In a buffered MFC system, the proton concentration is stable due to the buffer effect. Take phosphate buffer as an example,

$$H_3PO_4 \overset{K_1}{\Leftrightarrow} H^+ + H_2PO_4^- \qquad K_1 = \frac{[H^+][H_2PO_4^-]}{[H_3PO_4]} = 6.5 \times 10^{-3}, \qquad \text{eq. 6-30}$$

$$H_2PO_4^- \overset{K_2}{\Leftrightarrow} H^+ + HPO_4^{2-} \qquad K_2 = \frac{[H^+][HPO_4^{2-}]}{[H_2PO_4^-]} = 6.2 \times 10^{-8}, \qquad \text{eq. 6-31}$$

$$HPO_4^{2-} \overset{K_3}{\Leftrightarrow} H^+ + PO_4^{3-} \qquad K_3 = \frac{[H^+][PO_4^{3-}]}{[HPO_4^{2-}]} = 3.6 \times 10^{-13}. \qquad \text{eq. 6-32}$$

If enough buffer is added to the system, then the pH is maintained stably, which means at steady state, the overall concentration of proton vs time follows

$$\frac{\partial}{\partial t}[H^+] = 0. \qquad \text{eq. 6-33}$$

In the actual reactor protons are produced in the anode and must move to the cathode; therefore, the proton flux and balance are significant. In this study the electron balance instead of the proton balance was chosen to build the model, therefore, the proton flux and balance were not further developed.

6.1.2.4 Anode model implementation

The equations derived in this section were built into the anode model worksheet as shown in Figure 6-2 (a). The constants and operational parameters were imported into the input area. The example below presents the implementation process of the initial status when using the standard medium (COD ~1000 mg/L), the step numbers are noted in Figure 6-5 to aid understanding.

1) The operational parameters were initialized with given conditions (T = 296 K, pH = 6.5, S_A = 0.00456 m^2, x = 0.0003 m, R_{Ext} = 10000 Ω),
2) The initial substrate concentrations ($[Sub]_{bio}$) were imported to cell H11 (ethanol = 298 mg/L) and cell S11 (glucose = 281 mg/L),
3) The overall COD was calculated in cell AA11 as presented in eq. 6-1 to 6-10. The substrate consumption rate ($r_{sub,A}$) was calculated in cell K11 (for ethanol) and cell V11 (for glucose) using built-in eq. 6-13,
4) The endogenous respiration rate in the anode biofilm ($r_{res,A}$) was calculated in cell AG11 using built-in eq. 6-14,
5) The current density in the anode biofilm (i_A) was calculated in cell AM12 using eq. 6-12 and eq. 6-15,
6) The anode potential (E_A) was calculated in cell AS11 – AU11 using eq. 6-18; various losses were calculated in AW11 – BC11 using eq 6-19 to eq. 6-24.

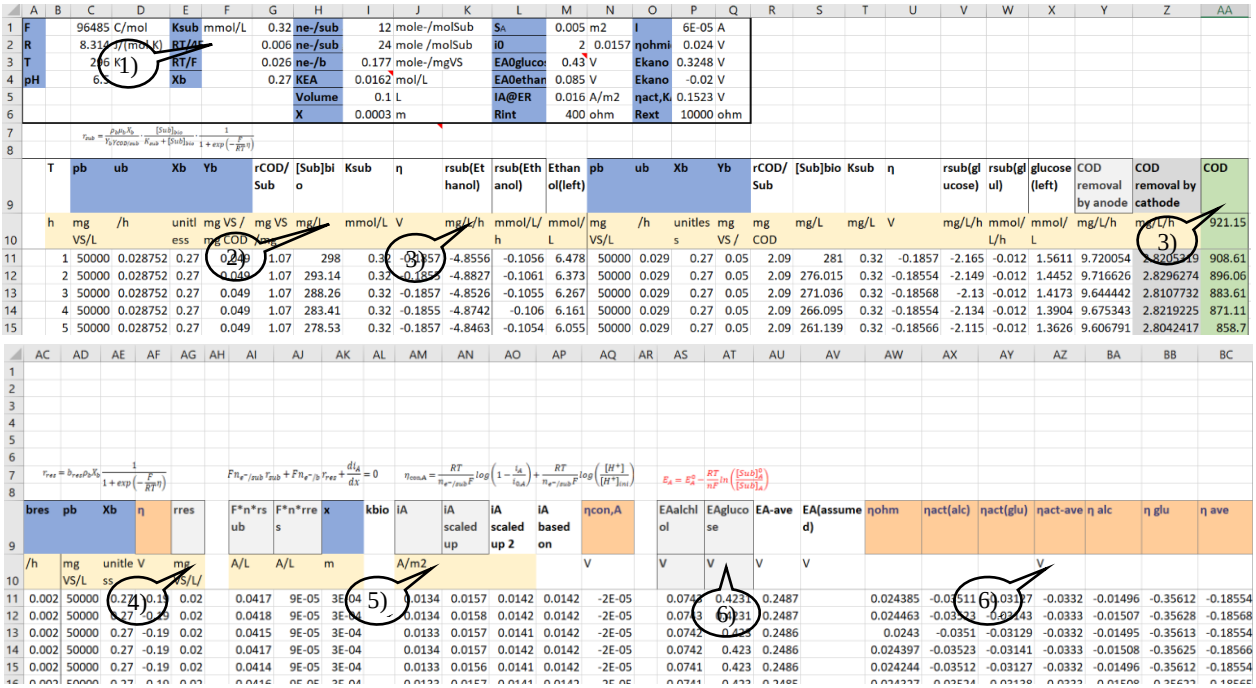

Figure 6-5 Anode half-cell model implementation process

6.1.3 Cathode steady state half-cell model

The cathode structure is more complex, contains four domains from the air side to the solution side, the PTFE diffusion layer (4 sub layers), the carbon cloth, the Pt/C catalyst layer, and the biofilm. In the cathode half-cell model, the following assumptions were made:

- Oxygen diffusion was restricted to one direction from air side to solution side.
- The catalyst layer and carbon cloth were saturated with liquid, the PTFE layer was waterproof and non-conductive.
- The bacteria on the cathode were assumed to be all heterotrophic aerobic bacteria, as the contribution of autotrophic aerobic bacteria to oxygen reduction as the biocatalyst is minor compared to the Pt/C catalyst (Popat et al., 2012).
- The cathodic potential was assumed to be fixed at steady state so the influence of the electrochemical changes in the cathode were neglected.

- The thickness of each layer was assumed in Table 6-5:

Table 6-5 Thickness of different layers of MFC air cathode

Layer	Thickness (μm)	References
PTFE diffusion layer (×4)	100	Assumed (Ou et al., 2016)
Carbon cloth	410	Measured
Pt/C catalyst layer	100	Assumed
Biofilm	1000	Measured

6.1.3.1 Electron balance and oxygen diffusion

The reduction reaction occurring in the cathode normalized by electron can be expressed as

$$0.25O_2 + e^- + H^+ \rightarrow \frac{1}{2}H_2O. \quad \text{eq. 6-34}$$

The cathode electron balance equation represents that the electrons transferred to the cathode are equal to the electrons utilized by cathode bacterial respiration. The steady state electron balance equation for the cathode is as follows (Marcus et al., 2007; Merkey and Chopp, 2012):

$$\frac{\partial i_C}{\partial x} + \left(n_{O_2}F\right)r_{O_2,C} = 0 \quad \text{eq. 6-35}$$

$$I = S_C \int_0^{L_{cat}} di_C \quad \text{eq. 6-36}$$

where

i_C = current density in cathode, A/m^2,

n_{O_2} = electron equivalence of oxygen, mmol e- / mmol oxygen,

$r_{O_2,C}$ = oxygen reduction rate, mmol/(L.s),

I = current, A,

S_C = projected surface area of cathode, m^2,

L_{cat} = thickness of catalyst, m^2.

The oxygen reduction rate at the cathode was obtained through combining the Monod equation and the Butler Volmer equation (Sirinutsomboon, 2014; Torres et al., 2008) as:

$$r_{O_2,C} = k_{O_2} \frac{[O_2]_{cat/liq}}{K_{O_2} + [O_2]_{cat/liq}} \exp\left[(1-\alpha_C)\frac{n_{e^-/O_2}F}{RT}(E_C - E_C^0)\right] \quad \text{eq. 6-37}$$

where

k_{O_2} = oxygen reduction rate per area, mmol/dm^2/s,

$[O_2]_{cat/liq}$ = oxygen concentration at the cathode|liquid interface, mmol/L,

K_{O_2} = half velocity constant for oxygen, mmol/L,

α_C = electron transfer coefficient of cathode, unitless,

E_C = cathode potential, V,

E_C^0 = standard reduction potential for the cathode, V.

The oxygen consumed at the cathode was dissolved from air after diffusing through the PTFE diffusion layer. The oxygen solubility is strongly dependent on the temperature (decreases at higher temperatures), pressure (increases at higher pressure), and the ionic strength (decreases at higher concentration of electrolyte). The oxygen concentration when diffusing through the PTFE layers was calculated by Fick's law of diffusion (Rharbi et al., 1999; Sirinutsomboon, 2014; Zielke, 2006) as follows:

$$\frac{\partial}{\partial t}[O_2]_{PTFE} = D_{O_2,PTFE}\frac{\partial^2}{\partial y^2}[O_2]_{PTFE} \quad \text{eq. 6-38}$$

where

$[O_2]_{PTFE}$ = oxygen concentration in PTFE layer, mmol/L,

y = location in PTFE layer, μm,

$D_{O_2,PTFE}$ = diffusivity of oxygen in PTFE, constant, μm^2/s.

The differential equations documented above were solved by a numerical approximation technique, using the implicit finite difference method (Zielke, 2006; Sirinutsomboon, 2014). Take the oxygen diffusion concentration for example, when the oxygen diffusion reaches steady state, in other words the diffusing concentration remains constant at all points on each side of the PTFE diffusion layers, the equation above then can be reduced to

$$\frac{\partial^2}{\partial y^2}[O_2]_{PTFE} = 0. \qquad \text{eq. 6-39}$$

Simplify the equation above by integrating twice with respect to y and introducing the boundary conditions at y = 0 and l (thickness of PTFE diffusion layer),

$$\frac{[O_2] - [O_2]_1}{[O_2]_2 - [O_2]_1} = \frac{x}{l}. \qquad \text{eq. 6-40}$$

As the concentration changes linearly from $[O_2]$ to $[O_2]_1$ through PTFE layer and the diffusion rate is the same across all sections. Therefore, the diffusion rate per unit area of section is calculated as

$$J = -D_{O_2,PTFE}\frac{d[O_2]_{PTFE}}{dy} = D_{O_2,PTFE}\frac{[O_2]_{air} - [O_2]_{cat/liq}}{l} \qquad \text{eq. 6-41}$$

where

J = diffusion rate per area,

$[O_2]_{air}$ = oxygen concentration in air, mmol/L,

$[O_2]_{PTFE|cc}$ = oxygen concentration at the PTFE|carbon cloth interface, mmol/L.

6.1.3.2 Cathode potential

Cathode potential was obtained using the Nernst equation:

$$E_C = E_C^0 - \frac{RT}{n_{e^-/o_2}F} ln\left(\frac{1}{[O_2]_{cat/liq}[H^+]^4_{cat/liq}}\right) \qquad \text{eq. 6-42}$$

where

$[H^+]_{cat/liq}$ = proton concentration at the cathode|liquid interface, mol/L.

At the boundary conditions, the cathode and anode voltage balance can be expressed as

$$E_C - E_A - IR_{Ext} = 0. \quad \text{eq. 6-43}$$

6.1.3.3 Heterotrophic Aerobic Bacteria

Glucose and ethanol are used as the carbon source and electron donor in this model. For glucose the electron donor reaction (R_d), electron acceptor reaction (R_a) and the bacterial synthesis reaction for HAB (R_c) are shown as:

R_d: $$\frac{1}{24}C_6H_{12}O_6 + \frac{1}{4}H_2O \rightarrow \frac{1}{4}CO_2 + H^+ + e^-;\ \Delta G_p^{0'} = -41.0\ \text{kJ/e}^-\ \text{eq} \quad \text{eq. 6-44}$$

R_a: $$0.25O_2 + e^- + H^+ \rightarrow \frac{1}{2}H_2O;\ \Delta G_p^{0'} = -78.7\ \text{kJ/e}^-\text{eq} \quad \text{eq. 6-45}$$

R_c $$\frac{1}{5}CO_2 + e^- + H^+ + \frac{1}{20}HCO_3^- + \frac{1}{20}NH_4^+ \rightarrow \frac{1}{20}C_5H_7O_2N + \frac{9}{20}H_2O \quad \text{eq. 6-46}$$

where the total energy released from glucose redox reaction

$$\Delta G_r^{0'} = (-78.7\ \text{kJ/e}^-\text{eq}) + (-41.0\ \text{kJ/e}^-\text{eq}) = -119.7\ \text{kJ/e}^-\ \text{eq.} \quad \text{eq. 6-47}$$

Ammonium is the nitrogen source; pyruvate is assumed to be the cellular intermediate in the conversion of a carbon source in cellular carbon. The standard free energy of carbon source converted to pyruvate ($\Delta G_p^{0'}$ = -5.9 kJ/e$^-$eq) can be derived by the sum of energy from electron donor reaction (-41.0 kJ/e$^-$eq) and the pyruvate production reaction (35.1 kJ/e$^-$eq). The energy required to synthesize one mole of cells ($C_5H_7O_2N$) from pyruvate ($\Delta G_{pc}^{0'}$ = 18.8 kJ/e$^-$eq) is based on an assumption of 10.5 g of cell dry weight per mole of ATP consumed and a free energy of 52.3 kJ/mol for ATP hydrolysis under physiological conditions (Grady et al., 2011; Ou et al., 2016; Roden and Jin, 2011). The energy and electron balance between

anabolism/catabolism of HAB is calculated based on Grady's (Grady et al., 2011) interpretation of McCarty's (1971) model.

$$\frac{f_e^0}{f_s^0} = \frac{-\left(\frac{\Delta G_p^{0'}}{\sigma^n} + \frac{\Delta G_{pc}^{0'}}{\sigma}\right)}{\sigma \Delta G_r^{0'}} \quad \text{eq. 6-48}$$

$$f_e^0 + f_s^0 = 1 \quad \text{eq. 6-49}$$

where

f_e^0 = the fraction of electrons directed by HAB from the cathode to O_2,

f_s^0 = the fraction of electrons that go from the cathode to biomass,

σ = the energy transfer coefficient (σ=0.6) (Grady et al., 2011),

n = the influence factor that equals to

$$n = \begin{cases} -1, & \Delta G_p^0 < 0 \\ +1, & \Delta G_p^0 > 0 \end{cases}. \quad \text{eq. 6-50}$$

Here f_e^0 is calculated to be 0.279 and f_s^0 0.721.

The final reaction is achieved as

$$C_6H_{12}O_6 + 1.67O_2 + 0.865HCO_3^- + 0.865NH_4^+ = 2.54CO_2 + 5.13H_2O + 0.865C_5H_7O_2N \quad \text{eq. 6-51}$$

The HAB biomass yield ($Y_{bio,HAB}$) and oxygen yield ($Y_{O_2,HAB}$) from glucose are

$Y_{bio,HAB}$ = 0.865 mol HAB / mol glucose, eq. 6-52

$Y_{O_2,HAB}$ = 1.67 mol O_2 / mol glucose, eq. 6-53

and the reaction rate of biomass ($r_{bio,HAB}$) and oxygen ($r_{O_2,HAB}$) can be derived as

$$r_{bio,HAB} = -Y_{bio,HAB} \cdot r_{Ac,HAB} \quad \text{eq. 6-54}$$

$$r_{O_2,HAB} = Y_{O_2,HAB} \cdot r_{Ac,HAB}.$$ eq. 6-55

Similarly, with ethanol as the electron donor,

R_d: $$\frac{1}{12}CH_3CH_2OH + \frac{1}{4}H_2O \rightarrow \frac{1}{6}CO_2 + H^+ + e^-;\ \Delta G_p^{0'} = -33.0\ \text{kJ/e}^-\ \text{eq}$$ eq. 6-56

R_a: $$0.25O_2 + e^- + H^+ \rightarrow \frac{1}{2}H_2O;\ \Delta G_p^{0'} = -78.7\ \text{kJ/e}^-\text{eq}$$ eq. 6-45

R_c $$\frac{1}{5}CO_2 + e^- + H^+ + \frac{1}{20}HCO_3{}^- + \frac{1}{20}NH_4{}^+ \rightarrow \frac{1}{20}C_5H_7O_2N + \frac{9}{20}H_2O$$ eq. 6-46

$\Delta G_r^{\circ'}$ = (-78.7 kJ/e$^-$eq) + (-33.0 kJ/e$^-$eq) = -111.7 kJ/e$^-$ eq, eq. 6-57

f_e^0 = 0.341, eq. 6-58

f_s^0 = 0.659. eq. 6-59

The final reaction is achieved as

$$CH_3CH_2OH + 1.02O_2 + 0.395HCO_3{}^- + 0.395NH_4{}^+ = 0.418CO_2 + 2.61H_2O + 0.395C_5H_7O_2N.$$ eq. 6-60

The HAB biomass yield ($Y_{bio,HAB}$) and oxygen yield ($Y_{O_2,HAB}$) from ethanol are

$Y_{bio,HAB}$ = 0.395 mol HAB/mol ethanol, eq. 6-61

$Y_{O_2,HAB}$ = 1.02 mol O_2/mol ethanol. eq. 6-62

6.1.3.4 Cathode model implementation

The equations derived in this section were built into the cathode model worksheet as shown in Figure 6-2 (b). The constants and operational parameters were imported into the input area. An example was given as

follows to present the implementation process of the initial status when using the standard medium (COD ~1000 mg/L), the step numbers are further noted in Figure 6-6 for clarity.

1) The operational parameters were initialized with given condition (T = 296 K, pH = 6.5, S_C = 0.00456 m^2, L_C = 100 µm = 0.0001 m).
2) The diffusion rate of oxygen per area (J) was calculated in cell G10 using eq. 6-41.
3) The E_C was calculated in cell M10 using built-in eq. 6-42. The column M was then used to calculate output V by using eq. 6-43.
4) The reaction rate of biomass ($r_{bio,HAB}$) and oxygen ($r_{O_2,HAB}$) was calculated in cell N10 and O10 using eq. 6-54 and 6-55 respectively.
5) The COD consumed (glucose equivalent) was calculated in Q10 using eq. 6-1 and 6-8, this portion of COD was then added to column AA in the anode model for overall COD consumption.

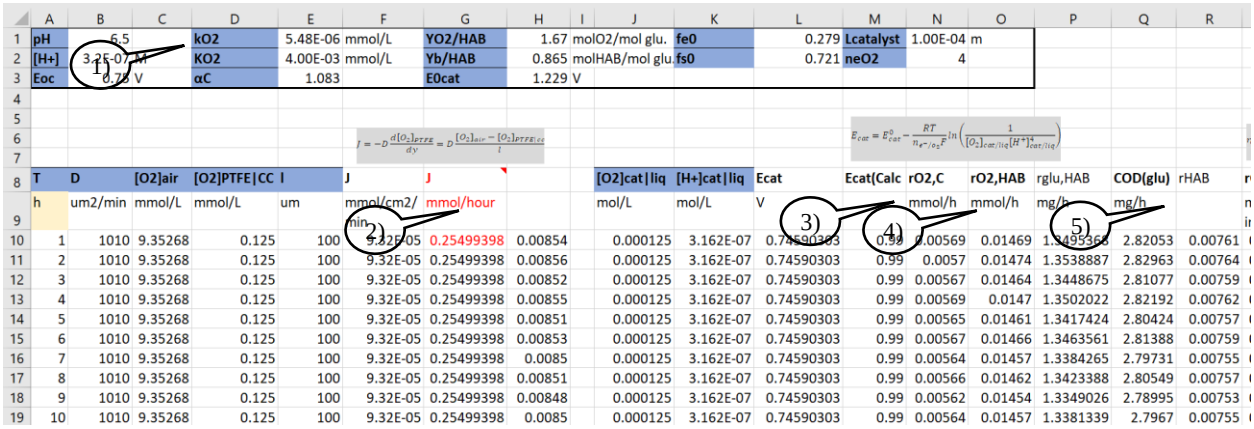

	A	B	C	D	E	F	G	H	I	J	K	L	M	N	O	P	Q	R
1	pH	6.5		kO2	5.48E-06	mmol/L	YO2/HAB	1.67	molO2/mol glu.	fe0	0.279	Lcatalyst	1.00E-04	m				
2	[H+]	3.2E-07	M	KO2	4.00E-03	mmol/L	Yb/HAB	0.865	molHAB/mol glu	fs0	0.721	neO2	4					
3	Eoc	0.79	V	αC	1.083		E0cat	1.229	V									
8	T	D	[O2]air	[O2]PTFE|CC	l	J	J			[O2]cat|liq	[H+]cat|liq	Ecat	Ecat(Calc	rO2,C	rO2,HAB	rglu,HAB	COD(glu)	rHAB
9	h	um2/min	mmol/L	mmol/L	um	mmol/cm2/min	mmol/hour			mol/L	mol/L	V		mmol/h	mmol/h	mg/h	mg/h	
10	1	1010	9.35268	0.125	100	9.32E-05	0.25499398	0.00854		0.000125	3.162E-07	0.74590303	0.99	0.00569	0.01469	1.3499368	2.82053	0.00761
11	2	1010	9.35268	0.125	100	9.32E-05	0.25499398	0.00856		0.000125	3.162E-07	0.74590303	0.99	0.0057	0.01474	1.3538887	2.82963	0.00764
12	3	1010	9.35268	0.125	100	9.32E-05	0.25499398	0.00852		0.000125	3.162E-07	0.74590303	0.99	0.00567	0.01464	1.3448675	2.81077	0.00759
13	4	1010	9.35268	0.125	100	9.32E-05	0.25499398	0.00855		0.000125	3.162E-07	0.74590303	0.99	0.00569	0.0147	1.3502022	2.82192	0.00762
14	5	1010	9.35268	0.125	100	9.32E-05	0.25499398	0.00851		0.000125	3.162E-07	0.74590303	0.99	0.00565	0.01461	1.3417424	2.80424	0.00757
15	6	1010	9.35268	0.125	100	9.32E-05	0.25499398	0.00853		0.000125	3.162E-07	0.74590303	0.99	0.00567	0.01466	1.3463561	2.81388	0.00759
16	7	1010	9.35268	0.125	100	9.32E-05	0.25499398	0.0085		0.000125	3.162E-07	0.74590303	0.99	0.00564	0.01457	1.3384265	2.79731	0.00755
17	8	1010	9.35268	0.125	100	9.32E-05	0.25499398	0.00851		0.000125	3.162E-07	0.74590303	0.99	0.00566	0.01462	1.3423388	2.80549	0.00757
18	9	1010	9.35268	0.125	100	9.32E-05	0.25499398	0.00848		0.000125	3.162E-07	0.74590303	0.99	0.00562	0.01454	1.3349026	2.78995	0.00753
19	10	1010	9.35268	0.125	100	9.32E-05	0.25499398	0.0085		0.000125	3.162E-07	0.74590303	0.99	0.00564	0.01457	1.3381339	2.7967	0.00755

Figure 6-6 Cathode half-cell model implementation process

6.2 Model verification (1000 mg/L COD, R_{Ext} = 10 KΩ)

The model verification process was completed assuming a feed strength of 1000 mg/L COD and an external resistance of 10 KΩ. The simulated and measured results on output voltage and COD removal are compared in Figure 6-7. Figure (a) reveals the simulated output voltage fit well with the previous results. The COD trend from the model also predicted the measured result (Figure (b)), both of which showed a constant

degradation rate at the beginning of the cycle, followed by a stable reading at the end, which agreed with the power output under the same feed strength (constant output after feed followed by 0 outcome when fuel ran out). The summary of the curves in the COD degradation phase are not identical and the experimental system did achieve slightly better overall COD removal. A summary of the verification results is given in Table 6-6. The results indicated that when using 1000 mg/L SWW (COD strength), the model fit well with the measured results on both COD removal (24 h and overall) and energy output (voltage, power and max. out period).

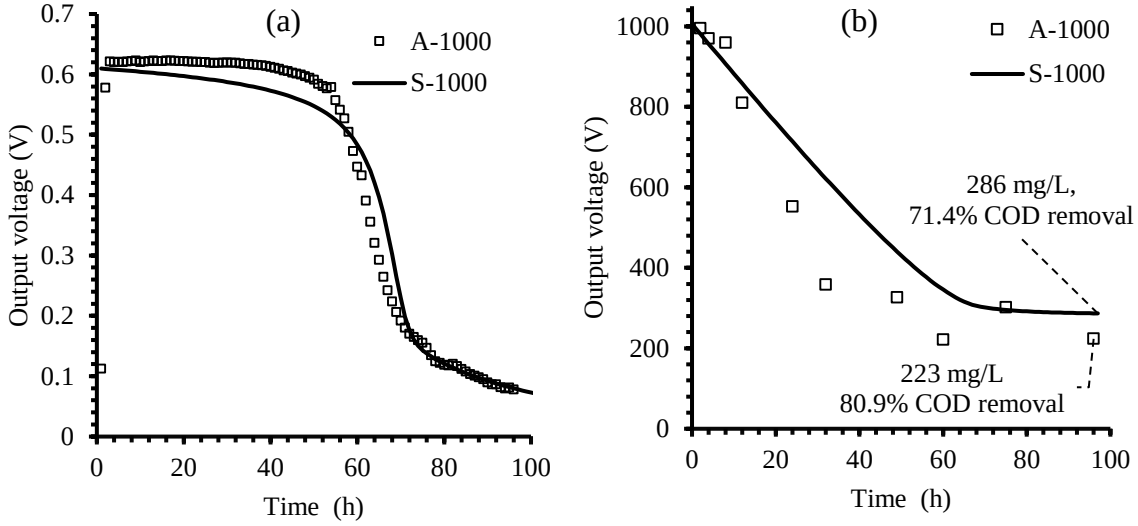

Figure 6-7 MFC model training results (1000 mg/L COD)
a) Output voltage comparison; b) COD removal comparison
'A' and 'S' in the legend stands for 'actual value' and 'simulated value' respectively; R_{Ext} = 10 KΩ.

Table 6-6 Summary of MFC model training results (1000 mg/L COD)

Media COD (mg/L)	1000	1000
	Actual	Simulated
COD removal 24h (%)	79±3	29
COD removal/cycle (%)	82±7	71.4
Max. output V (V)	0.60	0.61
Max. output P (mW) (ER=10KΩ)	0.036	0.037
Max. output period (h) (90% of Max V)	45	50

*Column in shade represents simulated values

6.3 Model validation

The model was further validated with higher COD strengths and different external resistances. The output voltage, COD, the effects of feed composition, external and internal resistance are discussed in detail respectively as follows:

6.3.1 Output voltage

Figure 6-8 gives a summary of the simulated output voltage from the model with increasing COD strength as input, indicating the trend that the maximum output voltage period increases with respect to the feed strength. Figure 6-9 further compares the model output voltage with different input COD to measured results from Chapter 4 respectively. Figure (a) (1000 mg/L COD) and (b) (2000 mg/L COD) fit reasonably well with the previous results; however, (c) and (d) reveal that the predicted data do not match the measured results as well as the feed strength increases. It becomes more obvious when the COD strength is 4000 mg/L, the actual output voltage differentiates itself from the simulated output voltage with more fluctuation (caused by temperature or decomposition of biofilm as discussed in Chapter 4), which was not predicted by the model.

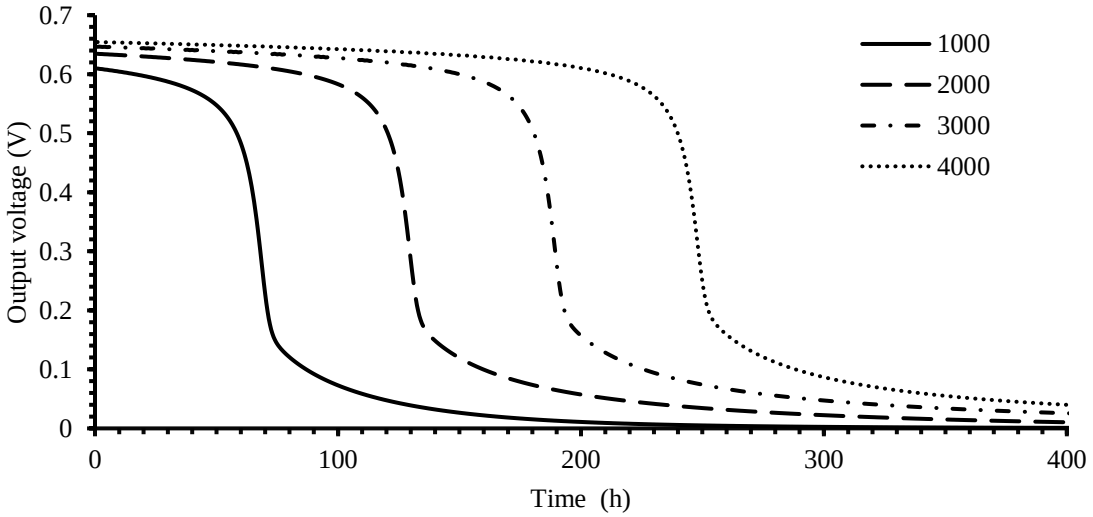

Figure 6-8 Model output (voltage) under different COD strengths
Numbers in the legend stand for input COD concentrations (mg/L); R_{Ext} = 10 KΩ

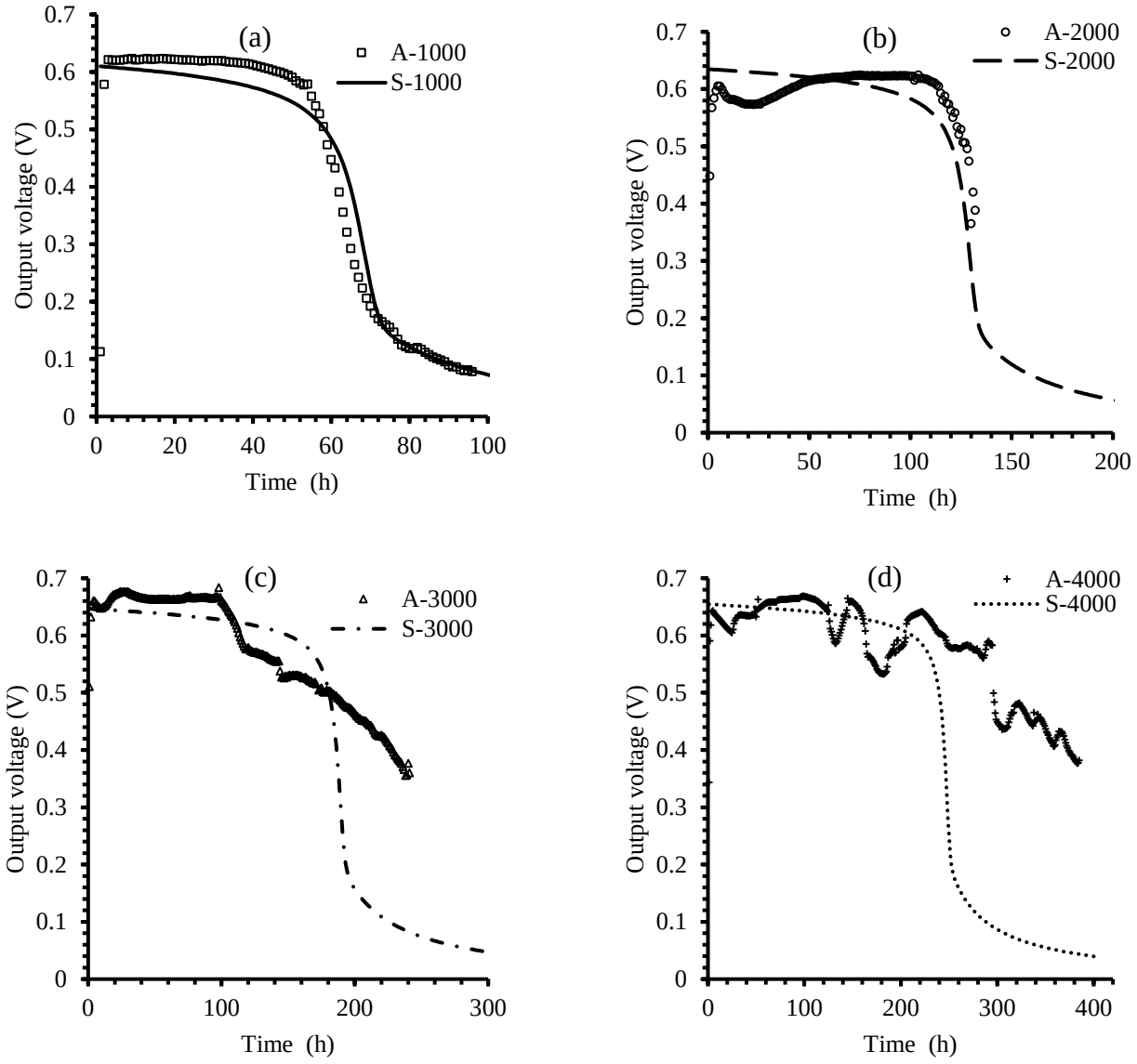

Figure 6-9 Comparison of measured and simulated output voltage under different COD strengths
'A' and 'S' in the legend stands for 'actual value' and 'simulated value' respectively; numbers stand for the COD concentration (mg/L); R_{Ext} = 10 KΩ.

6.3.2 COD degradation

Similarly, The COD degradation efficiencies predicted from the model with varied COD strengths indicate that, with the increase of the feed strength, the time for degradation also increased (Figure 6-10). Figure 6-11 gives the comparison of corresponding COD degradation efficiencies (feed strength 1000 - 4000 mg/L

COD). The model predicted the results at 1000 mg/L COD in Figure 6-11 (a), however, with the increase of feed strength, the simulated data start to deviate from the experimental results. They are slightly different from the actual performance of the reactors, in which the COD usually dropped sharply at the beginning of each cycle, and then started to stabilize at the end of cycle, whereas the simulated COD followed a more linear decrease until it stabilized at the end.

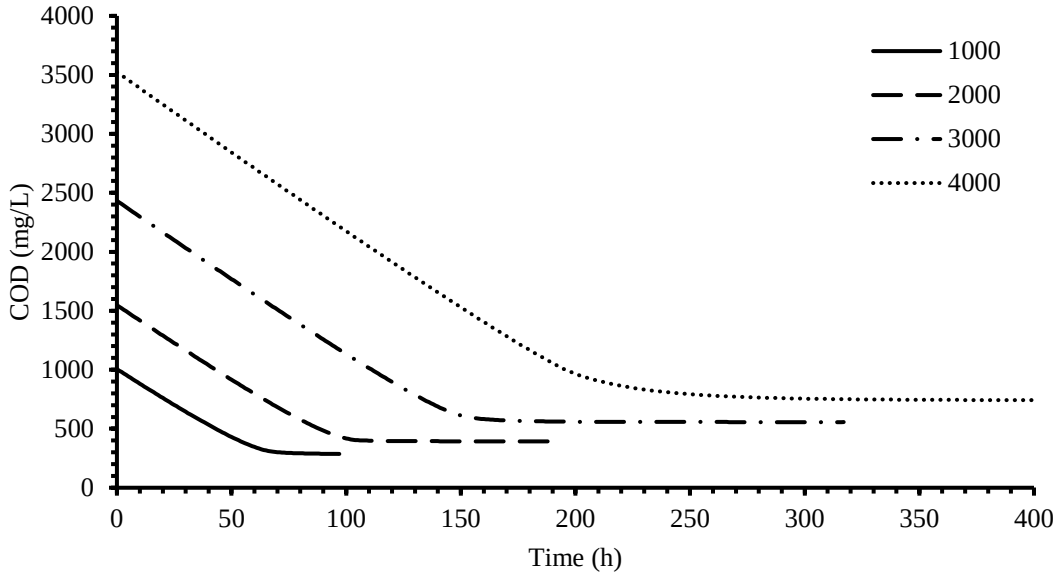

Figure 6-10 COD degradation efficiency under different COD strengths
Numbers in the legend stand for input COD concentrations (mg/L); R_{Ext} = 10 KΩ

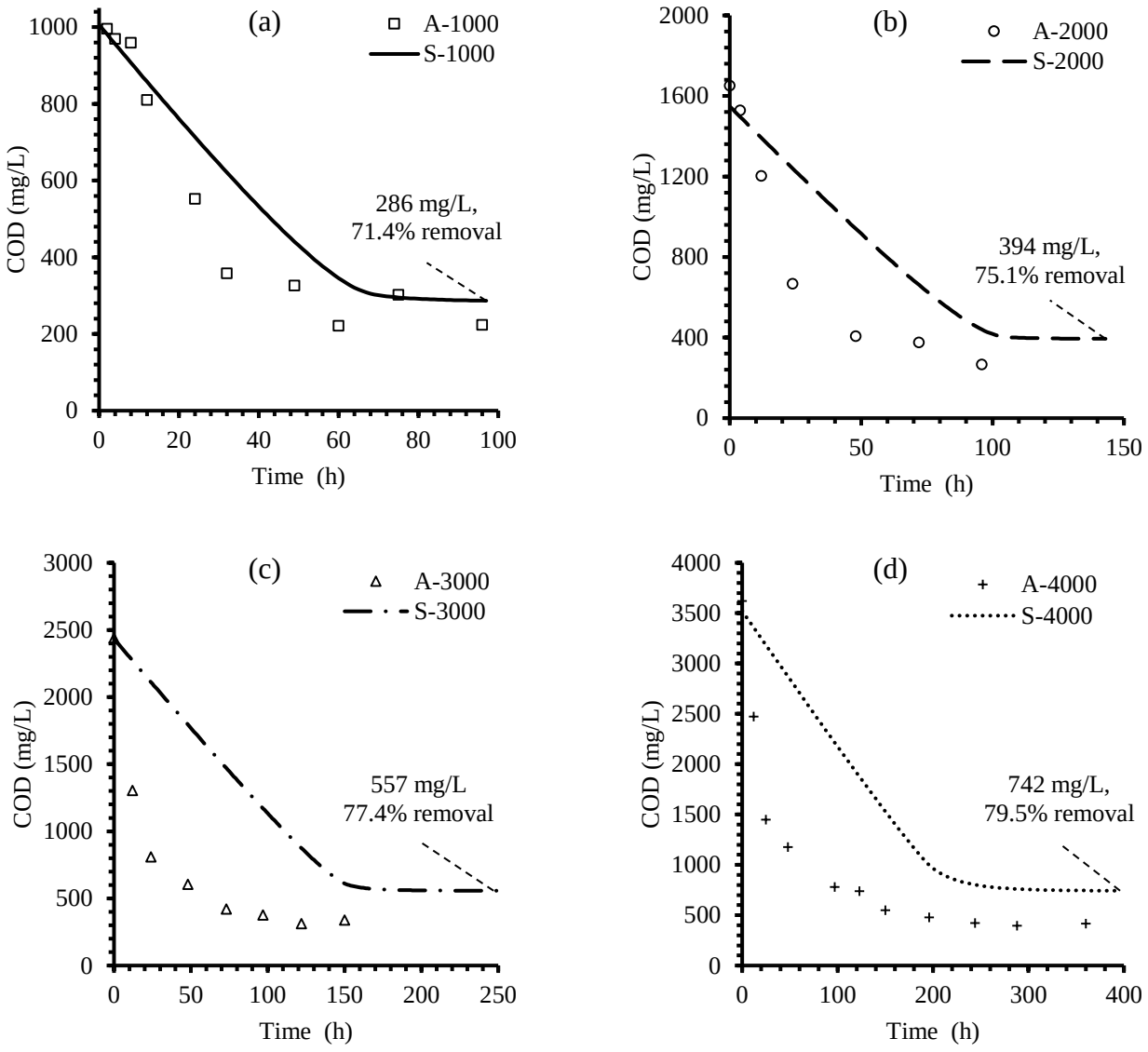

Figure 6-11 Comparison of actual and simulated COD degradation efficiency
'A' and 'S' in the legend stands for 'actual value' and 'simulated value' respectively, numbers stand for the COD concentration (mg/L); the value by the dash lines represents the residual COD (mg/L) and overall COD removal within this cycle. R_{Ext} = 10 KΩ.

Further to the finding above, the area between the curves for the simulated and measured COD before they stabilized (the accumulated COD difference (∑(ΔCOD.T)(mg/L*h), defined as y) was found to correlate to the feed strength (defined as x) with a relation of $y = 0.0006x^{2.4088}$ (R^2=0.9924), as shown in Figure 6-12.

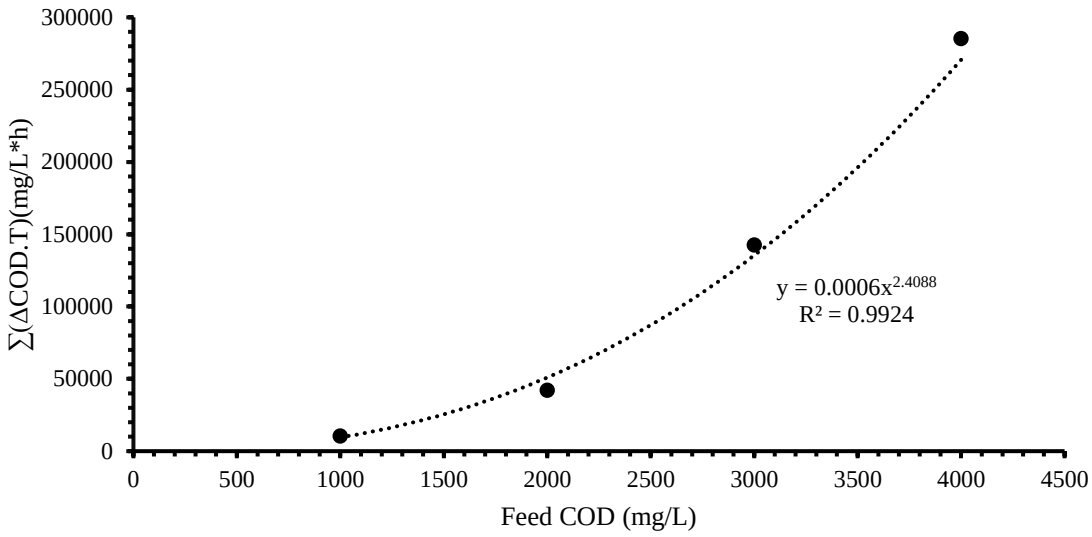

Figure 6-12 Correlation between the accumulated COD difference and feed COD

Table 6-7 presents a more detailed summary of the model output and experimental results. The electrical parameters (the maximum output voltage/power as well as the maximum output period) simulated by the model correspond well to the actual reactor. However, the actual COD removal rates within first 24 h are much higher than given in the model in every feed strength. The overall COD removal per cycle also follow a similar trend.

Table 6-7 Comparison of actual and simulated MFC reactor performance

Feed COD (mg/L)	Training		Validation					
	1000		2000		3000		4000	
	Actual	Simulated	Actual	Simulated	Actual	Simulated	Actual	Simulated
COD removal 24h (%)	79±3	29	73±4	20	67±1	13	59±1	9.3
COD removal/cycle (%)	82±7	71.4	86±5	75.1	90±3	77.4	91±4	79.5
Max. output V (V)	0.60	0.61	0.62	0.63	0.68	0.65	0.67	0.65
Max. output P (mW) (ER=10KΩ)	0.036	0.037	0.038	0.040	0.046	0.042	0.045	0.042
Max. output period (h) (90% of Max V)	45	50	120	107	112	165	196	220

*Columns in shade represent simulated values

The results presented in Figure 6-8 to Figure 6-12 and Table 6-7 can be explained by the complexity of the microbial community in the actual reactor. In the anode half-cell model several assumptions were made to

simplify the anode and anodic biofilm. Firstly, the biofilm was assumed to be all EABs and mature. However, the actual reactor was inoculated with anaerobic sludge, which is a complex mixed culture with the existence of various non-EABs as well as even yeast. These microorganisms can degrade the organic matter without transferring electrons to the anode, which explains why the actual COD can be degraded faster compared to the simulated results, but without correspondingly higher output power. Another assumption made was that the planktonic bacteria could be neglected in the model, which was common in previous MFC model studies (Ou et al., 2016; Pinto, 2011; Zeng et al., 2010). However, results from this study revealed the limits of this assumption. Figure 6-12 shows the accumulated COD difference increased sharply with the increase of feed strength. The proposed reason is the growth of planktonic cells due to excessive load supplement. When the reactor was fed with low COD medium, most of the organic matter was degraded by biofilm, which also explained that the predicted results fit well with the measured results when feed COD was 1000 mg/L. However, the increase of COD strength (from 2000 to 4000 mg/L) exceeded the degradation capacity of the biofilm, resulting in the growth of planktonic cells. This suggested that the higher the feed strength, the more significant role the planktonic cells played. The difference of the curve shape can also be explained by the complexity of the biofilm community and the impact of planktonic cells. Experimental results indicated that the COD removal in MFC reactors fit first-order kinetics, which has been reported by previous studies (Zhang et al., 2015); whereas the model predicted the COD degradation at close to zero-order kinetics before reaching 0 at the end of cycle (Figure 6-11), similar to other model studies (Picioreanu et al., 2007; Zeng et al., 2010). The excessive load may have caused the growth of planktonic cells and led to rapid consumption at the beginning of each cycle, followed by a decay stage at the end of cycle when load was limited. These findings indicate the limit of the biofilm anode/cathode model when applied to simulate an MFC reactor with excess load supply.

The model also shows that the COD degradation rate achieved by the anode is much higher than the cathode. An example (S-1000) is given in Figure 6-13, the COD removal speed (mg/L/h) of the anode is ~3.5x that

of the cathode (shown in (a)), and the overall COD removal (%) is 3.3x compared to that of the cathode (shown in (b)).

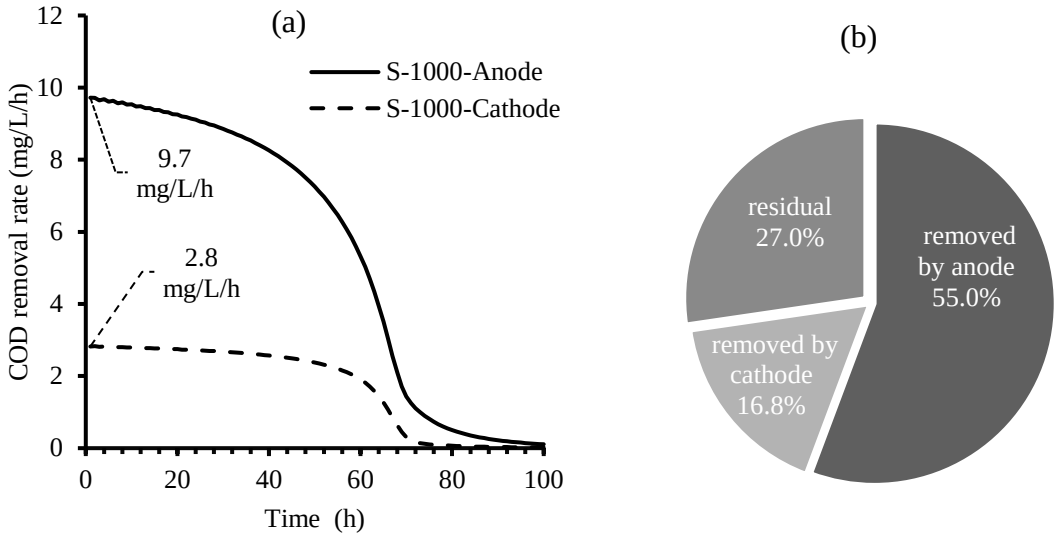

Figure 6-13 Simulated COD degradation by anode and cathode respectively (R_{Ext} = 10 KΩ)
(a): the degradation rate of anode and cathode when fed with SWW (COD 1000 mg/L), 'S' in the legend stands for 'simulated'; (b): the overall COD removal (%) accomplished by anode and cathode respectively.

Further analysis of the anode/cathode degradation ratio revealed that with the increase of feed strength from 1000 mg/L to 10000 mg/L COD, the ratio also increased relatively from 3.28 to 3.53 (Anode/cathode ratio = 0.1084 ln (feed COD) + 2.5647, R^2 = 0.8997) (Figure 6-14); Meanwhile the portion removed by the anode showed a higher increase from 55.0% (1000 mg/L COD) to 62.2% (10000 mg/L COD), compared to 16.8% to 17.6% by the cathode, as shown in Figure 6-15. This suggests that the anode plays a more essential role in an air cathode MFC in terms of COD removal, with the increase of feed strength, the anode accounts for more COD removal compared to the cathode. This has also been observed in other research (Gil et al., 2003; Hamelers et al., 2011; Marcus et al., 2007). The anode performance depends on various limiting factors; biofilm conductivity and electron donor concentration are two common ones usually discussed in MFC modelling. The conductivity of the anodic biofilm is usually contributed by the conductive nanowires in the EPS matrix of exoelectrogens (e.g. *Shewanella oneidensis MR-1* (Gorby et al., 2006; Marcus et al., 2007)). Inoculation of relative strains or creating a suitable environment for these species can improve the

conductivity and eventually improve the power generation efficiency of the reactor. This finding also suggests that the anode is more likely the limiting factor of an MFC system; anode optimization may be more efficient compared to cathode optimization in terms of COD removal.

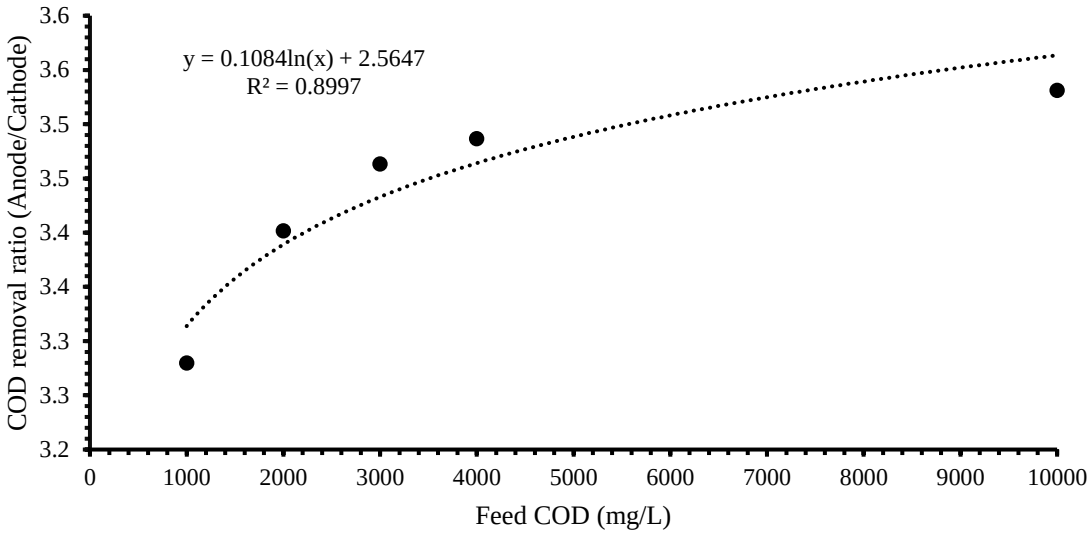

Figure 6-14 COD removal ratio (anode/cathode) under different COD strength.

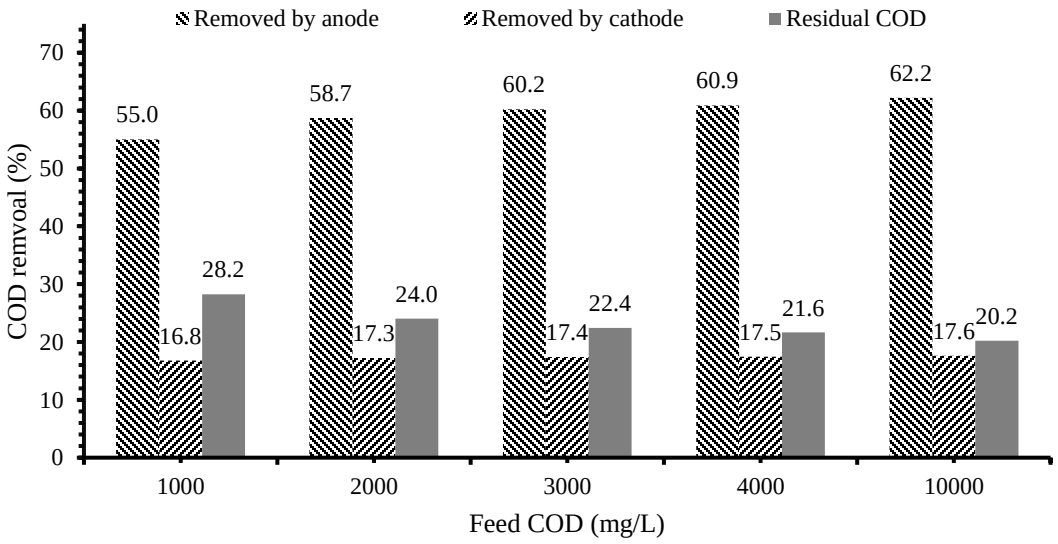

Figure 6-15 Simulated COD removal (%) by anode and cathode, respectively, under different COD strength.

6.4 Sensitivity analysis

The sensitivity analysis of this model was accomplished for three factors, the sensitivity to changes in feed composition, external resistance, and biofilm thickness.

6.4.1 Feed composition

The model output showed different patterns when changes to the feed composition were examined. The change of ethanol/glucose ratio resulted in a corresponding change in the power generation efficiency. A comparison example is given in Figure 6-16. As calculated in Section 6.1.1, the simplified SWW medium (COD 1000 mg/L) contains 298 mg/L ethanol and 281 mg/L glucose, with the concentration ratio of ~1 (298 mg/L : 281 mg/L). In order to compare the impact of composition, two additional types of media with same strength of COD (~1000 mg/L) but different ratio of ethanol to glucose were tested using the model, the compositions are shown in Table 6-8.

Table 6-8 Simulated SWW medium (~1000 mg/L COD) with different ethanol to glucose ratios

Concentration ratio	Ethanol (mg/L)	Glucose (mg/L)	COD (mg/L)
0.6	200	331	~1000
1	298	281	~1000
1.4	353	252	~1000

The simulated results generated from the model, including COD degradation curve and output voltage, are presented in Figure 6-16. The results indicated that the model showed low sensitivity on COD degradation efficiency, as all the media have the same COD strength. However, the output voltage showed different patterns, the medium with higher ethanol (or lower glucose) content resulted in higher and more constant output voltage.

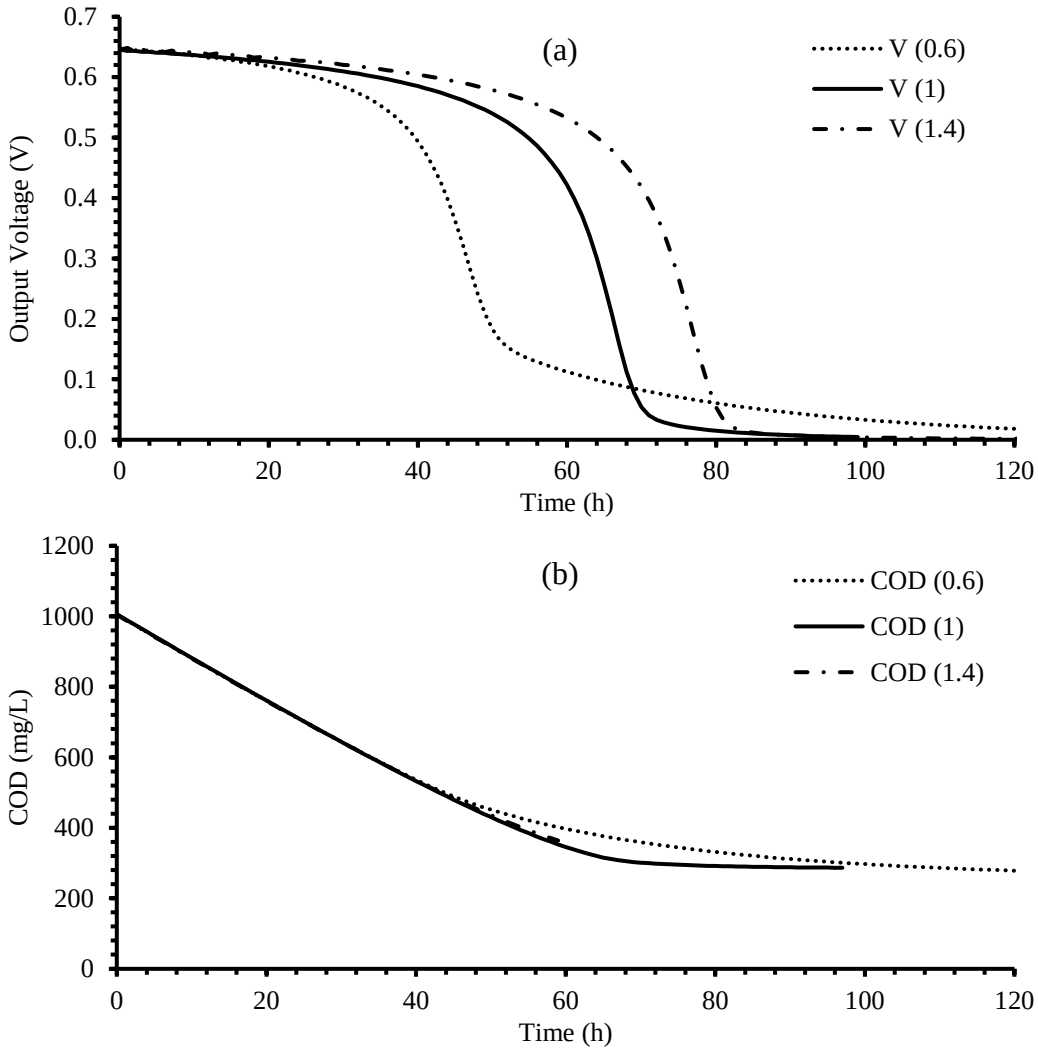

Figure 6-16 Impact of ethanol:glucose ratio on MFC model output voltage (a) and COD degradation (b) 0.6, 1 and 1.4 stand for medium with corresponding ratio as given in Table 6-8. R_{Ext} = 10 KΩ.

The explanation is that under the same mass concentration, ethanol has a much higher molar concentration (4.29x of glucose). This means ethanol contributes 2.15x more electrons than glucose under the same mass concentration (eq. 6-1 and 6-2). One of the applications for this finding is to pre-analyze the winery wastewater before using as MFC fuel. The contents of wastewaters from different wineries vary depending on the type of wine they produce, the technology they use for fermentation, etc. With help of the modelling, we can understand the wastewater containing highest ethanol tends to generate more power for the same COD strength. Furthermore, the model input can be increased to include more components in order to analyze the power generation potentials of different media.

6.4.2 Internal and external resistance

This model solely focuses on the stable state of the MFC reactor; therefore, the internal resistance was initially assumed to be stable (an estimated value of 400 Ω derived from Chapter 5 was given as input). Multiple methods can be used to estimate the reactor performance under different resistances. When the output voltage was derived using the current density i_A (i_A*S_A*R_{Ext}) calculated from eq. 6-17, the simulated results were very different from the actual data except when R_{Ext} = 10 KΩ, as shown in Figure 6-17 (a) vs (b). The possible reason was that in the physical system, the decrease of external resistance may have increased the activity and growth of EABs, which increased the thickness and conductivity of the anodic biofilm. As shown in eq. 6-15 and eq. 6-17 respectively, the increase in either biofilm conductivity or thickness would increase the current density proportionally.

An example of the sensitivity analysis on anodic biofilm thickness is given in Figure 6-18, increasing 0.1 mm of the anodic biofilm thickness (from 0.3 mm to 0.4 mm) resulted in an increase of 11.9% of maximum output voltage (25% of maximum output power), whereas decreasing by 0.1 mm (from 0.3 mm to 0.2 mm) led to a 21.9% and 39.0% loss in maximum output voltage and power respectively. Interestingly the change of anodic biofilm thickness did not result in a dramatically different COD removal as shown in Figure 6-18, revealing that the increase in biofilm would also lead to a higher columbic efficiency. The prediction of columbic efficiency is well paired with the observation in Chapter 5, that decreasing the external resistance closely to internal resistance would boost the columbic efficiency. To obtain a better prediction of output voltage using different external resistance, an alternative method was chosen by achieving anode and cathode potential respectively, and linking with Ohm's Law (by using OCV, external and internal resistance, as shown in eq. 6-18, eq. 6-42, and eq. 6-43). This method minimizes the impact of biofilm (conductivity, thickness) and provides an accurate description of the electrical performance. The optimized results are more in accordance with experimental data as shown in Figure 6-17 (c).

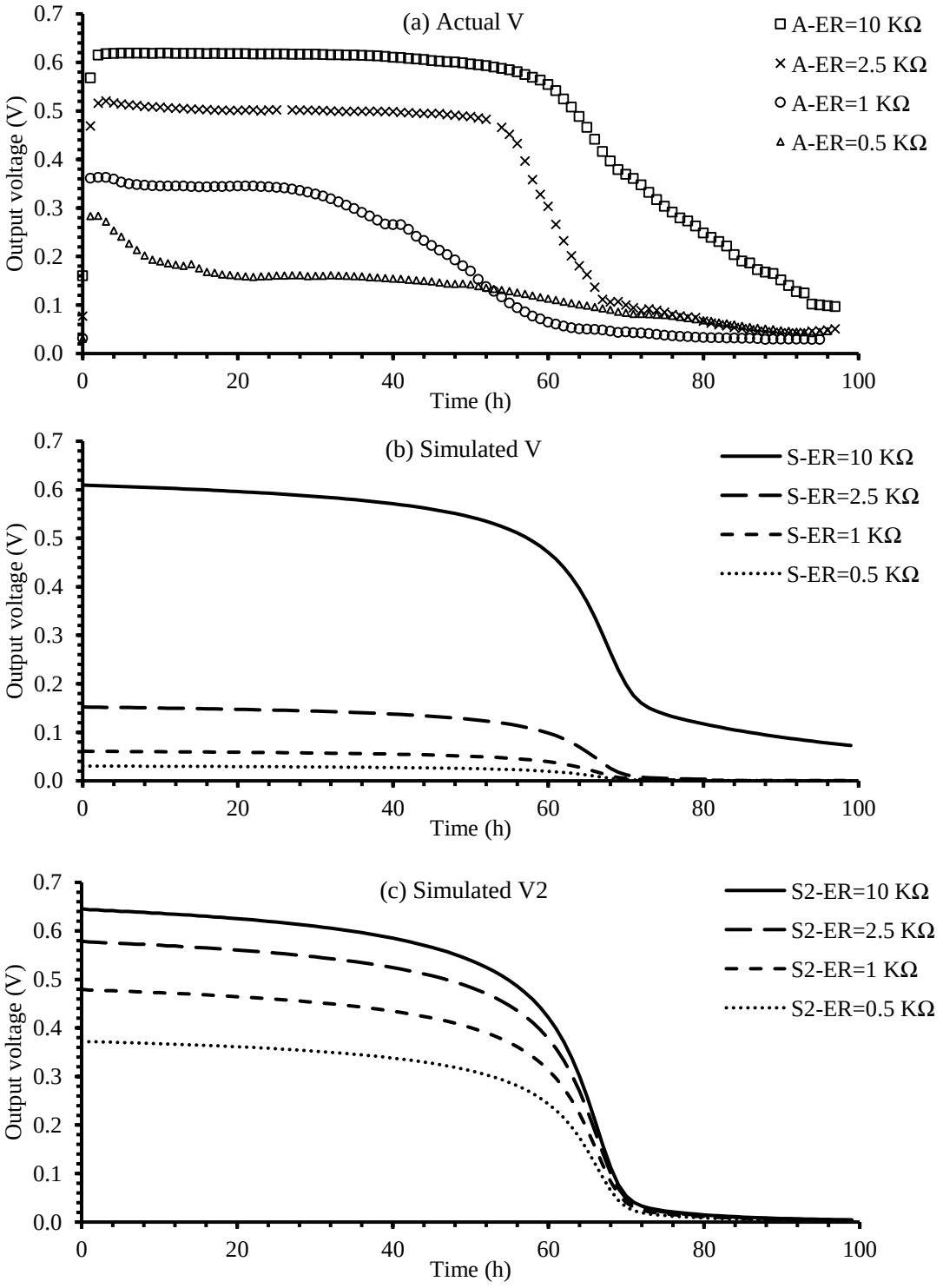

Figure 6-17 Comparison of actual and simulated output voltage using different external resistance 'A' and 'S' in the legend stands for 'actual and 'simulated' value respectively; (a): actual output voltages using different R_{Ext}; (b) simulated output voltages derived using current density (i_A); (c) simulated output voltages derived using electrode potentials.

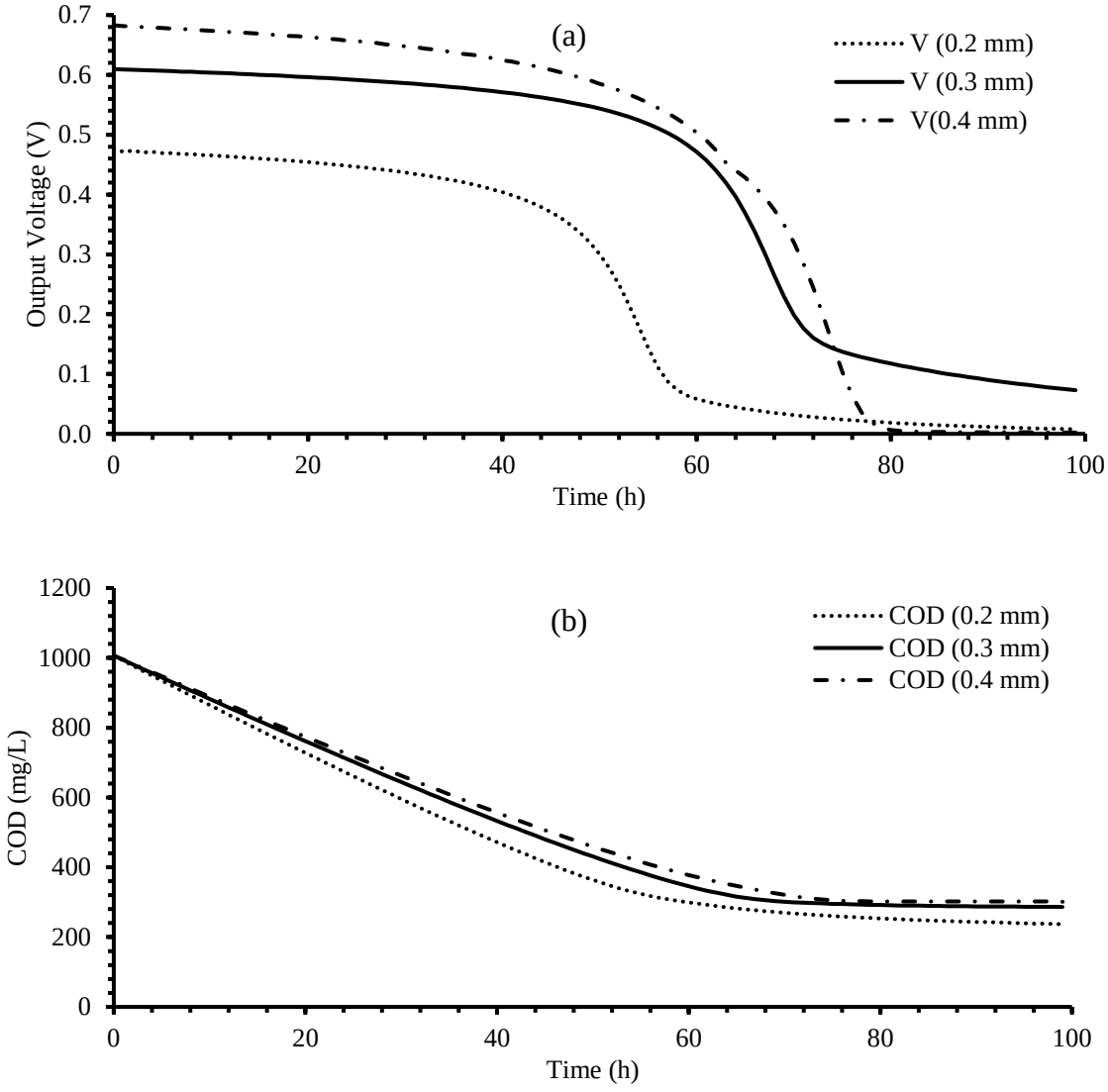

Figure 6-18 Impact of biofilm thickness on MFC model output voltage (a) and COD degradation (b) 0.2, 0.3 and 0.4 mm stand for anodic biofilm thicknesses. R_{Ext} = 10 KΩ

Polarization and power density curves simulated by this model (Figure 6-19) demonstrated that with internal resistance input, the model is capable of simulating what the power density and polarization curve would be if the biofilm of the reactor matured. As described in Section 5.2.2 overshoot phenomenon occurred when developing the polarization curve within one feed cycle due to the insufficient time that biofilm required to adapt to changed external resistance. Watson and Logan (2011) suggested a multi-cycle

method to allow the biofilm to mature when the external resistance changed in order to develop a more accurate polarization curve. This model could be used as an alternative way to simulate the polarization curve and power density analysis with a known internal resistance.

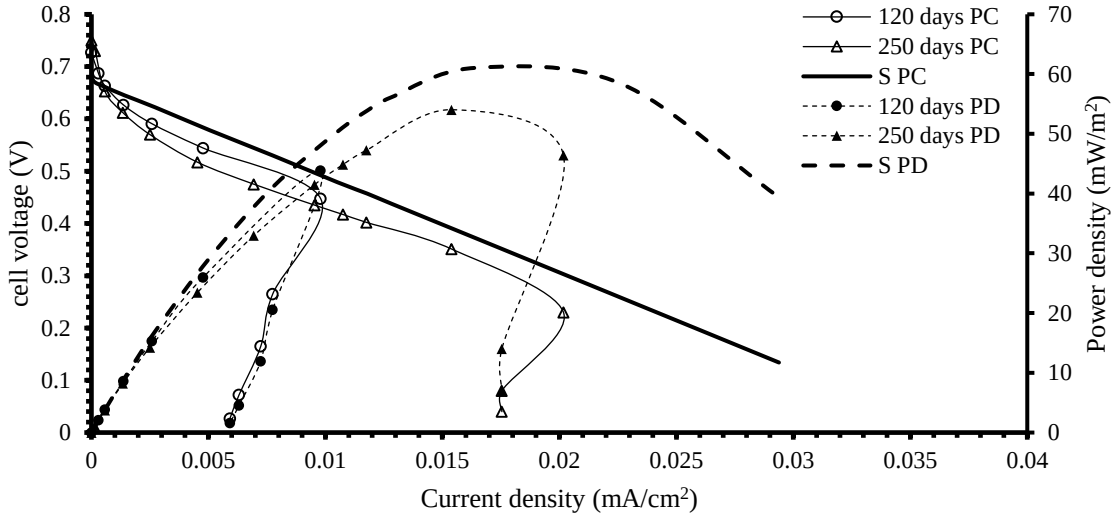

Figure 6-19 Comparison of actual and simulated polarization and power density curve
S: simulated value PC: Polarization curve; PD: Power density

6.5 Summary

This chapter presented the research progress in the development of various mathematical models for the simulation of MFC using SWW as substrate, followed by the development and use of a dynamic mathematical model of a single chamber MFC specifically for treating winery wastewater.

The biofilm anode was assumed and described using the Nernst-Monod equation, the anodic potential was described using the Nernst equation. The cathode was assumed to have a biofilm layer, oxygen diffusion was described using Fick's law of diffusion, oxygen reduction rate was estimated using the Monod equation and Butler Volmer equations. Finally, the two half-cell models were linked using mass and electron balance and Ohm's law. Constants, assumptions and boundary conditions were obtained by referring to published papers and experimental data obtained in lab studies.

The output voltage corresponded well with the actual data, however, the COD degradation efficiency showed a gap between the actual and simulated results, which was probably caused by the existence of non-EABs and the growth of planktonic cells at higher COD strength (≥ 2000 mg/L). The model revealed the anode of an air cathode MFC degraded more COD (~2.28x) than the cathode; with the increase of feed strength, the anode accounted for more COD removal compared to the cathode. The model also predicted that a higher power production can be obtained if using a SWW medium containing higher ethanol concentration. The thickness of the anodic biofilm was proportionally related to the external resistance; increasing the anode biofilm thickness was more effective to obtain a higher output voltage. Constant anodic biofilm thickness with respect to external resistance resulted in less accurate voltage simulation results. The model was more capable of simulating output voltage for different external resistances by using the potential balance equation.

Chapter 7. Conclusions

7.1 Summary of Work

The goal of the thesis was to investigate the application of microbial fuel cell (MFC) technology to winery wastewater treatment. In order to achieve this, single chamber air cathode MFCs were designed and fabricated, the impact of pH and buffer, seasonality, external and internal resistances were investigated and, a mathematical model was developed to describe the working mechanism of MFC fed SWW. Each specific objective was accomplished as follows:

- Design and fabricate an MFC reactor for the treatment of winery wastewater.

A 100 mL tubular shape single chamber air cathode MFC reactor was designed and constructed for the purpose of winery wastewater treatment. A 3K carbon fiber mesh was chosen as the anode, a pre-treated carbon cloth coated with PTFE (diffusion layers) and Pt/C (as catalyst layers) was designed as the cathode. Synthetic winery wastewater (SWW) medium was prepared by referring to the characterization results of winery wastewater sampled from vineyards. The MFC reactors were inoculated with anaerobic sludge and operated in batch mode. The medium was changed by replacing 80% of the volume with fresh feed based on either voltage drop or chemical oxygen demand (COD) consumption. Samples were taken routinely for further analysis required in this research. The reactor was loaded with an external resistance and the output voltage was continuously monitored every 2 min by a developed MFC monitoring system.

- Investigate the pH and buffer impact on MFC fed synthetic winery wastewater

The pH was found to be essential for the inoculation and maintenance of the MFC reactor. An optimum pH of 6.5 maintained by phosphate buffer was determined to provide stable MFC performance (both power production and COD removal). Other pHs or buffer (bicarbonate buffer) resulted in much lower power performance. Interestingly COD removal was unaffected by pH fluctuations, suggesting the sensitivity of

EABs to pH compared to the COD consuming microbial population. When the reactor was maintained at COD 1000 mg/L, PB 10 mM and pH 6.5, the highest COD removal rate was reached within 4 h after feed. The maximum output voltage was obtained 0.5 hour after feed and lasted for 60±3 h; COD removal reached ~80% within 60 h. An optimum COD:PB ratio (COD(mg/L):PB(mM)=100:1) was proposed for the purpose of cost effectiveness for the first time.

- Investigate the impact of seasonal changes of the synthetic winery wastewater as feed stock on the efficiency of MFC reactors

This study provides evidence that dog food is an effective alternative feed to maintain an active microbial population during the off season of a wastewater treatment plant (WWTP). The MFC was able to generate voltage from either SWW or dog food with no lag period after changing the feed. This reveals a great promise for the use of MFCs to treat agricultural wastes even when the seasonality of waste production is a challenge. Moreover, the performance of MFC fed SWW highly depends on the COD strength of the feed. With sufficient buffer supply to maintain pH stable at 6.5, when the COD of SWW feed was increased, the maximum voltage output did not increase, but instead the length of the period of maximum power increased. Overall, the energy recovery per cycle improved with increasing COD concentration in the wastewater up to about 0.042 kWh/kg COD removed.

- Investigate the impact of external and internal resistance on MFC treating synthetic winery wastewater

External resistance was found to be an effective control strategy to optimize MFC system performance by proper adjustment based on the purpose of the system. An external resistance set close to internal resistance maximized the treatment efficiency, whereas an external resistance higher than internal resistance increased the energy extracted from wastewater. The reason proposed was that decreasing the external resistance close to the internal resistance promoted the activation of EAB and resulted in faster COD degradation by exponentially improving the COD removal rate before reaching the limitation of the reactor. The study also

reinforced the need for proper pH buffer concentration adjustment as the change of external resistance may change the pH due to the alteration of the COD consumption rate; therefore, pH buffer concentration adjustment is mandatory. In addition, high salt condition (340 mM) failed to improve the reactor performance; increasing the time the reactor operated under optimum conditions, however, reduced the internal resistance and provided better output power density.

- Construct a numerical model describing the working mechanism of MFC treating winery wastewater

A numerical model was developed to understand the working mechanism of a single chamber MFC specifically for treating winery wastewater. Biofilm anode and cathode were described using the Nernst equation, the Nernst-Monod equation, and Fick's law of diffusion respectively, then linked together using mass & electron balance and Ohm's law. The model matched well on the output voltage when compared to experimental data, however, did not capture the COD removal rate well at higher COD strength (≥2000 mg/L). The proposed reason was the existence of non-EABs in the actual reactor consuming a fair amount of COD, and the planktonic cells in the anode chamber degrading more COD at higher feed strength. The model also revealed that the anode played a more essential role in an air cathode MFC in terms of COD removal, accounting for 3.28x or higher COD removal compared to the cathode. The reactor tended to generate more power if using a SWW medium containing higher ethanol concentration. The thickness of the anodic biofilm was proportionally related to the external resistance and, increasing the anode biofilm thickness resulted in an increase of output voltage.

7.2 Major contributions

This study demonstrated that MFC technology can be adopted for winery wastewater treatment and the treatment efficiency can be significantly improved with a better understanding of pH, seasonality, and operational parameters. The major original contributions of this thesis work are summarized as follows:

- This is the first experimental demonstration that an ideal phosphate buffer at a ratio of 1 mM buffer to each 100 mg/L COD could counter pH fluctuations during MFC operation.
- This is the first experimental demonstration that commercial dog food was an effective carbon source to maintain microbial activity and overcome the challenge of seasonality of a winery WWTP and MFC.
- This is the first model to suggest that the impact of planktonic cells can not be ignored when there was excessive load in the MFC system.

7.3 Limitations

The limitations of this study include:

- The reactor volume is restricted to 100 mL as a lab scale study; however, previous studies suggested that scaling up the reactor may lead to a decrease in efficiency. Therefore, further investigation needs to be done for larger scale studies.
- The model is currently limited by the range of assumptions used, such as equal area of anode and cathode, constant room temperature, a fixed reactor volume of 100 mL, etc.

7.4 Future work

Various aspects of the MFC treating winery wastewater were investigated throughout the study and opened up further investigation.

- The application of novel findings into retrofit or pilot scale MFC reactor

The findings from this thesis should be verified in a larger scale MFC. To continue this study, the Biological Solution Laboratory (BSL) has started another project developing an onsite MFC retrofit in Tantalus

Vineyards. The output power of the retrofit was measured as 50x more than discovered in this study, which is an exploration of the potential of MFC being used in actual wastewater treatment system.

- The use of the MFC model for extended applications

The numerical MFC model developed in this thesis can be further extended. The next-step study can be further divided into three directions.

1) Many previous studies assumed the activity of planktonic cells can be neglected, however, a significant finding from this model is that the contribution of planktonic cells on COD removal could not be ignored when the system was supplied with higher loads. As a future work a submodel to describe the contribution of planktonic cells on COD removal at excessive load supply is suggested to improve the simulation.
2) The model can be extended to cover not only the steady state but the overall process including the inoculation, growth, and decay state. Paired experiments need to be designed during the model development for verification and support.
3) Essential parameters for model development (e.g. K_{bio}) demand further investigation; Some parameters (e.g. Anodic and cathodic potential, the concentration of each specific medium component etc.) can be measured as real-time input for better simulation.
4) Another interesting direction is to apply this model to other wastes to verify if it can be used for more waste types, especially those that have not been tested as MFC feed before, to demonstrate the potential of resource recovery from these wastes. BSL lab is currently studying the application of MFC technology used in solid fruit waste treatment. This model can be adjusted using the characterization results of fruit waste results, in order to validate its flexibility under different circumstances.

References

Aaron, D., Tsouris, C., Hamilton, C.Y., Borole, A.P., 2010. Assessment of the effects of flow rate and ionic strength on the performance of an air-cathode microbial fuel cell using electrochemical impedance spectroscopy. Energies 3, 592–606. https://doi.org/10.3390/en3040592

Abrevaya, X.C., Sacco, N., Mauas, P.J.D., Cortón, E., 2011. Archaea-based microbial fuel cell operating at high ionic strength conditions. Extremophiles 15, 633–642. https://doi.org/10.1007/s00792-011-0394-z

Addi, H., Mateo-Ramírez, F., Ortiz-Martínez, V.M., Salar-García, M.J., Hernández-Fernández, F.J., de los Ríos, A.P., Godínez, C., Lotfi, E.M., Mahi, M. El, Blanco, L.J.L., 2018. Treatment of mineral oil refinery wastewater in microbial fuel cells using ionic liquid based separators. Appl. Sci. 8, 1–10. https://doi.org/10.3390/app8030438

Aelterman, P., Rabaey, K., Pham, H.T., Boon, N., Verstraete, W., 2006. Continuous electricity generation at high voltages and currents using stacked microbial fuel cells. Environ. Sci. Technol. 40, 3388–3394. https://doi.org/10.1021/es0525511

Aelterman, P., Versichele, M., Marzorati, M., Boon, N., Verstraete, W., 2008. Loading rate and external resistance control the electricity generation of microbial fuel cells with different three-dimensional anodes. Bioresour. Technol. 99, 8895–8902. https://doi.org/10.1016/j.biortech.2008.04.061

Asai, Y., Miyahara, M., Kouzuma, A., Watanabe, K., 2017. Comparative evaluation of wastewater-treatment microbial fuel cells in terms of organics removal, waste-sludge production, and electricity generation. Bioresour. Bioprocess. 4, 30. https://doi.org/10.1186/s40643-017-0163-7

Ayyaru, S., Dharmalingam, S., 2011. Development of MFC using sulphonated polyether ether ketone (SPEEK) membrane for electricity generation from waste water. Bioresour. Technol. 102, 11167–11171. https://doi.org/10.1016/j.biortech.2011.09.021

Bataineh, M., Scott, A.C., Fedorak, P.M., Martin, J.W., 2006. Capillary HPLC/QTOF-MS for characterizing complex naphthenic acid mixtures and their microbial transformation. Anal. Chem. 78, 8354–8361. https://doi.org/10.1021/ac061562p

Bird, R.B., Stewart, W.E., Lightfoot, E.N., 2012. Transport phenomena, second edition, Contraceptive delivery systems. https://doi.org/10.1002/aic.690070245

Bolzonella, D., Papa, M., Da Ros, C., Anga Muthukumar, L., Rosso, D., 2019. Winery wastewater treatment: a critical overview of advanced biological processes. Crit. Rev. Biotechnol. 39, 489–507.

https://doi.org/10.1080/07388551.2019.1573799

Bond, D.R., Lovley, D.R., 2003. Electricity production by Geobacter sulfurreducens attached to electrodes. Appl. Environ. Microbiol. 69, 1548–1555. https://doi.org/10.1128/AEM.69.3.1548-1555.2003

Borole, A.P., O'Neill, H., Tsouris, C., Cesar, S., 2008. A microbial fuel cell operating at low pH using the acidophile Acidiphilium cryptum. Biotechnol. Lett. 30, 1367–1372.

Buick, D., Holdstock, M., 2003. The relationship between acetic acid and volatile acidity. Adelaide, SA, Australia.

Calignano, F., Tommasi, T., Manfredi, D., Chiolerio, A., 2015. Additive Manufacturing of a Microbial Fuel Cell - A detailed study. Sci. Rep. 5. https://doi.org/10.1038/srep17373

Cang, Y., Roberts, D.., Clifford, D.., 2004. Development of cultures capable of reducing perchlorate and nitrate in high salt solutions. Water Res. 38, 3322–3330. https://doi.org/10.1016/J.WATRES.2004.04.020

Cao, X.X., Huang, X., Liang, P., Xiao, K., Zhou, Y.J., Zhang, X.Y., Logan, B.E., 2009. A New Method for Water Desalination Using Microbial Desalination Cells. Environ. Sci. Technol. 43, 7148–7152. https://doi.org/10.1021/es901950j

Cecconet, D., Molognoni, D., Callegari, A., Capodaglio, A.G., 2018. Agro-food industry wastewater treatment with microbial fuel cells: Energetic recovery issues. Int. J. Hydrogen Energy 43, 500–511. https://doi.org/https://doi.org/10.1016/j.ijhydene.2017.07.231

Cetinkaya, A.Y., Ozdemir, O.K., Demir, A., Ozkaya, B., 2017. Electricity Production and Characterization of High-Strength Industrial Wastewaters in Microbial Fuel Cell. Appl. Biochem. Biotechnol. 182, 468–481. https://doi.org/10.1007/s12010-016-2338-7

Champine, J.E., Underhill, B., Johnston, J.M., Lilly, W.W., Goodwin, S., 2000. Electron Transfer in the Dissimilatory Iron-reducing Bacterium Geobacter metallireducens. Anaerobe 6, 187–196. https://doi.org/https://doi.org/10.1006/anae.2000.0333

Chaudhuri, S.K., Lovley, D.R., 2003. Electricity generation by direct oxidation of glucose in mediatorless microbial fuel cells. Nat. Biotechnol. 21, 1229–1232. https://doi.org/10.1038/nbt867

Chen, F., Zeng, S., Luo, Z., Ma, J., Zhu, Q., Zhang, S., 2019. A novel MBBR–MFC integrated system for high-strength pulp/paper wastewater treatment and bioelectricity generation. Sep. Sci. Technol. 0, 1–10. https://doi.org/10.1080/01496395.2019.1641519

Cheng, S., Liu, H., Logan, B.E., 2006. Power densities using different cathode catalysts (Pt and CoTMPP) and polymer binders (Nafion and PTFE) in single chamber microbial fuel cells. Environ. Sci. Technol.

40, 364–369. https://doi.org/10.1021/es0512071

Cheng, S., Logan, B.E., 2011. Increasing power generation for scaling up single-chamber air cathode microbial fuel cells. Bioresour. Technol. 102, 4468–4473. https://doi.org/10.1016/j.biortech.2010.12.104

Cheng, S., Logan, B.E., 2007. Ammonia treatment of carbon cloth anodes to enhance power generation of microbial fuel cells. Electrochem. commun. 9, 492–496. https://doi.org/10.1016/j.elecom.2006.10.023

Cheng, S., Wu, J., 2013. Air-cathode preparation with activated carbon as catalyst, PTFE as binder and nickel foam as current collector for microbial fuel cells. Bioelectrochemistry 92, 22–26. https://doi.org/10.1016/J.BIOELECHEM.2013.03.001

Cho, Y.K., Donohue, T.J., Tejedor, I., Anderson, M.A., McMahon, K.D., Noguera, D.R., 2008. Development of a solar-powered microbial fuel cell. J. Appl. Microbiol. 104, 640–650. https://doi.org/10.1111/j.1365-2672.2007.03580.x

Choi, J., Liu, Y., 2014. Power generation and oil sands process-affected water treatment in microbial fuel cells. Bioresour. Technol. 169, 581–587. https://doi.org/10.1016/J.BIORTECH.2014.07.029

Clauwaert, P., Aelterman, P., Pham, T.H., De Schamphelaire, L., Carballa, M., Rabaey, K., Verstraete, W., 2008. Minimizing losses in bio-electrochemical systems: The road to applications. Appl. Microbiol. Biotechnol. 79, 901–913. https://doi.org/10.1007/s00253-008-1522-2

Conradie, A., Sigge, G.O., Cloete, T.E., 2014. Influence of winemaking practices on the characteristics of winery wastewater and water usage of wineries. South African J. Enol. Vitic. 35, 10–19.

Cooney, M.J., Roschi, E., Marison, I.W., Comminellis, C., von Stockar, U., 1996. Physiologic studies with the sulfate-reducing bacterium Desulfovibrio desulfuricans: Evaluation for use in a biofuel cell. Enzyme Microb. Technol. 18, 358–365. https://doi.org/https://doi.org/10.1016/0141-0229(95)00132-8

Coulter, A., 2018. Volatile Acidity. Aust. New Zeal. Grapegrow. Winemak. 16.

Crittenden, S.R., Sund, C.J., Sumner, J.J., 2006. Mediating electron transfer from bacteria to a gold electrode via a self-assembled monolayer. Langmuir 22, 9473–9476. https://doi.org/10.1021/la061869j

Cusick, R.D., Bryan, B., Parker, D.S., Merrill, M.D., Mehanna, M., Kiely, P.D., Liu, G., Logan, B.E., 2011. Performance of a pilot-scale continuous flow microbial electrolysis cell fed winery wastewater. Appl. Microbiol. Biotechnol. 89, 2053–2063. https://doi.org/10.1007/s00253-011-3130-9

Cusick, R.D., Kiely, P.D., Logan, B.E., 2010. A monetary comparison of energy recovered from microbial fuel cells and microbial electrolysis cells fed winery or domestic wastewaters. Int. J. Hydrogen Energy 35, 8855–8861. https://doi.org/10.1016/j.ijhydene.2010.06.077

D'Angelo, A., Mateo, S., Scialdone, O., Cañizares, P., Fernandez-Morales, F.J., Rodrigo, M.A., 2017. Optimization of the performance of an air–cathode MFC by changing solid retention time. J. Chem. Technol. Biotechnol. 92, 1746–1755. https://doi.org/10.1002/jctb.5175

Dannys, E., Green, T., Wettlaufer, A., Madhurnathakam, C.M.R., Elkamel, A., 2016. Wastewater Treatment with Microbial Fuel Cells: A Design and Feasibility Study for Scale-up in Microbreweries. J. Bioprocess. Biotech. 6, 1–6. https://doi.org/10.4172/2155-9821.1000267

De Borba, B.M., Jack, R.F., Rohrer, J.S., Wirt, J., Wang, D., 2014. Simultaneous determination of total nitrogen and total phosphorus in environmental waters using alkaline persulfate digestion and ion chromatography. J. Chromatogr. A 1369, 131–137. https://doi.org/10.1016/j.chroma.2014.10.027

del Campo, A., Cañizares, P., Lobato, J., Rodrigo, M., Fernandez Morales, F.J., 2016. Effects of External Resistance on Microbial Fuel Cell's Performance, in: Lefebvre, G., Jiménez, E., Cabañas, B. (Eds.), Environment, Energy and Climate Change II: Energies from New Resources and the Climate Change. Springer International Publishing, Cham, pp. 175–197. https://doi.org/10.1007/698_2014_290

Deval, A.S., Parikh, H.A., Kadier, A., Chandrasekhar, K., Bhagwat, A.M., Dikshit, A.K., 2016. Sequential microbial activities mediated bioelectricity production from distillery wastewater using bio-electrochemical system with simultaneous waste remediation. Int. J. Hydrogen Energy 42, 1130–1141. https://doi.org/10.1016/j.ijhydene.2016.11.114

Dong, Y., Qu, Y., He, W., Du, Y., Liu, J., Han, X., Feng, Y., 2015. A 90-liter stackable baffled microbial fuel cell for brewery wastewater treatment based on energy self-sufficient mode. Bioresour. Technol. 195, 66–72. https://doi.org/10.1016/J.BIORTECH.2015.06.026

Du, Z., Li, H., Gu, T., 2007. A state of the art review on microbial fuel cells: A promising technology for wastewater treatment and bioenergy. Biotechnol. Adv. 25, 464–482. https://doi.org/10.1016/j.biotechadv.2007.05.004

Eaktasang, N., Kang, C.S., Lim, H., Kwean, O.S., Cho, S., Kim, Y., Kim, H.S., 2016. Production of electrically-conductive nanoscale filaments by sulfate-reducing bacteria in the microbial fuel cell. Bioresour. Technol. 210, 61–67.

Eaton, A.D., Clesceri, L.S., Rice, E.W., Greenberg, A.E., Franson, M., 2005. APHA: standard methods for the examination of water and wastewater. Centen. Ed. APHA, AWWA, WEF, Washington, DC.

Fan, L.P., Li, J.J., 2016. Overviews on internal resistance and its detection of microbial fuel cells. Int. J. Circuits, Syst. Signal Process. 10, 316–320.

Fan, Y., Hu, H., Liu, H., 2007. Sustainable power generation in microbial fuel cells using bicarbonate buffer and proton transfer mechanisms. Environ. Sci. Technol. 41, 8154–8158. https://doi.org/10.1021/es071739c

Fan, Y., Sharbrough, E., Liu, H., 2008. Quantification of the internal resistance distribution of microbial fuel cells. Environ. Sci. Technol. 42, 8101–8107. https://doi.org/10.1021/es801229j

Fedorovich, V., Varfolomeev, S.D., Sizov, A., Goryanin, I., 2009. Multi-electrode microbial fuel cell with horizontal liquid flow. Water Sci. Technol. 60, 347–355. https://doi.org/10.2166/wst.2009.139

Feng, C., Li, J., Qin, D., Chen, L., Zhao, F., Chen, S., Hu, H., Yu, C.-P., 2014. Characterization of exoelectrogenic bacteria Enterobacter strains isolated from a microbial fuel cell exposed to copper shock load. PLoS One 9, e113379.

Feng, Q., Song, Y.C., Bae, B.U., 2016. Influence of applied voltage on the performance of bioelectrochemical anaerobic digestion of sewage sludge and planktonic microbial communities at ambient temperature. Bioresour. Technol. 220, 500–508. https://doi.org/10.1016/j.biortech.2016.08.085

Feng, Y., Wang, X., Logan, B.E., Lee, H., 2008. Brewery wastewater treatment using air-cathode microbial fuel cells. Appl. Microbiol. Biotechnol. 78, 873–880. https://doi.org/10.1007/s00253-008-1360-2

Fillaudeau, L., Bories, A., Decloux, M., Esteban-Decloux, M., 2008. Brewing, winemaking and distilling: An overview of wastewater treatment and utilisation schemes, in: Handbook of Water and Energy Management in Food Processing. pp. 929–995. https://doi.org/10.1533/9781845694678.6.929

Franks, A.E., Nevin, K.P., Jia, H., Izallalen, M., Woodard, T.L., Lovley, D.R., 2009. Novel strategy for three-dimensional real-time imaging of microbial fuel cell communities: Monitoring the inhibitory effects of proton accumulation within the anode biofilm. Energy Environ. Sci. https://doi.org/10.1039/b816445b

Freguia, S., Masuda, M., Tsujimura, S., Kano, K., 2009. Lactococcus lactis catalyses electricity generation at microbial fuel cell anodes via excretion of a soluble quinone. Bioelectrochemistry 76, 14–18.

Friman, H., Schechter, A., Ioffe, Y., Nitzan, Y., Cahan, R., 2013. Current production in a microbial fuel cell using a pure culture of C upriavidus basilensis growing in acetate or phenol as a carbon source. Microb. Biotechnol. 6, 425–434. https://doi.org/10.1111/1751-7915.12026

Fultz, M. Lou, Durst, R.A., 1983. Investigation of two multichannel image detectors for use in

spectroelectrochemistry. Talanta 30, 933–939. https://doi.org/10.1016/0039-9140(83)80216-1

Ganguli, R., Dunn, B.S., 2009. Kinetics of Anode Reactions for a Yeast-Catalysed Microbial Fuel Cell. Fuel Cells 9, 44–52. https://doi.org/10.1002/fuce.200800039

Ge, Z., He, Z., 2016. Long-term performance of a 200 liter modularized microbial fuel cell system treating municipal wastewater: treatment, energy, and cost. Environ. Sci. Water Res. Technol. 2, 274–281.

Gil-Carrera, L., Escapa, A., Carracedo, B., Morán, A., Gómez, X., 2013. Performance of a semi-pilot tubular microbial electrolysis cell (MEC) under several hydraulic retention times and applied voltages. Bioresour. Technol. 146, 63–69. https://doi.org/10.1016/j.biortech.2013.07.020

Gil, G.C., Chang, I.S., Kim, B.H., Kim, M., Jang, J.K., Park, H.S., Kim, H.J., 2003. Operational parameters affecting the performance of a mediator-less microbial fuel cell. Biosens. Bioelectron. 18, 327–334. https://doi.org/10.1016/S0956-5663(02)00110-0

Gonzalez del Campo, A., Lobato, J., Cañizares, P., Rodrigo, M.A., Fernandez Morales, F.J., 2013. Short-term effects of temperature and COD in a microbial fuel cell. Appl. Energy 101, 213–217. https://doi.org/10.1016/j.apenergy.2012.02.064

Goold, H.D., Kroukamp, H., Williams, T.C., Paulsen, I.T., Varela, C., Pretorius, I.S., 2017. Yeast's balancing act between ethanol and glycerol production in low-alcohol wines. Microb. Biotechnol. 10, 264–278. https://doi.org/10.1111/1751-7915.12488

Gorby, Y.A., Yanina, S., McLean, J.S., Rosso, K.M., Moyles, D., Dohnalkova, A., Beveridge, T.J., Chang, I.S., Kim, B.H., Kim, K.S., Culley, D.E., Reed, S.B., Romine, M.F., Saffarini, D.A., Hill, E.A., Shi, L., Elias, D.A., Kennedy, D.W., Pinchuk, G., Watanabe, K., Ishii, S., Logan, B., Nealson, K.H., Fredrickson, J.K., 2006. Electrically conductive bacterial nanowires produced by Shewanella oneidensis strain MR-1 and other microorganisms. Proc. Natl. Acad. Sci. 103, 11358–11363. https://doi.org/10.1073/pnas.0604517103

Goswami, R., Mishra, V.K., 2018. A review of design, operational conditions and applications of microbial fuel cells. Biofuels 9, 203–220. https://doi.org/10.1080/17597269.2017.1302682

Goud, R.K., Babu, P.S., Mohan, S.V., 2011. Canteen based composite food waste as potential anodic fuel for bioelectricity generation in single chambered microbial fuel cell (MFC): Bio-electrochemical evaluation under increasing substrate loading condition. Int. J. Hydrogen Energy 36, 6210–6218. https://doi.org/https://doi.org/10.1016/j.ijhydene.2011.02.056

Grady, C.P.L., Daigger, G.T., Love, N.G., Filipe, C.D., 2011. Biological wastewater treatment, 3rd ed. CRC Press： IWA Pub., c2011., Boca Raton, FL.

Greenman, J., Gálvez, A., Giusti, L., Ieropoulos, I., 2009. Electricity from landfill leachate using microbial fuel cells: Comparison with a biological aerated filter. Enzyme Microb. Technol. 44, 112–119. https://doi.org/10.1016/j.enzmictec.2008.09.012

Gude, V.G., 2016. Wastewater treatment in microbial fuel cells - An overview. J. Clean. Prod. https://doi.org/10.1016/j.jclepro.2016.02.022

Gunawardena, A., Fernando, S., To, F., 2008. Performance of a yeast-mediated biological fuel cell. Int. J. Mol. Sci. 9, 1893–1907. https://doi.org/10.3390/ijms9101893

Guo, X., Zhan, Y., Chen, C., Cai, B., Wang, Y., Guo, S., 2016. Influence of packing material characteristics on the performance of microbial fuel cells using petroleum refinery wastewater as fuel. Renew. Energy 87, 437–444. https://doi.org/https://doi.org/10.1016/j.renene.2015.10.041

Hamamoto, K., Miyahara, M., Kouzuma, A., Matsumoto, A., Yoda, M., Ishiguro, T., Watanabe, K., 2016. Evaluation of microbial fuel cells for electricity generation from oil-contaminated wastewater. J. Biosci. Bioeng. 122, 589–593. https://doi.org/https://doi.org/10.1016/j.jbiosc.2016.03.025

Hamelers, H.V.M., ter Heijne, A., Stein, N., Rozendal, R.A., Buisman, C.J.N., 2011. Butler–Volmer–Monod model for describing bio-anode polarization curves. Bioresour. Technol. 102, 381–387. https://doi.org/10.1016/J.BIORTECH.2010.06.156

He, W., Zhang, X., Liu, J., Zhu, X., Feng, Y., Logan, B.E., 2016. Microbial fuel cells with an integrated spacer and separate anode and cathode modules. Environ. Sci. Water Res. Technol. 2, 186–195.

He, Z. (Jason, Huang, Y., Manohar, A.K., Mansfeld, F., K Manohar, A., Mansfeld, F., Manohar, A.K., Mansfeld, F., 2008. Effect of electrolyte pH on the rate of the anodic and cathodic reactions in an air-cathode microbial fuel cell. Bioelectrochemistry 74, 78–82. https://doi.org/10.1016/j.bioelechem.2008.07.007

Heilmann, J., Logan, B.E., 2006. Production of Electricity from Proteins Using a Microbial Fuel Cell. Water Environ. Res. 78, 531–537. https://doi.org/10.2175/106143005X73046

Hernández-Fernández, F.J., Pérez De Los Ríos, A., Salar-García, M.J., Ortiz-Martínez, V.M., Lozano-Blanco, L.J., Godínez, C., Tomás-Alonso, F., Quesada-Medina, J., 2015. Recent progress and perspectives in microbial fuel cells for bioenergy generation and wastewater treatment. Fuel Process. Technol. https://doi.org/10.1016/j.fuproc.2015.05.022

Holmes, D.E., Bond, D.R., Lovley, D.R., 2004. Electron Transfer by Desulfobulbus propionicus to Fe(III) and Graphite Electrodes. Appl. Environ. Microbiol. https://doi.org/10.1128/AEM.70.2.1234-1237.2004

Holmes, D.E., Nicoll, J.S., Bond, D.R., Lovley, D.R., 2009. Erratum: Potential role of a novel psychrotolerant member of the family geobacteraceae, geopsychrobacter electrodiphilus gen. nov., sp. nov., in electricity production by a marine sediment fuel cell (Applied and Environmental Microbiology (2004) 70: 10 (6. Appl. Environ. Microbiol. 75.

Hoskins, D.L., Zhang, X., Hickner, M. a., Logan, B.E., 2014. Spray-on polyvinyl alcohol separators and impact on power production in air-cathode microbial fuel cells with different solution conductivities. Bioresour. Technol. 172, 156–161. https://doi.org/10.1016/j.biortech.2014.09.004

Huang, J., Sun, B., Zhang, X., 2010. Electricity generation at high ionic strength in microbial fuel cell by a newly isolated Shewanella marisflavi EP1. Appl. Microbiol. Biotechnol. 85, 1141–1149. https://doi.org/10.1007/s00253-009-2259-2

Huang, J., Yang, P., Guo, Y., Zhang, K., 2011. Electricity generation during wastewater treatment: An approach using an AFB-MFC for alcohol distillery wastewater. Desalination 276, 373–378. https://doi.org/10.1016/j.desal.2011.03.077

Huang, L., Logan, B.E., 2008. Electricity generation and treatment of paper recycling wastewater using a microbial fuel cell. Appl. Microbiol. Biotechnol. 80, 349–355.

Huggins, T., Fallgren, P.H., Jin, S., Ren, Z.J., 2013. Energy and performance comparison of microbial fuel cell and conventional aeration treating of wastewater. J. Microb. Biochem. Technol. 5. https://doi.org/10.4172/1948-5948.s6-002

Ichihashi, O., Hirooka, K., 2012. Removal and recovery of phosphorus as struvite from swine wastewater using microbial fuel cell. Bioresour. Technol. 114, 303–307. https://doi.org/https://doi.org/10.1016/j.biortech.2012.02.124

Ieropoulos, I., Winfield, J., Greenman, J., 2010. Effects of flow-rate, inoculum and time on the internal resistance of microbial fuel cells. Bioresour. Technol. 101, 3520–3525. https://doi.org/10.1016/j.biortech.2009.12.108

Ioannou, L.A., Puma, G.L., Fatta-Kassinos, D., 2015. Treatment of winery wastewater by physicochemical, biological and advanced processes: A review. J. Hazard. Mater. 286, 343–368. https://doi.org/10.1016/j.jhazmat.2014.12.043

Jadhav, G.S.S., Ghangrekar, M.M.M., 2009. Performance of microbial fuel cell subjected to variation in pH, temperature, external load and substrate concentration. Bioresour. Technol. 100, 717–723. https://doi.org/10.1016/j.biortech.2008.07.041

Jang, J.K., Pham, T.H., Chang, I.S., Kang, K.H., Moon, H., Cho, K.S., Kim, B.H., 2004. Construction and

operation of a novel mediator- and membrane-less microbial fuel cell. Process Biochem. 39, 1007–1012. https://doi.org/10.1016/S0032-9592(03)00203-6

Janicek, A., Fan, Y., Liu, H., 2014. Design of microbial fuel cells for practical application: a review and analysis of scale-up studies. Biofuels 5, 79–92. https://doi.org/10.4155/bfs.13.69

Jiang, Y., Liang, P., Liu, P., Yan, X., Bian, Y., Huang, X., Yong Jiang, Peng Liang*, Panpan Liu, Xiaoxu Yan, Yanhong Bian, X.H., 2015. A cathode-shared microbial fuel cell sensor array for water alert system. Environ. Sci. Technol. Lett. 2, 206–214. https://doi.org/10.1016/j.ijhydene.2016.12.050

Jo, Y., Kim, J., Hwang, S., Lee, C., 2015. Anaerobic treatment of rice winery wastewater in an upflow filter packed with steel slag under different hydraulic loading conditions. Bioresour. Technol. 193, 53–61.

Jung, S., Mench, M.M., Regan, J.M., 2011. Impedance characteristics and polarization behavior of a microbial fuel cell in response to short-term changes in medium pH. Environ. Sci. Technol. 45, 9069–9074. https://doi.org/10.1021/es201737g

Jung, S., Regan, J.M., 2011. Influence of external resistance on electrogenesis, methanogenesis, and anode prokaryotic communities in microbial fuel cells. Appl. Environ. Microbiol. 77, 564–571. https://doi.org/10.1128/AEM.01392-10

Jussier, D., Dubé Morneau, A., Mira de Orduña, R., 2006. Effect of Simultaneous Inoculation with Yeast and Bacteria on Fermentation Kinetics and Key Wine Parameters of Cool-Climate Chardonnay. Appl. Environ. Microbiol. 72, 221 LP – 227. https://doi.org/10.1128/AEM.72.1.221-227.2006

Kaiser, P., Reich, S., Leykam, D., Willert-Porada, M., Greiner, A., Freitag, R., 2017. Electrogenic Single-Species Biocomposites as Anodes for Microbial Fuel Cells. Macromol. Biosci. 17, 1600442.

Katuri, K.P., Scott, K., Head, I.M., Picioreanu, C., Curtis, T.P., 2011. Microbial fuel cells meet with external resistance. Bioresour. Technol. 102, 2758–2766. https://doi.org/10.1016/j.biortech.2010.10.147

Kim, B.H., Kim, H.J., Hyun, M.S., Park, D.H., 1999. Direct electrode reaction of Fe(III)-reducing bacterium, Shewanella putrefaciens. J. Microbiol. Biotechnol. 9, 127–131.

Kim, H., Kim, B., Kim, J., Lee, T., Yu, J., 2014. Electricity generation and microbial community in microbial fuel cell using low-pH distillery wastewater at different external resistances. J. Biotechnol. 186, 175–180. https://doi.org/10.1016/j.jbiotec.2014.06.012

Kim, H.J., Park, H.S., Hyun, M.S., Chang, I.S., Kim, M., Kim, B.H., 2002. A mediator-less microbial fuel cell using a metal reducing bacterium, Shewanella putrefaciens. Enzyme Microb. Technol. 30, 145–152. https://doi.org/10.1016/S0141-0229(01)00478-1

Kim, K.Y., Yang, W., Logan, B.E., 2015. Impact of electrode configurations on retention time and domestic

wastewater treatment efficiency using microbial fuel cells. Water Res. 80, 41–46. https://doi.org/10.1016/j.watres.2015.05.021

Kodama, Y., Shimoyama, T., Watanabe, K., 2012. Dysgonomonas oryzarvi sp. nov., isolated from a microbial fuel cell. Int. J. Syst. Evol. Microbiol. 62, 3055–3059.

Kokabian, B., Gude, V.G., 2015. Sustainable photosynthetic biocathode in microbial desalination cells. Chem. Eng. J. 262, 958–965. https://doi.org/10.1016/J.CEJ.2014.10.048

Larrosa-guerrero, A., Scott, K., Head, I.M., Mateo, F., Ginesta, A., Godinez, C., 2010. Effect of temperature on the performance of microbial fuel cells. Fuel 89, 3985–3994. https://doi.org/10.1016/j.fuel.2010.06.025

Ledezma, P., Stinchcombe, A., Greenman, J., Ieropoulos, I., 2013. The first self-sustainable microbial fuel cell stack. Phys. Chem. Chem. Phys. 15, 2278. https://doi.org/10.1039/c2cp44548d

Lee, D.S., Jeon, C.O., Park, J.M., 2001. Biological nitrogen removal with enhanced phosphate uptake in a sequencing batch reactor using single sludge system. Water Res. 35, 3968–3976. https://doi.org/10.1016/S0043-1354(01)00132-4

Lefebvre, O., Tan, Z., Kharkwal, S., Ng, H.Y., 2012. Effect of increasing anodic NaCl concentration on microbial fuel cell performance. Bioresour. Technol. 112, 336–340. https://doi.org/10.1016/j.biortech.2012.02.048

Li, C., Lesnik, K.L., Fan, Y., Liu, H., 2016. Millimeter scale electron conduction through exoelectrogenic mixed species biofilms. FEMS Microbiol. Lett. 363.

Li, J.T., Zhang, S.H., Hua, Y.M., 2013. Performance of denitrifying microbial fuel cell subjected to variation in pH, COD concentration and external resistance. Water Sci. Technol. 68, 250–256. https://doi.org/10.2166/wst.2013.250

Li, S., Chen, G., 2018. Factors Affecting the Effectiveness of Bioelectrochemical System Applications: Data Synthesis and Meta-Analysis. Batteries 4, 34. https://doi.org/10.3390/batteries4030034

Li, W.-W., Yu, H.-Q., He, Z., 2014. Towards sustainable wastewater treatment by using microbial fuel cells-centered technologies. Energy Environ. Sci. 7, 911–924. https://doi.org/10.1039/c3ee43106a

Li, X., Cheng, K., Selvam, A., Wong, J.W.C., 2013. Bioelectricity production from acidic food waste leachate using microbial fuel cells: Effect of microbial inocula. Process Biochem. 48, 283–288. https://doi.org/https://doi.org/10.1016/j.procbio.2012.10.001

Liang, P., Huang, X., Fan, M.-Z., Cao, X.-X., Wang, C., 2007. Composition and distribution of internal resistance in three types of microbial fuel cells. Appl. Microbiol. Biotechnol. 77, 551–558.

Liang, Y., Feng, H., Shen, D., Li, N., Guo, K., Zhou, Y., Xu, J., Chen, W., Jia, Y., Huang, B., 2017. Enhancement of anodic biofilm formation and current output in microbial fuel cells by composite modification of stainless steel electrodes. J. Power Sources 342, 98–104. https://doi.org/10.1016/J.JPOWSOUR.2016.12.020

Litaor, M.I., Meir-Dinar, N., Castro, B., Azaizeh, H., Rytwo, G., Levi, N., Levi, M., MarChaim, U., 2015. Treatment of winery wastewater with aerated cells mobile system. Environ. Nanotechnology, Monit. Manag. https://doi.org/10.1016/j.enmm.2015.03.001

Liu, G., Yates, M.D., Cheng, S., Call, D.F., Sun, D., Logan, B.E., 2011. Examination of microbial fuel cell start-up times with domestic wastewater and additional amendments. Bioresour. Technol. 102, 7301–7306. https://doi.org/10.1016/j.biortech.2011.04.087

Liu, H., Cheng, S., Logan, B.E., 2005a. Power Generation in Fed-Batch Microbial Fuel Cells as a Function of Ionic Strength, Temperature, and Reactor Configuration. Environ. Sci. Technol. 39, 5488–5493. https://doi.org/10.1021/es050316c

Liu, H., Grot, S., Logan, B.E., 2005b. Electrochemically Assisted Microbial Production of Hydrogen from Acetate. Environ. Sci. Technol. 39, 4317–4320. https://doi.org/10.1021/es050244p

Liu, H., Logan, B.E., 2004. Electricity Generation Using an Air-Cathode Single Chamber Microbial Fuel Cell in the Presence and Absence of a Proton Exchange Membrane. Environ. Sci. Technol. 38, 4040–4046. https://doi.org/10.1021/es0499344

Liu, H., Ramnarayanan, R., Logan, B.E., 2004. Production of Electricity during Wastewater Treatment Using a Single Chamber Microbial Fuel Cell. Environ. Sci. Technol. 38, 2281–2285. https://doi.org/10.1021/es034923g

Liu, J., Zhang, F., He, W., Yang, W., Feng, Y., Logan, B.E., 2014. A microbial fluidized electrode electrolysis cell (MFEEC) for enhanced hydrogen production. J. Power Sources 271, 530–533. https://doi.org/10.1016/j.jpowsour.2014.08.042

Liu, T., Yu, Y.Y., Li, D., Song, H., Yan, X., Chen, W.N., Ning Chen, W., Chen, W.N., 2016. The effect of external resistance on biofilm formation and internal resistance in Shewanella inoculated microbial fuel cells. RSC Adv. 6, 20317–20323. https://doi.org/10.1039/c5ra26125b

Liu, Z., Liu, J., Zhang, S., Su, Z., 2009. Study of operational performance and electrical response on mediator-less microbial fuel cells fed with carbon- and protein-rich substrates. Biochem. Eng. J. 45, 185–191. https://doi.org/10.1016/J.BEJ.2009.03.011

Logan, B.E., 2010. Scaling up microbial fuel cells and other bioelectrochemical systems. Appl. Microbiol.

Biotechnol. 85, 1665–1671. https://doi.org/10.1007/s00253-009-2378-9

Logan, B.E., 2008. Microbial fuel cells. John Wiley & Sons.

Logan, B.E., Hamelers, B., Rozendal, R., Schröder, U., Keller, J., Freguia, S., Aelterman, P., Verstraete, W., Rabaey, K., 2006. Microbial fuel cells: Methodology and technology. Environ. Sci. Technol. 40, 5181–5192. https://doi.org/10.1021/es0605016

Logan, B.E., Regan, J.M., 2006. Electricity-producing bacterial communities in microbial fuel cells. Trends Microbiol. https://doi.org/10.1016/j.tim.2006.10.003

Logan, D.E., Wright, C.J., Galpin, M.R., 2009. Correlated electron physics in two-level quantum dots: Phase transitions, transport, and experiment. Phys. Rev. B 80, 125117.

Lovley, D.R., Coates, J.D., Blunt-Harris, E.L., Phillips, E.J.P., Woodward, J.C., 1996. Humic substances as electron acceptors for microbial respiration. Nature 382, 445.

Lu, N., Zhou, S. gui, Zhuang, L., Zhang, J. tao, Ni, J. ren, 2009. Electricity generation from starch processing wastewater using microbial fuel cell technology. Biochem. Eng. J. 43, 246–251. https://doi.org/10.1016/j.bej.2008.10.005

Luo, Y., Zhang, F., Wei, B., Liu, G., Zhang, R., Logan, B.E., 2011. Power generation using carbon mesh cathodes with different diffusion layers in microbial fuel cells. J. Power Sources 196, 9317–9321. https://doi.org/10.1016/j.jpowsour.2011.07.077

Lyon, D.Y., Buret, F., Vogel, T.M., Monier, J.M., 2010. Is resistance futile? Changing external resistance does not improve microbial fuel cell performance. Bioelectrochemistry 78, 2–7. https://doi.org/10.1016/j.bioelechem.2009.09.001

Malandra, L., Wolfaardt, G., Zietsman, A., Viljoen-Bloom, M., 2003. Microbiology of a biological contactor for winery wastewater treatment. Water Res. 37, 4125–34. https://doi.org/10.1016/S0043-1354(03)00339-7

Manohar, A.K., Mansfeld, F., 2009. The internal resistance of a microbial fuel cell and its dependence on cell design and operating conditions. Electrochim. Acta 54, 1664–1670. https://doi.org/10.1016/j.electacta.2008.06.047

Marcus, A.K., Torres, C.I., Rittmann, B.E., 2011. Analysis of a microbial electrochemical cell using the proton condition in biofilm (PCBIOFILM) model. Bioresour. Technol. 102, 253–262. https://doi.org/10.1016/j.biortech.2010.03.100

Marcus, A.K., Torres, C.I., Rittmann, B.E., 2007. Conduction-based modeling of the biofilm anode of a microbial fuel cell. Biotechnol. Bioeng. https://doi.org/10.1002/bit.21533

Marsili, E., Baron, D.B., Shikhare, I.D., Coursolle, D., Gralnick, J.A., Bond, D.R., 2008. Shewanella secretes flavins that mediate extracellular electron transfer. Proc. Natl. Acad. Sci. 105, 3968–3973.

Martin, E., Savadogo, O., Guiot, S.R., Tartakovsky, B., 2010. The influence of operational conditions on the performance of a microbial fuel cell seeded with mesophilic anaerobic sludge. Biochem. Eng. J. 51, 132–139. https://doi.org/10.1016/j.bej.2010.06.006

Mateo, S., Zamorano-López, N., Borras, L., Fernandez-Morales, F.J., Cañizares, P., Seco, A., Rodrigo, M., 2018. Effect of sludge age on microbial consortia developed in MFCs. J. Chem. Technol. Biotechnol. 93, 1290–1299. https://doi.org/10.1002/jctb.5488

Mathuriya, a S., 2014. Eco-affectionate face of microbial fuel cells. Crit. Rev. Environ. Sci. Technol. 44, 97–153. https://doi.org/10.1080/10643389.2012.710445

McCarty, P.L., 1971. Energetics and bacterial growth. Org. Compd. Aquat. Environ. 1, 157–172.

McCarty, P.L., Bae, J., Kim, J., 2011. Domestic Wastewater Treatment as a Net Energy Producer–Can This be Achieved? Environ. Sci. Technol. 45, 7100–7106. https://doi.org/10.1021/es2014264

Merkey, B. V, Chopp, D.L., 2012. The Performance of a Microbial Fuel Cell Depends Strongly on Anode Geometry: A Multidimensional Modeling Study . Bull. Math. Biol. . https://doi.org/10.1007/s11538-011-9690-0

Metcalf & Eddy, A., Tchobanoglous, G., Stensel, H.D., Tsuchihashi, R., Burton, F.L., Abu-Orf, M., Bowden, G., Pfrang, W., Eddy, M.&, 2014. Wastewater engineering: treatment and resource recovery, Fifth. ed. McGraw-Hill Education, New York, NY.

Michie, I.S., Kim, J.R., Dinsdale, R.M., Guwy, A.J., Premier, G.C., 2011. Operational temperature regulates anodic biofilm growth and the development of electrogenic activity. Appl. Microbiol. Biotechnol. 92, 419–430. https://doi.org/10.1007/s00253-011-3531-9

Middaugh, J., Cheng, S., Liu, W., 2006. How to Make Cathodes with a Diffusion Layer for Single-Chamber Microbial Fuel Cells.

Min, B., Cheng, S., Logan, B.E., 2005. Electricity generation using membrane and salt bridge microbial fuel cells. Water Res. 39, 1675–86. https://doi.org/10.1016/j.watres.2005.02.002

Mink, J.E., Qaisi, R.M., Logan, B.E., Hussain, M.M., 2014. Energy harvesting from organic liquids in micro-sized microbial fuel cells. NPG Asia Mater. 6, e89. https://doi.org/10.1038/am.2014.1

Miran, W., Nawaz, M., Kadam, A., Shin, S., Heo, J., Jang, J., Lee, D.S., 2015. Microbial community structure in a dual chamber microbial fuel cell fed with brewery waste for azo dye degradation and electricity generation. Environ. Sci. Pollut. Res. 22, 13477–13485. https://doi.org/10.1007/s11356-

015-4582-8

Miyahara, M., Kouzuma, A., Watanabe, K., 2015. Effects of NaCl concentration on anode microbes in microbial fuel cells. AMB Express 5. https://doi.org/10.1186/s13568-015-0123-6

Mohammad Reza Miroliaei, Abdolreza Samimi, Davod Mohebbi-Kalhori, M.K., Qasemic, A., 2014. Competition Between E. coli and Shewanella sp. for Electricity Generation in Air Cathode MFC in Presence of Methylene Blue as Artificial Mediator. Environ. Sci. Technol. 33, 482–489. https://doi.org/10.1002/ep

Mohan, Y., Das, D., 2009. Effect of ionic strength, cation exchanger and inoculum age on the performance of Microbial Fuel Cells. Int. J. Hydrogen Energy 34, 7542–7546. https://doi.org/10.1016/j.ijhydene.2009.05.101

Mohanakrishna, G., Mohan, S.K., Mohan, S. V, 2012. Carbon based nanotubes and nanopowder as impregnated electrode structures for enhanced power generation: Evaluation with real field wastewater. Appl. Energy 95, 31–37. https://doi.org/10.1016/j.apenergy.2012.01.058

Molognoni, D., 2014. Microbial Fuel Cells Application to Wastewater Treatment: laboratory experience and controlling strategies.

Moon, H., Chang, I.S., Kim, B.H., 2006. Continuous electricity production from artificial wastewater using a mediator-less microbial fuel cell. Bioresour. Technol. 97, 621–627. https://doi.org/10.1016/j.biortech.2005.03.027

Mosse, K.P.M., Patti, A.F., Christen, E.W., Cavagnaro, T.R., 2011. Review: Winery wastewater quality and treatment options in Australia. Aust. J. Grape Wine Res. 17, 111–122. https://doi.org/10.1111/j.1755-0238.2011.00132.x

Nandy, A., Kumar, V., Kundu, P.P., 2016. Effect of electric impulse for improved energy generation in mediatorless dual chamber microbial fuel cell through electroevolution of Escherichia coli. Biosens. Bioelectron. 79, 796–801. https://doi.org/10.1016/j.bios.2016.01.023

Nandy, A., Kumar, V., Kundu, P.P., 2013. Utilization of proteinaceous materials for power generation in a mediatorless microbial fuel cell by a new electrogenic bacteria Lysinibacillus sphaericus VA5. Enzyme Microb. Technol. 53, 339–344.

Newman, D.K., Kolter, R., 2000. A role for excreted quinones in extracellular electron transfer. Nature 405, 94.

Nimje, V.R., Chen, C.-Y., Chen, C.-C., Jean, J.-S., Reddy, A.S., Fan, C.-W., Pan, K.-Y., Liu, H.-T., Chen, J.-L., 2009. Stable and high energy generation by a strain of Bacillus subtilis in a microbial fuel cell.

J. Power Sources 190, 258–263.

Nimje, V.R., Chen, C.-Y., Chen, H.-R., Chen, C.-C., Huang, Y.M., Tseng, M.-J., Cheng, K.-C., Chang, Y.-F., 2012. Comparative bioelectricity production from various wastewaters in microbial fuel cells using mixed cultures and a pure strain of Shewanella oneidensis. Bioresour. Technol. 104, 315–323. https://doi.org/10.1016/J.BIORTECH.2011.09.129

Oh, S., Logan, B.E., 2005. Hydrogen and electricity production from a food processing wastewater using fermentation and microbial fuel cell technologies. Water Res. 39, 4673–4682. https://doi.org/https://doi.org/10.1016/j.watres.2005.09.019

OIV, 2018. GLOBAL ECONOMIC VITIVINICULTURE DATA, OIV publications.

Oliveira, A., Markoski, M.M., Marcadenti, A., Garavaglia, J., Olivaes, J., 2016. Molecular Properties of Red Wine Compounds and Cardiometabolic Benefits. Nutr. Metab. Insights 9, NMI.S32909. https://doi.org/10.4137/nmi.s32909

Oliveira, V.B., Simões, M., Melo, L., Pinto, A., 2013. Overview on the developments of microbial fuel cells. Biochem. Eng. J. 73, 53–64. https://doi.org/10.1016/j.bej.2013.01.012

Ortiz-Martínez, V.M.M., Salar-García, M.J.J., de los Ríos, A.P.P., Hernández-Fernández, F.J.J., Egea, J.A.A., Lozano, L.J.J., 2015. Developments in microbial fuel cell modeling. Chem. Eng. J. 271, 50–60. https://doi.org/10.1016/j.cej.2015.02.076

Ou, S., Kashima, H., Aaron, D.S., Regan, J.M., Mench, M.M., 2016. Multi-variable mathematical models for the air-cathode microbial fuel cell system. J. Power Sources 314, 49–57. https://doi.org/10.1016/j.jpowsour.2016.02.064

Park, D.H., Zeikus, J.G., 2003. Improved fuel cell and electrode designs for producing electricity from microbial degradation. Biotechnol. Bioeng. 81, 348–355.

Park, D.H., Zeikus, J.G., 2000. Electricity Generation in Microbial Fuel Cells Using Neutral Red as an Electronophore. Appl. Environ. Microbiol. 66, 1292 LP – 1297. https://doi.org/10.1128/AEM.66.4.1292-1297.2000

Park, Y.H., Smith, G., Park, E., 2016. Mediator-less microbial fuel cell employing Shewanella Oneidensis. Energy Sources, Part A Recover. Util. Environ. Eff. 38, 1779–1784. https://doi.org/10.1080/15567036.2014.969815

Penteado, E.D., Fernandez-Marchante, C.M., Zaiat, M., Cañizares, P., Gonzalez, E.R., Rodrigo, M.A., 2016a. Influence of sludge age on the performance of MFC treating winery wastewater. Chemosphere 151, 163–170. https://doi.org/10.1016/j.chemosphere.2016.01.030

Penteado, E.D., Fernandez-Marchante, C.M., Zaiat, M., Cañizares, P., Gonzalez, E.R., Rodrigo, M.A.R., 2016b. Energy recovery from winery wastewater using a dual chamber microbial fuel cell. J. Chem. Technol. Biotechnol. 91, 1802–1808. https://doi.org/10.1002/jctb.4771

Penteado, E.D., Fernandez-Marchante, C.M., Zaiat, M., Gonzalez, E.R., Rodrigo, M.A., 2018. Optimization of the performance of a microbial fuel cell using the ratio electrode-surface area / anode-compartment volume. Brazilian J. Chem. Eng. 35, 141–146. https://doi.org/10.1590/0104-6632.20180351s20160411

Penteado, E.D., Fernandez-Marchante, C.M., Zaiat, M., Gonzalez, E.R., Rodrigo, M.A., 2017a. On the Effects of Ferricyanide as Cathodic Mediator on the Performance of Microbial Fuel Cells. Electrocatalysis 8, 59–66. https://doi.org/10.1007/s12678-016-0334-x

Penteado, E.D., Fernandez-Marchante, C.M., Zaiat, M., Gonzalez, E.R., Rodrigo, M.A., 2017b. Influence of carbon electrode material on energy recovery from winery wastewater using a dual-chamber microbial fuel cell. Environ. Technol. (United Kingdom) 38, 1333–1341. https://doi.org/10.1080/09593330.2016.1226961

Pepe Sciarria, T., Merlino, G., Scaglia, B., D'Epifanio, A., Mecheri, B., Borin, S., Licoccia, S., Adani, F., 2015. Electricity generation using white and red wine lees in air cathode microbial fuel cells. J. Power Sources 274, 393–399. https://doi.org/10.1016/j.jpowsour.2014.10.050

Pham, C.A., Jung, S.J., Phung, N.T., Lee, J., Chang, I.S., Kim, B.H., Yi, H., Chun, J., 2003. A novel electrochemically active and Fe(III)-reducing bacterium phylogenetically related to Aeromonas hydrophila, isolated from a microbial fuel cell. FEMS Microbiol. Lett. 223, 129–134. https://doi.org/10.1016/S0378-1097(03)00354-9

Pham, T.H., Rabaey, K., Aelterman, P., Clauwaert, P., De Schamphelaire, L., Boon, N., Verstraete, W., 2006. Microbial fuel cells in relation to conventional anaerobic digestion technology. Eng. Life Sci. 6, 285–292. https://doi.org/10.1002/elsc.200620121

Philamore, H., Rossiter, J., Walters, P., Winfield, J., Ieropoulos, I., 2015. Cast and 3D printed ion exchange membranes for monolithic microbial fuel cell fabrication. J. Power Sources 289, 91–99. https://doi.org/10.1016/j.jpowsour.2015.04.113

Picioreanu, C., Head, I.M., Katuri, K.P., van Loosdrecht, M.C.M., Scott, K., 2007. A computational model for biofilm-based microbial fuel cells. Water Res. 41, 2921–2940. https://doi.org/10.1016/j.watres.2007.04.009

Pinto, R.P., 2011. Dynamic Modelling and optimisation of microbial fuel cells and microbial electrolysis cells 154.

Pinto, R.P., Srinivasan, B., Uiot, S.R., Tartakovsky, B., 2011. The effect of real-time external resistance optimization on microbial fuel cell performance. Water Res. 45, 1571–1578. https://doi.org/10.1016/j.watres.2010.11.033

Popat, S.C., Ki, D., Rittmann, B.E., Torres, C.I., 2012. Importance of OH- transport from cathodes in microbial fuel cells. ChemSusChem 5, 1071–1079. https://doi.org/10.1002/cssc.201100777

Potter, M.C., 1911. Electrical Effects Accompanying the Decomposition of Organic Compounds. II.--Ionisation of the Gases Produced During Fermentation. Proc. R. Soc. B Biol. Sci. 84, 260–276. https://doi.org/10.1098/rspb.1915.0030

PR Newswire Association, 2016. Global Wine Market 2016-2020, PR Newswire. PR Newswire Association LLC, New York.

Premier, G.C., Kim, J.R., Michie, I., Dinsdale, R.M., Guwy, A.J., 2011. Automatic control of load increases power and efficiency in a microbial fuel cell. J. Power Sources 196, 2013–2019. https://doi.org/10.1016/J.JPOWSOUR.2010.09.071

Prokhorova, A., Sturm-Richter, K., Doetsch, A., Gescher, J., 2017. Resilience, dynamics, and interactions within a model multispecies exoelectrogenic-biofilm community. Appl. Environ. Microbiol. 83, e03033-16.

Puig, S., Serra, M., Coma, M., Cabré, M., Dolors Balaguer, M., Colprim, J., 2011. Microbial fuel cell application in landfill leachate treatment. J. Hazard. Mater. 185, 763–767. https://doi.org/10.1016/J.JHAZMAT.2010.09.086

Qiang, L., Yuan, L., Ding, Q., 2011. Influence of buffer solutions on the performance of microbial fuel cell electricity generation. Huanjing kexue 32, 1524–1528.

Rabaey, K., Verstraete, W., 2005. Microbial fuel cells: Novel biotechnology for energy generation. Trends Biotechnol. 23, 291–298. https://doi.org/10.1016/j.tibtech.2005.04.008

Raghavulu, S.V., Venkata Mohan, S., Venkateswar Reddy, M., Mohanakrishna, G., Sarma, P.N., 2009. Behavior of single chambered mediatorless microbial fuel cell (MFC) at acidophilic, neutral and alkaline microenvironments during chemical wastewater treatment. Int. J. Hydrogen Energy 34, 7547–7554. https://doi.org/10.1016/j.ijhydene.2009.05.071

Rajagopal, R., Saady, N.M.C., Torrijos, M., Thanikal, J. V., Hung, Y.T., 2013. Sustainable agro-food industrial wastewater treatment using high rate anaerobic process. Water (Switzerland) 5, 292–311. https://doi.org/10.3390/w5010292

Reguera, G., McCarthy, K.D., Mehta, T., Nicoll, J.S., Tuominen, M.T., Lovley, D.R., 2005. Extracellular

electron transfer via microbial nanowires. Nature 435, 1098.

Ren, Z., Ward, T.E., Regan, J.M., 2007. Electricity production from cellulose in a microbial fuel cell using a defined binary culture. Environ. Sci. Technol. 41, 4781–4786. https://doi.org/10.1021/es070577h

Rengasamy, K., Berchmans, S., 2012. Simultaneous degradation of bad wine and electricity generation with the aid of the coexisting biocatalysts Acetobacter aceti and Gluconobacter roseus. Bioresour. Technol. 104, 388–393. https://doi.org/10.1016/j.biortech.2011.10.092

Reshetilov, A., Alferov, S., Tomashevskaya, L., Ponamoreva, O., 2006. Testing of bacteria gluconobacter oxydans and electron transport mediators composition for application in biofuel cell. Electroanalysis 18, 2030–2034. https://doi.org/10.1002/elan.200603624

Rharbi, Y., Yekta, A., Winnik, M.A., 1999. A method for measuring oxygen diffusion and oxygen permeation in polymer films based on fluorescence quenching. Anal. Chem. https://doi.org/10.1021/ac990193c

Rismani-Yazdi, H., Christy, A.D., Carver, S.M., Yu, Z., Dehority, B.A., Tuovinen, O.H., 2011. Effect of external resistance on bacterial diversity and metabolism in cellulose-fed microbial fuel cells. Bioresour. Technol. 102, 278–283. https://doi.org/10.1016/j.biortech.2010.05.012

Roden, E.E., Jin, Q., 2011. Thermodynamics of microbial growth coupled to metabolism of glucose, ethanol, short-chain organic acids, and hydrogen. Appl. Environ. Microbiol. 77, 1907–1909. https://doi.org/10.1128/AEM.02425-10

Rodrigo, M.A., Cañizares, P., Lobato, J., 2010. Effect of the electron-acceptors on the performance of a MFC. Bioresour. Technol. 101, 7014–7018. https://doi.org/https://doi.org/10.1016/j.biortech.2010.04.013

Roh, S.-H., Kim, S.-I., 2012. Construction and performance evaluation of mediator-less microbial fuel cell using carbon nanotubes as an anode material. J. Nanosci. Nanotechnol. 12, 4252–4255.

Roller, S.D., Bennetto, H.P., Delaney, G.M., Mason, J.R., Stirling, J.L., Thurston, C.F., 1984. ELECTRON-TRANSFER COUPLING IN MICROBIAL FUEL CELLS: 1. COMPARISON OF REDOX-MEDIATOR REDUCTION RATES AND RESPIRATORY RATES OF BACTERIA. J. Chem. Technol. Biotechnol. Biotechnol. 34 B, 3–12.

Rosso, D., Bolzonella, D., 2009. Carbon footprint of aerobic biological treatment of winery wastewater. Water Sci. Technol. 60, 1185–1189. https://doi.org/10.2166/wst.2009.556

Rowe, A.R., Chellamuthu, P., Lam, B., Okamoto, A., Nealson, K.H., 2015. Marine sediments microbes capable of electrode oxidation as a surrogate for lithotrophic insoluble substrate metabolism. Front.

Microbiol. 5, 784. https://doi.org/10.3389/fmicb.2014.00784

Samsudeen, Nainamohamed, Radhakrishnan, T.K., Matheswaran, M., 2015. Performance comparison of triple and dual chamber microbial fuel cell using distillery wastewater as a substrate. Environ. Prog. Sustain. Energy 34, 589–594. https://doi.org/10.1002/ep.12005

Samsudeen, N, Radhakrishnan, T.K., Matheswaran, M., 2015. Bioelectricity production from microbial fuel cell using mixed bacterial culture isolated from distillery wastewater. Bioresour. Technol. 195, 242–247. https://doi.org/10.1016/j.biortech.2015.07.023

Santos, J.B.C., Silva De Barros, V. V., Linares, J.J., 2017. The hydraulic retention time as a key parameter for the performance of a cyclically fed glycerol-based microbial fuel cell from biodiesel. J. Electrochem. Soc. 164, H3001–H3006. https://doi.org/10.1149/2.0011703jes

Sayed, E.T., Barakat, N.A.M., Abdelkareem, M.A., Fouad, H., Nakagawa, N., 2015. Yeast extract as an effective and safe mediator for the baker's-yeast-based microbial fuel cell. Ind. Eng. Chem. Res. 54, 3116–3122. https://doi.org/10.1021/ie5042325

Schaetzle, O., Barrière, F., Baronian, K., 2008. Bacteria and yeasts as catalysts in microbial fuel cells: electron transfer from micro-organisms to electrodes for green electricity. Energy Environ. Sci. 1, 607–620. https://doi.org/10.1039/B810642H

Scott, K., J. Philips, Verbeeck, K., Rabaey, K., Arends, J.B.A., Dumitru, A., Bajracharya, S., ElMekawy, A., Srikanth, S., Pant, D., Premier, G.C., Michie, I.S., Boghani, H.C., Fradler, K.R., Kim, J.R., Gude, V.G., Cotterill, S., Heidrich, E., Curtis, T., Yu, E.H., Di Lorenzo, M., I. Ieropoulos, J. Winfield, I. Gajda, A. Walter, G.P., Jimenez, I.M., Pasternak, G., You, J., Tremouli, A., Stinchcombe, A., Forbes, S., Greenman, J., 2016. Microbial Electrochemical and Fuel Cells: Fundamentals and applications, Woodhead Publishing Series in Energy. https://doi.org/10.1016/B978-1-78242-375-1.00012-5

Scott, K., Murano, C., 2007. Microbial fuel cells utilising carbohydrates. J. Chem. Technol. Biotechnol. Int. Res. Process. Environ. Clean Technol. 82, 92–100.

Serrano, L., de la Varga, D., Ruiz, I., Soto, M., 2011. Winery wastewater treatment in a hybrid constructed wetland. Ecol. Eng. 37, 744–753. https://doi.org/10.1016/J.ECOLENG.2010.06.038

Shehab, N. a., Amy, G.L., Logan, B.E., Saikaly, P.E., 2014. Enhanced water desalination efficiency in an air-cathode stacked microbial electrodeionization cell (SMEDIC). J. Memb. Sci. 469, 364–370. https://doi.org/10.1016/j.memsci.2014.06.058

Shin, C., Kim, K., McCarty, P.L., Kim, J., Bae, J., 2016. Development and application of a procedure for evaluating the long-term integrity of membranes for the anaerobic fluidized membrane bioreactor

(AFMBR). Water Sci. Technol. https://doi.org/10.2166/wst.2016.210

Shizas, I., Bagley, D.M., 2004. Experimental Determination of Energy Content of Unknown Organics in Municipal Wastewater Streams. J. Energy Eng. 130, 45–53.

Siegert, M., Yates, M.D., Call, D.F., Zhu, X., Spormann, A., Logan, B.E., 2014. Comparison of nonprecious metal cathode materials for methane production by electromethanogenesis. ACS Sustain. Chem. Eng. 2, 910–917. https://doi.org/10.1021/sc400520x

Sirinutsomboon, B., 2014. Modeling of a membraneless single-chamber microbial fuel cell with molasses as an energy source. Int. J. Energy Environ. Eng. 5, 1–9. https://doi.org/10.1007/s40095-014-0093-5

Sirrine, K.L., Russell, P.H., Makepeace, J., 1977. Winery wastewater characteristics and treatment. Industrial Environmental Research Laboratory, Office of Research and Development, U.S. Environmental Protection Agency, Cincinnati, Ohio.

Sonawane, J.M., Marsili, E., Ghosh, P.C., 2014. Treatment of domestic and distillery wastewater in high surface microbial fuel cells. Int. J. Hydrogen Energy 39, 21819–21827. https://doi.org/10.1016/j.ijhydene.2014.07.085

Srikanth, S., Kumar, M., Singh, D., Singh, M.P., Das, B.P., 2016. Electro-biocatalytic treatment of petroleum refinery wastewater using microbial fuel cell (MFC) in continuous mode operation. Bioresour. Technol. 221, 70–77. https://doi.org/https://doi.org/10.1016/j.biortech.2016.09.034

Stamatelatou, K., Antonopoulou, G., Tremouli, A., Lyberatos, G., 2010. Production of gaseous biofuels and electricity from cheese whey. Ind. Eng. Chem. Res. 50, 639–644.

Stumm, W., Morgan, J.J., 1996. Oxidation and Reduction; Equilibria and Microbial Mediation, in: Aquatic Chemistry: Chemical Equilibria and Rates in Natural Waters. pp. 425–515.

Sun, Y., Zuo, J., Cui, L., Deng, Q., Dang, Y., 2010. Diversity of microbes and potential exoelectrogenic bacteria on anode surface in microbial fuel cells. J. Gen. Appl. Microbiol. 56, 19–29.

Sustarsic, M., 2009. Wastewater Treatment: Understanding the Activated Sludge Process. Chem. Eng. Prog. 26–29.

SWBC, 2018. Winery Process Wastewater Management Handbook : Best Practices and Technologies.

Syron, E., Casey, E., 2015. Membrane bioreactors for wastewater treatment, in: Handbook of Membrane Separations: Chemical, Pharmaceutical, Food, and Biotechnological Applications, Second Edition. Elsevier, pp. 741–758. https://doi.org/10.1201/b18319

Tang, Y.L., He, Y.T., Yu, P.F., Sun, H., Fu, J.X., 2012. Effect of temperature on electricity generation of single-chamber microbial fuel cells with proton exchange membrane, in: Advanced Materials

Research. Trans Tech Publ, pp. 1169–1172.

Tkach, O., Sangeetha, T., Maria, S., Wang, A., 2017. Performance of low temperature Microbial Fuel Cells (MFCs) catalyzed by mixed bacterial consortia. J. Environ. Sci. (China) 52, 284–292. https://doi.org/10.1016/j.jes.2016.11.006

Toh, H., Sharma, V.K., Oshima, K., Kondo, S., Hattori, M., Ward, F.B., Free, A., Taylor, T.D., 2011. Complete genome sequences of Arcobacter butzleri ED-1 and Arcobacter sp. strain L, both isolated from a microbial fuel cell.

Torres, C.I., Marcus, A.K., Rittmann, B.E., 2008. Proton transport inside the biofilm limits electrical current generation by anode-respiring bacteria. Biotechnol. Bioeng. 100, 872–881. https://doi.org/10.1002/bit.21821

Tursun, H., Liu, R., Li, J., Abro, R., Wang, X., Gao, Y., Li, Y., 2016. Carbon material optimized biocathode for improving microbial fuel cell performance. Front. Microbiol. 7, 1–9. https://doi.org/10.3389/fmicb.2016.00006

U.S.EPA, 2014. Energy Efficiency in Water and Wastewater Facilities. U.S. Environ. Prot. Agency 49.

Vázquez-Larios, A.L., Solorza-Feria, O., Poggi-Varaldo, H.M., de Guadalupe González-Huerta, R., Ponce-Noyola, M.T., Ríos-Leal, E., Rinderknecht-Seijas, N., 2014. Bioelectricity production from municipal leachate in a microbial fuel cell: Effect of two cathodic catalysts. Int. J. Hydrogen Energy 39, 16667–16675. https://doi.org/https://doi.org/10.1016/j.ijhydene.2014.05.178

Vega, C.A., Fernández, I., 1987. Mediating effect of ferric chelate compounds in microbial fuel cells with Lactobacillus plantarum, Streptococcus lactis, and Erwinia dissolvens. Bioelectrochemistry Bioenerg. 17, 217–222. https://doi.org/https://doi.org/10.1016/0302-4598(87)80026-0

Velasquez-Orta, S.B., Head, I.M., Curtis, T.P., Scott, K., 2011. Factors affecting current production in microbial fuel cells using different industrial wastewaters. Bioresour. Technol. 102, 5105–5112. https://doi.org/https://doi.org/10.1016/j.biortech.2011.01.059

Velvizhi, G., Venkata Mohan, S., 2011. Biocatalyst behavior under self-induced electrogenic microenvironment in comparison with anaerobic treatment: Evaluation with pharmaceutical wastewater for multi-pollutant removal. Bioresour. Technol. 102, 10784–10793. https://doi.org/https://doi.org/10.1016/j.biortech.2011.08.061

Venkata Mohan, S., Mohanakrishna, G., Sarma, P.N., 2010. Composite vegetable waste as renewable resource for bioelectricity generation through non-catalyzed open-air cathode microbial fuel cell. Bioresour. Technol. 101, 970–976. https://doi.org/10.1016/j.biortech.2009.09.005

Venkata Mohan, S., Veer Raghavulu, S., Sarma, P.N., 2008. Influence of anodic biofilm growth on bioelectricity production in single chambered mediatorless microbial fuel cell using mixed anaerobic consortia. Biosens. Bioelectron. 24, 41–47. https://doi.org/10.1016/j.bios.2008.03.010

Vidyalakshmi, R., Paranthaman, R., Bhakyaraj, R., 2009. Sulphur Oxidizing Bacteria and Pulse Nutrition - A Review. World J. Agric. Sci. 5, 270–278.

Vlyssides, A.G., Barampouti, E.M., Mai, S., 2005. Wastewater characteristics from Greek wineries and distilleries. Water Sci. Technol. 51, 53–60. https://doi.org/10.2166/wst.2005.0007

Von Canstein, H., Ogawa, J., Shimizu, S., Lloyd, J.R., 2008. Secretion of flavins by Shewanella species and their role in extracellular electron transfer. Appl. Environ. Microbiol. 74, 615–623.

Walter, X.A., Forbes, S., Greenman, J., Ieropoulos, I.A., 2016. From single MFC to cascade configuration: The relationship between size, hydraulic retention time and power density. Sustain. Energy Technol. Assessments 14, 74–79. https://doi.org/10.1016/j.seta.2016.01.006

Wang, H., Qu, Y., Li, D., Ambuchi, J.J., He, W., Zhou, X., Liu, J., Feng, Y., 2016. Cascade degradation of organic matters in brewery wastewater using a continuous stirred microbial electrochemical reactor and analysis of microbial communities. Sci. Rep. 6, 27023. https://doi.org/10.1038/srep27023

Wang, X., Cheng, S., Feng, Y., Merrill, M.D., Saito, T., Logan, B.E., 2009. Use of carbon mesh anodes and the effect of different pretreatment methods on power production in microbial fuel cells. Environ. Sci. Technol. 43, 6870–6874. https://doi.org/10.1021/es900997w

Wang, X., Feng, Y., Liu, J., Shi, X., Lee, H., Li, N., Ren, N., 2010. Power generation using adjustable Nafion/PTFE mixed binders in air-cathode microbial fuel cells, Biosensors and Bioelectronics. https://doi.org/10.1016/j.bios.2010.06.026

Watson, V.J., Logan, B.E., 2011. Analysis of polarization methods for elimination of power overshoot in microbial fuel cells. Electrochem. commun. 13, 54–56. https://doi.org/10.1016/j.elecom.2010.11.011

Wei, J., Liang, P., Huang, X., 2011. Recent progress in electrodes for microbial fuel cells. Bioresour. Technol. 102, 9335–9344. https://doi.org/https://doi.org/10.1016/j.biortech.2011.07.019

Welz, P.J., Holtman, G., Haldenwang, R., Le Roes-Hill, M., 2016. Characterisation of winery wastewater from continuous flow settling basins and waste stabilisation ponds over the course of 1 year: Implications for biological wastewater treatment and land application. Water Sci. Technol. 74, 2036–2050. https://doi.org/10.2166/wst.2016.226

Wen, Q., Wu, Y., Cao, D., Zhao, L., Sun, Q., 2009. Electricity generation and modeling of microbial fuel cell from continuous beer brewery wastewater. Bioresour. Technol. 100, 4171–4175.

https://doi.org/10.1016/j.biortech.2009.02.058

Wen, Q., Wu, Y., Zhao, L., Sun, Q., Kong, F., 2010. Electricity generation and brewery wastewater treatment from sequential anode-cathode microbial fuel cell. J. Zhejiang Univ. Sci. B 11, 87–93. https://doi.org/10.1631/jzus.B0900272

Wrighton, K.C., Agbo, P., Warnecke, F., Weber, K.A., Brodie, E.L., DeSantis, T.Z., Hugenholtz, P., Andersen, G.L., Coates, J.D., 2008. A novel ecological role of the Firmicutes identified in thermophilic microbial fuel cells. ISME J. 2, 1146–1156. https://doi.org/10.1038/ismej.2008.48

Wrighton, K.C., Thrash, J.C., Melnyk, R.A., Bigi, J.P., Byrne-Bailey, K.G., Remis, J.P., Schichnes, D., Auer, M., Chang, C.J., Coates, J.D., 2011. Evidence for direct electron transfer by a Gram-positive bacterium isolated from a microbial fuel cell. Appl. Environ. Microbiol. 77, 7633–7639.

Wu, S., Li, H., Zhou, X., Liang, P., Zhang, X., Jiang, Y., Huang, X., 2016. A novel pilot-scale stacked microbial fuel cell for efficient electricity generation and wastewater treatment. Water Res. 98, 396–403. https://doi.org/10.1016/j.watres.2016.04.043

Xing, D., Cheng, S., Logan, B.E., Regan, J.M., 2010. Isolation of the exoelectrogenic denitrifying bacterium Comamonas denitrificans based on dilution to extinction. Appl. Microbiol. Biotechnol. 85, 1575–1587.

Xing, D., Zuo, Y., Cheng, S., Regan, J.M., Logan, B.E., 2008. Electricity Generation by Rhodopseudomonas palustris DX-1. Environ. Sci. Technol. 42, 4146–4151. https://doi.org/10.1021/es800312v

Yamashita, T., Ishida, M., Ogino, A., Yokoyama, H., 2016. Evaluation of organic matter removal and electricity generation by using integrated microbial fuel cells for wastewater treatment. Environ. Technol. (United Kingdom) 37, 228–236. https://doi.org/10.1080/09593330.2015.1066874

Yan, M., Fan, L., 2013. Constant voltage output in two-chamber microbial fuel cell under fuzzy pid control. Int. J. Electrochem. Sci. 8, 3321–3332.

Yang, Q., Wu, Z., Liu, L., Zhang, F., Liang, S., 2016. Treatment of oil wastewater and electricity generation by integrating constructed wetland with microbial fuel cell. Materials (Basel). 9. https://doi.org/10.3390/ma9110885

Yang, W., He, W., Zhang, F., Hickner, M.A., Logan, B.E., 2014. Supporting Information to: Single-Step Fabrication Using a Phase Inversion Method of Poly(vinylidene fluoride) (PVDF) Activated Carbon Air Cathodes for Microbial Fuel Cells. Environ. Sci. Technol. Lett. 1, 416–420. https://doi.org/10.1021/ez5002769

You, J., Preen, R.J., Bull, L., Greenman, J., Ieropoulos, I., 2017. 3D printed components of microbial fuel cells: Towards monolithic microbial fuel cell fabrication using additive layer manufacturing. Sustain. Energy Technol. Assessments 19, 94–101. https://doi.org/http://dx.doi.org/10.1016/j.seta.2016.11.006

You, S.J., Zhao, Q.L., Jiang, J.Q., Zhang, J.N., 2006. Treatment of domestic wastewater with simultaneous electricity generation in microbial fuel cell under continuous operation. Chem. Biochem. Eng. Q. 20, 407–412.

Zeng, Y., Choo, Y.F., Kim, B.H., Wu, P., 2010. Modelling and simulation of two-chamber microbial fuel cell. J. Power Sources 195, 79–89. https://doi.org/10.1016/j.jpowsour.2009.06.101

Zhang, F., Chen, G., Hickner, M.A., Logan, B.E., 2012. Novel anti-flooding poly(dimethylsiloxane) (PDMS) catalyst binder for microbial fuel cell cathodes. J. Power Sources 218, 100–105. https://doi.org/10.1016/J.JPOWSOUR.2012.06.088

Zhang, F., Cheng, S., Pant, D., Bogaert, G. Van, Logan, B.E., 2009. Power generation using an activated carbon and metal mesh cathode in a microbial fuel cell. Electrochem. commun. 11, 2177–2179. https://doi.org/10.1016/j.elecom.2009.09.024

Zhang, F., Merrill, M.D., Tokash, J.C., Saito, T., Cheng, S., Hickner, M.A., Logan, B.E., 2011a. Mesh optimization for microbial fuel cell cathodes constructed around stainless steel mesh current collectors. J. Power Sources 196, 1097–1102. https://doi.org/10.1016/j.jpowsour.2010.08.011

Zhang, F., Pant, D., Logan, B.E., 2011b. Long-term performance of activated carbon air cathodes with different diffusion layer porosities in microbial fuel cells. Biosens. Bioelectron. 30, 49–55. https://doi.org/10.1016/j.bios.2011.08.025

Zhang, F., Saito, T., Cheng, S., Hickner, M.A., Logan, B.E., 2010. Microbial fuel cell cathodes with poly(dimethylsiloxane) diffusion layers constructed around stainless steel mesh current collectors. Environ. Sci. Technol. 44, 1490–1495. https://doi.org/10.1021/es903009d

Zhang, L., Li, C., Ding, L., Xu, K., Ren, H., 2011. Influences of initial pH on performance and anodic microbes of fed-batch microbial fuel cells. J. Chem. Technol. Biotechnol. 86, 1226–1232. https://doi.org/10.1002/jctb.2641

Zhang, L., Zhou, S., Zhuang, L., Li, W., Zhang, J., Lu, N., Deng, L., 2008. Microbial fuel cell based on Klebsiella pneumoniae biofilm. Electrochem. commun. 10, 1641–1643. https://doi.org/https://doi.org/10.1016/j.elecom.2008.08.030

Zhang, P.Y., Liu, Z.L., 2010. Experimental study of the microbial fuel cell internal resistance. J. Power

Sources 195, 8013–8018. https://doi.org/10.1016/j.jpowsour.2010.06.062

Zhang, X., He, W., Ren, L., Stager, J., Evans, P.J., Logan, B.E., 2015. COD removal characteristics in air-cathode microbial fuel cells. Bioresour. Technol. 176, 23–31. https://doi.org/10.1016/j.biortech.2014.11.001

Zhang, X., Xia, X., Ivanov, I., Huang, X., Logan, B.E., 2014. Enhanced Activated Carbon Cathode Performance for Microbial Fuel Cell by Blending Carbon Black. https://doi.org/10.1021/es405029y

Zhou, M., Wang, H., Hassett, D.J., Gu, T., 2013. Recent advances in microbial fuel cells (MFCs) and microbial electrolysis cells (MECs) for wastewater treatment, bioenergy and bioproducts. J. Chem. Technol. Biotechnol. 88, 508–518. https://doi.org/10.1002/jctb.4004

Zhu, X., Logan, B.E., 2013. Copper anode corrosion affects power generation in microbial fuel cells. https://doi.org/10.1002/jctb.4156

Zhuang, L., Zheng, Y., Zhou, S., Yuan, Y., Yuan, H., Chen, Y., 2012. Scalable microbial fuel cell (MFC) stack for continuous real wastewater treatment. Bioresour. Technol. 106, 82–88.

Zhuang, L., Zhou, S., Li, Y., Yuan, Y., 2010. Enhanced performance of air-cathode two-chamber microbial fuel cells with high-pH anode and low-pH cathode. Bioresour. Technol. 101, 3514–3519.

Zielke, E., 2006. Numerical Analysis of a one dimensional Diffusion Equation for a single chamber Microbial Fuel Cell using a Linked Simulation Optimization (LSO) technique, E521: Advanced Numerical Methods.

Zuo, K., Wang, Z., Chen, X., Zhang, X., Zuo, J., Liang, P., Huang, X., 2016. Self-Driven Desalination and Advanced Treatment of Wastewater in a Modularized Filtration Air Cathode Microbial Desalination Cell. Environ. Sci. Technol. 50, 7254–7262. https://doi.org/10.1021/acs.est.6b00520

Zuo, Y., Xing, D., Regan, J.M., Logan, B.E., 2008. Isolation of the exoelectrogenic bacterium Ochrobactrum anthropi YZ-1 by using a U-tube microbial fuel cell. Appl. Environ. Microbiol. 74, 3130–3137. https://doi.org/10.1128/AEM.02732-07